DOCTOR OF PHILOSOPHY

Molecular Analysis of Hepatitis C Virus Envelope Glycoprotein E2 Binding and Entry

Alshehri, Ahmad A.

Award date:
2017

Molecular Analysis of Hepatitis C Virus Envelope Glycoprotein E2 Binding and Entry

Ahmad A. Alshehri

Submitted for the degree of Doctor of Philosophy

School of Medcine

University of Dundee

February 2017

Table of Contents

LIST OF TABLES

Table

LIST OF FIGURES

Figure

LIST OF ABBREVIATIONS

Abbreviation	Meaning
a.a	Amino acid(s)
AASLD	Association for the Study of Liver Diseases
IgG	Immunoglobulin G
ApoE	Apolipoprotein E
BCA	Bicinchninic Acid Assay
BSA	Bovine Serum Albumin
BVDV	Bovine Viral Diarrhea virus
cat. no.	catalogue number
CCR-5	Chemokine Receptor-5
CD81	Cluster of Differentiation 81
CHC	Clathrin Heavy Chain
CHO	Chinese Hamster Oocytes
CIDEB	Cell-death-Inducing DFFA-like Effector B
CLDN-1	Claudin-1
CS	Cleavage site
CVB	Coxsackievirus B
D.W	Distilled Water
DAPI	4',6-Diamidino-2-phenylindole
DC-SIGN	Dendritic Cell Specific Intercellular adhesion molecule 3-grabbing Non-integrin
DCs	Dendritic Cells
DNA	Deoxyribo Nucleic acid
DS2ES	*Drosophila melanogaster* Schneider 2 cell expression system
E.coli	*Escherichia coli*
E1	Envelope 1
E2	Envelope 2
EBV	Epstein Barr virus
ECL	Extracellular loop
EGFR	Epidermal Growth Factor Receptor

ELISA	Enzyme-linked Immunosorbent Assay
EphA2	Ephrin receptor A2
ER	Endoplasmic reticulum
EtBr	Ethidium Bromide
EtOH	Ethanol
FBS	Fetal Bovine Serum
FCM	Flow Cytometer
FDA	Food and Drug Administration
FITC	Fluorescein Isothiocyanate
GAG	Glycosaminoglycan
GBD	Global Burden of Disease studies
gp120	Glycoproteins 120
gp46	Glycoproteins 46
HAV	Hepatitis A Virus
HBsAg	Hepatitis B surface Antigen
HBV	Hepatitis B Virus
HCC	Hepatocellular carcinoma
HCV	Hepatitis C Virus
HCVcc	Hepatitis C Virus cell culture
HCVpp	Hepatitis C virus pseudoparticle
HDL	High Density Lipoprotein
HEK	Human Embryonic Kidney
hFAS	human Fatty Acid Synthase
HIV	Human Immunodeficiency virus
HPLC	High Performance Liquid Chromatograhy
hPSCs	human Pluripotent Stem Cells
HPV16	Human Papillomavirus 16
HSPG	Heparan Sulphate Proteoglycan
HSV	Herpes Simplex Viruses
HTLV-1	Human T-Cell Leukaemia Virus Type-1
HVR1	Hypervariable Region 1
ICTV	International Committee on Taxonomy of Viruses
IF	Immunofluorescence
IFN-α	Interferon Alpha

IL-2	Interlukin-2
IPSCs	Induced Pluripotent Stem Cells
IPTG	Isopropyl β-D-1-thiogalactopyranoside
IRES	Internal Ribosome Entry Site
JAM	Junctional Adhesion Molecule
ISGs	IFN-Stimulated Genes
LB	Lysogeny Broth
L-SIGN	Liver Specific Intercellular adhesion molecule 3-grabbing Non-integrin
LDL	Low-Density Lipoprotein
LDL-R	Low-Density Lipoprotein Receptor
LSEC	Liver Sinusoidal Endothelial Cells
LTRs	Long Terminal Repeats
LVP	Lipoviroparticle
M2	Matrix protein 2
MBP	Maltose Binding Protien
MDBK	Madin-Darby Bovine Kidney
MLV	Murine Leukaemia Virus
NANB	non-A, non-B hepatitis
NEAA	Non Essential Amino Acids
NK	Natural Killer
no.	Number
NPC1L1	Niemann-Pick C1-like 1
NS	Non-Structural proteins
OCLN	Occludin
ORF	Open Reading Frame
OST	Oligosaccharyl Transferase
PAGE	Polyacrylamide Gel Electrophoresis
PBS	Phosphate-Buffered Saline
PCR	Polymerase Chain Reaction
PFA	Paraformaldehyde
pMt	Metalthionine promoter
poly A	polyadenylation
PTH	Post Transfusion Hepatitis
r	recombinant

RNA	Ribo Nucleic Acid
rRVGP	recombinant Rabies Virus Glycoproteins
RTKs	Receptor Tyrosine Kinases
S2	Schneider 2
SDS	Sodium Dodecyl Sulphate
SEL	Small Extracellular Loop
SOC	Super Optimal broth with Catabolite repression
SR-B1	Scavenger Receptor class B type 1
srE2	Secreted (or Soluble) Envelope 2
$srE2^{332}$	srE2 full length lacking TMD
SS	Single Stranded
SV40 poly	Simian Virus 40 PolyA
SVR	Sustained Viral Response
TAG	Triglyceride
TAPA-1	Target of an Anti-Proliferative Antibody
TC	Thrombin Cleavage
TMB	3,3',5,5'-Tetramethylbenzidine
TJs	Tight Junction proteins
TMD	Transmembrane Domain
tPA	tissue Plasminogen Activator
TSFR1	Transferrin Receptor 1
VLDL	Very Low-Density Lipoprotein
VSV	Vesicular Stomatitis Virus
WB	Western Blotting

Superscript:

The number on the upper right-hand side of the envelope E2 and single amino acid indicates the postion of truncation and the site of residue respectively on the recombinant protein sequences.

Subscript:

The number on the lower right-hand side of the envelope E2, glycosylation site and single amino acid indicates the postion of truncation, glycan site and the site of residue respectively on the reference protein sequences.

AMINO ACIDS

Amino acid	One letter code
Alanine	A
Arginine	R
Asparagine	N
Aspartic acid	D
Cysteine	C
Glutamine	Q
Glutamic acid	E
Glycine	G
Histidine	H
Isoleucine	I
Leucine	L
Lysine	K
Methionine	M
Phenylalanine	F
Proline	P
Serine	S
Threonine	T
Tryptophan	W
Tyrosine	Y
Valine	V

ACKNOWLEDGEMENTS

This thesis could not have existed without the assistance of certain individuals who have lent their time, effort and experience to assist me with my research, thus providing me with the opportunity to enrich my knowledge. I would like to express my deepest gratitude to Dr. David W. Brighty and Professor John F. Dillon, my project supervisors, who have guided me throughout the entire project, sharing their experiences and insights about the research process with me. Thank you for providing me with valuable advice and always being very patient with me, especially when I asked many, many questions. I am also indebted to Dr. David Meek, chair of my thesis monitoring committee, and his colleagues, who have provided assistance and support during my studies. Many thanks for Dr. Gareth and his team (university of Oslo) for collaboration with my group. I must express gratitude especially to my beloved wife, Amal Alahmari, for her invaluable and enthusiastic support. I also thank my children, Abdullah and Almohanad, for their endless love. My deepest thanks go to my parents, Abdullah and Fatemah, as well as my extended family, for their spiritual encouragement and their belief in me. I would also like to mention my good friends Adem Dawed and Abdulrazzag Othman who has shared his valuable opinions with me along the way. I wish to articulate sincere appreciation for all those who have provided me with technical help and have shared ideas with me, including all the doctoral students and staff in the School of Medicine – and Dr. Sharon Kuo, Dr. Lindsay Tulloch and Dr. Roger Tavendale in particular.

Finally, I am extremely grateful to Najran University and to Saudi royal embassy at London for funding this project and offering a massive amount of support to me throughout my studies.

DECLARATION

I hereby declare that the candidate, Ahmad A. Alshehri is the author of the thesis presented herein; that, unless otherwise stated, all references cited have been consulted by the candidate; that the work of which the thesis is a record has been done by the candidate, and that it has not been previously accepted for a higher degree.

Signature:

All conditions stated within the Ordinance and Regulations of the University of Dundee have been strictly adhered to and fulfilled by the candidate, Ahmad A. Alshehri.

Supervisor's Signature: Dr. David Brighty and Professor John Dillon

ABSTRACT

The envelope of the hepatitis C virus (HCV) mediates entry into cells by binding directly to the cluster of differentiation 81 receptor (CD81) and to the scavenger receptor class B type 1 (SR-B1). The critical incorporation of claudin-1 receptor (CLDN-1) and occludin receptor (OCLN) (indirect interaction) has been reported. Then, fusion process is intiated between viral and cellular membranes following acidification of endosomes. All known HCV-receptor interactions are mediated by HCV envelope protein 2 (E2) but the manner in which E2 coordinates interactions with multiple entry receptors and cell surface co-factors in order to promote viral entry are only just beginning to be understood. Here, we have developed soluble recombinant forms of the E2 protein, which are fused to the Fc region of human IgG for use in the dissection of the E2 function and as molecular probes to interrogate the early events in the E2-dependent HCV entry pathway. These recombinant E2-immunoadhesins retain their immunological profile, as well as the cell surface and CD81-binding specificity that are typical of native E2. We have demonstrated that E2, in the complete absence of all other viral protein, is competent both for targeted binding and for internalisation into hepatoma cells. Rates of E2-Fc internalisation differ between cell types, being dependent on the density of the CD81 receptors displayed on the cell surface, to an extent. Internalised E2-immunoadhesin localises with endocytosis markers and tends to accumulate in early endosomes in target cells. Although binding to CD81 promotes and accelerates E2 internalisation rates, high-level expression, along with the display of CD81, is not sufficient to drive the internalisation of E2 in 293T cells, which confirms that the recruitment of CD81 to a multi-component entry complex is a critical event in the rapid attachment and endocytosis of E2. We have also identified important residues located somewhere within $E2^{195}$ immunoadhesin, which undergo remarkably direct interactions with alternative host surface factors, when known HCV receptors are engaged. Our data enables us to speculate that the alternative factor has not defined yet and need further study.

Chapter 1 Introduction

1.1 General Overview

1.1.1 History of hepatitis C virus

From the mid 1950s till late 1970s, evidence based on epidemiological data, transmission studies and serological markers revealed the existence of an unknown causative agent for hepatitis. Applying the analytical systems of the day confirmed the presence of distinct forms of Hepatitis that differed from hepatitis A virus (HAV) and hepatitis B virus (HBV) and was therefore termed non-A, non-B hepatitis (NANB). Other hepatotropic viruses, mainly the cytomegalovirus, and the Epstein-Barr virus, were excluded as the agents responsible for NANB hepatitis (Alter *et al.*, 1975; Feinman *et al.*, 1980; Feinstone *et al.*, 2001).

Importantly, (Prince *et al.*, 1974) demonstrated that 71% of post transfusion hepatitis (PTH) cases were exposed to the NANB infectious agent and suggested the term hepatitis C. Screening blood donations for Hepatitis B surface antigen (HBsAg) resulted in a significant reduction of post-transfusion HBV cases. However, 90% of donor samples were infected with hepatitis agents that were not serologically linked to exposure to HAV or HBV (Alter *et al.*, 1975). Moreover, 22 cases of patient hepatitis were recorded after transfusion with HBV-negative blood; suggesting that a significant proportion of PTH cases were infected with undefined hepatitis agents (Feinstone *et al.*, 1973; Feinstone *et al.*, 2001). Additional cases of hepatitis were also observed in recreational intravenous drug users and were reported to be caused by unrecognized etiologic agents that were neither HAV nor HBV (Mosley *et al.*, 1977). Between 1968 and 1970, follow up of 29 patients in haemodialysis units who were infected with NANB hepatitis identified 8 cases of chronic liver

disease, 37.5% of whom reported with severe hepatitis and cirrhosis (Galbraith *et al.*, 1975).

Additionally, frozen sera, collected in early 1950s, from volunteers who had received serum from asymptomatic blood donors showed signs of a transmissible NANB agent (negative for HBV, HAV, cytomegalovirus, and Epstein-Barr virus) and the existence of a chronic carrier state in blood donors (Hoofnagle *et al.*, 1977). Moreover, liver biopsy samples from chimpanzees undergoing experimental inoculation with NANB infected human serum showed presence of a NANB hepatitis agent. Furthermore inoculation of chimpanzees with serum from a NANB-infected chimpanzee transmitted hepatitis to the recipient animal exemplifying continuous passage of NANB hepatitis transmission (Hollinger *et al.*, 1978; Tabor *et al.*, 1978).

In the 1980s, two distinctive findings were achieved: First, the NANB agent was found to be sensitive to chloroform. Chimpanzees inoculated with NANB-serum pre-treated with chloroform failed to become infected and did not show evidence of hepatitis suggesting that the NANB agent contains lipid and that chloroform strips this lipid content. This suggested that the NANB agent belongs to enveloped viruses, which have a lipid envelope as part of their structural features (Bradley *et al.*, 1983; Feinstone *et al.*, 1983). The second finding was extraction of NANB agent from chimpanzee plasma through microfiltration techniques and electron microscopy determination of severe changes in hepatocytes from liver biopsy make an expectation that this agent is 30 to 60nm envelope RNA virus which was not related to retroviruses (Bradley *et al.*, 1985; He *et al.*, 1987). However despite all this evidence, it is worth noting that the low titre of NANB recovered from chimpanzee serum, the absence of effective cell culture models for NANB antigen propagation and the paucity of conventional immunology and virology methods for the agent limited progress and characterization of this etiological agent.

1.1.2 Discovery of Hepatitis C virus genome sequence

In 1989, Choo and colleagues applied molecular approaches to identify the genetic characteristics of the post transfusion NANB agent recovered from chimpanzee plasma samples. Plasma was exposed to extensive centrifugation to pellet virus and nucleic acid fragments. cDNA constructs were obtained using nonspecific primers with DNA polymerase or reverse transcriptase. The resultant cDNA libraries were inserted into the bacteriophage λgt11 vector for expression in *Escherichia coli* (*E.coli*). From a total of $10x^6$ individual clones, cross reactivity analysis between expressed viral proteins and NANB antisera from chronic NANB hepatitis patients identified two positive clones named clone 5-1-1 and an overlapping clone 81. The isolated clonal DNA did not hybridise to host genomic DNA. By contrast, the isolated probes hybridized to RNA recovered from NANB infected chimpanzees and failed to hybridise with RNA from uninfected chimpanzees confirming specific isolation of NANB sub-genomic sequences. Hybridisation signals were detected upon treating samples with deoxyribonuclease, but not with ribonuclease, providing evidence that NANB genome is comprised of RNA. Further analysis of the NANB viral RNA revealed a genome size of approximately 9700 nucleotides. The genome is a positive sense and single stranded (SS) RNA and the discovered virus was termed Hepatitis C virus (Choo *et al.*, 1989).

Analysis of the HCV RNA genome revealed a single long open reading frame (ORF). Overall the homology of HCV RNA and the encoded proteins were unique providing evidence of a new virus. Taxonomic classification of viruses relies on factors such as replication mechanisms, virus structure and the functional properties of encoded proteins; based on the genomic features HCV shows similarities to the flaviviruses and pestiviruses which are all members of the flaviviridae family (Choo *et al.*, 1991). HCV is now classified as a member of the *Hepacivirus* genus in the *Flaviviridae* family according to International Committee on Taxonomy of Viruses (ICTV) as it is mainly a hepatotropic virus unlike the largely non-hepatotropic infections cause by flaviviruses and pestivirses (Lindenbach & Rice, 2013).

1.1.3 Clinical picture of HCV infection

HCV is primarily a hepatotropic infection and is the leading cause of liver transplantation in the resource-rich world (Bowen & Walker, 2005; Chen & Morgan, 2006). Two clinically relevant stages has been identified following infection with HCV: The acute hepatitis stage which may produce only brief symptoms within 3 to 12 weeks after capturing the infection and approximately 15-25% of cases spontaneously clear the infection. Whereas, about 75-85% of acute hepatitis cases fail to clear virus and progress to the chronic hepatitis stage (Alter & Seeff, 2000; Flint *et al.*, 1999a; Maheshwari *et al.*, 2008). Most identified HCV persistent cases are asymptomatic and untreated or failing to respond to therapy develop hepatic fibrosis, steatosis, progress to cirrhosis in up to 35% of cases after about 25 years and possibly developing Hepatocellular carcinoma (HCC) in about 17% of western cirrhotic *c*ases based on 5 years cumulative incidence (Fattovich *et al.*, 2004; Hofmann *et al.*, 2012; Poynard *et al.*, 1997). The chronicity rate is different in range between infected individuals (mild, moderate and severe) and the differential outcome of infection is linked, at least in part, to viral genotype and quasispecies evolution. Moreover, host factors are also implicated including race, age, gender, individual life style and immune status (Howell *et al.*, 2000; Kenny-Walsh & Irish Hepatol Res, 1999; Thomas *et al.*, 2000; Vogt *et al.*, 1999).

1.1.3.1 Acute self limiting stage

20% of all causes of acute hepatitis is due HCV infection (Gerlach *et al.*, 2003). Most acute HCV cases are asymptomatic and only about one third develop clinical symptoms including Jaundice, fatigue, nausea, weakness and elevated blood alanine aminotransferase (ALT) levels. Symptoms may last up to 3 months following exposure and mostly spontaneous recovery is achieved (Alter & Seeff, 2000; Chen & Morgan, 2006). Acute course is characterised by detection of virus RNA in serum at 7-14 days post-exposure to infection (Thimme *et al.*, 2001). High viremia is identified in the first few weeks followed by fast decline in viremia reaching level of 10^5-10^7 IU/mL (Alter *et al.*, 1995).

ALT typically rises above the upper normal value by 4 weeks of exposure and may reach 8-10 fold higher than the upper normal limit (Hoofnagle, 2002). Immunological assays detect anti-HCV antibody in 60% of patients at onset of symptoms. Surprisingly, upon long-term following up, some self-limiting HCV cases show no presence of anti-HCV in serum which has not yet been fully understood; indicating, no correlation between presence of anti HCV and infection persistence (Farci *et al.*, 1991; Hoofnagle, 2002). Analysis of RNA provide early detection of cases during the acute phase of viral infection making RNA analysis more reliable than anti-HCV to identify acute stage cases (Chen & Morgan, 2006; Chung, 2005).

1.1.3.2 Chronic infection stage

This stage is defined as continuous detection of RNA genome beyond 6-months of infection. Most cases are asymptomatic, the first stage of chronic infection lasts for about 12 weeks after the infection and its features are similar to the acute stage (Hoofnagle, 2002). The second stage features are persistent viremia and marked ALT fluctuations along the duration of disease and in some cases show no correlation with progress to liver disease complications (Thomas *et al.*, 2000).

The mechanism by which HCV causes lipid accumulation in liver (steatosis) has not been elucidated. Yamaguchi *et al.*, (2005) reported that transfecting mouse hepatocytes with a construct expressing the HCV core resulted in down-regulation of some genes involved in lipid metabolism and elevated triglyceride (TAG) accumulation.

The direct involvement of HCV in the pathogenesis of liver cancer is still under investigation. Interestingly (Moriya *et al.*, 1998) two transgenic mouse lines expressing HCV core showed accumulation of lipid droplets in the cytoplasm of hepatocytes within 16 months of birth. Of these lines those exhibiting high core expression progressed rapidly to hepatic tumours. The tumours in transgenic mice showed similarities with HCV-induced hepato-carcinogenesis. Other viral proteins than core including E2, NS3, NS5A and NS5B (**Fig. 1.3-1)**

have been associated variously with activation or inactivation of cellular signalling pathways which were similar to pathways that resulte in rapid progression to HCC (Goossens & Hoshida, 2015; Tan *et al.*, 1999; Zhao *et al.*, 2005). Clearly, interaction of HCV proteins with hepatocytes is a complex and multi-layered process and the contribution of individual proteins to hepatocellular carcinoma are yet to be resolved.

1.1.4 Seroprevalence distribution and mode of transmission

An estimated 185 million people are infected with HCV worldwide with prevalence rate of 2.8% for period from 2001 to 2015 (Hanafiah *et al.*, 2013; Messina *et al.*, 2015). However, comprehensive seroprevleance analysis is confounded by the asymptomatic pattern of acute infection, inadequate community-infection tracking systems, socio-economic status, the type of population based studies (focusing on highly selective groups), and the inability of available assays to discriminate between acute, chronic, and spontaneous clearance (Alter, 2007; Hagan *et al.*, 2002; Lavanchy, 1999). Hanafiah *et al.*, (2013) in a meta-analysis of 232 published studies and based on detection of anti-HCV markers estimated a prevalence rate of < 1.5% (low) in north America and tropical part of southern America, 1.5-3.5% (moderate) in sub-saharine Africa, south and south east Asia, Europe (east, central and west regions), middle and south America, and high infection rates > 3.55% in north Africa, middle east, and central and eastern Asia (**Fig. 1.1-1**). The highest prevalence rates registered for a single country were reported for Egypt (14.3 %) and this extensive transmission is likely due to mass campaign of anti-schistosomal treatment that was suspended in 1980s and included reuse of contaminated needles (Frank *et al.*, 2000; Miller & Abu-Raddad, 2010).

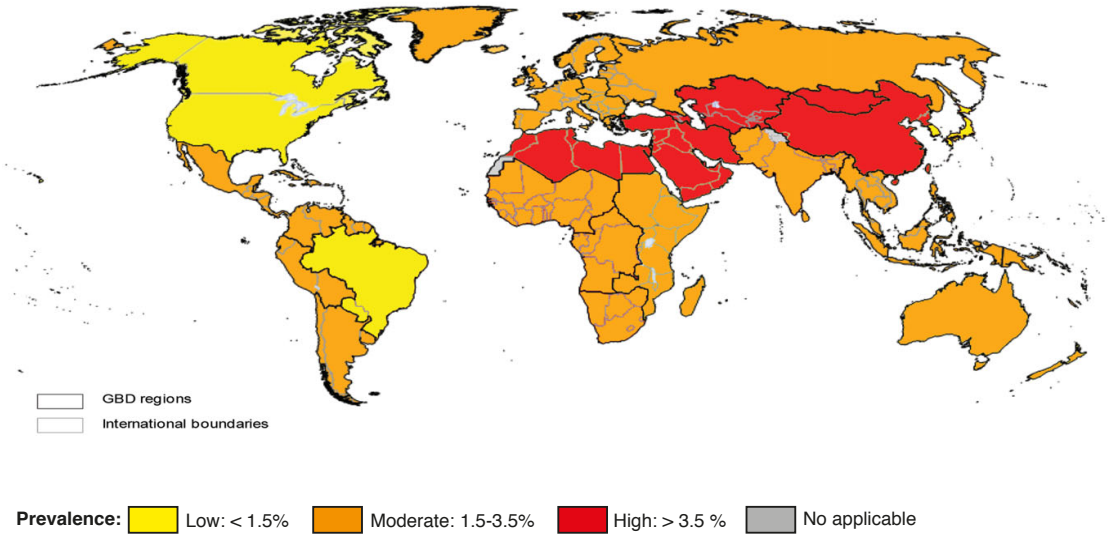

Figure 1.1-1 Seroprevalence of HCV infection according to anti-HCV parameter.
Data were collected from 232 published studies at period from 1997-2007 and from USA National Health and Nutrition Examination Survey at period up to 2010. The estimation of prevalence were calculated by meta-analysis, standardized according to international age weight parameter (1990-2005) and mapped into 21 GBD (Global Burden of Disease studies) region. Adapted with permission from Hepatology journal © Hanafiah *et al.*, (2013).

Seven genotypes of HCV (1-7) have been identified according to their RNA nucleotide sequence and phylogenic features (Simmonds *et al.*, 1994) (**Fig. 1.1-2**). Genotypes differ in nucleotide sequence by 30-35% and within specific genotypes subtype strains differ genomically by less than 15% (Smith *et al.*, 2014). HCV genotypes differ in global distribution, progress to liver disease, immune evasion and response to treatment (Zein, 2000). In terms of geographical distribution of HCV genotypes (**Fig. 1.1-3**), some sub-types are considered epidemic strains (GT1a, 1b, 2a, 3a) due to rapid distribution in economically developed countries. One hypothesis suggests that the distribution of subtype 1a and b is due to contamination of blood products before implementation of HCV screening in the 1990s. Sharing drug needles and migration from Pakistan and India has been suggested as a route for dissemination of subtype 3a. As subtype 2a is common in West Africa and parts of South America, the slave trade may have played a role into circulating

this subtype around the world (Alter *et al.*, 1989; Magiorkinis *et al.*, 2009; Thomson, 2009). Other subtypes are considered regionally endemic as there is no significant circulation to other regions. Such regionally restricted subtypes include subtype 1 and 2 in west Africa, subtype 3 in south Asia, subtype 4 in central Africa and middle east, subtype 5 in southern region of Africa and subtype 6 in south east Asia and the single GT 7 isolate from central African immigrants in Canada (Messina *et al.*, 2015; Pybus *et al.*, 2009). Recent literature studies pooled data from 1217 published papers to study genotype prevalence by region. Genotype 1 is the most widely distributed type (46.2%). Genotype 3 (30.1%) is the second common circulating infection. GT 2, 4 and 6 contribute 9.1% of HCV infection rate whereas GT5 is the lowest distributed around the world accounting for less than 1% (Messina *et al.*, 2015).

The route of HCV transmission in developed countries is mainly through exposure to infected blood through blood transfusion, contaminated renal dialysis machines, and organ transplantation. Sharing intravenous drug needles between addicts is a major source of infection in advanced countries. Other routes of transmission such as unprotected sexual activity, perinatal passage from infected mothers and occupational needle stick injuries are less efficient vehicles for transmission as they tend to be small-dose exposures (1998; Puro *et al.*, 1995; Roberts & Yeung, 2002; Terrault, 2002; Thomson, 2009).

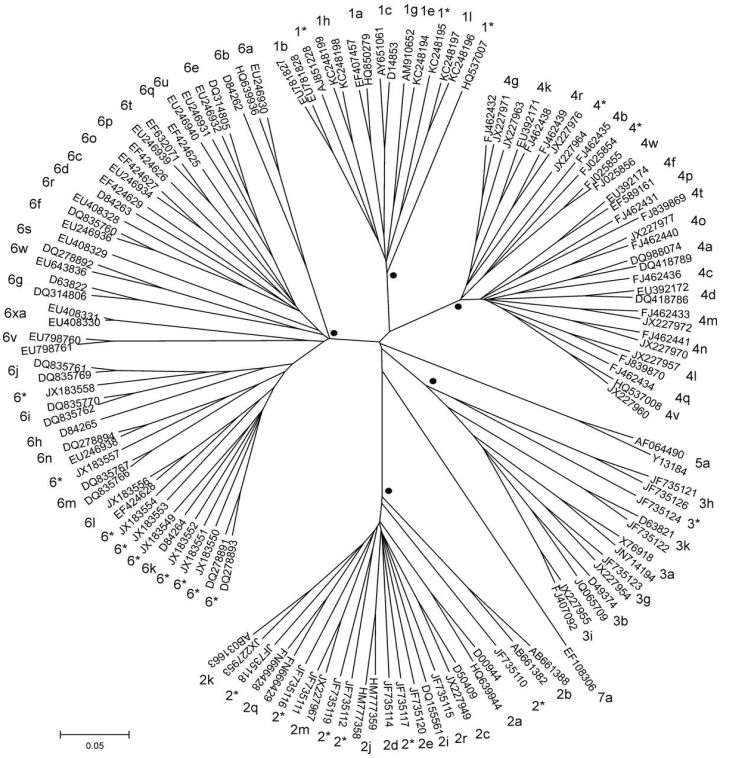

Figure 1.1-2 Phylogenetic tree of HCV.

129 whole genome sequences (reference code) are divided into 1-7 genotypes. Labelled tips represent 67 confirmed subtypes (accession number and letter) and 20 unassigned subtypes (accession number and star). Lowest shared branch for genotypes 1,2,3,4 and 6 is labelled by black dot. Adapted with permission from Hepatology journal © Smith *et al.*, (2014).

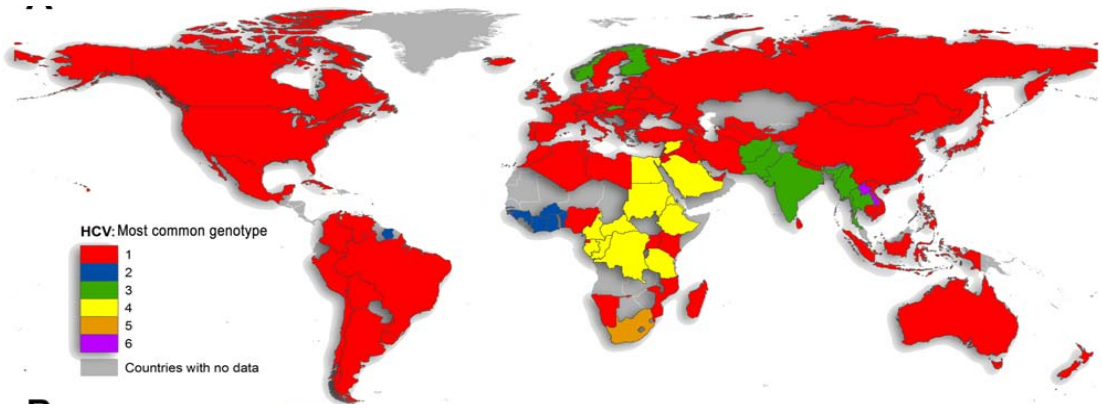

Figure 1.1-3 Distribution of major HCV genotype (GT1 to GT6) per GBD country.
Data were collected from 1217 studies and covered 117 countries (90% of global populated area). Adapted with permission from Hepatology journal © Messina *et al.*, (2015).

1.1.5 Diagnosis and screening of HCV

Most acute HCV cases are considered asymptomatic and rare diagnosis of such cases are based on routine testing. Symptomatic signs of HCV infection associated mainly with persistent infection are systemic need for doing diagnosis. Serological anti-HCV immunoglobulin G (anti-HCV IgG) and molecular (HCV RNA) assays are the routine laboratory methods to manage HCV infection for diagnostic and therapeutic purposes in respectively. Detection of anti-HCV IgG in patient plasma or serum against various recombinant HCV epitopes (core, NS3, NS4 and NS5) by third generation enzyme-linked immunosorbent assay (ELISA) or immunoblotting assay provides information about immune response but does not discriminate between acute or resolved infection. Rapid test assay which awarded U.S. Food and Drug Administration (FDA) approval is introduced for ≥ 15 years old individuals providing fast result within an hour of sample collection from blood or by fingerstick. Identification of anti HCV IgG is valuable to evaluate the immune response to anti-viral therapy (Kamili *et al.*, 2012). Detection and quantification of viral RNA is mandatory for designing therapeutic strategies in terms of drug dose, duration, and end stage of treatment when patient be able to form sustained virological response (Chevaliez & Pawlotsky, 2007).

Screening of HCV promotes managing of HCV infection. It has positive impact on efficient cure when detected at early stage and reduces the transmission of virus between people. The American Association for the Study of Liver Diseases (AASLD) reported that individuals who received blood products, share needles, are HIV immunocompromised, have sexual activities with a HCV infected partner, are the children of a HCV infected mother or who have been on renal dialysis are considered to be at high risk for HCV infection and they are advised for to be tested (Gupta *et al.*, 2014).

1.1.6 Treatment strategies

The standard “classical” treatment for HCV employs pegylated interferon alpha (IFN-α) and ribavirin as combination therapy, which provides greater success in clearing virus than using monotherapy alone. Approximately, 54–56% of patients experience a sustained viral response (SVR) to therapy; indicating that about half of patients are unable to develop a sustained response and progress to chronic HCV infection (Feld & Hoofnagle, 2005). SVR is defined as clearance of HCV genome during therapy and for 6 months after therapy termination. For patients many inter-related factors such as gender, age, body weight, progression of liver disease, HIV co-infection, renal failure; along with viral genotype, viremia, quasispecies diversity, and acute or chronic infection determine the outcome of treatment (Feld & Hoofnagle, 2005; Ghany *et al.*, 2009). In severe cases of decompensated cirrhosis and HCC, liver transplantation is an option but does not treat the infection (Brown, 2005).

The exact process how INF-alpha or ribavirin suppress HCV replication is not completely understood. INF-alpha is an endogenous antiviral molecule that is secreted in response to HCV infection and induces a strong innate immune reaction and an increase IFN-stimulated genes expression (Tovey *et al.*, 1987; Tsugawa *et al.*, 2014). By contrast, ribavirin is a guanosine analogue pro-drug that is phosphorylated in the hepatocyte cytoplasm and inhibits the viral RNA polymerase resulting in terminated and mutated genomic RNA resulting in reduced HCV infectivity (Dixit *et al.*, 2004).. However, INF-alpha and ribavirin

are costly, have severe side effects, and are ineffective for more than 50% of patients, these drawbacks have encouraged the search for better drugs (Brennan & Shrank, 2014). New drug therapies involving sofosbuvir (inhibitor for NS5B replication), ombitasvir (NS5A suppressor) and paritaprevir (NS3/4A serine protease inhibitor) have revolutionised the treatment of hepatitis C (Ahmed & Felmlee, 2015) and in some cases confer SVRs approaching 100%.

A prophylactic subunit vaccine (recombinant protein, envelope, core, peptide and DNA forms) is not yet available, but candidates are in human clinical trials (Halliday *et al.*, 2011).

1.2 Immune response to HCV infection

It is proposed that escape of HCV from the immune response is key to persistent HCV infection. Failure of the immune response to clear virus is thought to be due to HCV modulation of innate and adaptive immune pathways. HCV entry into hepatocytes and initiation of its RNA replication leads to induction of the first host immune response by natural killer (NK) cells, the first line of innate defence, and an increase in their frequency in liver than in peripheral blood through secretion of INF-gamma or by mediating a Th1 immune response. A study reported that clearance of acute HBV from the liver of chimpanzees without cytopathic effect association is due to initial secretion of INF-gamma by NK cells before the onset of hepatocytes destruction occurred by NK mediated $CD8^+$ cytotoxic T cell immune response (Guidotti *et al.*, 1999). In addition, macrophages and dendritic cells (DCs) play roles in innate response through capturing and presenting virus antigen to components of adaptive immune system. Altogether, there is an increase in INF- type-1 and IFN-stimulated gene expression (ISGs) resulting in secretion of INF- α and β, which block or attenuate virus amplification (Banchereau *et al.*, 2000; Su *et al.*, 2002). HCV modulates the innate immune response by interfering with key factors important for the INF signaling mechanism (blocking of STAT1, ISGs and JAC-STAT) resulting in failure to clear virus and thus the establishment of persistent infection (Foy *et al.*, 2003; Foy *et al.*, 2005). B lymphocytes secrete

high amounts of antibody during natural HCV infection, but the inability of antibody to clear infection is incompletely understood. Though antibodies can target any region on HCV proteins; E1 and E2 are the common targets for neutralizing Ab activity in vitro (Bartosch *et al.*, 2003a; Meunier *et al.*, 2008). A study conducted on a persistently infected patient before and after INF-α treatment demonstrated continuous immune pressure on virus that was associated with a shift in sequence of the hypervariable region 1 (HVR1) of E2 that narrowed the neutralisation capacity of the antibodies and helped the virus to evade the humoral immune response (Pawlotsky *et al.*, 1999). Masking of envelope by lipid when circulating in blood before entry into the liver might also be associated with in preventing mapping recognition by humoral immunity which suggest another strategy of escaping from immune response (Law *et al.*, 2013).

1.3 Structural features of envelope glycoprotiens

1.3.1 HCV genome and polyprotein processing

The HCV RNA genome encodes a single large polyprotein of approximately 3000 amino acids. The ORF is flanked by un-translated regions at both its 5' and 3' termini containing 341 and 230 nucleotides respectively (**Fig. 1.3-1**). Translation of HCV RNA is induced by ribosomes binding to the Internal Ribosome Entry Site (IRES) and leads to the synthesis of the polyprotein precursor (~ 3000 a.a). The precursor undergoes independent processing events that release 10 proteins. Cleavage by a cellular peptidase (host endoplasmic reticulum) yields the structural proteins core, E1, E2 and P7 (ion channel) and cleavage by the viral protease releases the non-structural proteins, NS2, NS3, NS4A, NS4B, NS5A, and NS5B (Clarke, 1997; Penin *et al.*, 2004). Association of non-structural proteins with the virus genome lead to formation of a replication complex which is transcribed to form a negative intermediate single stranded RNA (ssRNA), which is copied to yield the positive ssRNA genome. Cleaved mature core (capsid) multimerises with other

capsids (capsid assembly process) at the outer surface of ER (cytoplasmic side). Then, capsids interact with RNA genome, which form a protective layer for HCV RNA in the encapsidation process. Capsid then buds into the inner luminal side of the ER. Envelopes E1 and E2 interact to form a noncovalent heterodimer complex (envelope assembly process) and interact with of capsids. The formed HCV particles undergo maturation and associate with lipoproteins via the secretary process before leaving the cell (Polyak *et al.*, 2006; Rehermann, 2009). The non-structural protein functions are not yet fully understood. The available data indicate that NS2/NS3 degradation occurs by auto NS2/3 processing to release NS2, an important membrane protein required for HCV replication (Welbourn & Pause, 2006). NS3 has a serine protease activity, which cleaves NS3/4A/4B/5A/5B. NS4A is coupled with NS3 as serine protease cofactor. In addition, NS3 has helicase activity which employs ATP catalysis to unwind RNA (Frick, 2006; Lin, 2006). NS4B is reported to regulate virus replication through linking with the ER membrane to form a membranous web that is required for concentrating virus components at ER (Sklan & Glenn, 2006). NS5A is a phosphorylated protein that binds to host membranes and is key element of replicase required for HCV replication (He *et al.*, 2006). In addition, NS5B acts as RNA-dependent RNA polymerase to drive HCV replication (Ranjith-Kumar & Kao, 2006).

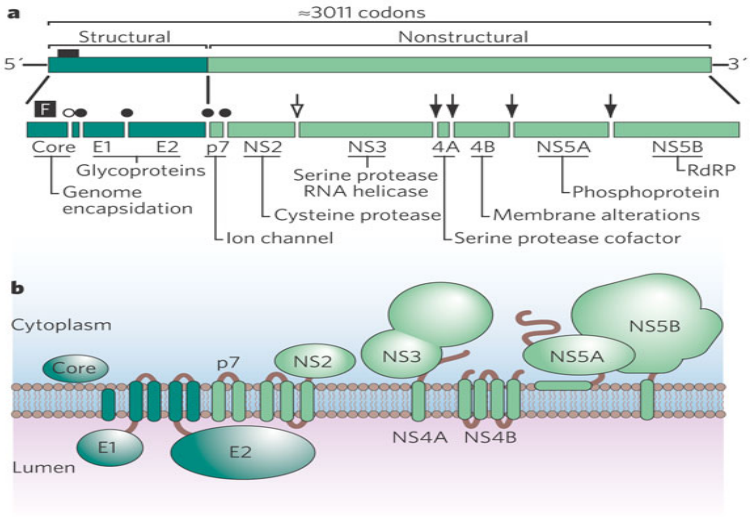

Figure 1.3-1 HCV genome and polyproteins

(A) Illustration of the long open reading frame of the HCV RNA genome, which encodes both structural and nonstructural protein products. Peptidase cleavage site is represented by closed circles (signal peptidase sites) and the open circle (the signal peptide peptidase site). viral protease cleavage site is represented by arrows. (b) HCV polyproteins are shown with the topology of the mature peptides shown relative to the membrane of the endoplasmic reticulum. Adapted with permission from Nature journal © Lindenbach & Rice, (2005).

1.3.2 Glycosylation of envelope E1 and E2

The mature noncovalent glycoproteins E1 and E2 are embedded in the outer fatty bilayer that envelops the virus RNA genome-containing capsid. They have two types of domain: N-terminal domains (ectodomain glycosylated site) and C-terminal domains (anchored site). N-linked glycosylation process involves addition of glycan from lipid (donor) to glycoprotein via asparagine amino acid (N) at the consensus sequence N-X- Threonine (T)/Serine (S) (acceptor) (X indicates any amino acid except proline residue) (Gavel & Vonheijne, 1990; Marshall, 1974). Glycan addition is induced by oligosaccharyl transferase (OST) after arrival of synthesised envelope at ER (Duvet *et al.*, 2002). Alignments of six HCV genotypes revealed that E2 is heavily glycosylated with total of 10-11 sequons and 20 cysteine amino acids in comparison with 5-7 sequons and 8 cysteine amino acids on E1 (Cormier *et*

al., 2004a; Merola *et al.*, 2001; Zhang *et al.*, 2004b). N-linked glycan position patterns of GT1a (H strain) glycoproteins are illustrated in figure (**1.3-2**).

Glycans are involved in the envelope's conformational folding, viral entry and immune responses evasion. This involvement is complicated and has not been fully understood yet (Hebert *et al.*, 1997; van Kooyk & Geijtenbeek, 2003; Wei *et al.*, 2003). Substitution at residue $E1N1_{196}$, $E1N4_{305}$, $E2N8_{556,}$ and $E2N10_{623}$ showed impairment of E1-E2 heterodimer formation (Goffard *et al.*, 2005; Meunier *et al.*, 1999). Mutation at $E1N1_{196,}$ $E1N2_{209,}$ $E1N4_{305,}$ $E2N1_{417}$ and $E2N11_{645}$ leads to reduction of HCVpp infectivity to less than 50% while mutation at $E2N1_{417,}$ $E2N2_{423,}$ $E2N4_{448}$, $E2N7_{540,}$ $E2N8_{556}$ and $E2N10_{623}$ significantly abolishes infection into Huh7. It is worth noting that mutation at $E2N8_{556}$ and $E2N10_{623}$ disrupted binding of HCV E1-E2 pseudoparticles (HCVpp) to soluble CD81 LEL; this indicate that some glycans have an influence on binding to CD81, but that does not mean subsequent effect on entry is always true (Goffard *et al.*, 2005; Owsianka, 2006). Immunizing mice with mutated $E1N4_{305}$ results in generation of antibody associated with enhancing recognition of insect derived viral particles (Fournillier *et al.*, 2001). Incubating single mutated E2 at glycan site $N1_{417}$ or $N6_{532}$ with patient sera increased the sensitivity of antibody for neutralising HCVpp infectivity (Dubuisson *et al.*, 2008; Falkowska *et al.*, 2007). This reflects that glycosylation sites mask important antigenic epitopes on HCV envelope to escape from immune response.

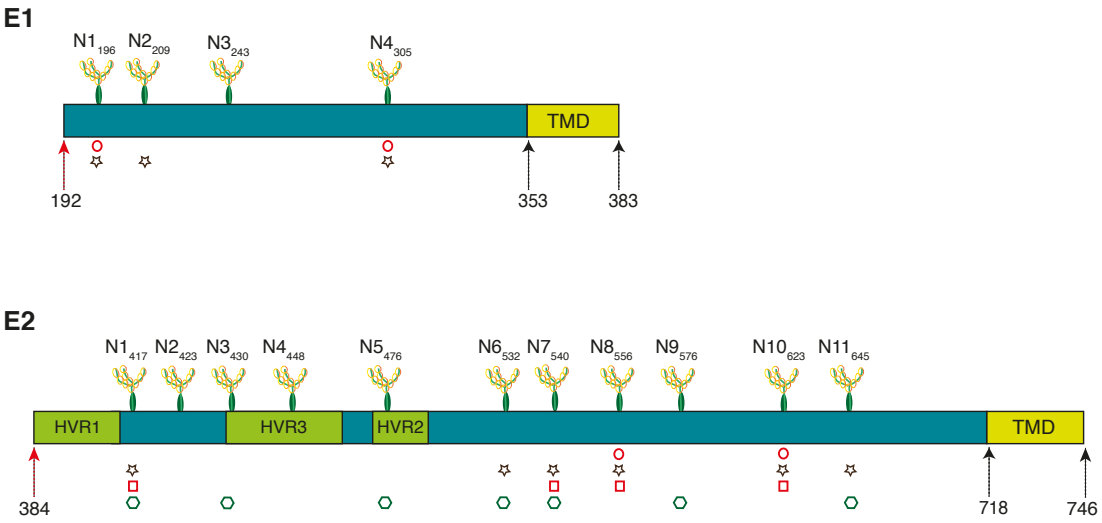

Figure 1.3-2 Schematic representation of GT1a envelope glycosylation sites. Glycosylation terminal is represented by N followed by number related to the relative glycan site in each protein. Red circles indicate glycan position involved in E1-E2 heterodimer complex and brown stars indicates glycosylation positions involved in entry of HCVpp. Sites involved in soluble HCVpp-CD81 LEL interaction is indicated by red square. Position involved in neutralizing of HCVpp entry is indicated by green polygon. Hypervariable region 1 (HVR1) is indicated by green box. The transmembrane domain (TMD) is represented by yellow filled box. Red arrow indicates start site of envelope while black arrow indicates start and end site of envelope TMD. Three hypervariable regions (HVR) within E2 are shown. Amino acids sites correspond to the native M62321 reference sequence (Choo *etal*., 1989; Lavie *et al*., 2007; Troesch *et al*., 2006).

1.3.3 Hypervariable regions of E2

The hypervariable region (HVR1) located at residues 384 to 410 of N-terminal of E2 reveal a highly variable sequence and makes an attractive target for most neutralising patient sera. The selective immune pressure drifts genetic mutation in HVR1 to evade the humoral immune response leading to persistent infection (Hijikata *et al.*, 1991; Korenaga *et al.*, 2001; Mondelli *et al.*, 2001). Deletion of HCVpp HVR1 has no effect on alteration of envelope folding or interaction with soluble CD81 large extracellular loop (CD81 LEL) but reduces virus entry (Forns *et al.*, 2000a). Residues number A_{397}, G_{398}, K_{408}, Q_{409} and N_{410} are binding site for scavenger receptor class B type 1 (SR-B1) (Guan *et al.*, 2012). Further variable regions located at site 474-482 (HVR2)

and site 431-466 (HVR3), have not been extensively studied but were suggested to have a role in binding and entry of HCV (Troesch *et al.*, 2006).

1.3.4 Transmembrane domain (TMD) and E1-E2 confirmation

The envelope transmembrane domain (TMD) of GT1a H77 is located at C-terminal side of E1 at position 353-383 (31 a.a) and E2 at position 718–746 (29 a.a). It acts as a hydrophobic stretch, which strictly anchors the glycoproteins to the membrane of the ER (Duvet *et al.*, 1998a; Lavie *et al.*, 2007). Any deletion or mutation of TMD charged residues is sufficient to decrease or inhibit signaling activity, which in turn impairs assembly of E1-E2 heterodimer proteins (Cocquerel *et al.*, 2000; Hsu *et al.*, 2003; Patel *et al.*, 2001; Selby *et al.*, 1994).

Membrane proximal heptad repeat is located outside TMD of E2 at position 675-699 and plays a role in E1E2 heterodimer formation and entry of HCVpp. Substitution of conserved a.a between 6 HCV genotypes at positions L_{675}, S_{678}, L_{689}, L_{692} disrupt stability of E1-E2 heterodimerisation and totally inhibit entry of HCVpp into Huh7. In addition, mutation at these sites did not alter binding of HCVpp to recombinant CD81 LEL. According to this study, no effect on mutated HCVpp-CD81 LEL interaction was expected because binding sites for CD81 and most neutralising antibodies locate at postion 384-661 of E2 (Drummer & Poumbourios, 2004; Yagnik *et al.*, 2000).

Expression of correctly folded versions of the full length E2 comprised of residues 384 to 715 and fused with TMD in the absence of E1 is still achievable and comparable to E1-E2 complex (Cocquerel *et al.*, 1998; Flint *et al.*, 2000; Michalak *et al.*, 1997; Pileri *et al.*, 1998). Protein expression in mammalian cells can be secreted into media when TMD of E2 is missing completely or at least 31 residues are deleted (Lucas *et al.*, 2003; Michalak *et al.*, 1997) (Selby *et al.*, 1994). Absence of E2 protein containing the TMD leads to E1-E1 complex aggregations, which involves different size of partial glycosylated noncovalent or covalent complex or even both (Cocquerel *et al.*,

2000; Patel *et al.*, 2001); these studies indicate that TMD of E2 acts as essential chepron-like structure which is required for correctly folded E1 expression.

1.4 HCV life cycle

Multi-complex steps for HCV replication into host liver cells are shown in Figure (**1.4-1**). It starts with attachment of virion envelope glycoproteins to several host surface factors and receptors **(1)**. Virion-receptor interaction involves complexing with a variety of other surface receptors and initiates alteration of virion glycoprotiens; this leads to virion internalisation into host cytoplasm via endocytosis process **(2)**. Fusion between virion and endosome membrane results in capsid disassembly and viral positive strand RNA release **(3).** Translation of RNA genome occurs to make polypeptides at ER **(4)**. Conjunction of virion proteins with other cell factors lead to membranous web formation which acts as a scaffold for RNA replication. Virus postive (+) RNA strand is synthesised from intermediate negative (-) RNA strand (**5**). Newly formed capsid encapsulates the RNA genome (Nucleocapsid), assembles with envelopes and buds into ER lumen (**6**). Maturation of virion takes place through the secretory pathway (**7**) and the formed virion is released from host cell (**8**).

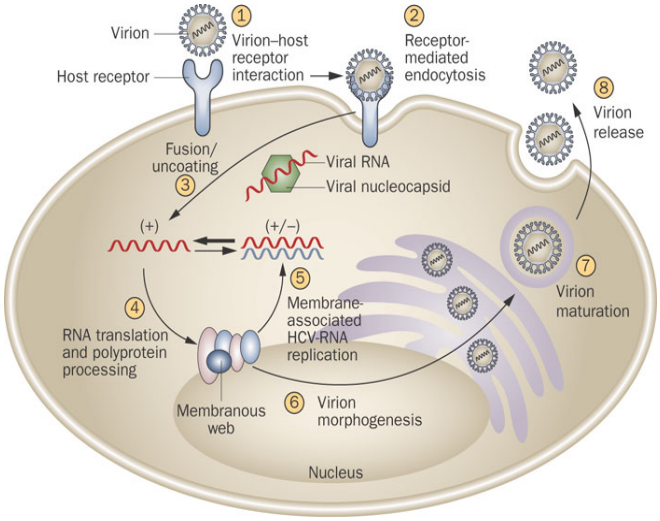

Figure 1.4-1 HCV life cycle.
Adapted with permission from Nature reviews gastroenterology & Hepatology journal © Pereira & Jacobson, (2009).

1.5 Virus binding and entry

Concentration of virus on the cell surface is initiated through interaction with factors including lipoproteins such as low-density lipoprotein (LDL) and very low-density lipoprotein (VLDL), Heparan sulphate proteoglycan (HSPG), C-type lectins such as Liver or dendritic cell specific intercellular adhesion molecule 3-grabbing non-integrin (L/DC-SIGN) (Chang *et al.*, 2007a; Lindenbach & Rice, 2013). Then, multiple undefined events are induced and resulted in virus entry. The envelope glycoproteins interact with four specific entry receptors on host cells: Cluster of differentiation 81 (CD81), scavenger receptor class B type 1 (SR-B1), claudin-1 (CLDN1) and occludin (OCLN). Then, followed by fusion proteins process into host cytosol (Bartosch & Cosset, 2006; Cocquerel *et al.*, 2006; Dubuisson *et al.*, 2008; Lindenbach & Rice, 2013; Sabahi, 2009).

1.5.1 Attachment factors

1.5.1.1 LDL and VLDL

In vivo, recovered HCV virion from chronic infected patient plasma showed association with a large range of low density fractions of the main proteins that exist in LDL and VLDL including apolipoprotein B and E (ApoB and ApoE) (Catanese *et al.*, 2013; Xu *et al.*, 2015). HCV RNA containing particles circulate in patients' blood as lipoviroparticle (LVP) (Andre *et al.*, 2002; Andre *et al.*, 2005; Hino *et al.*, 1997). Presence of ApoB and ApoE fractions in sera from chronic infected patients or recurrent acute infected patients is associated with presence of viral E1, E2 and core. E2-specific antibody results in immunoprecipitation of LVP containing E2 from patient serum or liver derived antigen. This indicates formation of HCV particle into blood and liver (Nielsen *et al.*, 2004; Nielsen *et al.*, 2006; Nielsen *et al.*, 2008; Prince *et al.*, 1996).

In vitro, secreted LVPs from stable HCV cell culture (HCVcc) hepatoma cell lines showed association with virus particles. Down-regulation of ApoE expression leads to reduction in infectious HCVcc secreted in media with no effect on virion replication (Chang *et al.*, 2007a; Cun *et al.*, 2010; Jiang *et al.*, 2012; Shi *et al.*, 2013). In a more recent report, N-terminal domain of ApoE initiates attachment of HCV to Huh7.5 cell surface through HSPGs and incubating cells with Heparinase prevent binding of virus to host cell surface (Jiang *et al.*, 2012). All together these findings demonstrate that the aim of HCV association with lipid is to mediate virus binding to surface receptors and facilitate its release from cells.

1.5.1.2 Lectins DC-SIGN and L-SIGN

Lectin DC-SIGN is 44 kDa protein receptor which is highly expressed on dendritic cells of myloid origin (Gardner *et al.*, 2003). C-type Lectin molecule on DC recognises glycan on ICAM-3 receptor expressed on T cell for adaptive immunological synaptic response. C-type lectin is considered an attachment factor for HIV by interaction with glycoprotein 120 (gp120). C-type lectin was

reported to act as trans receptor through mediating HIV-1 internalisation into dendritic cells to enhance infection of $CD4^+$T lymphocyte, (Geijtenbeek *et al.*, 2000). L-SIGN is an antigen presenting protein and is highly expressed by liver sinousidial endothelial cells (not present on hepatocyte) and lymph nodes (Ludwig *et al.*, 2004).

Gardner *et al.*, (2003) showed that secreted $E2_{665}$ interacts more with Hela cells expressing L-SIGN/DC-SIGN than parental Hela cells and binding is blocked in the presence of mannan (mannose binding lectin) or Antibody targeting lectin binding domain. Further studies showed binding of pesudotyped E1E2 particle to cells expressing L-SIGN and DC-SIGN and binding capacity is enhanced if E2 is heavily mannosylated. L-SIGN and DC-SIGN are absent on Huh7 surface and expression of these factors did not enhance entry of HCVpp (Lozach *et al.*, 2003; Lozach *et al.*, 2004). Overall, Lectin domain on L-SIGN and DC-SIGN are binding sites for mannose N-glycans on HCV envelope E2.

However DC-SIGN and L-SIGN are not recognizable receptors on liver and not considered as sole factor for hepatic tropism; they seem to play a role in chronicity of HCV infection. Interaction of envelopes E1 and E2 with DC-SIGN on immature Dcs has no effect on expression of maturation markers and supports the idea that HCV may not alter cells but use them to escape from immune response. This is consistent with reporting healthy DCs in infected chronic patient (Longman *et al.*, 2004; Ludwig *et al.*, 2004). Liver sinusoidal endothelial cells (LSEC) express L-SIGN on their surface and bind HCV envelopes (Ludwig *et al.*, 2004). LSEC form a blood barrier between liver and vessels (Akbar *et al.*, 2001; Breiner *et al.*, 2001). Although it was proposed that this enhances passing capacity of HCV from blood to hepatocyte; large diameter of HCV (up to 50nm) makes the passive diffusion unlikely to initiate efficient liver attack as LSEC restrict passing of molecules greater than 12nm diameter. It is likely that LSEC capture viruses through lectin forming a reservoir for trafficking infection to adjacent hepatocyte and may alter DCs (antigen presenting cells for immune response mediation), subsequently

reduce efficiency of immune response and lead to form chronic infection (Lozach *et al.*, 2004).

1.5.1.3 HSPG

HSPG are surface expressed macromolecules that belong to glycosaminoglycan (GAG) family and present ubiquitously on most adherent cells (Lin, 2004). Recombinant intracellular $E2_{673}$ and insect-derived HCV-LPs interact with HSPG on hepatoma cells (Barth *et al.*, 2003). Compared to the wild type HCVcc, deletion of HVR1 of HCVcc does not significantly alter binding to Huh7. Moreover, HCV HVR1 has no effect on binding E2 to HSPG cell surface or mediate binding to cell surface through ApoE (Xu *et al.*, 2015).

Indeed, HSPG mediates indirect interaction of virion to cell surface through binding with the N-terminal domain of ApoE (region required for apoliporotein uptake) and does not play a direct role in virus entry according to the following evidences: i) addition of monoclonal antibody-specific for ApoE to Huh7.0 or primary hepatocyte in the presence of HCVcc at 4°C reduces surface binding by 60% and addition of anti-ApoE after binding of HCVcc particles has no effect on infectivity rate ii) treating Huh7.5 cells with heparinase reduces attachment of HCV by 75-85% iii) down-regulation of CD81, SRB1, CLDN-1, OCLN and LDLr does not inhibit binding of HCVcc to cell surface but reduces its entry into Huh7.5 by 80-95% (Jiang *et al.*, 2012; Shi *et al.*, 2013). All evidences agree with the initial attachment which occur by binding of ApoE that anchores with HCV particles to HSPG on cell surface and HCV E2 acts post attachment with entry co-receptors CD81, SR-B1, CLDN-1, OCLN and LDL before entry.

1.5.2 Interaction with entry receptors

1.5.2.1 CD81 receptor

Human CD81 (previously called target of an anti-proliferative antibody, TAPA-1) is non glycosylated, 26 kDa molecule, widely expressed on cell surface and belong to the tetraspanin superfamily. Engagement of CD81 with other surface

molecules induce signal based response that has influences on cell physiology functions such as proliferation, adhesion, activation, movement and morphology. The biological structure of CD81 (**Fig. 1.5-1A**) involves four transmembrane passages, small and large extracellular loops (SEL and LEL), and two intracellular sites (Cocquerel *et al.*, 2003; Levy, 2014; Oren *et al.*, 1990). CD81 was identified for the first time to be a putative binding receptor for HCV through binding of GT1a truncated $E2_{661}$ to soluble LEL of CD81 (Pileri *et al.*, 1998). An E2-CD81 interaction is restricted to cells of human, chimpanzee and tamarine origin and do not bind to CD81 of African green monkey or mouse origin (Allander *et al.*, 2000; Meola *et al.*, 2000). Different genotypes have different binding capacity for CD81 in which E2 of GT1a has best affinity interaction to CD81 (Roccasecca *et al.*, 2003).

Four cysteines are situated in LEL at sites 156,157,175 and 190 and form two disulfide bonds. Mutation of these amino acids inhibit binding of soluble $E2_{715}$ to CD81 LEL which confirms that disulfide bridges are potential binding sites for E2 (Petracca *et al.*, 2000). Alignment of human CD81 with African green monkey CD81 sequence revealed only four amino acid differences located within the human LEL at site T_{163}, F_{186}, E_{188} and D_{196}. Mutation of these residues showed that F_{186} is a critical site for interaction with $E2_{661}$ (Higginbottom *et al.*, 2000). Further study reported that F_{186} situated on subdomain head of LEL and together with the hydrophobic a.a such as I_{181}, I_{182} and L_{185}, form a ridge cluster. This cluster is close to the polar region which is formed by B_{184} and T_{166} and is close to another weak polarity region. This indicates that residues involve in the E2-CD81 LEL interaction is hydrophobic amino acids (Drummer *et al.*, 2006; Owsianka *et al.*, 2006).

In terms of mapping E2 amino acids that are required for interaction with CD81, three monoclonal linear neutralising antibodies that bind soluble $E2_{661}$ (H77 strain) at different sites are able to recognise $E2_{661}$ epitopes at residues 436 to 447 (GWLAGLFYRHKF), 480 to 493 of HVR2 (PDQRPYCWHYPP) and 544 to 551 (PPLGNWFG) and block attachment of $E2_{661}$ to CD81 expressed on cells–(Flint *et al.*, 1999a). Mutagenesis analysis of a conserved motif

(G_{436}WLAGLFY) located on E2 in the region between HVR1 and HVR2 indicates its role in modulating interaction with CD81 LEL. Removing HVR1 does not affect binding of truncated $E2_{661}$ (H77c strain) to native CD81. In addition, different mutations at this motif lead to significant decrease in internalisation of E1-E2 pseudo typed particles into Huh7 cell (Drummer *et al.*, 2006). Further study identified E2 residues (GT1a H77) W_{420}, Y_{527}, W_{529}, G_{530}, and D_{535} to be important for CD81 binding (Falkowska *et al.*, 2007). Recent crystal structural and functional studies mapped E2 amino acids that are required for interaction with CD81 and these E2 residues form part of a discontinuous CD81-binding motif. These studies revealed additional residues on E2 of GT1a H77 strain involving residues, Y_{614}, H_{618} and Y_{619} (Castelli *et al.*, 2014; Deng *et al.*, 2014; Khan *et al.*, 2014; Kong *et al.*, 2013).

The role of CD81 in HCV binding and entry were concluded originally from anti-E2 neutralising data that showed correlation between inhibition of E2-CD81 interaction *in vitro* and neutralising of infectivity in chimpanzee *in vivo* (Cocquerel *et al.*, 2003; Scarselli *et al.*, 2002). In addition, availability of anti-CD81 sera enrich the understanding of CD81 in HCV infection. For example, binding of $E2_{661}$ to CD81 on cells is significantly blocked by MAb (5A6) specific to CD81 (Flint *et al.*, 1999a; Zhang *et al.*, 2004a). Infectivity of HCVpp and HCVcc in selected hepatoma cell lines are inhibited by anti-CD81 in dose dependent manner. Down regulation of CD81 on hepatoma cells showed reduction in internalisation of HCVpp and ectopic expression of CD81 on HepG2 cell associate with promoting entry and infectivity of HCVpp (Zhang *et al.*, 2004a; Zhong *et al.*, 2005).

This gives rise to the question whether CD81 is a primary receptor (essential for binding and entry) or just entry mediation co-receptor. Kinetic study showed that adding HCVpp to pre-incubated Huh7 with anti-CD81 (JS/81) at 4^{o}C leads to 20% increase in entry upon shifting temperature to 37°C comparing with HCVpp entry in cells not treated with anti-CD81. Moreover, addition of anti-CD81 to pre-incubated Huh7 with HCVpp and anti-CD81 or to pre-incubated with HCVpp alone indicates inhibition of HCVpp entry (Cormier *et al.*, 2004b).

Non-hepatic cell lines express high levels of CD81 and are reported to be weak or not permissive for HCVpp infection. This is relevant to conclude HCV is hepatic based infection (Scarselli *et al.*, 2002). Although different style of experiments were done involving different affinity of common anti-CD81 sera (anti-GST MAb, JS/81 and 5A6), available evidences suggest importance of CD81 as post-binding co-receptor, a necessary but not sufficient factor for virus entry and that association with other liver specific molecules is important to mediate HCV entry.

1.5.2.2 SR-B1

SR-B1 is 82 kDa integral surface protein belonging to CD36 superfamily. It is about 509 amino acids that are arranged in horseshoe shape multi-ligands. SR-B1 is composed of transmembrane domains (N and C termini) and joined to the inside of cytoplasm with 2 short N and C termini and outside with one large extracellular domain (Krieger, 2001; Rhainds *et al.*, 2004) (**Fig. 1.5-1B**). SR-B1 was demonstrated initially as a binding receptor for acetylated LDL, oxidized LDL (not native LDL). Then, SR-B1 was identified as a high affinity binding site for high density lipoproteins (HDL) and found to mediate delivery of HDL-cholesterol ester (not its protein part) to cells. SR-B1 is highly expressed in liver and steroidogenic tissues such as adrenal gland and gonads (Acton *et al.*, 1996; Acton *et al.*, 1994; Landschulz *et al.*, 1996a). In addition, SR-B1 was reported to bind beta-VLDL (Van Eck *et al.*, 2008).

Scarselli *et al.*, (2002) identified SR-B1 for the first time as a binding receptor for recombinant HCV (1a H77c and 1b BK isolates) envelope E2 and it was selective based binding in which no interaction with a closely related member of CD36 family, a highly expressed factor in macrophages and endothelial tissues, is identified which support targeting hepatic tissue by HCV. Soluble $E2_{661}$ from both isolates showed no interaction with closely related mouse SR-B1 (80% a.a identity), which makes human SR-B1 a target for infection. Deleting HVR1 does not affect proper folding of modified E2 and keep E2-CD81 LEL interaction but leads to inhibitory effect on binding native SR-B1

which indicates that HVR1 is the specific binding site for SR-B1 interaction (Forns *et al.*, 2000a; Scarselli *et al.*, 2002). Modified RNA genome which includes E2 HVR1 deletion results in attenuated infectively in comparsion with wildtype genome; this gives an evidence that HVR1 enhances binding possibly through interaction with SR-B1 and entry of wild type HCV into cells (Forns *et al.*, 2000b). HCVpp that include deletion of E2 HVR1 tend to be more sensitive to neutralising antibodies more than HCVpp harbouring original E1-E2. Thus, HVR1 of E2 seem to: support evasion of immune response mediated by neutralising antibodies; support entry into cells; and contribute to chronicity of infection (Bartosch *et al.*, 2005; Dreux *et al.*, 2006).

The HCV-SRB1-HDL interaction is reported to attenuate neutralisation of infectivity of circulating HCV *in vivo*, and both HCVpp and HCVcc *in vitro*. LDL associates with physical contact with virions containing HCV glycoproteins and possibly forms a mask to escape from neutralising antibodies. This cannot be stated for HDL in which no interaction between HDL and HCV glycoproteins is reported. Thus, virus is not using SR-B1 as an attachment receptor only but exploits the functional interplay that exist between SR-B1 and HDL to accelerate the rate of virion uptake by cells and this might promote faster escape from immune response. One possible explanation for this event is that HDL binding to SR-B1 facilitates HDL endocytosis and in turn to HCV E2 which already interacts with the same receptor. Second explanation may be that HDL-SR-B1 interplay has an influence on changes occurring at the cell membrane level including dynamic lipid uptake, localisation of surface receptors, membrane motility, cytoskeleton rearrangement and endocytosis. All these changes might make the cell more permissive and may favour more endocytosis of HCV-CD81 compexes which leads to effcient entry of virion and evading immune response. (Bartosch *et al.*, 2005; Dreux *et al.*, 2006; Grove *et al.*, 2007; Voisset *et al.*, 2005).

1.5.2.3 CLDN-1

CLDN-1 is 21 kDa molecule and belongs to claudin superfamily that include 24 members. CLDN-1 is part of tight junction proteins (TJs) that include OCLN and junctional adhesion molecule (JAM) and together modulate TJs strands functions. The liver is the main site for CLDN-1 expression, which is located at cell-cell contact region with other TJs. Other epithelial tissues that are part of pancreas, colon, skin, prostate, choroidal plexus and placenta are also predominant places for CLDN-1 expression. The CLDN-1 molecule consists of four transmembrane-spanning passages, one intracellular loop and two intracellular domains (N and C domains) and two extracellular loops (ECL 1 ≈ 50 a.a and ECL 2 ≈15 a.a) (**Fig. 1.5-1C**). CLDN-1 acts as a gate for paracellular pathway to facilitate transport of molecules such water and salts between adjacent cells. In addition, it establishes a polarity pathway, which allows exchange of molecules between apical and basolateral domains of cell membrane (Furuse *et al.*, 2002; Furuse & Tsukita, 2006; Gumbiner, 1993; Heiskala *et al.*, 2001).

A novel finding reported by Evans *et al.*, (2007a) shows that ectopic CLDN-1expression on 293T cells rescues the entry of HCVpp harboring glycoproteins isolated from genotype 1a, 1b, 2a and 2b in comparison with parental non permissive CLDN-1 deficient-293T cells. Moreover, CLDN-1 expressing 293T cells showed susceptibility for HCVcc infection and measuring NS5A expression showed an Infectivity rate 1000 fold lower than the rate seen in Hu7.5; indicating that CLDN-1 expression confers entry of HCV into 293T but does not support RNA genome replication which determine the liver as a site for entry and replication of HCV. Parental HepG2 cells (non detectable CD81, CLDN-1+ve) remain resistance to HCVpp infectivity. Over expression of CLDN 7 and 3 on 293T cells, high homology for Claudin compared with CLDN-1 by 60% and 49% respectively, did not support HCVpp infectivity (Evans *et al.*, 2007). These findings prove that HCV entry requires human host factors and CLDN-1 beside CD81 and SRB1 are required but not sufficient to internalise HCV glycoproteins.

In terms of identifying sites on CLDN-1 responsible for initiating HCV entry, two residues (I_{32} and E_{48}) located in N-terminal third of ECL 1, two residues (F_{148} and R_{158}) in ECL2 of CLDN-1 are critical residues mediating entry of HCV (Evans *et al.*, 2007; Liu *et al.*, 2009). another group reported 6 high conserved motifs of CLDN-1 ECL1 (W_{30}-G_{49}-L_{50}-W_{51}-C_{54}-C_{64}) to play key role in localisation of CLDN-1 at cell-cell adhesion region which involve site for other related TJs molecules that are required for facilitate uptake of HCV (Cukierman *et al.*, 2009).

However, while there are no decisive data showing clear direct binding of HCV envelope proteins to CLDN-1, it cannot be denied that the envelope proteins may undergo conformational alteration initiated by binding with CD81 and SR-B1 receptors on the target cell. This is necessary to interact with CLDN-1 and might be parallel to events that occur with HIV-1 gp120 early binding with chemokine receptor (CCR-5) before interaction with CD4 (Evans *et al.*, 2007; Wu *et al.*, 1996).

A study published by Krieger *et al.*, (2010) showed that incubating Huh7.0 cells at 37°C for 60 minutes with polyclonal anti-CLDN1 sera which target half of N terminus of ECL1 has no effect on modifying TJs, and then transfecting cells with HCV strain leads to neutralising the infectivity of HCVcc. In the same work, to study association between CD81, SR-B1 and claudin-1 receptors, single antibody targeting each receptor had inhibitory effect on HCVpp infectivity at a range of 40-60%. Combination of the two antibodies target receptors (CD81-CLDN1, CD81-SRB1 and SRB1-CLDN1) improved inhibitory effect at average of 80%. Combination of three antibodies against receptors has more inhibitory effect in which the HCVpp infectivity was reduced by more than 90%. All together these prove association between CLDN-1, CD81 and SRB1.

1.5.2.4 OCLN

OCLN is ≈ 65 kDa membrane component of TJs which include CLDN-1, binds with intracellular connector such as zonula occludens protein 1 (ZO-1) which

links directly actin cytoskeleton, and OCLN interacts directly with F-actin. The structure of the OCLN molecule (**Fig. 1.5-1D**) includes four transmembrane-spanning passages and two extracellular loops (ECL1 ≈ 46 a.a and ECL2 ≈ 48 a.a) and one cytosolic loop, intracellular N and C domains (Hartsock & Nelson, 2008; Paris *et al.*, 2008). Extracellular loops initiate cell-cell interaction and ECL 2 is responsible for aggregation with other TJs such as CLDN-1 and JAM (Heiskala *et al.*, 2001; Nusrat *et al.*, 2005).

Over expression of OCLN on permissive hepatoma derived cells including Huh7.5, Hep3B, which naturally express OCLN, has no effect on infectivity rate of HCVpp. CD81-deficient HepG2 and 293T remain resistant to HCVpp infection when transfected with OCLN. Ectopic CLDN-1 and OCLN co-expression on Hela cell surfaces confer susceptibility of cells for HCVpp infection. Down-regulation of OCLN on Huh7.5 and Huh7 cells showed marked reduction in infectivity of HCVpp and HCVcc. Overall, these evidences prove that OCLN is a fourth important factor for HCV entry (Benedicto *et al.*, 2009; Ploss *et al.*, 2009).

Introduction of chimeric fusion containing ECL1 and ECL2 that are linked with C terminus of OCLN confers susceptibility of HCVpp infection to 293T cells. Replacing CLDN-1 with both ECLs of OCLD and the tail of CLDN-1 keeps 293T cell resistant for HCVpp infection. This indicates existence of CLDN-1/OCLN interaction, which is essential for mediating virion entry. Further data reported that recombinant HCV GT1a $E2_{384-715}$ or $E1E2_{193-746}$ proteins bind to Huh7 and complex with CD81 followed with lateral co-localisation to cell-cell contact region, which cluster with CLDN-1, ZO-1 and OCLD. This data proved that lateral migration of E2-CD81 to cell-cell contact area happen by at least CD81 as down-regulation of CD81 expression result in marked decrease in co-localisation with TJs at head-head cell contact (Brazzoli *et al.*, 2008; Liu *et al.*, 2009b).

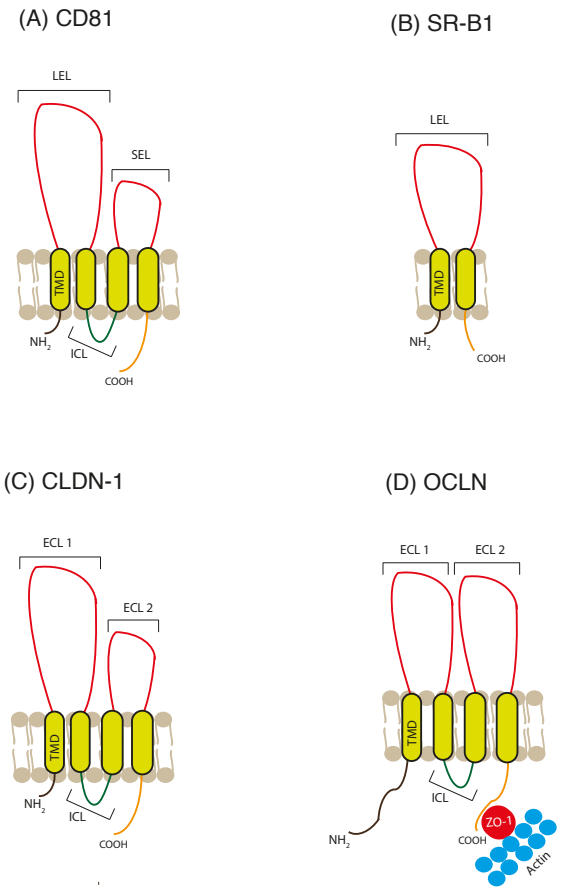

Figure 1.5-1 HCV entry receptors.
LEL: large extracellular loop; SEL: small extracellular loop; ECL 1: extracellular loop 1; ECL 2: extracellular loop 2; ICL: intracellular loop; COOH; c-terminal domain; NH_2: N-terminal domain; ZO-1: zonula occludens protein 1.

1.5.2.5 Other receptors

1.5.2.5.1 NPC1L1

The structure of Niemann-Pick C1-like 1 (NPC1L1) cholesterol absorption receptor is composed of 13 transmemebrane domains, three large extracellular loops (LEL1, 2 and 3), five cytosolic loop, extracellular N domain and intracellular C domain (Yu, 2008). Presence of NPC1L1 is identified on the surface of hepatocyte and intestinal cells. It functions as a gate for cholesterol

absorption and homeostasis (Altmann *et al.*, 2004). Knockdown of NPC1L1 on the surface of Huh7.0 cells resulted in marked decrease of HCVcc entry. Antibody targeting LEL1 of NPC1L1 (not LEL2 or LEL3) leads to reduction of HCVcc infectivity rate into Huh7.0 cell. HCV RNA replication or HCVcc release are not affected by NPC1L1 down-regulation. Treating Huh7.0 with HCVcc was associated with significant decrease in the presence of NPC1L1 which has not yet been understood (Sainz *et al.*, 2012). All indicate that NPC1L1 LEL is post binding entry domain for HCV. Direct or indirect HCV- NPC1L1 interaction to mask HCV glycoproteins or alter its folding features which is required for mediating entry is not defined yet.

1.5.2.5.2 EGFR and EphA2

Epidermal growth factor receptor (EGFR) and Ephrin receptor A2 (EphA2) are Receptor tyrosine kinases (RTKs) abundantly expressed on hepatocytes. Downregulation of EGFR and EpHA2, targeting them by specific antibodies, blocking them by Erlotinib and Dasatinib (an inhibitor for EGFR and EphA2 respectively) result in marked decrease for entry of HCVpp and HCVcc but did not affect the binding to permissive hepatoma cells. Further kinetic analysis, showed similar half maximal time for inhibition of HCVpp entry by anti-CD81 and Erlotinib. Addition of Erlotinib or silencing EGFR on hepatocyte disrupt CD81/CLDN-1 co-factors organisation. All together this demonstrated that EGFR and EphA2 are post binding entry factors and work through enhancing CD81/CLDN-1 association to form complex with their receptors and initiate virus entry (Lupberger et al., 2011).

1.5.2.5.3 TSFR1

Transferrin receptor 1 (TSFR1) is a membrane glycoprotein, which mediates iron uptake through endocytosis and its functional activity is important for iron homeostasis (Ponka & Lok, 1999). Patients with chronic infection develop iron overload and that suggested disruption of iron metabolism by HCV (Milic *et al.*, 2016). Novel work performed by Martin & Uprichard, (2013) showed that incubating Huh7.0 with HCVcc for 8 days resulted in reduction of mRNA copies

of TSFR1 in comparison with mock cells. Moreover, incubating Huh7.0 with anti-TSFR1 resulted in marked reduction in entry of HCVpp harbouring different genotypes envelopes (GT1a, 1b and 2a). These findings indicate that TSRF1 is an additional HCV entry co-receptor with no link of TSFR1 to virion replication. For kinetic study purpose, Huh7.0 cells were treated with anti-CD81 or anti-TSFR1 for 1 hour followed with HCVcc addition at 4°C for binding. Then, anti-CD81 or anti-TSFR1 was added to the corresponding Huh7.0 at 37°C. Measuring level of HCV genome after 30 hours post-infection indicates lss of activity of anti-TSRF1 and anti-CD81 by 4 hours and 2 hours post-infection respectively. This demonstrates the action of TSRF1 to be after binding of the virus to CD81.

1.5.3 Cell endocytosis and endosomal membrane fusion

Following virus binding with attachment factors on cell surfaces (e.g GAGS, ApoE), interaction with entry receptors (CD81, SR-B1, CLDN-1, and OCLN) and mediating conformational changes of the envelope heterodimers, internalisation of the virus into the host cell occurs through clathrin-mediated endocytosis (Blanchard *et al.*, 2006; Coller *et al.*, 2009a; Coller *et al.*, 2009b; Meertens *et al.*, 2006; Tscherne *et al.*, 2006). Such conclusion is based on the following evidences: i) treating cells with chlorpromazine, which prevents clathrin lattice assembly at cell surface allow assembly of clathrin coated pits on endosomes (Wang *et al.*, 1993). This leads to blockage of HCVpp (1a subtype) and the HCV clone (subtype 2a) entry into PLC/PRF/5 hepatoma cells and Huh7 respectively. ii) Down-regulation of clathrin heavy chain (CHC) resulted in partial inhibition of HCVpp (60%) into PLC/PRF/5 hepatoma and Huh7 and 80% inhibition of HCVcc entry into Huh7. Vesicular stomatitis virus (VSV) that relays on clathrin endocytosis showed similar results for partial inhibition of psudo typed VSV-Gpp. The authors suggested that this is likely due to incomplete knock down of CHC to approximately 20% rather than existing of other internalisation pathway for HCV (Blanchard *et al.*, 2006; Sun *et al.*, 2005; Tscherne *et al.*, 2006).

HCV envelope mediates fusion with endosomes in acidic pH environment presumably in a similar style to well-studied members of the Flavi virus genera through inducing conformational modification of the envelope protein. Exact endosome features that are incorporated into HCV fusion process are still undefined. Incubating Huh7.5 cells for three hours with an inhibitor for acidity of endosome such as bafilomycin A1 or concanamycin A (an inhibitor of early endosomal vacuoles H^+ ATPase leading to neutralising acidic pH of endosome) (Huss *et al.*, 2002; Johnson *et al.*, 1993a), and ammonium chloride (NH4Cl, an inhibitor for lysosome fusion with endosome of phagosme) (Hart & Young, 1991) before addition of HCVpp leads to inhibition of virion entry (Blanchard *et al.*, 2006; Meertens *et al.*, 2006; Tscherne *et al.*, 2006).

During virus the life cycle, some envelope glycoproteins are formed as immature and require maturation and activation steps before release from the cell. An example is a flavivirus inactive precursor protein named PreM which is assembled with glycoprotein E to form an immature heterodimer protein on the virion surface at ER and is resistant to cellular low pH environment. Then, following budding from the ER into vesicle for transportation to trans Golgi cleavage by furin protease results in maturation of PreM into M and making it fully functional for acid dependant fusion with endosome, where it await release from cells (MacKenzie & Westaway, 2001; Stadler *et al.*, 1997). In the case of HCV, generated HCVpp is identified to be mature in terms of binding to CD81 and recognition by produced monoclonal antibodies and polyclonal antibodies from patient sera. In addition, some antibodies neutralise the infectivity of native HCV strain. In comparison with pestiviruses, no cleavage by endoprotease during transport of HCV E1-E2 through secretory pathway has been observed. It is stated that exposing HCVpp to acidic pH brings changes in conformation of E1-E2 heterodimer. Some mAbs that recognise native HCVpp show low signal and some lost signal during recognition of HCVpp that was incubated at pH 5.5. Pull down of treated HCVpp at low pH revealed 75% dissociation of E1 from E2 with low molecular size for E1 band (De Beeck *et al.*, 2004; Lavillette *et al.*, 2006). This strongly indicates that HCV

glycoproteins become acidic activated protein during internalisation process of the virus. During fusogenicity process, the HCV lipid layer joins the host endosomal cell membrane causing formation of vesicles and this leads to the release of the HCV genome into the cytoplasm of the host cells for replication purposes (Meertens *et al.*, 2006).

1.5.4 Envelope glycoproteins are class II fusion proteins

Previous data suggest that HCV envelope protein confirmation is similar to class II fusion proteins, similar pattern for flavivirdae, which are composed of a non-cleavage beta sheet structure with folded internal peptide loops (Lindenbach, 2007). In addition, during their biological synthesis, Type II proteins form a complex through association with another partner possesing chaperone activity. Degradation of the associated protein induces fusogenic activity of the fusion protein, followed by conformational changes in the presence of cellular factors such as cellular binding or acidic pH; this results in stable trimer formation. Consequently, the fusion peptide and its insertion site are exposed to the host cell membrane, meaning that both TMD and the fusion peptide are important candidates in initiating the fusion process (Dubuisson *et al.*, 2008).

Best crystallography model of class II fusion protein which has been studied and possibly form homologous template for understanding HCV E2 (not E1) performing fusion with cell endsome is flavivirus tick-borne encephalitis virus (TBEV). Before fusion, Flavivirus envelope E lay on viral membrane and consist mainly of Beta strands and involve three domains (I,II and III) joined together at site of domain II and forming homodimer structure. Domain I and III were joined by a flexible linker. In addition, Domain II contain an internal hydrophobic membrane binding loops joined two beta sheets and named fusion peptide loops (FL) which is masked by domain I and II. In the presence of acidic pH trigger, conformation changes involving disassociation of dimeric to trimeric form occurred, flexable linker folds back domain III at the region of Domain I and subsequently pushing Domain II toward fusion membrane and

exposing FL which fused with endosome membrane. According to cystography structure, TMD act as anchored for envelope E and support stability of folded envelope (Bressanelli *et al.*, 2004; Heinz *et al.*, 2004; Stiasny & Heinz, 2006; White *et al.*, 2008).

It has been shown that the HCV E1 and E2 proteins with an altered TMD, have a negative impact on E1-E2 heterodimerisation, affect the oligomeric properties of the fusion protein, subsequently affect virus entry and fusion process (Ciczora *et al.*, 2007).

Many studies have initially proposed that E2 is the class II fusion protein according to predicated sequence analysis that showed classical fusion peptide features at $E2_{429-452}$ (CNESLNTGWLAGLFYQHKFNSSGC), however this area later has been shown to be CD81 binding sites (Delos *et al.*, 2000; Drummer *et al.*, 2006). In addition, similar to flaviviruses envelope E protein, HCV $E2_{675-699}$ (H77 isolate) contain conserved and alpha helix hydrophobic region named membrane-proximal heptad repeat region which join $TMD_{716-746}$ and has been demonstrated to play a role in E1-E2 heterodimersation and HCVpp entry into Huh7 cell. Mutation to this region has no effect on binding of envelope to CD81 (Drummer & Poumbourios, 2004).

HCV $E1_{330-347}$ region (AALVVAQLLRIPQAIMDM) contain hydrophobic residues and were considered as class II fusion peptide (Drummer *et al.*, 2007). E1 protein has not been reported to play an essential role in virus entry and membrane fusion. Initial studies showed that Mab specific to E1 (H111) neutralised HCVpp and HCVcc infectivity in terms of blocking binding to cell surface (Dreux *et al.*, 2006; Keck *et al.*, 2004). Glycoprotein E1 contains a putative fusion peptide sequence, which can be considered as a companion protein. $E1_{272-304}$ **(C**SALYVGDL**C**GSVFLVGQLFTFSPRRHWTTQD**C),** which contain predicted fusion loops (underline), proline and three cysteine residues (bold) make it a homologous truncated class II fusion protein (Flint *et al.*, 1999a; Garry & Dash, 2003).

A recent study predicted six regions that resemble the hallmark of fusion

peptide; one at E1 and five across E2. Accumulated mutagenesis data from HCVpp/liposome fusion assay and syncytium assay for psudotyped H77 E1E2 showed three conserved mapped regions among HCV genotypes, which are critical for fusion process involving $E1_{270-284}$ (Y_{276} and Y_{282}), $E2_{416-430}$ (G_{418}) and $E2_{600-620}$ (W_{616}). Introducing mutations has no effect on either the stability of E1-E2 heterodimer formation or binding to CHO cells expressing CD81 and SR-B1. In terms of infectivity, a significant reduction in infectivity at a range of 20-100 fold lower than the wild H77 was detected (Dubuisson *et al.*, 2008; Lavillette *et al.*, 2007). In a further study, substitution of F_{285} with A on E1 at motif (VFLVG) proved to inhibit HCVpp entry while keeping stability of E1-E2 heterodimersation. It is worth noting that F_{285} is conserved between most HCV genotypes except GT 2 which contain M (Drummer *et al.*, 2007) and more research is required to analyse the effect of mutagenesis of this residue on heterodimerisation, entry and fusion of virus glycoproteins. Mutations to GWG (W_{469}) and WHY (Y_{489}) motifs at regions $E2_{467-473}$ and $E2_{482-515}$ respectively has no effect on binding, entry or fusion of HCVpp; however these motifs were identified by others as important flavi viurses fusion residues (Yagnik *et al.*, 2000). Overall, this indicates regions containing these residues may play key role in fusion of glycoproteins with endosomal membrane and it is possible that residues taking part in binding and entry may not be essential for the fusion process. In agreement with this view Lavillette *et al.*, 2007, suggests that both envelope proteins contain fusion determinants, which work alongside each other, and play a functional role in establishing the full fusion mechanism. Differences between initial prediction data and updated data for region incorporated into fusion may stress some controversy about absolute identity of HCV, which might have a unique style to fuse with endosome in a way not known yet.

1.5.5 Proposed mechanism of HCV E2 binding and entry

Up to date, identical putative pathway of envelope E2 surface interaction and internalisation into cytoplasm of hepatocyte can be described as follows: LVPs interact with HSPG, LDLR and SR-B1 (**Fig. 1.5-2A**). The E2-SRB1 interaction

results in alteration of E2 (**Fig. 1.5-2B**) and initiates E2-CD81 complex formation, which in turn leads to a signal transduction probably through EGFR, Rho GTPase and Ras (**Fig. 1.5-2C**). CLDN-1, OCLN, TSFR1 (also called TfR1) and NPC1L1 are involved post E2-CD81 interaction in E2 diffusion according to undefined mechanism yet; these events induce accumulation of E2 at point of cell-cell contact. E2-CD81-CLDN-1 complex triggers entry via clathrin-mediated endocytosis pathway (**Fig. 1.5-2D**). In the presence of acidic environment, fusion process occurs between E2 and cell endosome (**Fig. 1.5-2E**). Recently, the cell-death-inducing DFFA-like effector B (CIDEB) was defined to play a role after internalisation of E2 perhaps at fusion step.

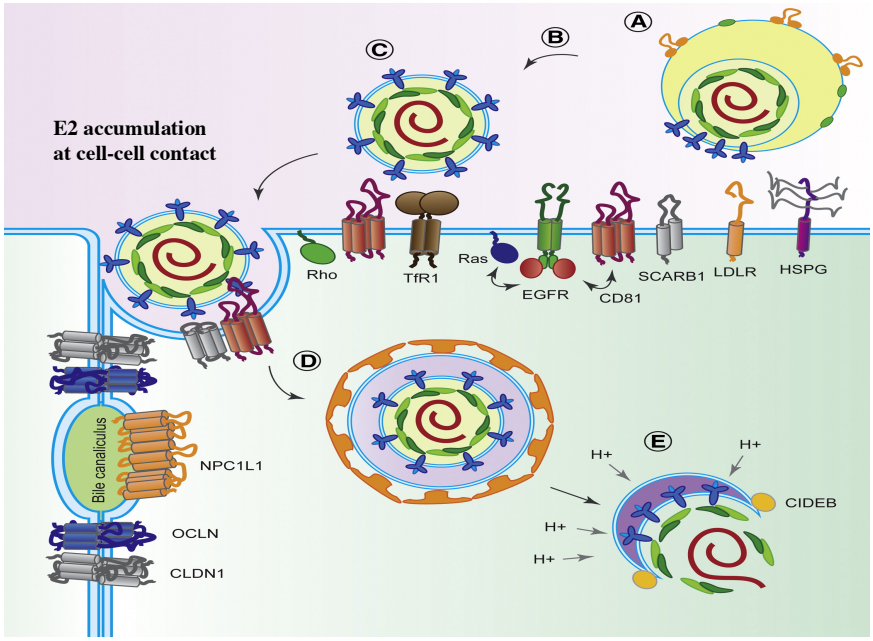

Figure 1.5-2 Model for HCV binding and E2 entry.
SCARBI is SR-B1. Adapted with permission from Cell host & microbe journal © Ding *et al.*, (2014).

1.6 Models to study HCV entry

Since the period of HCV genome identification, there have been many obstacles to understand the mechanism of HCV entry and promote therapeutic

and vaccine development. One of these problems is the lack of a robust cell culture system capable to amplify the HCV. Absence of efficient small animal model is another obstacle preventing *in vivo* exploration of virus binding, entry and rest of its life cycle (Dubuisson *et al.*, 2008; Lindenbach & Rice, 2013; 2008).

Nevertheless, there have been many dramatic achievements to understand each step of virus entry. The first achievement is generating soluble $E2_{384-661}$ derived from GT1a H77 strain. This recombinant form helped to identify the surface receptors on the target cell that interact with envelope but was not enough to investigate the full process of virus entry (Cocquerel *et al.*, 2006; Flint *et al.*, 1999a; Forns *et al.*, 2000a; Pileri *et al.*, 1998). Further achievement is developing baculovirus system containing cDNA of HCV genotype 1b J-strain (Core, E1,E2, p7 and 21 residues of NS2) to produce virus-like particles in insect cells Which helped to understand the folding of E1-E2 heterodimers and their functional properties (Baumert *et al.*, 1998; Cocquerel *et al.*, 2006). These particles were not functionally helpful to study the glycoprotein-receptor interaction, entry and fusion process as the expressed particles were kept in the cytoplasmic compartment.

A model involving replacing retroviruses or lentiviruses glycoproteins, with different viral glycoproteins on their core particles and encapsidation of the genetic reporter gene into the target cell membrane, has been exploited as the first robust productive model of full length HCV E1-E2 pseudo particles (HCVpp) which facilitated understanding of virus life cycle up to the entry step (Bartosch & Cosset, 2009; Negre *et al.*, 2002; Sandrin *et al.*, 2002). The strategy of production of psudotype retroviral particles includes co-transfection of embryo kidney HEK 293T cells with three expression vectors to produce HCVpp on the surface of the murine leukaemia virus (MLV) or human immunodeficiency virus (HIV). The first vector induces glycosaminoglycan (Gag)-Pol protein expression. The Gag protein is well known as a retroviral protein for encapsidation of RNA and for budding the particle at the plasma membrane and Pol is an enzymatic reverse transcriptase. The second

expression vector involves two long terminal repeats (LTRs) for the packaging signal and encodes the luciferase protein reporter that can be measured to evaluate the infectivity of the virus in the target cell. The third vector encoded the native HCV E1-E2 protein with its TMD. All expression vectors involve a human cytomegalovirus (CMV) promoter. The successfully expressed envelope protein is delivered to the plasma membrane, the site in which retrovirus assembly takes place, and released into media. Infecting target Huh7 with HCVpp results in binding of the envelope to receptor complexes which mediate entry (Bartosch & Cosset, 2006).

More recently, a robust cell-culture-derived infectious HCV (HCVcc) was achieved to replicate the full-length virus RNA genome without adaptive mutations. This is based on amplification of HCVcc through transfection of stable human Huh-7 with a virus genome initially cloned from the HCV GT2a RNA of Japanese fulminant hepatitis (JFH-1) (Kato *et al.*, 2001; Wakita *et al.*, 2005). This yielded 10^8 particle per ml of culture media and transfecting naive Huh7.5.1 with JFH-1 particles that were isolated from stable Huh7 yielded a higher infection titre (Cai *et al.*, 2005). HCVcc was identified to be infectious when injected in a chimpanzee, the closest host model for HCV, and in human hepatocytes transplanted into a mouse (Lindenbach & Rice, 2005). Generation of JFH-1 infectious particle is valuable to create deep understanding not only of virus entry but also other steps of the lifecycle involving replication and budding, assembly and release. In contract, this system is associated with limitation in terms of safety and using one particular isolate, which is not effective for studying other virus genotypes (Bartosch *et al.*, 2003b; Lohmann & Bartenschlager, 2014; Yi *et al.*, 2006).

Plasma derived HCV virion was used to study the early steps of HCV life cycle but there was insufficient *in vitro* replication in hepatoma cells. This could possibly be due to an interferon induced mechanism which blocked virual growth and was an obstacle for many years (Dubuisson *et al.*, 2008).

Another attempt to produce effective cell culture system for HCV propagation

was the replicon model. There are two types of replicons: HCV sub-genomic and genomic replicons which are a modified RNA system used to replicate non-structural or both structural and non-structural genes respectively (Lohmann *et al.*, 1999). This system improved the study of RNA replication, intracellular host cell factors and was an effective approach for screening regions on the replicon sensitive to antiviral therapy (Bartenschlager, 2002). In contrast, it was not an efficient model to study virus binding to cell surface factors and entry.

1.7 Hypothesis and aims

Previous studies have demonstrated the ability of permissive hepatoma cells to bind, take up, and allow entry of HCV particles and retroviral particles psudotyped with HCV E1 & E2. With these viral particles viral entry and infection is absolutely dependent on the presence of both envelope proteins E1 and E2. However, using viral particles to explore viral entry makes it difficult to resolve the distinct roles of E2 versus E1 and there is considerable evidence that these factors have unique functions during viral entry. To overcome these confounding effects, I wished to explore the functions of HCV E2 during attachment to cells in the complete absence of all other viral proteins. It was important to determine which domains of E2 are required for binding to cells and whether E2 in the absence of all other viral proteins is capable of directing entry into the cytoplasm of cells. Moreover, most published data have focused on the molecular interaction of E2 with the critical cellular entry receptor CD81, but have not examined the impact of E2 binding on CD81 localisation and function.

Here, we hypothesized that E2 alone is likely to be functionally sufficient not only for binding to the cell surface but also for orchestrating the early events of viral entry. The aims of this project were to express soluble and functional forms of HCV E2 (full length and its derivatives) for use as molecular probes to examine receptor binding by E2 and E2 domain structure and function. Here I generate soluble functional forms of HCV E2 fused to epitope tags such as the Fc-domain of human IgG. These E2 molecular probes were used to:

- Examine and probe the functional receptors on cells.
- To determine why some cells fail to support viral attachment or entry.
- To identify the role of critical cellular factors in the entry pathway.
- To examine the hypothesis that novel cell surface factors involved in HCV entry remain to be identified.

- To examine the hypothesis that E2 plays a highly dynamic role in orchestrating the early events of attachment and entry.

  And

- Finally, in this project I aimed to confirm that our major findings apply equally to primary hepatocytes the critical cell type infected by HCV.

Chapter 2 Material and methods

2.1 Molecular cloning

2.1.1 Reverse transcription

Reverse transcription reactions were prepared with the following constituents: 20 μg mRNA, 1μl oligo $(dT)_{23}$ primer, 1 x 1st strand buffer (Tris-HCl pH 8.5, KCl, MgCl2), 10 mM Dithiothreitol (DTT) reducing agent, 0.5 mM Deoxynucleotide Triphosphate (dNTP) mix, 200 units Superscript™ II reverse transcriptase, dH_20 to a 20 μl final volume in an Eppendorf microcentrifuge tube. The mRNA and oligo $(dT)_{23}$ were preheated at 75°C for 10 minutes in a Dri-block heater (Techne) and rapidly placed on ice before adding any other components. The reactions were then incubated at 47°C for 1 hour in a water bath (Grant Instruments Ltd). mRNA was for full length HCV genotype 1a Wychowski strain (GenBank: AX663428) and strain). Supercript™ II reverse transcriptase, 5 x 1st strand buffer and 0.1 M DTT (Cat. No. 18064-014) were supplied by Life Technologies, Inc. Oligo $(dT)_{23}$ by Sigma-Aldrich (Cat. No. O4387).

2.1.2 Polymerase chain reaction (PCR)

Hot start PCR reactions were performed in a progene FPR0G050 DNA thermal cycler (Techne) according to manufacture's instructions. The reaction was set up with the following constituents: 50ng DNA template; 200μM dNTP mix; 0.30μM forward primer and 0.30μM reverse primer; 1.5mM $MgSO_4$; 1 x reaction buffer for Taq Polymerase 200 mM (Tris-HCl pH 8.4 and 500 mM KCl); 5 units of Taq Polymerase to 50μl with dH_20. KOD Polymerase PCR reactions were set up with the following constituents: 50ng DNA template; 200μM dNTP mix; 1mM $MgSO_2$; 0.3 μM forward and reverse primers; 1 x KOD hot start DNA Polymerase reaction buffer (ready manufacturer); 1 unit of KOD

DNA Polymerase to 50 μl with dH_20. The yield of the PCR product was checked by running 5 μl of the reaction on agarose gel. All primers were supplied by MWG-Biotech or Operon. KOD Hot Start DNA Polymerase product was supplied by Novagen (cat. no. 71086-3).

Table 2.1-1 KOD Polymerase cycling parameters

Number	Cycle	Temperature	Time
1	Hot Start	95°C	2 minutes
40	Denaturation	95°C	20 seconds
	Annealing	60°C	30 seconds
	Extension	70°C	30 seconds
1	Final Extension	70°C	5 minutes

2.1.3 PCR fragments purification

50μl DNA solution was mixed with equal volume dH_2O and then added with 100μl phenol. Sample was mixed vigorously using Vortex-Genie 2 Shaker (Cole-parmer) for 15 seconds then samples were centrifuged at speed of $16x10^3$ gravity for 2 minutes. A soluble DNA partition into the aqueous phase was extracted and equal volume of chloroform: isomyl alcohol 24:1 was added to DNA fraction followed with repeating vortex mixing and centrifugation steps. DNA containing aqueous layer was collected. Phenol (cat. no.16018), chloroform Isomyl alcohol 24:1 (cat. no. C0549) were supplied by Sigma Aldrich.

2.1.4 Ethanol precipitation

DNA was precipitated with 0.1 volume v 3 M sodium acetate and 2.5-3 volumes of ice cold absolute EtOH in a microcentrifuge tube. The DNA was pelleted by centrifuging at 16000 x g for 10 minutes. The supernatant was

recovered and the pellet was washed with 70% EtOH, and centrifuged again for a further 5 minutes. The supernatant was removed and the DNA pellet was dried under heat vacuum in a Savant speedVac concentrator (Thermo scientific). The DNA was then resuspended in either dH_20 or TE buffer and stored at -20°C.

2.1.5 Restriction Endonuclease Digestion

Analytical restriction fragments were performed in a 20μl volume with 5μl mini-prep DNA, 2μl 10 x restriction enzyme buffer (New England Biolabs), 10-20 units of restriction enzyme (New England Biolabs) and dH_20 to a final volume of 20μl in eppendorff tube. For cloning purposes restriction fragments were carried out in a 40 μl total volume using 7-8 μg of DNA. Fragments were incubated in water bath (Grants Instruments) at 37°C for 3-5 hours.

2.1.6 DNA Gel Electrophoresis

Agarose gels (0.8%, 1.2%, 2%) in 100 mL 1x Tris-borate-EDTA (TBE) (**Table 2.1-2**) were heated up in a microwave oven until the agarose is completely dissolved. After allowing to cool down to about 50°C, ethidium bromide (EtBr) was added to a final concentration of 0.25 μg/ml and the solidified gel was placed into a Sub-Cell GT casting unit (BIORAD). An 8/12 wide comb was well placed into the casting tray and the gel was allowed to completly solidify for 30 minutes at RT or 10 minutes at 4C°C. The comb was removed and the gel transferred to a horizontal gel electrophoresis tank (BIORAD), 1X TBE was added to cover completely the gel. DNA digested samples were mixed with one sixth volume of 6X blue gel loading dye and loaded into the wells of gel. 2-Log DNA Ladder (1ug) was diluted into loading buffer (6x) and loaded into the first lane of the gel. Gels were run at 80 to 120 V for 1 hour using a power pack supply (BIORAD). Gels were visualised using a UV transilluminator (Appligene ONCOR) under 302 nm UV light and photographed with the aid of a monitor (Sony), camera (UVP) and printer (Sony). EtBr was supplied by life technology

Inc. (cat. no. 15585011). 2-Log DNA Ladder (cat. no. N3200) and 6X blue Gel Loading Dye, Blue (cat. no. B7021) were provided by New England Biolabs.

2.1.7 Purification and precipitation of DNA digests

Digested DNA was purified using preparatory agarose gels (0.8-2% w/v). Wide well combs were used to accommodate the entire 40μl DNA products. Gels were run at 80-120 V for 1 hour in horizontal gel electrophoresis tank (BIORAD). The EtBr stained gel was visualised under 260 ultraviolet light with a UV transilluminator box (Appligene ONCOR) in a dark room. The desired sized DNA bands were excised from the gel, cut into pieces and placed into microcentrifuge tubes. Enough TE buffer (**Table 2.1-2**) was added to submerge the gel pieces and the gel pieces containing the DNA were incubated at 37°C overnight. Following incubation, the excised band gel pieces were snap frozen in liquid nitrogen and the frozen gel pellets were placed in Costar Spin-X centrifuge tube filters. The gel pieces were thawed out at 37°C and centrifuged at 16000 x g for 10 minutes at RT. Recovered supernatant was recovered and the DNA was then precipitated using cold EtOH (section 2.1.4) and resuspended in 30μl of dH_20. To estimate the concentration of DNA required for ligation reaction, 5μl DNA 5μl was then added to 6x loading buffer and electrophoresed on a 0.8% agarose gel. Costar Spin-X centrifuge tubes were supplied by Sigma (cat. no. CLS8162).

2.1.8 Ligation reaction

Ligation reactions were carried out using a 3:1 ratio of plasmid: insert in a 20μl volume consisting of 10μl of 2 x T4 DNA ligase reaction buffer (Tris-HCl pH 7.6, $MgCl_2$, ATP, DTT); 150 units of T4 DNA ligase and dH_20 to a final volume of 20μl in a eppendorff tube. Ligation reactions were incubated at RT for 30 to 60 minutes. Ligation reagents were supplied by New England Biolabs (cat. no. M0318).

2.1.9 Transformation of DNA into *E.coli* cells

Frozen NEB 5-alpha Competent *E. coli* cells competent cells at -80°C were thawed on ice for 10 minutes. To a pre-chilled falcon tube, 4μl ligation reaction, 8μl dH_20 and 50μl competent cells were flicked 4-5 times and incubated on ice for 30 minutes. Cells were heat shocked at 42°C for 55 seconds and then placed on ice for 2 minutes. 200μl of super optimal broth with catabolite repression (SOC) out growth media was added and the cells were incubated at 37°C with shaking vigorously at 250 rpm in a shaker incubator (New Brunswick Scientific Co.,) for 1 hour. LB plates were pre-warmed to 37°C. Following incubation, 200μl of the culture was spread on pre-warmed LB agar plates containing the appropriate antibiotic. Plates were incubated at 37°C in an incubator (Gallenhamp) for 17 hours. DH5α competent cells (cat. no. C2987H), SOC media (cat. no. B9020) were provided by New England Biolabs.

2.1.10 Competent cells

E.coli cells DH5α were grown by picking a single bacterial colony from an agar plate and transferring into 50 ml lysogeny broth (LB) media (**Table 2.1-2**) in a 250 ml conical flask. This was incubated overnight at 37°C with vigorous shaking at 250 rpm in an incubator shaker (New Brunswick Scientific Co., Inc). Following incubation 10 mls of culture was inoculated into 200 ml fresh LB media in a 1 L conical flask and incubated with moderate shaking until the optical density 650 (OD_{650}) reached approximately 0.3 compared to a sterile LB blank. The cultures vessel were divided equally into four 50 ml falcon tubes and incubated on ice for 15 minutes. Cells were pelleted by centrifugation in Sorvall RC-5B Superspeed Centrifuge using GSA rotor (Sorvall) at 2500 x g for 7 minutes at 4°C. The supernatants were removed and the pellets were resuspended on ice by gentle pipetting in 16 mls of transformation buffer 1 per 50 ml original culture (**Table 2.1-2**). Cells were incubated on ice for 15 minutes and harvested as above; the cells were then resuspended in 4 ml of transformation solution 2 (**Table 2.1-2**). Resuspended cells were dispensed in

200μl aliquots into pre-chilled sterile microcentrifuge tubes and immediately flash frozen in liquid nitrogen. Cells were stored at -80°C until used.

2.1.11 Mini-prep for Plasmid isolation

Transformed bacterial cultures were grown by inoculating a single colony into 4 ml of LB media (**Table 2.1-2**) containing 100 μg/ml Ampicillin (cat. no. A0166 by Sigma). Cultures were incubated overnight at 37°C with vigorous shaking at 250 rpm in a shaking incubator (New Brunswick Scientific Company). 1.5 ml of culture was transferred to a microcentrifuge tube and pelleted at 4°C by centrifugation at 6000 x g for 2 minutes in a eppendorf microcentrifuge (Cole-Parmer). The supernatant was aspirated and the pellet was resuspended in 200μl of ice-cold Alkaline lysis solution I (**Table 2.1-2**) with gentle inverted mixing. Next 200μl of ice-cold solution II (**Table 2.1-2**) was added and the tubes were inverted a few times to mix the solution. Following this ice-cold 200μl of solution III (**Table 2.1-2**) was added; the contents of the tubes were mixed then centrifuged at 16000 x g for 10 minutes at 4°C. The supernatants were collected into a fresh microcentrifuge tube to which 600μl of phenol (Sigma-Aldrich) was added. Microcentrifuge tubes were vortexed and then centrifuged at 16000 x g for 10 minutes. The upper layer supernatant containing DNA was removed into a fresh microcentrifuge tube. The DNA was then ethanol precipitated and dissolved into 25μl of TE (pH 8.0) containing 20μg of RNaseA (cat. no. EN0531 by life technology Inc) and stored at -20°C.

2.1.12 Maxi-Prep for Plasmid isolation

Bacterial cultures were grown by picking a single colony and inoculating into 2 mls LB medium containing ampicillin (100 μg/ml). The culture was grown at 37°C for 6-8 hours with vigorous shaking at 250 rpm in a shaker incubator (New Brunswick Scientific Company). This culture was then used to inoculate 400 ml LB containing ampicillin culture medium in a 2 L conical flask. The culture was grown at 37°C overnight with shaking at 250 rpm in a shaker incubator. Following incubation, cells were placed into polypropylene 1 L

bottles (Nalgene) and centrifuged at 2700 x g for 20 minutes at 4°C in the LYNX 6000 superspeed centrifuge using the Fiberlite F10-4x1000 LEX rotor (Sorvall). The supernatants were removed and the pellets were resuspended in 10 ml of ice-cold plasmid-prep solution I (**Table 2.1-2**). Resuspended pellets were transferred to 50 ml polypropylene tubes (Beckman) and incubated on ice for 5 minutes. 10 ml of ice-cold Plasmid-prep solution II (**Table 2.1-2**) was added to the tubes and the contents were gently inverted few seconds to achieve complete mixing and then incubated for 5-7 minutes at RT. 10 ml of Cold Plasmid-prep solution III (**Table 2.1-2**) was then added to the tubes. The tubes were shaken by gentle inversion and then left on ice for a further 5 minutes. Samples were centrifuged at 17500 x g for 20 minutes at 4°C in a RC-5B Plus centrifuge, using an SS-34 rotor (Sorvall). The supernatants were filtered through a miracloth filter (Calbiochem) into a fresh 50 ml falcon tube and 8/10 fraction volume isopropanol was added, mixed well and incubated for 5 minutes at RT. The sample were transferred to 50 ml polypropylene tubes and centrifuged at 175000 x g for 20 minutes at 37°C in a RC5B Plus centrifuge (Sorvall) using an SS-34 rotor. The supernatants were removed and the tube containing pellets were inverted to allow air-dry for approximately 10 minutes. Pellets were resuspended in 4.5 ml of TE buffer and placed into a fresh 15 ml falcon tube containing 4.8 g of cesium chloride ($CsCl_2$) (**Table 2.1-2**) and mixed until fully dissolved in water bath at 37°C. EtBr with final concentration of 0.25 mg/ml was added and the samples were transferred to 6 ml polycarbonate Ultracrimp centrifuge tubes (Sorvall). The samples were ultra-centrifuged at 239000 x g for 15-18 hours at 20°C in an ultra pro80 ultracentrifuge (Sorvall), using a TFT 45.6 fixed angle rotor to allow the caesium chloride gradient to form.

Then plasmid DNA bands were recovered by side piercing the tube with 1 ml syringe and 19 gauge needle. DNA was placed into a 15 ml falcon tube and an equal volume of $CsCl_2$ saturated isopropanol added and allowed for settlement. The upper bright pink layer containing EtBr was pipetted out and the process was repeated until all the EtBr had been discarded. The DNA was transferred to a clean 15 ml corex tube and 3 volumes of dH_20 was added,

1/10 volume of sodium acetate and an equal volume of isopropanol was added. The samples were centrifuged at 17500 x g for 20 minutes at 4^{o}C in an RC5C Plus centrifuge (Sorvall), using an SS-34 rotor. Supernatants were removed and the pellets were dissolved in 400μl of TE. The DNA was then precipitated with EtOH and dissolved in 200μl of TE. The DNA concentration was estimated and the samples were frozen at -20^{o}C until required.

2.1.13 Plasmid DNA Concentration

DNA concentrations of plasmids were measured at absorbance 260nm (A_{260}) using an ultraspec 2000 ultraspectrophotometer (Pharmacia Biotech). Turbidity of samples were determined by measuring absorbance at 320nm (A_{320}) Samples were prepared for analysis by diluting 5μl of DNA in 500μl of dH_20. Samples were transferred to a quartz cuvette and the A_{260} was read against a dH_20 reference. A_{260} readings were converted to DNA concentrations in μg/ml using the following formulae:

Double Stranded DNA:

(A_{260} reading – A_{320} reading) X Dilution Factor X 50 = [DNA] μg/ml; A_{260} = 1 = 50 μg/ml

Single Stranded DNA:

A_{260} X Dilution Factor X 25 = [DNA] μg / ml; A_{260} = 1 = 25 μg /ml

2.1.14 DNA sequencing

Double stranded DNA plasmid at concentration of 150-500 ng/μl was transported on ice to Tayside center for genomic analysis (University of Dundee) to sequence generated Plasmid containing target DNA by capillary electrophoresis technique using 3130XL Genetic Analyser (Applied Biosystems).

Table 2.1-2 Recipe for stock reagents used in molecular cloning

Name	**Preparation**
TE buffer	10 mM Tris-HCl; pH 7.5, 1 mM EDTA; pH 8.0
1x TBE	10.8 g Tris-base, 5.5 g boric acid, 4 ml 0.5M EDTA (pH 8.0); to 1L with dH_2O
Agarose Gel	0.8% / 2% (w/v) agarose, 0.25 μg/ml Ethidium Bromide; 1 x TBE to 100 mls with dH_20
Transformation Buffer 1	0.1 M RbCl, 0.05 M $MnCl_2$, 0.01 M $CaCl_2$, 15% w/v Glycerol; pH 5.8
Transformation Buffer 2	0.2 M MOPS, 0.01 M RbCl, 0.075 M $CaCl_2$, 15% (w/v) Glycerol; pH 6.8
Luria-Bertani (LB) Agar	10 g NaCl; 10 g tyrptone; 5 g Yeast Extract; 20 g Agar to 1 L with dH_2O
LB Medium	10 g NaCl; 10 g Tryptone; 5 g Yeast Extract To 1 L with dH_20; pH 7.0 with 5 M NaOH, Autoclave
Plasmid Prep Solution I	50mM Glucose, 10mM EDTA, 25 mM Tris-HCl; pH 6.0. Sterilise by filtration, store at 4^oC
Plasmid Prep Solution II	200 mM NaOH, 1% (w/v) SDS. Sterilise by filtration, store at RT
Plasmid Prep Solution III	3 M Potassium acetate; pH 4.0. Sterilise by filtration, store at 4^oC
$CsCl_2$ saturated with isopropanol	10-15 g $CsCl_2$; 1X 5-10 ml TE buffer; 20 ml of Isopropanol. Store at RT

2.2 Protein Biochemistry

2.2.1 Generation of stable *Drosophila* cell lines expressing srE2-Fc fusion protein

Drosophila melanogaster Schnieder 2 cells were maintained in Shields and Sang M3 medium (**Table 2.2-1**) supplemented with 10% (v/v) 65°C heat treated fetal bovine serum (FBS) and 10% (v/v) insect medium supplement. Insect S2 cell in 4ml of media at density of 3 x 10^6 in T-25 flask (Nunclon) were incubated overnight at 24°C. Next day, insect cells were transiently transfected by calcium phosphate ($CaPO_4$) precipitation method with the Plasmid pMtE2-Fc plasmid carrying the HCV GT1a E2 coding sequence of strain in a combination with pCOhygro resistant plasmid to produce stable cell line. In brief, Solution 1 contained a mixture of 19 μg of envelope expression vector, 1 μg of pCOhygro, 1 μl 1 M $CaCl_2$ to 375 μl with dH_2O was prepared into microcentrifuge tube and were gently mixed. Mock control lacking the pCOHygro vector was also prepared in 375 μl $CaCl_2$ solution. Solution 2 contained 2X HEPES-Buffer (375 μl) (**Table 2.2-1**) was added as well to second microcentrifuge tube. Solution A was added slowly drop-wise to solution B with continuous gentle mixing and incubated at RT for 40 minutes. The mixture was added dropwise to cells in M3 culture media supplemented containing 10% FBS with continuous swirling and incubated for 24 hours at 24°C using P33 Precision Incubator (LEEC). To remove the calcium phosphate solution, cell culture then was placed into 15 ml Falcon tube and spun for 5 minutes at 1000x g in a TC6 centrifuge with an H400 rotor (Sorvall). Supernatants were removed and cells were dissolved into 5 mls of M3 media supplemented with 10% FBS and centrifuges again. Supernatants were removed and cell pellets were loosened and resuuspended in 5 mls M3 containing 10% FBS and transferred to T-25 flask and incubated 48 hours in at 24°C. Transfected S2 cells or Mock cells were pelleted by centrifugation and cell pellets were dissolved in 5 ml M3 selection media supplemented with 10% FBS, 1% penicillin/streptomycin solution and 0.1% Hygromycin-B to begin

selection at 24°C. Cells were pelleted by centrifugation every 5 days and resuspended in 5 mls M3 selection media. The establishment of the selected cell line was measured against negative control cells (empty vector) which had died off. The established cell line culture was transferred to T75 flasks, scaled up until 12 mls with M3 selection media and seeded at density of 2 x 10^6 cells per ml every 6-7 days. When grown cultures had reached a cell density of 4-6 x10^6 cells/ml (log phase), cells culture were transferred to 15 ml falcon tube and the samples were centrifuged at 700 x rpm for 5 minutes in Labofuge 400 centrifuge (Heraeus) to remove the calcium phosphate solution. Supernatants were aspirated and pellets were resuspended into fresh S2 media and harvested as above. Then cell pellet were resuspended into 5 mls media containing 500 μM Cu_2SO_4 for inducing expression from the metalothionein promoter. Then cell culture were incubated 4-6 days at 24°C. For analysing transient expression, samples were collected on daily basis course. 100 μl of secreted media were placed into eppendorf for centrifugation using Labofuge 400 centrifuge (Heraeus). Supernatants containing the expected expressed protein fusions were collected and passed through filter apparatus and filter sterilised. Samples were stored at 4°C for immediate western blotting analysis.

When transfected cells demonstrated protein expression, expansion of stable transfected cells was conducted. Cell cultures that had reached density of 6x10^6 M/ml in T-25 flask were harvested in 15 ml falcone tube using Labofuge 400 centrifuge (Heraeus) at 700 rpm for 5 minutes. Supernatant was aspirated and the pellet was resuspended into fresh media containing Hygromycin-B (50 μg/ml) and seeded into two T-75 flasks at density of 2x10^6/ml. Cell culture were incubated at 24°C for 4-6 days. Upon reaching desired density of 6x10^6M/ml, 24 ml of transfected S2 cells were transferred to sterilse conical 150 ml flask with 2.25 volume of prepared sterilized large scale M3 medium and incubated at 24°C with shaking at 80 rpm for 4-5 days using New Brunswick Innova 2100 Shaker (eppendorf). The process of cell expantion was continued until reaching 3-7 L of cell culture. Cu_2SO_4 at final concenteration of 500 μM were added immediately to cell culture at density of 4-6x10^6 /ml in

flask and incubated for further 5 days at medium at 24°C with shaking. Cells were harvested gently at 1500 rpm for 10 minutes at 4°C in in the LYNX 6000 superspeed centrifuge using the Fiberlite F10-4x1000 LEX rotor (Sorvall). Supernatants were gently poured through a sterilising filter with a pore size of 0.22 µm using vacuum filtration rapid-Filtermax (TPP). Samples were stored on ice for next day purification.

Table 2.2-1 Recipes used for stable transfected Drosophila production

Reagent	Preparation
2X HEPES solution 2	50 mM HEPES,1.5 mM Na2HPO4, 280 mM NaCl, pH 7.1. Sterilise by filtration
1L large scale Schneiderís insect Medium	24.5 g of insect media (S9895), 0.5g $NaHCO_3$, 10% insect supplement, 3.5% substance X and top up 1L with dH_2O, filter-sterilize store at 4°C

2.2.2 Expression of MBP-CD81 LEL fusion

The pMALc2 vector was obtained from NEW England Biolabs (NEB). pMALc2MBP-CD81 LEL plasmid was transformed into competent BL21 E.coli cells (BL21) and the transformants were spread out on selection LB agar plate supplied with 100 µg/ml ampicillin. Optimised CD81 LEL was cloned into the pMALc2 vector (NEB) in correct reading frame with the maltose binding protein (MBP). pMALc2-MBP-CD81 LEL vector was transformed into competent BL21 (pMALc2) cells (NEB) and the transformants were selected on prewarmed agar plate containing 100 µg/ml ampicillin. Plates were incubated at 37°C in an incubator (Gallenhamp) for 17 hours.

A single colony from the pMALc2-MBP-CD81 LEL was resuspended into 2 ml LB media containing 100 µg/ml ampicillin. The cells were incubated at 37°C with vigorous shaking at 170-250 rpm in an incubator shaker (New Brunswick Scientific Co., Inc) until the OD_{600} reached 0.5-0.75. Then 2 mls freshly grown

cell culture was used to inoculate 200 mls of LB-Amp medium supplemented with glucose at final concentration of 2 g/L in 1L glass conical flask. The cells were incubated with shaking at 37°C until the OD_{600} had reached 0.5-0.75. Once an optimum OD_{600} was reached, 2 mls of the cell culture was removed for an uninduced control and final concentration of 0.4 mM Isopropyl β-D-1-thiogalactopyranoside (IPTG) was added to the remaining of the cell culture. The sample was further incubated for another 2-3 hours on shaker at 37°C for optimum protein expression.

The induced cells were harvested by centrifugation at 5000 x g for 15 minutes at 4°C. The supernatant was poured off the flask and the pellet was resuspended in 1/10 of the bacterial culture volume lysis buffer (**Table 2.2-2**), 1/10 the volume 1% Triton X-100 and 1% (v/v) Protease Inhibitor Cocktail were added. The sample was incubated at 30°C for 15 minutes. The sample was placed in an ice-water bath and sonicated 3-5 times in a Soniprep 150 Ultrasonicator (Sanyo) at 18 Hz frequency for 15 seconds. Sonicate was transferred to a corex tube and cleared by centrifugation at 12000 x g for 10 minutes at 4°C in an RC 5B Plus centrifuge (Sorvall) using an SS34 rotor. Supernatants (containing soluble lysate) were collected and passed through millex syringe filter units with pore size 0.20 micron (Sigma-Aldrich). 10-20 μl aliquot of induced cells and 50 μl of uninduced cells were mixed with 5 μl of 5 X sample buffer and run on a 10% polyacrylamide gel and Coomassie stained for western blotted. The rest of lysate was placed on ice for next day purification stage.

Table 2.2-2 Recipe used for MBP-CD81 LEL expression

Reagent	**Preparation**
Lysis buffer	50 mM Tris HCl pH 7.4, 200mM NaCl, 50 μg/ml lysozyme with Triton.

2.2.3 Transient CD81 expression on HepG2 cells

HepG2 cells in MEM media supplied with 10% (v/v) FBS, 1% (v/v) non-essential amino acids (NEAA) were cultured into 6-well dishes (Nunc) and incubated at 37°C using Hera Cell 240 CO_2 Incubator (thermo scientific). When the cultures had reached confluence of 70-85%, cells were transfected with DNA-lipid complex by using Lipofectamine 3000 transfection reagent (life technology). In brief, 5 µg of pcDNA3.1-CD81 plasmid was diluted into 125 µl of Opti-MEM Medium and mixed well. In other two tubes, Lipofectamine 3000 reagent (3.75ul and 7.5ul) was diluted into 125 µl of Opti-MEM Medium and mixed on vortex for 3 seconds. Diluted DNA was transferred to each diluted Lipofectamine 3000 Reagent at ratio of 1:1 and incubated at RT for 15 minutes. DNA-lipid mix at final volume 250 µl was added to each well and plate was incubated for 2 days at 37°C. Opti-MEM Medium were aspirated and fresh MEM media supplied with 10% (v/v) FBS, 1% (v/v) NEAA and selective G-418 sulfate to a final concentration of 800 µg/ml were added to transfected cells and incubated for further 2-3 days at 37°C. Growth was evaluated against parental HepG2 cell (no vector) which were treated with same media. Transfected cells were then passaged into T-25 flask in MEM media supplied with 10% (v/v) FBS, 1% (v/v) NEAA and selective G418 to a final concentration of 400 µg/ml and incubated for 5 days in 5% CO_2 at 37°C. An aliquot used for flow cytometric and confocal analysis.

2.2.4 SDS-PAGE gel

Hand casting and running of Sodium Dodecyl Sulphate Polyacrylamide Gel Electrophoresis (SDS-PAGE) gels were performed using the Bio-Rad mini-protean II cell gel system. The casting unit was prepared by placing 0.75 mm (or 1.5mm) spacer plate with short plate to form to form cassette sandwiches and and fastening them onto the Bio-Rad gel clamp assembly unit. This was then clamped into the Bio-Rad gel casting stand. Separating gel (**Table 2.2-3**) was poured into the gap between the two glass plates and water was layered until it overflowed onto the gel to achieve a horizontal gel edge. The gel was

allowed to polymerise for 20-30 minutes at RT. The layered water was discarded and stacking gel (**Table 2.2-3**) was poured onto the top of separating gel. A 10 well-forming comb was inserted and the gel was allowed to set for 20 minutes at RT. The comb was removed from the gel and the gel plate assembly was removed from the casting stand and was fitted into the Protean II buffer tank. Running buffer (**Table 2.2-3**) was poured into inner chamber of the tank until it overflowed and to fill 25% of the outer chamber. Up to 20 μl of desired prepared protein sample (section 2.2.5) were loaded into each lane of gel. 10 μl of broad range (7-175 kDa) pre-stained protein marker (New England Biolabs) were also loaded. The gel was run at 100 V through stacking gel and at 150-200 through separating gel for 60-90 minutes using powerPac HV Power Supply (BIORAD). The gel tank assembly unit was removed from the tank and the gel was removed from the plates and Coomassie stained or western blotted.

Table 2.2-3 Recipes for SDS-PAGE

Reagent	**Preparation**
Separating gel	8%/12%/15% (v/v) Acrylamide: Bisacrylamide: 29:1; 373mM TrisHCL (pH 8.8); 0.1% (w/v) SDS; 40 μl of 10% (w/v) Ammonium persulfate (APS); 15 μl of *N*,*N*,*N*′,*N*′-Tetramethylethylenediamine (TEMED) to 10 mls with d_2H0
Stacking Gel	4.5% (v/v) Bisacrylamide: 29:1, 125mM Tris-HCL (pH6.8); 0.1% (w/v) SDS; 30 μl 10% (w/v) APS; 8 μl TEMED to 5 mls dH_20.
1x Running Buffer per 1L	25 mM Tris; 190 mM Glycine, 10 mls of 10% (w/v) SDS; to up to 1L with dH_2O
5 X Sample Buffer	250 mM Tris-HCl (pH6.8); 10% SDS; 50% Glycerol; 15% β-Mercaptoethanol; 0.02% Bromophenol Blue

2.2.5 Preparation of samples for SDS-PAGE

Bicinchninic Acid (BCA) Assay was used to measure produced protein in bacterial cell lysate (section 2.2.2) or secreted by Drosophila *S2* cells (section 2.2.1). The assay was setup in a 96 well microplate using the following components: BCA reagent A was mixed with BCA reagent B at ration of 50:1 and mixed well. 200 μl working reagent (A+B) was added to each well containing 25 μl of test sample or to blank PBS sample (1:8 sample to working reagent ration). Microplate was mixed on shaker for 30-45 seconds and then incubated for 30 minutes at 37°C in an incubator (Gallenhamp). Diluted bovine serum albumin (BSA) standards with concentration of 5-250 μg/ml were prepared and incubated with working reagents as above. The optical density readings were measured at OD_{562} using Gemini XPS Microplate Reader (Molecular device Inc.). All samples readings were subtracted from blank reading and standard curve were plotted to determine the unknown concentration of test samples. The relative concentration of protein in a sample was ascertained using the OD_{562} reading. Protein concentration in a sample was normalised with PBS to volume of 20 μl. Typically, 5 to 20 μl of sample originated from *E.coli* or insect cells was mixed with 5 x sample buffer (**Table 2.2-3**), heated at 99°C in a heating block (Techne) for 3 minutes, placed on ice for 90 seconds and then loaded on to an SDS-PAGE gel.

2.2.6 Western blotting

Protein samples were transferred to a nitrocellulose membrane using the Trans-Blot Cell and Criterion Blotter equipment (BIORAD). The SDS-PAGE gels were placed into the gel holder cassette as follows: open cassette was immersed into transfer buffer (**Table 2.2-4**) with a foam pad and a sheet of 3MM Whatman filter paper (Schleicher and Schuell). Gel was then placed on Whatman filter paper and covered with Protean nitrocellulose membrane (Schleicher and Schuell). Nitrocellulose membrane was layered with Whatman paper and another sheet of sponge. Bubbles were carefully removed after each layer. Transfer cassette was then closed and placed in an electrode

assembly unit, and then transfer buffer was poured into the tank. Ice packs was placed into the tank to keep transfer buffer cold. Standard stir bar was placed to the bottom of tank keep optimum ion distribution and tank was placed on magnetic plate using UC-152 magnetic stirrer plate (Stuart). Protein was western blotted to nitrocellulose membrane at 150-200 v for 1-2 hours.

Nitrocellulose membrane was removed from the tank and placed in 20 mls of blocking buffer (**Table 2.2-4**) overnight at 4^{o}C under gentle agitation on Spiramix 5 Roller Mixer (Denley). Membrane was rinsed briefly twice in 10 mls washing buffer for 10 minutes with shaking on SSM1 orbital shaker (Stuart). Membrane was incubated with 15 mls dilute solution of primary antibody (**Table 2.2-4**) at RT for 1 hour under gentle agitation. Membrane was then rinsed three times with 10 mls of wash buffer for 10 minutes at a time. The membrane was exposed to 15 mls of secondary antibody (**Table 2.2-4**) at RT for 1 hour under gentle agitation. The membrane was rinsed three times with wash buffer. Membrane was incubated with enhanced chemiluminescence solutions (ECL) as following: 3 mls ECL solution I (**Table 2.2-4**) and 3 mls ECL solution II (**Table 2.2-4**) for 1 minute were mixed well and placed on membrane for 3 minutes. For visualization of developing blots, the membrane was finally exposed to Super RX medical X-ray film (Fuji) in dark room for various exposure times and the film processed in Compact X4 Automatic X-Ray Film Processor (Xograph Imaging Systems).

Table 2.2-4 Recipes for WB

Reagent	**Preparation**
Transfer Buffer per 1 L	25 mM Tris; 190 mM Glycine; 20% v/v Methanol; top up to 1L dH_2O
Blocking Buffer per 100 mls	5% w/v Skimmed milk powder; 0.25% v/v Triton X-100 PBS in 100 mls PBS
Wash Buffer	0.1% w/v Marvel; 0.025% v/v Triton X-100 PBS in 500mls PBS

Primary Antibody Solution	Primary antibody diluted in 10% v/v BSA or marvel; 0.02% Sodium Azide PBS
Secondary Antibody Solution	Secondary antibody diluted 10% v/v BSA or marvel in PBS
ECL I	176 mM Coummaric acid; 400 μM Luminol; 0.1 M Tris-HCL (pH8.5)
ECL II	0.02% (v/v) Hydrogen peroxide; 0.1 M TrisHCL (pH 8.5).

Table 2.2-5 Antibodies used in Westerns

Antibody	Dilution / Concentration	Cat. No.	Source
Goat α-Human IgG (Fc specific)	1:1000	I2136	Sigma
Monoclonal Mouse 15B1	1 μg/ml	--	Homemade
Donkey α-Sheep/goat HRP	1:2000	AB324P	Sigma
Goat α-Mouse HRP	1:5000	AP308P	Sigma

2.2.7 Coomassie Blue Staining of SDS-PAGE gels

Gels were stained with Coomassie blue (**Table 2.2-6**) for 20 minutes and with gentle agitating and then de-stained with de-staining solution (**Table 2.2-6**) for couples of time until background of gel is completely destained. Stained gel was finally placed in dH2O and visualised using GeneFlash Bio Imaging Gel Documentation System equipped with Pulnix-300 camera and printer (Syngene).

Table 2.2-6 Recipes for Coomassie Blue Staining

Reagent	Preparation
Coomassie Blue Solution	50% methanol, 10% acetic acid, 0.25% Coomassie blue R250 in dH_2O
Destaining Solution	10% methanol, 10% acetic acid in dH_2O

2.2.8 srE2-Fc fusion Purification using Protein A

HiTrap XK 16/40 column (GE healthcare) was packed with 3-5 ml protein A-spherose. 20 column volumes (CV 60-100) of PBS were pumped over the column at 3 ml/minute at RT using peristaltic pump P-1 (GE healthcare) and the collected flow was discarded. Filtered 500 ml of bottle of drosophila medium (containing secreted srE2-Fc fusion) were pumped over the column at 3 ml/minutes and any unbound fraction was collected into a fresh sterile beaker. Once the medium had passed through the column, same medium was passed through again to enhance binding of any unbound srE2-Fc protein. Total of about 18 hours was required to load 3.2 L through equilibrated column. Then, the unbound protein to the column was washed with 20 CV loading buffer (**Table 2.2-7**) at 3 ml/minute and the collected flow was removed. 5-10 CV Elution buffer (**Table 2.4-1**) was applied to the column and the eluate was collected into fresh sterile 50 ml Falcon tube and placed on ice at 4^{o}C. For column stripping and storage purpose, the column was loaded with 5 CV stripping buffer (100mM citrate pH 2.5) followed with further 5CV of wash buffer and finally 5CV of 20% EtOH in sterile, filtered and de-gassed dH_2O. The eluted fractions were applied to VivaSpin20 centrifugal concentrator with 10kDa molecular weight cutoff (Sartorius) and centrifuge at 3500 rpm using RT-7 Plus centrifuge (Sorvall) at 4^{o}C. The concentrated fractions were loaded into SnakeSkin dialysis tubing (Thermo Fisher) and sealed with clips. The tube then was placed into 1 L dialysis buffer for 30 minutes at RT and process was

repeated twice with using fresh dialysis buffer every time and finally dialysed into PBS at 4^{o}C overnight. The final fraction were assayed for protein by BCA assay, dispensed into 50ul aliquots and stored at -20^{o}C.

Table 2.2-7 Recipes used for srE2-Fc fusion purification

Reagent	Preparation
Loading buffer	50 mM TRIS HCL pH7.4/ 200mM NaCl in dH_2O

2.2.9 MBP-CD81 LEL purification using amylose resin

Amylose resin (5 ml) was poured gently into column. The column was washed with 3 CV dH_2O (each CV= 5 ml), followed with 10 CV filtered column buffer (**Table 2.2-8**). Filtered bacterial soluble lysate was applied to column at flow rate of 1 ml/minute and collected flow in 50 ml Falcon tube was discarded. Unbound protein remaining on the column was washed through with 20 CV volumes of column buffer. 10 CV of elution buffer (**Table 2.2-8**) was then applied to the column and the flows (containing rMBP-CD81 LEL) were collected in sterile 50 ml Falcon tube passed through filter with 0.20 μm pore size and placed on ice. The filtered eluted fractions were concentrated, dialysed and measured for protein concentration as mentioned in section (2.2.8). The total yield was dispensed into 50ul aliquots and stored at -20^{o}C.

Table 2.2-8 Recipes used for MBP-CD81 LEL fusion purification

Reagent	Preparation
Column Buffer	20 mM Tris-HCl (pH 7.4) 200 mM NaCl 1 mM EDTA
Elution Buffer	20 mM Tris-HCl (pH 7.4) 0.2 M NaCl supplementd with 10mM maltose

2.3 Cell biology

2.3.1 Human cell culture

Huh7 subclone (Huh7.0 and Huh7.5) cell lines were cultured in Dulbecco's Modified Eagle Medium (DMEM) provided with 10% (v/v) 55°C heat treated FBS. The cells that had reached 70-80% confluence rate were split using the following method: culture media was discarded and the cells were washed once with PBS. The cells were dissociated from the flask by adding 2 ml of 0.05% Trypsin-EDTA solution (Gibco) or homemade solution (**Table 2.3-1**) per 75cm^2 T-flask and incubated at 37°C for 10-20 minutes. The dissociated cells were resuspended in 2 mls of fresh warm media and were centrifuged at 700 rpm using for 5 minutes in Labofuge 400 centrifuge (Heraeus). The supernatant was discarded and the cell pellet was resuspended into 6 mls of DMEM media and 1 ml of cell suspension was added to 11 mls of fresh growth DMEM media in a new T-75 flask. The flask was then incubated in CO_2 incubator at 37°C and the cells were allowed to grow until they formed a confluent monolayer.

HepG2 cell lines were maintained in Minimum Essential Medium (MEM) supplemented with 10% (v/v) 55°C heat treated FBS and 1% (v/v) non-essential amino acids (NEAA) and were split as mentioned above. Fibroblast HEK 293T cells were cultured in DMEM provided with 10% (v/v) 55°C heat treated FBS. Culture media was aspirated and the cells were washed once with PBS. 8 ml of pre-warm fresh DMEM media was added to flask and the cells were detached by pipetting gently up and down and new cells were cultured at 1:8 splitting ratio. The flask was then incubated in CO_2 incubator at 37°C and the cells were allowed to grow until confluent.

Frozen seed stocks of cells were prepared (**Table 2.3-1**) by placing 10 mls of cell suspension into a 15 ml falcon tube. The cells were then spun at 500-700 rpm in a Labofuge 400 centrifuge (Heraeus) for 5 minutes. The supernatant was discarded and the cell pellet was resuspended in pre-cold freezing media to a cell density of 1 x 10^7 cells/ml. The cell suspension was aliquoted into 1.8

ml cryogenic tubes (Nalgene) and left to freeze overnight at -80◦C in Mr. Frosty freezing container (Thermo fisher). The following day the cells were transferred to the liquid nitrogen tank for long cell preservation. Live cells density was assessed using IX51 inverted microscope (OLYMPUS) and counted using a Bright-Line hemacytometer (Sigma-Aldrich).

Table 2.3-1 Recipes used for cell culture

Reagent	Preparation
1x Trypsin/EDTA	1 mM EDTA, 0.25% Trypsin in PBS
Freezing Media	8% (v/v) DMSO, 20% (v/v) FBS in DMEM or MEM

2.3.2 Insect cell culture

Final density of 2 x 10^6 cells per 1ml *of Drosophila melanogaster* Schneider 2 (S2) cells were cultured in M3 media (Sigma) supplemented with 10% of 65°C heat inactivated FBS and insect supplement. The cells were then left to grow at 23°C and once their density had reached 15 x 10^6 the insect cells were split into fresh media. For seeds stocks, cells were frozen as discussed above.

2.3.3 Immunofluorescence staining

After 90% of cells confluence, cells were cultured at a density of 3x10^5 cells/ml and then 50-100 μl of cells in medium was placed in each single open well of μ-Slide 8 Well (IBIDI) and incubated for 18-24 hours in CO_2 incubator at 37°C. Medium was discarded and cells were then washed with PBS. Cells were fixed with 50 μl of 4% (w/v) paraformaldehyde (PFA) in PBS pH 7.4 at RT for 15-20 minutes. PFA was removed and the cells were rinsed twice with 2mM glycine/ PBS. Cells were permeabilised by adding cooled 0.1-0.2% Triton X-100 in PBS at 4°C for 3-5 minutes and then cells were washed twice (5 minutes each) with 2 mM glycine/PBS. Cells were blocked by adding 150 μl of 5% BSA in

PBS and incubated 40-60 minutes at RT. The blocking solution was decanted and the cells were incubated with 100 µl diluted primary antibody in 5% BSA in PBS at RT for 1 hour. Antibody solution was decanted and cells were washed three times with 0.1% BSA in PBS for 5 minutes each. Diluted secondary antibody (100 µl) in 5% BSA in PBS was added cells in each chamber for 1 hour at RT in the dark. Secondary antibody solution was decanted and cells were rinsed three times (5 minutes each) with 0.1% BSA in PBS. Cells were incubated with 50 µl of 0.5 µg/ml DAPI stain (Sigma-Aldrich) for 5 minutes and then rinsed twice with dH_2O and finally with PBS. Cells in each well were mounted with 1-2 drops of optimised mounting medium (IBIDI) and stored at 4°C. The slides were viewed using the TCS SP5 confocal microscopy (63x scanning objective) and images were captured using the LAS AF software (Leica Microsystems). Images were further processed through ImageJ software (FIJI) and Illustrator CC software (Adobe system). Some sets of experiments required treating live cells grown on coverslip with antibodies or srE2-Fc variants at different time points and incubated in CO_2 incubator at 37°C. Medium was then discard and cells were then fixed with 4% PFA solution at RT for 15-20 minutes. Washing cells, permeabilisation, adding primary or secondary antibodies, counter staining and mounting coverslip were done as discussed above.

Table 2.3-2 Antibodies used in Immunofluorescence

Antibody	**Dilution/ Concenterati on**	**Cat. No.**	**Source**
Goat anti-Human IgG (Fc specific)-FITC	1:50	F9512	Sigma-Aldrich
Rabbit anti-Human IgG (Fc)-Texas Red	1:50	SAB3701287	Sigma-Aldrich
Monoclonal Mouse anti- CD81(5A6)	15 µg/ml	Sc-23962	Santa Cruz
Mouse anti-claudin-1 (A-9)	15 µg/ml	Sc-166338	Santa Cruz
Goat anti-occludin (Y-12)	10 µg/ml	Sc-27151	Santa Cruz

Goat anti-mouse alexa Fluor 647	1:150	4410S	Cell signaling
Donkey anti-goat FITC	1:30	Sc-2024	Santa Cruz
Mouse anti-heavy chain clathrin	7 μg/ml	MA1065	Thermo fisher
Rabbit anti-SRB (1 and 2)	1:30	Ab36970	Abcam
Donkey anti-goat IgG Alexa Fluor 647	1:75	Ab150131	Abcam

2.3.4 Flow cytometer

Target cells ($1x10^6$) were incubated with purified recombinant proteins (srE2-Fc, its derivatives, control tPA-Fc, rMBP-CD81LEL) or specific antibodies and suitable medium supplemented with 10% FBS in a total volume of 1 ml in microcentrifuge tube. Samples were incubated on SB3 rotator (Stuart) at 10 rpm for 30-60 minutes at RT. The cells were pelleted at 2000 rpm, in an Eppendorf C5415C microfuge (Beckman) for 2.5 minutes. Supernatants were aspirated and pellet was gently suspended in 1 ml of washing solution (PBS with 0.1% sodium azide) and pelleted as above. Supernatants were removed and cell the pellet were resuspended into diluted secondary conjugated antibody in 500 ml appropriate medium at room temperature for 30-60 minutes in the dark. The cells were pelleted, washed, fixed (0.5 % paraformaldehyde in PBS pH 7.4), and stored in the dark at 4°C until assayed by FACScan or LSRFortessa cell analyser (Becton-Dickinson). Data were analysed by Prism 6 (GraphgPad).

Table 2.3-3 Antibodies used in Flow cytometry

Antibody	**Cat. No.**	**Source**
Monoclonal Mouse anti- CD81 (5A6)	Sc-23962	Santa Cruz
Rabbit anti-SRB1 (H-180)	Sc-67098	Santa Cruz
Mouse anti-claudin-1 (A-9)	Sc-166338	Santa Cruz

Goat anti-occludin (Y-12)	Sc-27151	Santa Cruz
Goat anti-Human IgG (Fc specific)-FITC	F9512	Sigma-Aldrich
Monoclonal mouse anti-CD81 (5A6) PE conjugate	Sc-23962PE	Santa Cruz
Goat anti-mouse IgG Alexa Fluor 647 conjugate	4410S	Cell signaling
Goat anti-rabbit IgG (H+L) Alexa Fluor 647 conjugate	4414S	Cell signaling
Donkey anti-goat FITC	Sc-2024	Santa Cruz

2.3.5 Enzyme-linked immunosorbent assay (ELISA)

Microtitre Nunc MAXI-Sorp 96-well plates (Sigma-Aldrich) were coated with 100 μl of purified antigen (srE2-Fc or derivatives, or MBP-CD81 LEL), or conditioned insect cell medium supernatants containing srE2^{332}-HAH6 for 1 h at RT as indicated. Unbound proteins were pipetted out and the wells were washed 3x in fresh PBS (5 minutes each). The plates were incubated with 250 μl of blocking solution (**Table 2.3-5**) for each well at RT for 1 hour and then wells were washed twice in wash solution. Primary antibodies (100 μl) were added and incubated with the immobilized target Ag for 1 h at RT. Plates were washed extensively with wash buffer 3 times (**Table 2.3-5**), and 100 μl peroxidase-conjugated secondary IgG added and the plates incubated at RT for 1 hour and rinsed 3 times in washing buffer followed by 3 times with fresh PBS. Bound Ab was detected by adding 100 μl 3,3',5,5'-Tetramethylbenzidine (TMB) working solution (**Table 2.3-5**) to each well and incubated 10–20 minutes with gentle shaking and then 50 μl of stop solution (**Table 2.3-5**) were added to each well; The optical density readings were measured at OD_{450} using Gemini XPS Microplate Reader (Molecular device Inc.). Dose-dependent Ab binding was compared using Prism 6 (GraphPad).

Table 2.3-4 Antibodies used in ELISA

Antibody	**Cat. No.**	**Source**
Monoclonal mouse α-CD81 (5A6)	sc-23962	Santa Cruz
Goat α-mouse HRP	AP308P	Sigma-Aldrich
Goat α-human IgG (Fc specific) HRP	A0170	Sigma

Table 2.3-5 Recipes for ELISA

Reagent	**Preparation**
Blocking solution	5% skimmed milk powder or BSA in PBS and 0.025 % (v/v) Triton X-100
Washing solution	1% Marvel or BSA in PBS and 0.025 % (v/v) Triton X-100
TMB working solution	2 drops of buffer, 3 drops of TEMB and 2 drops of H_2O_2
Stop solution	0.5 M H_2SO_4

2.4 Ready-to-use manufactured Kits

Table 2.4-1 List of reagents and kits used

Reagent	**Cat. No.**	**Supplier**
Schneiderís insect medium with $NaHCO_3$	S0146	Sigma-Aldrich
FBS	10500064	Gibco-Thermo Fisher scientific
Insect medium supplement 10X	17267	Sigma-Aldrich
Schneiderís insect medium without $NaHCO_3$	S9895	Sigma-Aldrich

100X penicillin/streptomycin	15140122	Thermo fisher
Hygromycin B	H9773	Sigma-Aldrich
BL21 competent E.coli	C2530	NEB
IPTG	16758	Sigma-Aldrich
Protease inhibitor cocktail	Ab65621	Abcam
DMEM, high glucose, GlutaMAX supplement	41966047	Life technology- Gibco
MEM, GlutaMAX supplement	41090028	Life technology- Gibco
MEM NEAA solution (100X)	11140050	Life technology- Gibco
Trypsin-EDTA (0.05%)	25300054	Life technology- Gibco
TMB Peroxidase (HRP) kit	SK-4400	Vector
Prestained protein marker	P7708	NEB
Acrylamide/bis-Acrylamide, 29:1 Solution	A2455	Melford
APS	A3678	Sigma-Aldrich
TEMED	T9281	Sigma-Aldrich
BCA protein assay kit	23225	Pierce
BSA	A9418	Sigma-Aldrich
Gentle Ag/Ab elution buffer, pH 6.6	21027	Pierce
Protein A IgG binding buffer	21001	Pierce
Protein A sepharose	17528001	GE Healthcare
Amylose resin	E802	NEB
Geneticin (G-418 Sulfate)	11811023	Thermo Fisher Scientific
Lipofectamine 3000 transfection reagent	L3000008	Thermo Fisher Scientific

Chapter 3 An HCV E2-derived Immunoadhesin is Efficiently Targeted to Human Hepatoma Cells and is internalised in a Receptor Density-Dependent and Rate-Limited Manner

3.1 Drosophila melanogaster expression system

The fruit fly *Drosophila melanogaster* Schneider 2 cell expression system (DS2ES) has been demonstrated to be a powerful experimental tool for studying mechanisms of different human diseases and in particular understanding the host-virus interaction of some infectious viruses such as influenza A virus, human immunodeficiency virus 1(HIV) and Human T-Cell Leukaemia Virus Type-1 (HTLV-1) through expressing matrix protein 2 (M2), envelope glycoproteins 120 (gp120) and glycoproteins 46 (gp46) respectively (Adamson *et al.*, 2011; Brighty & Rosenberg, 1994; Hughes *et al.*, 2012). There are two significant advantages to the application of the DS2ES for expression of viral envelope proteins: The recombinant proteins accumulate abundantly in the insect media as a soluble secreted form, which can be easily purified; In addition, the expressed recombinant proteins frequently retain full glycosylation and functional activity, which results in robust affinity binding to host cellular receptors as is the case for recombinant HIV gp120 (affinity to CD4) and recombinant HTLV-1 gp46. Importantly, the recombinant envelope proteins are functionally comparable with the native proteins purified from viral particles (Brighty *et al.*, 1991; Ivey-Hoyle *et al.*, 1991; Jassal *et al.*, 2001). Based upon published methodologies from the Brighty laboratory, the S2 cells were transfected with plasmids encoding recombinant HCV glycoproteins E2 and derivatives there of. The absence of the transmembrane domain (TMD) at the C terminal of E2 allowed high quantity secretion of N-terminal E2 (srE2) into the culture medium, allowing rapid concentration and purification. The

expressed high affinity srE2 provide an important resource for the biological, biophysical and biochemical analysis that were carried out in this project.

3.1.1 pMT HCV GT1a E2-Fc Vectors

cDNA generated by reverse transcription of native HCV GT1a Wychowski RNA (**Fig. 3.1-1**) was a gift from François-Loïc Cosset and used for PCR amplification of full N-terminal $E2^{332}$ DNA **(Fig. 3.1-2).** E2 vectors encoding the targeted amino acids (a.a) sequences were constructed and stably transfected into our drosophila expression system for generation of five secreted forms of HCV glycoproteins E2 (**Fig. 3.1-3 A)**. The Drosphila Metalthionine promoter (pMt) was used as a conditional promoter to induce transcription in presence of the copper sulfate. Moreover, our expression system utilises the human tissue plasminogen activator (tPA), which acts as a signal sequence to aid secretion of the recombinant protein (Brighty et al., 1991). srE2 full length ($E2^{332}$) encodes coding regions from b.p 648 (GAA codon) to bp 1643 (AAG codon) was inserted into the pMT vector. In addition, four srE2 variants that encode deleted E2 forms of E2 named $E2^{295}$, $E2^{278}$, $E2^{265}$ and $E2^{195}$ were introduced into the plasmid (**Fig. 3.1-3 B**). The $E2^{332}$ construct and the E2 truncated forms contain no TMDs and thus the recombinant proteins will not be anchored to the plasma membrane. After Each E2 sequence, a thrombin cleavage site (LVPAGS) was introduced followed by the Fc-domain of human immunoglobulin G (IgG) located at b.p 1662 to b.p 2366). The transcription unit was terminated with the Simian virus 40 Polyadenylation signal (SV40 poly A), an ribonuclease cleavage signal that promotes poly-adenylation downstream of a hexanucleotide motif (AATAAA) and stabilizes the mRNA (Orozco *et al.*, 2002; Proudfoot, 1989; Proudfoot *et al.*, 2002). Expressed envelope proteins ($E2^{332}$, $E2^{295}$, $E2^{278}$, $E2^{265}$ and $E2^{195}$) are numbered from the start of E2 and are equivalent to the following coordinates on the HCV polyprotein $E2_{715}$, $E2_{678}$, $E2_{661}$, $E2_{648}$ and $E2_{578}$ resepctively, and illustrated in Fig. 3.1-1. An essentially identical set of E2 proteins were also constructed in which the human Fc-region was replaced by the influenza virus-derived HA-tag followed by a hexa-histidine tag (HAH6 tag) to ease purification.

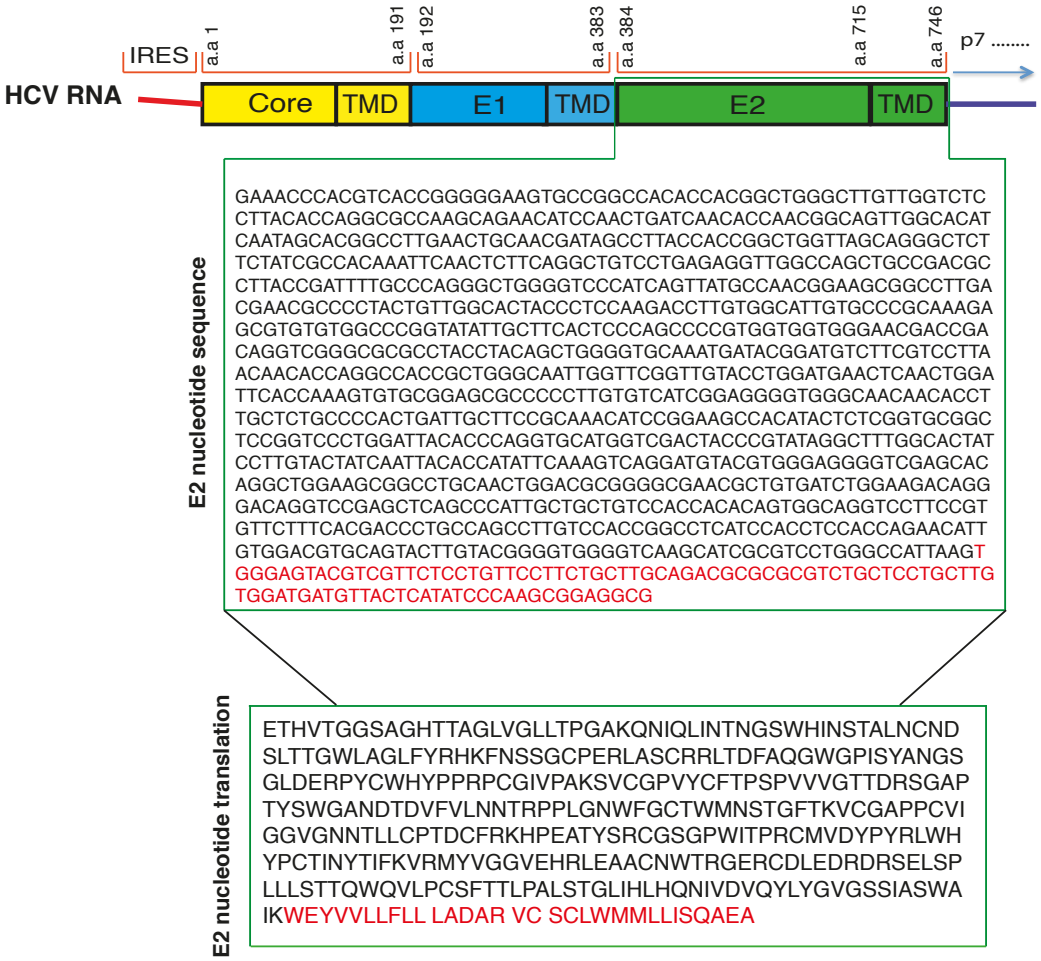

Figure 3.1-1 HCV GT1a glycoprotein E2 nucleotide and a.a Sequences.
A simplified diagram of the HCV RNA genome (Wychowski strain) illustrating IRES, N-termianl of core (yellow rectangle), N-terminal of E1 (blue rectangle), N-terminal of E2 (green rectangle) and p7 channel. Core, E1 and E2 were shown fused with its related transmembrane domain (TMD). a.a number represent position site of start and end of N-terminal regin of core (1-191), E1 (192-383), N-terminal E2 (384-715) and E2 TMD (716-746); all according to native plyprotien sequence. Nucleotide sequence and amino acid sequence of full N-terminal domain of E2 (total of 332 a.a) and TMD (31a.a) are illustrated in black letter and red letter respectively.

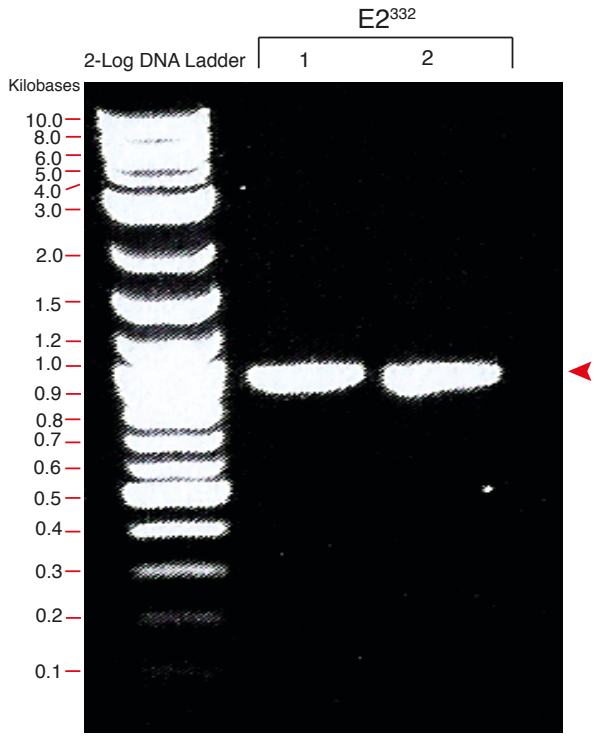

Figure 3.1-2 Agarose gel electrophoresis of glycoprotein E2^{332} PCR product.
After PCR processing (section 2.1.2), purification and precipitation of DNA digests from agarose gel (section 2.1.7), PCR samples 1 (167ng) and PCR sample 2 and (196 ng) and 2 μl of 2-Log DNA ladder were run on 1% agarose gel in 1X TBE at 80 to 120 V for 1 hour (section 2.1.6). 2-Log DNA ladder (first lane) and E2^{332} DNA reactions (second and third lanes) was visualised by EtBr staining at final concentration of 0.25 μg/ml and photographed under UV light. Red arrowhead indicate E2^{332} band with size of 996 nucleotides.

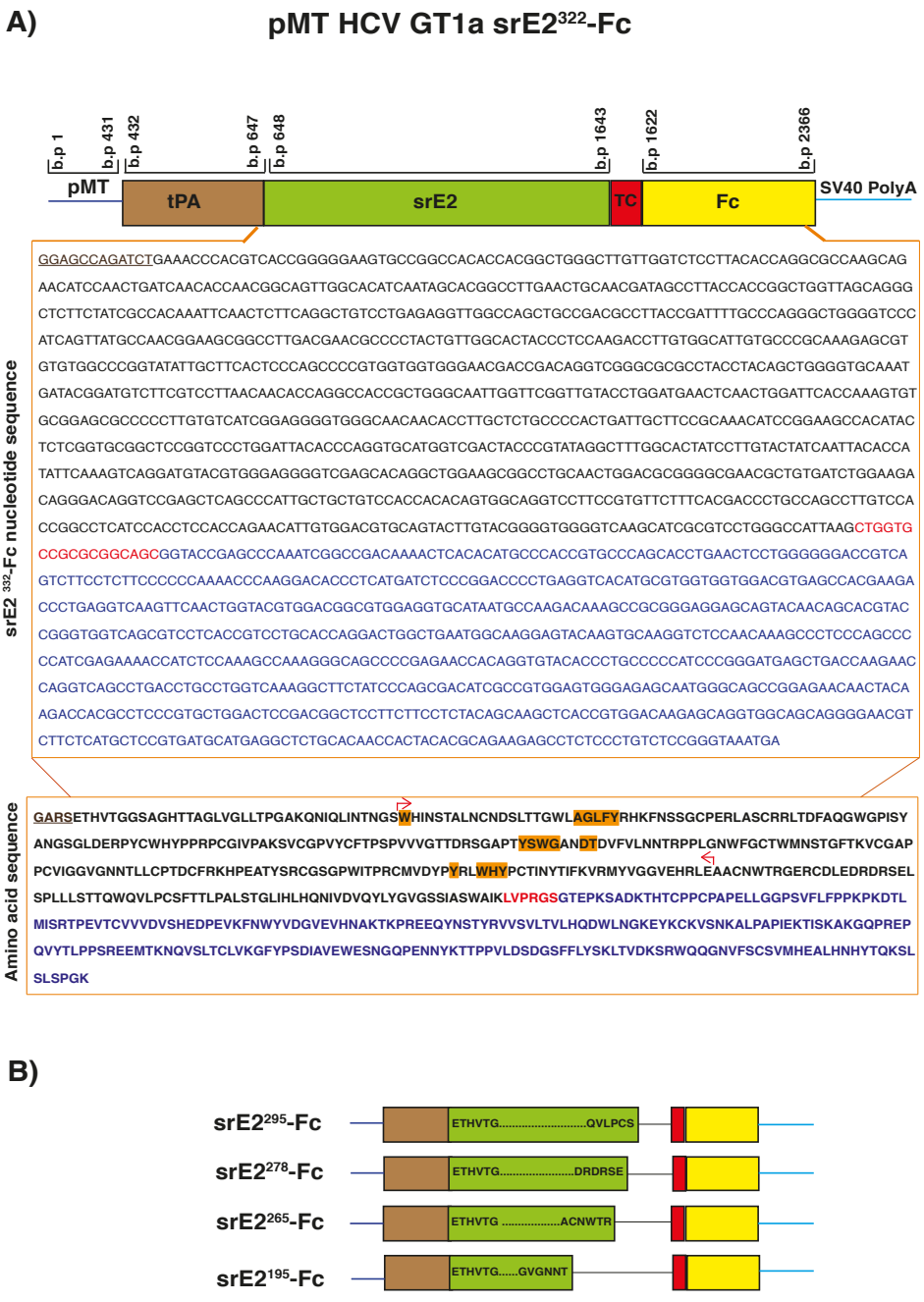

Figure 3.1-3 Expression of HCV E2 which fused to the Fc-region of IgG.

(A) Plasmid MtE2^{332}-Fc was used to express the HCV E2-immunoadhesin; number indicates start and end of each gene in plasmid vector. Nucleotide sequence of E2 (black), thrombin cleavge site, TC (red) and and Fc (Blue) are shown; the predicted amino acid sequence of the mature protein product is shown in one-letter amino acid code. Transcription was driven by the inducible Drosophila metallothionein promoter (pMT), and the transcripts terminated by the SV40 early polyadenylation sequences. To aid secretion the 36-amino-acid signal sequence from the human tPA gene (brown rectangle) was fused to the amino-terminus of E2 (Green

rectangle), the leader is removed upon secretion and leaves 4 amino acids (GARS, brown underline) fused to the E2 protein. At the carboxy-terminus the E2 transmembrane region was replaced by an in-frame fusion at amino acid K^{332} with the Fc-region of human IgG (yellow rectangle), a thrombin cleavage site (shown in red) was included to facilitate proteolytic removal of the Fc-region from the mature purified protein. The amino acid sequence of the mature processed fusion protein is illustrated in single letter amino acid code. The red arrows denote the core E2 region for which structural information is available. Amino acid residues known to interact with CD81 are highlighted in orange. (B) Additional forms of E2 truncated from the carboxy-terminus and fused to Fc were also generated; the numerical suffix refers to the amino acids retained in the truncated E2 numbered from residue 1 (Glu) of the full-length E2.

3.1.2 Soluble recombinant E2-Fc fusions

Both pMt srE2^{332}-FC and pCOhygro vectors were co-transfected in *Drosophila melanogaster* S2 cell and stable cell lines were selected using hygromycin B. The aim of adding hygromycin B containing media was to select cells lines that contain transfected transcription units (pMt srE2-Fc and pCOhygro) and cells that were untransfected with such pCOhygro unit, mock transfected Drosophila S2 cells, will be sensitive and not survive exposure to hygromycin B comparing with resistant cells containing pCOhygro unit. Cell lines stably transfected with pMt srE2^{332}-FC were generated after 42 days of continuous selection with media containing hygromycin B. Stable cell lines produced from cells transfected with pMt srE2-Fc were suspended in fresh FBS-free media and induced with 500uM $CuSO_4$ incubated at 25°C. Cell free media supernatants from the parental untransfected S2 cells and stable transfected Drosophila cells were assayed by WB using antibodies raised against Fc domain of human IgG demonstrated expression of the Fc domain that tagged with srE2^{332} domain. A similar sized antigen could not be detected similar in untransfected cells supernatant, indicating no cross reactivity with any component produced from untransfected S2 cell. All truncated forms (srE2^{295}-Fc, srE2^{278}-Fc, srE2^{265}-Fc and sE2^{195}-Fc) were efficiently secreted into the tissue culture medium and recognized by anti Fc conjugate (**Fig. 3.1-4 A & B**). Measuring the mobility of all E2-Fc form bands on SDS gel showed a small relative increase in protein migration compared to the predicted theoretical migration of the designed viral protein (**Table 3.1-1)** likely due to glycosylation of HCV E2 protein and its derivatives in S2 cells. The immunological fidelity of the secreted recombinant srE2-Fc was examined using anti-E2 polyclonal and monoclonal antibodies. Most importantly, the srE2^{332} tagged with the HAH6-domain was efficiently recognised by antisera from infected patients by ELISA (**Fig. 3.1-5 A)**. Moreover, mouse monoclonal antibodies raised against E2-derived peptides efficiently recognised the important domains of E2 by WB (**Fig. 3.1-5 B**). In addition, ELISA analysis showed binding capacity of mouse monoclonal anti-E2 to all unpurified srE2-Fc fusions (**Fig. 3.1-5 C**). Overall, this

evidence indicates functional recognition of the linear epitopes and native folded structure of secreted recombinant E2-Fc and derivatives. Incubating supernatant containing the control tPA-Fc fusion exhibited no HRP signal above background indicating that human Fc-domain does not cross react with mouse monoclonal anti GT1a E2.

A)

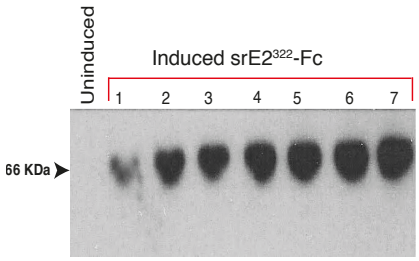

B)

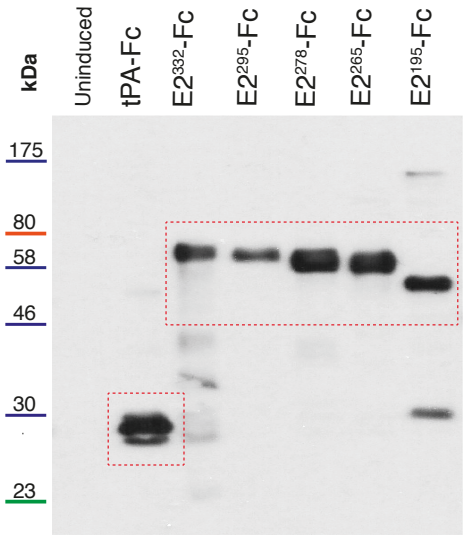

Figure 3.1-4 Recognition of correct folded Fc domain fused with srE2 forms. (A) Cell-free conditioned culture medium supernatants from uninduced (7 day incubation) and induced S2 cells (1-7 days incubation as indicated) transfected with pMtE2^{332}-Fc were assayed for srE2^{332}-Fc expression by reducing denaturing condition western blotting (WB) of total 3 µg in 10 µl 5x loading buffer per lane and probed with goat anti-human Fc (1:1000) and secondary donkey anti-sheep HRP (1:2000), as detailed in section 2.2.6 (B) Western analysis of culture supernatants from induced wild type insect cells and cells expressing "full-length" (srE2^{322}-Fc) and truncated derivatives of srE2-Fc (E2^{295}-Fc; E2^{278}-Fc; E2^{265}-Fc; srE2^{195}-Fc) bordered with red triangle and the control tPA-Fc bordered with red square. Minor proteolytic processing products are observed in some cultures and include the heavy band at approximately 30 kDa in the srE2^{195}-FC lane. ColorPlus Prestained Protein Marker was used as reference for band size and MW are indicated.

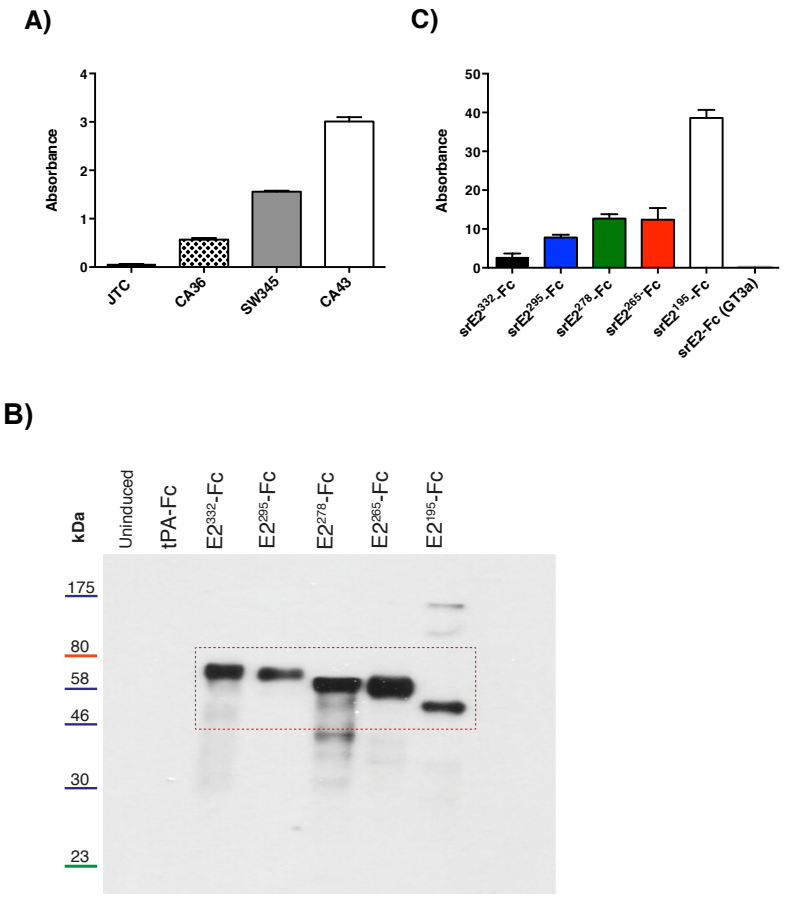

Figure 3.1-5 Recognition of srE2 domain by human patient sera and mouse anti-E2.

(A) Purified $E2^{332}$ -HAH6 with was coated onto ELISA plates and detected using sera from a healthy uninfected donor (JTC) or with sera from independent anonymous HCV infected patients (CA36, SW345 and CA43). Bound antibody was detected with anti-Human Fc HRP (1:5000) and absorbance was measured at 450nm (as described in section 2.3.5) (B) Western analysis of culture supernatants on 10% SDS-PAGE from induced wild type insect cells and cells expressing $srE2^{322}$-Fc and truncated derivatives of srE2-Fc ($E2^{295}$-Fc; $srE2^{278}$-Fc; $srE2^{265}$-Fc; $srE2^{195}$-Fc) and the control tPA-Fc. Total of 3 µg in 10 µl 5x loading buffer was placed in each lane. The western was probed with primary mouse monoclonal anti-E2 (LBT 15B10) at concentration of 1 µg/ml and secondary anti-mouse HRP (1:5000). Red rectangle indicates target bands of srE2-Fc fusions. ColorPlus Prestained Protein Marker was used as reference for band size. (C) Unpurified E2-Fc forms were coated onto ELISA plates and detected using mouse monoclonal anti-E2 (15B10) at dilution of 1:5000. Reaction probed with secondary sheep anti-mouse HRP (1 in 10000) and absorbance was measured at 450nm. All data was subtracted from tPA-Fc and are means and standard deviations from triplicate assays.

Table 3.1-1 Molecular weight of expected and achieved expressed srE2-Fc fusions.

Protein	Predicted MW (kDa)	Actual MW(kDa)
srE2^{332}-Fc	63.60712	≈66
srE2^{295}-Fc	59.66454	≈62
srE2^{278}-Fc	57.79632	≈60
srE2^{265}-Fc	56.23472	≈59
srE2^{195}-Fc	47.92106	≈52
tPa-Fc	26.21869	≈27

Predicted Molecular weight (M.W) of E2-Fc band of was measured by theoretical computation tool provided by ExPASy Bioinformatic resource portal. W.B analysis of E2-Fc fusion band, which was probed with anti-Fc, or primary mouse monoclonal anti-E2 (15B10) provided actual MW of E2-Fc which was measured against ColorPlus Prestained Protein Marker (sizes are given in kDa).

3.2 Purification and Concentration of srE2-Fc fusions

3.2.1 srE2^{332}-Fc and protein A sepharose affinity column

The availability of commercial antisera that bind Fc Tag and the availability of protein A sepharose was of particular advantage to this study, as these reagents along with the Fc-tag joining srE2, provided outstanding opportunities to detect, concentrate, and purify srE2-Fc immunadhesion from culture supernatants, aided by the strong interaction between the Fc-region and staphylococcal Protein A (SpA) (Jansson *et al.*, 1998; Nguyen *et al.*, 2000). This feature assisted in purification of large volumes of secreted E2-Fc by running it through a column containing Protein A sephrose and elution using gentle elution buffer. Collected sample elute was dialysed and concentrated using centrifugal filtration and the samples resolved by SDS-PAGE and stained with Commassie stain (**Fig. 3.2-1**). Concentration of purified srE2^{332}-Fc was measured by BCA method. We achieved high total protein yield of approximately 100mg purified and concentrated from 3.2L of induced drosophila cell culture. These finding again indicate functional folding of Fc-tag that correctly bound SpA. Due to the presence of the disulphide linked Fc-domain the purified E2-Fc is dimeric and displays two copies of E2.

3.2.2 Other soluble recombinant E2-Fc derivatives

In the same manner as for srE2^{332}-Fc purification, Protein A was able to bind correctly folded Fc that tagged with all srE2 forms (**Fig. 3.2-2**.). This advantage helped in achieving approximate yield of total of 50 mg from 1.7 L of cell culture for each E2 forms. A similar method for the concentration of the truncated protiens was applied. Purification and concentration of control tPA-Fc underwent same processing.

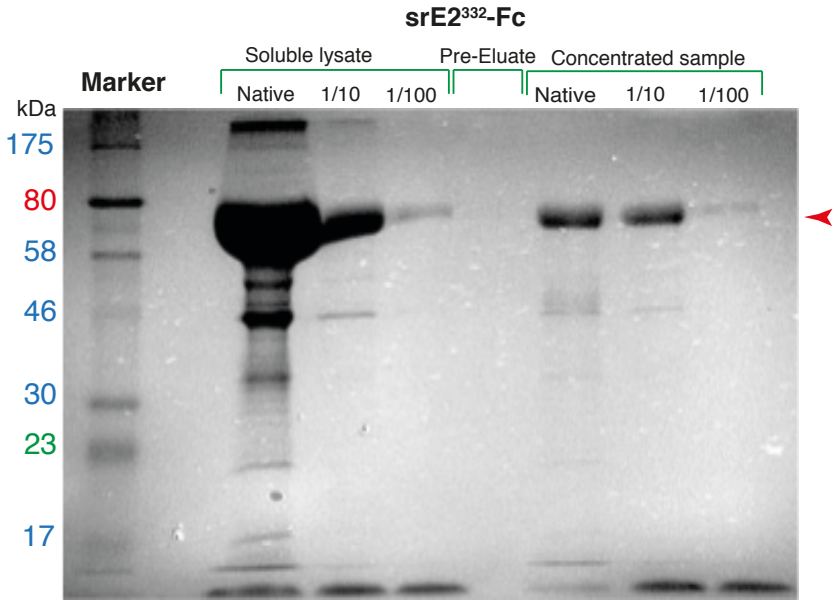

Figure 3.2-1 Coomassie blue staining of srE2^{332}-Fc fractions.

Large scale S2 cell culture conditioned medium containing srE2^{332}-Fc was harvested. Then, media was poured into filter apparatus and filter-sterilise (soluble lysate, second to furth lanes). Fraction was applied to column packed with protein A sepharose. Column was washed with 50mM TRIS pH7.4/200mM NaCl (pre-eluate fraction, fifth lane). Bound E2^{332}-Fc to column was eluted trough loading Pierce elution buffer. E2^{332}-Fc eluate fraction was concentrated using VivaSpin20 centrifugal concentrator (concentrated E2^{332}-Fc fraction, sixth to eighth lanes). Then, concentrated srE2^{332}-Fc was loaded into dialysis tube and was dialysed in 1L of 50mM TRIS pH7.4/200mM NaCl and finally in PBS. Unpurified soluble lysate (total of 5 µg reduced non-denatured of in 2x loading buffer. Purified native samples (total of 20ng reduced non-denatured of in 2x loading buffer) and diluted samples in PBS (1/10 and 1/100) were loaded on 10% SDS gel and srE2^{332}-Fc bands was visualised by Commassie blue dye. Red arrows denote target srE2^{332}-Fc band with M.W of 66 kDa. ColorPlus Prestained Protein Marker was reference leader for protein weight. Section 2.2.7 and 2.2.8 give further methodology details for coomassie staining and protein purification respectively.

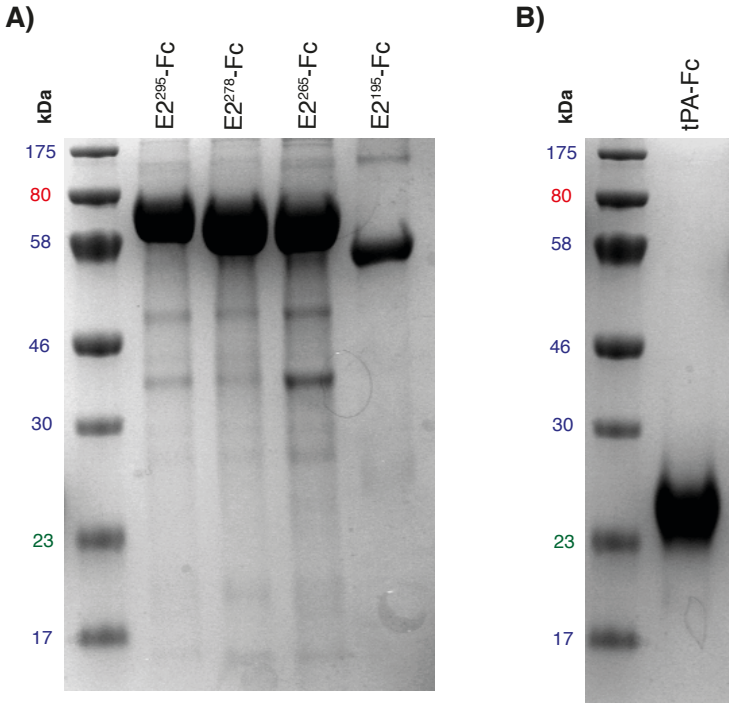

Figure 3.2-2 Commassie blue staining of srE2-Fc derivatives.

Expanded insect cell culture containing srE2-Fc variant (A) or tPA-Fc (control) was harvested to collect secreted protein in media. Then, media was poured into filter apparatus and filter-sterilise. Fraction was loaded into equilibrated column packed with protein A sepharose. Column was washed with loading buffer (50mM TRIS pH7.4/200mM NaCl). Bound E2-Fc variant to column was eluted using Pierce elution buffer. E2-Fc eluate was concentrated using VivaSpin20 centrifugal concentrator and dialysed in 1L of 50mM TRIS pH7.4/200mM NaCl and finally in PBS. Samples (total of 20ng reduced non-denatured of in 2x loading buffer) were loaded on 10% SDS gel and srE2^{332}-Fc bands was visualised by Commassie blue dye. ColorPlus Prestained Protein Marker was reference leader for protein weight.

3.3 The srE2^{332}-Fc immunoadhesin binds to human cell surface receptors

3.3.1 Analysing the binding capacity of srE2-Fc

3.3.1.1 srE2^{332}-Fc binding to a panel of human cell lines

Six human derived cell lines were used to test the functional reactivity of the srE2^{332}-Fc produced in drosophila S2 cells. Flow cytometry was used to examine binding activity to human fibroblast cells represented by HEK 293T and Hela cells, liver cells represented by HepG2 and human lymphocytes represented by Raji (B cells) and CEM (T cells). In addition, an immortalized B lymphocytes derived from patient infected with HCV attending Prof. Dillon' Clinic were used as well. In this experiment, cells were detached from the flask (fibroblast and HepG2 cells) or collected from suspension (cell derived lymphocytes) and washed with PBS. Subsequently, cells were incubated with a fixed amount of srE2^{332}-Fc at RT to allow glycoprotein envelope/receptor binding. Unbound envelope was removed through a PBS washing step followed by addition of secondary goat anti-Human Fc antibody conjugated with FITC to allow detection of soluble E2 fusion interaction. Then cells were washed with PBS and fixed in 0.5% PBS and bound srE2^{332}-Fc assayed by flow cytometry. Increased FITC-specific fluorescence was observed on all cell lines in the presence of srE2^{332}-Fc; indicating recognition of cell surface receptors by srE2-Fc. In addition, incubation of cells with the control protein tPA-Fc exhibited no FITC fluorescence detection indicating that the human Fc domain does not contribute to binding to the target cell surface and it is the srE2 domain that determines the binding capcity to cells.

Cells were incubated individually with each of the secondary anti-Fc antibodies in each experiment to exclude antibody reaction directly to cell surface and these results were always negative (**Fig. 3.3-1**). Our data indicate that receptors recognised by HCV E2 are widespread on human cells, but for this project we focused on the analysis of E2 binding to 293T cells and hepatoma

cell lines, which are considered the principle cells used by researchers to study HCV.

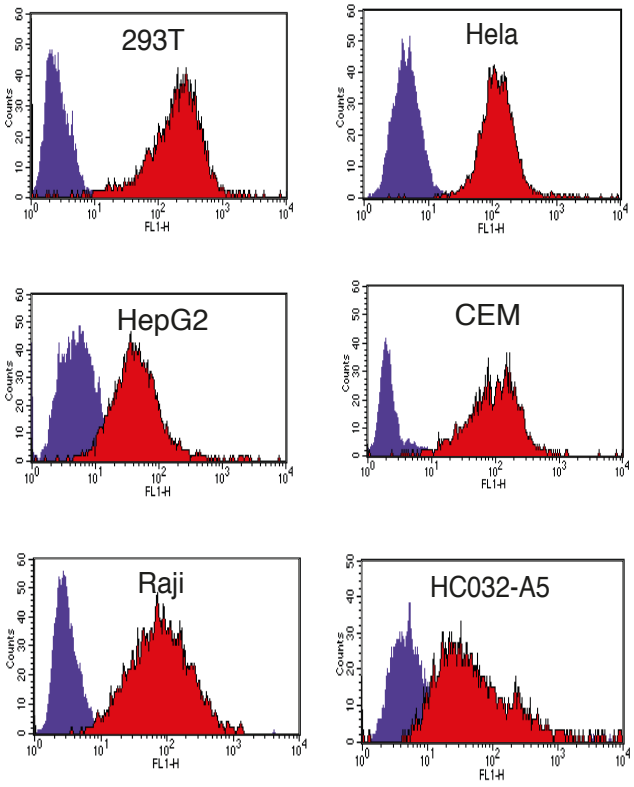

Figure 3.3-1 srE2^{332}-Fc interacts to various human cells.

Detached cells at density of 1x10^{6} / ml of culture media (DMEM for 293T, MEM for HepG2 and RPMI for other cells) containing 10% FBS were incubated with 15µg/ml of control tPA Fc (solid purple histogram), or srE2^{322}-Fc (solid red histogram). Cells were washed to remove unbound protein. The bound E2-Fc was probed with FITC-conjugated anti-human FC secondary (1:500). Samples were fixed with 0.5% PFA in PBS prior detection by FACS analysis. The above figures shows typical flow cytometry histograms for six human cell lines; 293T, Hela, Hep G2, CEM, Raji and HC032-A5 and CEM. FCM methodlgy is explained in section 2.3.4.

3.3.1.2 Dose dependent interaction of srE2^{332}-Fc to 293T cells

As an initial step in characterising the binding process of E2-Fc and therefore HCV to host cells binding to non-hepatic HEK 293T was examined. Our selection was supported by other resracher findings in recent years which showed that 293T is a competent experimental model to study HCV life cycle at surface binding level after expression of some key surface receptors (Da Costa *et al.*, 2012). As srE2^{332}-Fc showed binding to cell surface, we wanted to address if this interaction was receptor mediated through examining the effect of recombinant E2 fusion concentration on binding capacity. Upon incubating 293T with increasing concentration of E2^{332}-Fc, cells exhibited a pronounced and corresponding increase in FITC-specific fluorescence intensity (**Fig. 3.3-2**). Low srE2^{332}-Fc concentrations were associated with low level binding to 293T cell. Importantly, we noticed 293T cells continue to be sensitive to srE2^{332}-Fc addition till 100µg where cell receptors were saturated with reactant protein. Control 293T cells were incubated with tPA-Fc at increasing concentration and examined by FCM to exclude possibility of non-specific Fc tag binding to the examined cells (**Fig. 3.3-2**).

A)

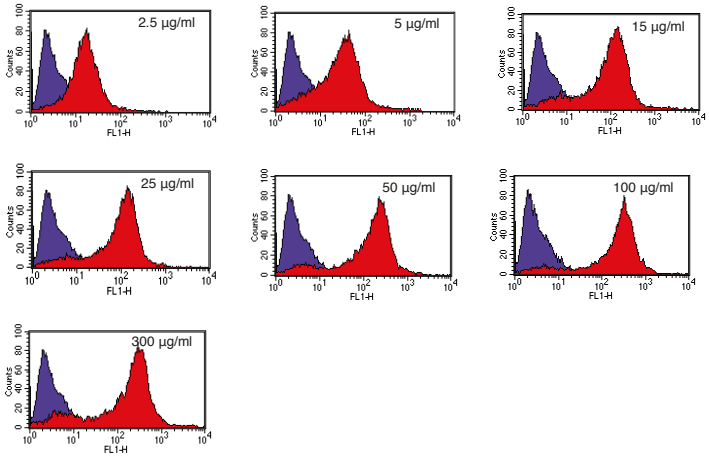

B)

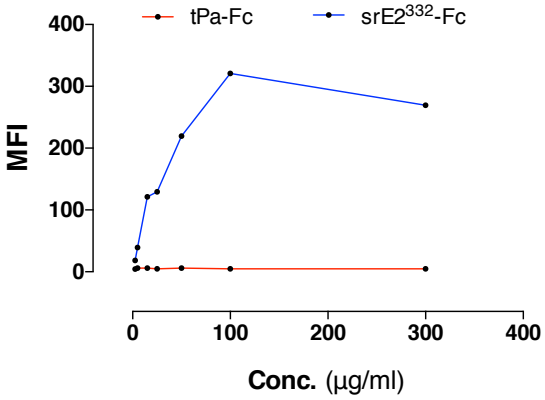

Figure 3.3-2 Dose dependent binding of srE2^{332}-Fc to 293T.

(A) 293T cells were detached from flask using DMEM/FBS media pipetting and counted at 1x10^6 for each sample test and were gently agitated at 37°C, 5% CO_2 for 20 minutes. Purified srE2^{332}-Fc fusion (solid red histogram) and tPA-Fc (purple solid histogram) was incubated with cells at the concentrations shown. Cells were probed for bound glycoprotein with secondary anti-human Fc FITC conjugate serum (1 in 500). Between steps, washing was carried out to remove unbound srE2^{332}-Fc. Samples were fixed with 0.5% PFA. FCM was used for sample analysis. (B) Dose dependent binding curve of srE2^{332}-Fc incubated with 293T.. The basal mean fluorescence intensity (MFI) from control data readings was subtracted from each of the data points shown.

3.3.1.3 Blocking CD81 and analysing srE2^{332}-Fc binding

The plasma membrane associated CD81 tetraspanin (Levy *et al.*, 1998) is known to play a key role mediating binding of truncated $E2_{661}$ and HCV pseudoparticles to cells (Cormier *et al.*, 2004b; Flint *et al.*, 1999b). Here, we wanted to determine if CD81 is a cell surface attachment factor that interacts with srE2^{332}-Fc. As an initial step, the presence of CD81 on 293T cell surface was confirmed: cells were detached from the flasks and incubated with increasing concentrations of mouse monoclonal anti-CD81-PE (5A6) conjugate serum. Our finding showed that MFI correlated with the concentration of anti-CD81PE, which represent the binding of anti-CD81PE to CD81. Surprisingly, despite a good binding affinity of anti-CD81 PE, high concentrations of anti-CD81 are required to saturate the available CD81 binding sites, which indicates that CD81 is expressed at high levels on the 293T cell surface (**Fig. 3.3-3 A**). To analyse the impact of anti-CD81 on the binding of srE2^{332}-Fc to the cell surface, 293T cells were incubated with serial dilutions of anti-CD81 (5A6) unconjugated sera for a short period of 30 minutes at RT. Constant concentration of srE2^{332}-Fc was added to cells and the reaction was probed with anti-human FC FITC secondary antibody. Flow cytometry showed that the FITC-specific srE2^{332}-Fc binding activity was reduced by up to 55% in the presence of anti-CD81 in comparsion with MFI of srE2^{332}-Fc in the absence of anti-CD81 and the 55% reduction was achieved at 0.325 µg/ml of anti-CD81. It is notable that further addition of anti-CD81 (up to 5 µg/ml), resulted in a constant FITC mean intensity reading and showed no extra antagonistic effect on srE2 fusion binding to 293T. This may indicates presence of alternative factors, other than CD81, that bind full-length srE2^{332}-Fc (**Fig. 3.3-3 B**).

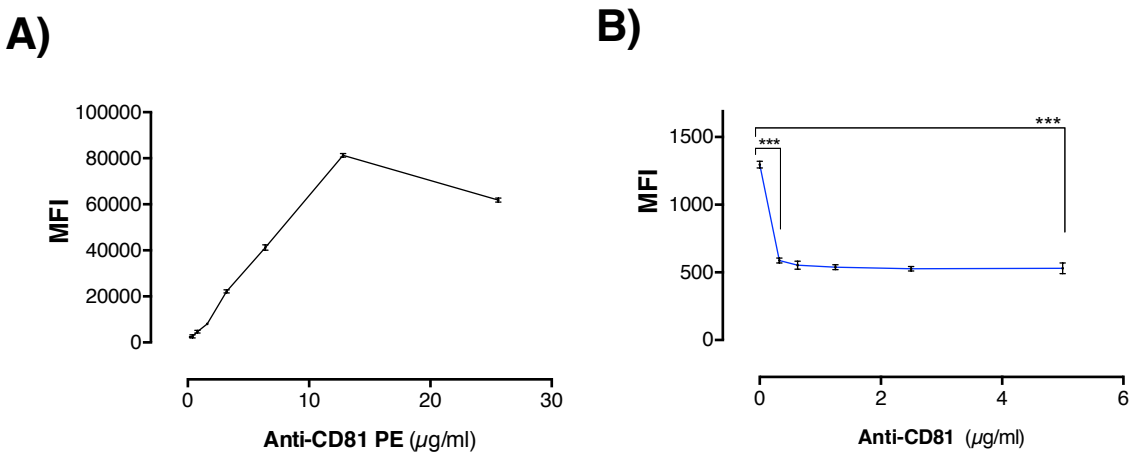

Figure 3.3-3 Binding of srE2^{322}-Fc is reduced in presence of anti-CD81 sera.

(A) Detached 293T cells at a density of 1x10^6 /ml were incubated for CD81 presence with mouse monoclonal anti-CD81 PE conjugate (5A6) serum at concentration shown for 60 minutes at RT. Unbound anti-CD81 was washed and cells were fixed with 0.5% PFA in PBS prior to analysis by flow cytomertry. Control samples were probed with irrelevant mouse anti-human IgG and basal mean fluorescence intensity from control was subtracted from each of the data point shown. (B) Detached 293T cells were treated with unconjugated mouse monoclonal anti-CD81 mouse sera (5A6) at concentration points shown for 30 minutes. For measuring glycoprotein binding capacity, cells were probed with 25 μg/ml srE2^{332}-Fc and reaction was labelled with FITC-conjugated anti-human Fc goat secondary (1:500) and measured by fortessa machine. The basal MFI from control tPA-Fc data reading was subtracted from each srE2^{332}-Fc reading at points shown. T-test ***: $p < 0.001$. Both (A) and (B) are data means and standard deviations from three independent assays.

3.3.1.4 Binding studies of MBP-CD81 LEL to srE2^{322}-Fc

3.3.1.4.1 Expression of MBP-CD81 LEL fusion in *E.coli*

The pMal-c2 expression system is routinely used to express heterologous proteins such as human fatty acid synthase (hFAS) and *Thermus thermophilus* proline dehydrogenase in *E.coli* (Huijbers & van Berkel, 2015; Jayakumar *et al.*, 1996).This system includes a strong promoter ($P_{tac)}$ that has been used to produce high levels (2% of total protein) of target protein fused to Maltose binding protein (MBP) and locate it in *E.coli* cytoplasm. In brief, the malE gene encoding MBP is fused with the target protein coding sequence and inserted downstream of the Ptac promoter in the pMal-c2 vector to express the MBP-target protein fusion (Lavallie *et al.*, 1993; Maina *et al.*, 1988). The MBP tag often improves solubility of the heterologous protein and enhances correct protein folding of the fused partner protein (Kapust & Waugh, 1999). In terms of biochemical properties advantage, generated MBP fusion protein tends to be mostly stable and resistance to proteolytic attack (Smyth *et al.*, 2003). Here, we employed these advantages by cloning human CD81 LEL in pMal-c2 linking our target sequence encoding CD81 LEL to the C-terminal end of MBP to generate a recombinant MBP-CD81 LEL fusion protein (**Fig. 3.3-4**).

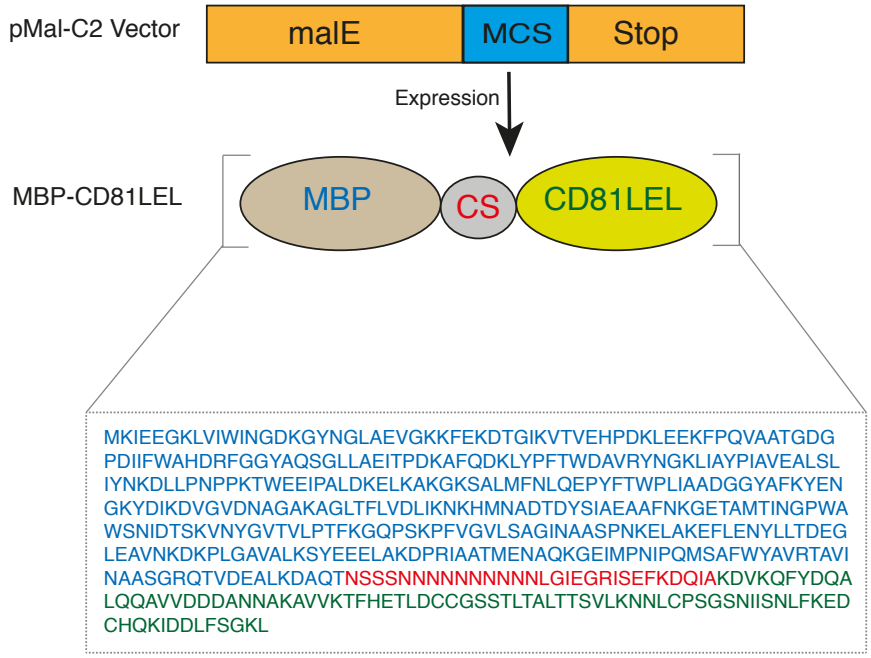

Figure 3.3-4 Schematic diagram of MBP-CD81 LEL expression system.
Plasmid pMal-C2-vector (coloured rectangles) containing CD81 LEL insert at multi-clonal site (MCS) located downstream malE gene was used to express the MBP-CD81 LEL (coloured oval shapes). Transcription of the open reading frame was driven by the inducible *E.coli* promoter (P_{tac}) and the transcripts terminated by the stop codon sequence. Expressed MBP joining CD81 LEL fusion accumulates in the E. coli cytoplasm. The cleavage site (CS) was included to facilitate proteolytic removal of the MBP-region from the mature purified protein (gray circle). The amino acid sequence of the mature fusion protein is illustrated in single letter amino acid code (MBP sequence shown in blue letters, CS in red letters and CD81 LEL in green letters).

3.3.1.4.2 Affinity purification and concentration of MBP-CD81 LEL

An important feature of *E.coli* MBP as a fusion tag is the ability to purify the fusion proteins from lysates by affinity chromatography (Bornhorst & Falke, 2000; Lavallie *et al.*, 1993; Pryor & Leiting, 1997). The MBP-domain link to CD81 LEL has specific affinity to amylose resin and this allows efficient separation from cell lysates and allows rapid fusion protein purification. To purify chimeric MPB-CD81 LEL, induced and clarified *E.coli* lysate was passed through an affinity amylose column and the eluted fractions dialysed and concentrated. The purified protein was examined by SDS-PAGE and coomassi blue analysis, yielding a protein with a molecular weight (about 52 kDa) consistent with MBP-CD81 LEL (**Fig. 3.3-5).**

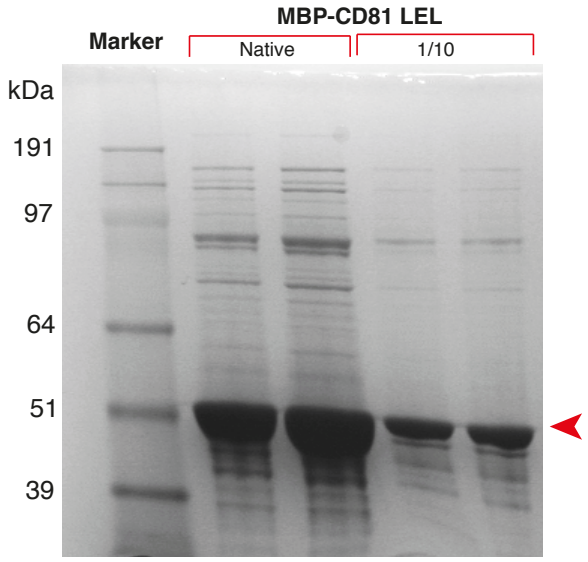

Figure 3.3-5 Commassie blue staining of purified MBP-CD81 LEL fraction.

Soluble lysate from *E.coli* cell pellet was prepared and filter-sterilised. Lysate was applied to Amylose resin column. Column was washed with 20mM TRIS pH7.4/200mM NaCl. Bound MBP-CD81 LEL to column was eluted with elution buffer (20mM TRIS pH7.4/200mM NaCl/ 10mM maltose). MBP-CD81 LEL eluate was loaded into dialysis tube and was dialysed in 1L of 50mM TRIS pH7.4/200mM NaCl. Dialysed fraction was concentrated using VivaSpin20 centrifugal concentrator (concentrated MB-CD81 fraction). In duplicate, purified native concentrated samples (total of 20ng reduced non-denatured of in 2x loading buffer), shown at second and third lanes, and diluted samples in PBS (1/10), shown at fourth and fifth lanes, were loaded on 10% SDS gel and MBP-CD81 LEL bands was visualised by Commassie blue dye. Red arrows denote target MBP-CD81 LEL band with M.W of 52.22 kDa as expected (average M.W of MBP= 40.33 kDa, cleavage site= 2.36 kDa and CD81 LEL=9.52 kDa. Nu PAGE Mops Marker was reference leader for protein weight (first lane). Further details for expression and purification of rMBP-CD81 LEL are decribed in section 2.2.2 and 2.2.9 resepctively.

3.3.1.4.3 Binding assay using anti-CD81

We wished to determine if the MBP-CD81 LEL produced in our *E.coli* system was functional and retained binding properties. A micro-well plate was coated with MBP-CD81 LEL and subsequently blocked in 5% milk in PBS-T blocking buffer, serial dilution of mouse anti-CD81 (5A6) sera was added and the bound antibody detected using HRP- labelled secondary anti-mouse antibody. The HRP signal was detectable indicating successful recognition of CD81 LEL tag by anti-CD81 sera demonstarting functional expression of recombinant fusion and indicating that this CD81 LEL tag folded in a manner comparable to LEL domain of native CD81 receptor. With increasing concentration of antibodies an increase in HRP-specific absorbance was observed, thus indicating binding of anti-CD81 sera to CD81 LEL in a dose dependent manner. In addition, saturation of binding reactivity was achieved upon adding 1 µg of anti-CD81 sera followed with gradual decrease in binding upon adding more anti-CD81 sera (>1µg) to the reaction (**Fig. 3.3-6**). As an experimental control, Anti-CD81 sera were incubated at same dilution points with MBP-STOP that lack expression of CD81 LEL domain to exclude antibody cross reactivity with the MBP tag and result was always negative.

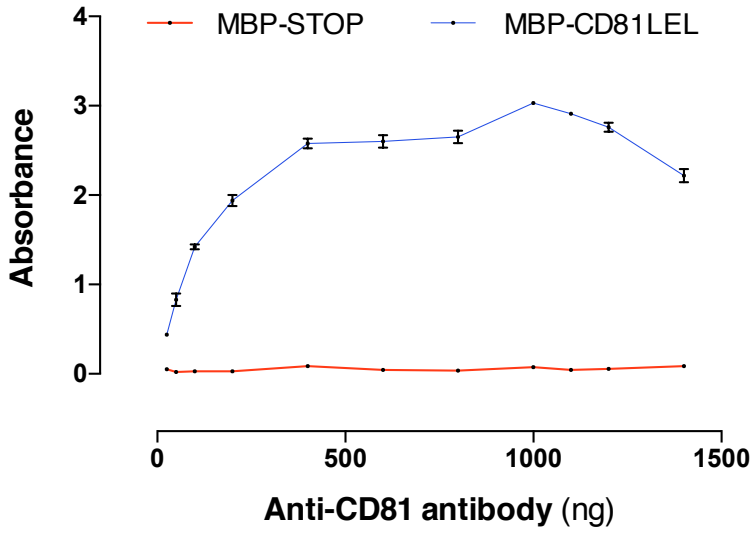

Figure 3.3-6 Recognition of MBP-CD81 LEL by mouse anti-CD81 sera.

MBP-CD81 LEL (10 ng/µl) was coated to a 96-well ELISA plate. 5% milk in PBS-T was loaded into the wells for blocking purpose. Serial concentration of anti-CD81 (5A6) at point shown incubated with MBP-CD81 LEL. The CD81 LEL bound reactivity detected using anti-mouse HRP (1 in 5000 in 5% milk in PBS) and unbound antibody washed away.. Absorbance of signal was measured at 450nm using ELISA plate reader. MBP-STOP control samples were incubated with anti-CD81 sera to exclude cross-reaction with the MBP domain. Data are mean and standard deviations of triplicate readings and background readings from irrelevant anti-mouse IgG were subtracted from the data shown. Method of ELISA is descriped in section (2.3.5).

3.3.1.4.4 Analysing binding of srE2^{332}-Fc to CD81 LEL

It has been reported that HCV glycoprotein E2 interacts with the large extracellular loop of human CD81 (Flint *et al.*, 1999b; Higginbottom *et al.*, 2000) and binding to the LEL of CD81 is crucial for HCV entry (Feneant *et al.*, 2014). We wanted to analyse if our recombinant srE2^{332} could recognise the large extracellular loops of CD81, to address this, we coated ELISA plates with 1µg of MBP-CD81 LEL. Serial dilutions of srE2^{322}-Fc were added followed by incubation with goat anti-human Fc specific HRP antibody. The signal generated from HRP was detected and reflected srE2^{332} fusion interaction to MBP-CD81 LEL. Interestingly soluble srE2^{322} protein bound to rCD81 LEL and 0.25 µg of srE2^{332}-Fc fusion was enough to saturate interaction with the immobilised MBP-CD81 LEL (**Fig. 3.3-7**). As a control, MBP-STOP which lacks the CD81 LEL was analysed for binding reactivity to srE2. Soluble E2-Fc did not bind to MBP-stop.

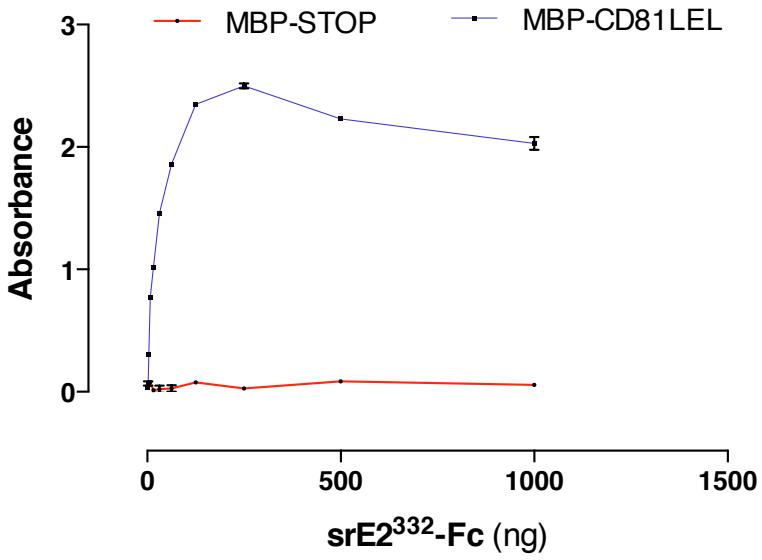

Figure 3.3-7 The srE2^{322}-Fc fusion interacts with CD81 LEL tag.

Purified srE2^{322}-Fc at the concentrations shown was added to a 96-well ELISA plate coated with 1µg of MBP-CD81 LEL fusion per well. The bound srE2^{322}-Fc reactivity was detected using anti-Human FC specific HRP conjugate secondary (1 in 5000 in 5% milk in PBS-T). Absorbance at 450nm was quantified using an ELISA plate reader. MBP-STOP control samples were incubated with srE2^{322}-Fc fusion to exclude cross-reactivity to the MBP domain. Data are the average and standard deviation of triplicate independent assays and background signals from control tPA-Fc were subtracted from the data shown.

3.3.1.5 Competition analysis of srE2^{332}-Fc binding toward MBP-CD81 LEL and 293Tcells

After demonstrating the interaction of secreted E2 to native CD81 on 293T and to recombinant MPB-CD81 LEL, we wanted to test competitive binding of srE2^{332}-Fc to 293T cell surface in presence of soluble rMBP-CD81 LEL. We designed a competitive assay by incubating a constant amount of soluble E2 envelope with increasing amounts of rMPB-CD81 LEL in the presence of 293T cells. As an experimental control, we incubated a set of cells with srE2^{332}-Fc in the absence of MBP-CD81 LEL. The binding was measured by flow cytometer. Our result revealed a gradual decrease of FITC mean intensity associated with increasing concentration of MBP-CD81 LEL incubated with 293T cells comparing with higher mean intensity of anti-Fc FITC that bound srE2^{332}-Fc in MBP-CD81 LEL free sample tube. The result showed significant reduction when srE2^{332}-Fc incubated with 1 µg/ml MBP-CD81 LEL. These observations indicate competitive binding between 293T cells and MBP-CD81 LEL to bind the srE2^{332} fusion. Moreover a decrease in FITC fluorescence was detected at high concentrations of CD81 LEL fusion, but high concentratios of MBP-CD81 LEL were not sufficient to inhibit srE2-Fc binding completely. This suggests that srE2^{322}-Fc may bind to additional factors other than CD81 on the 293T cell surface (**Fig. 3.3-8**).

A)

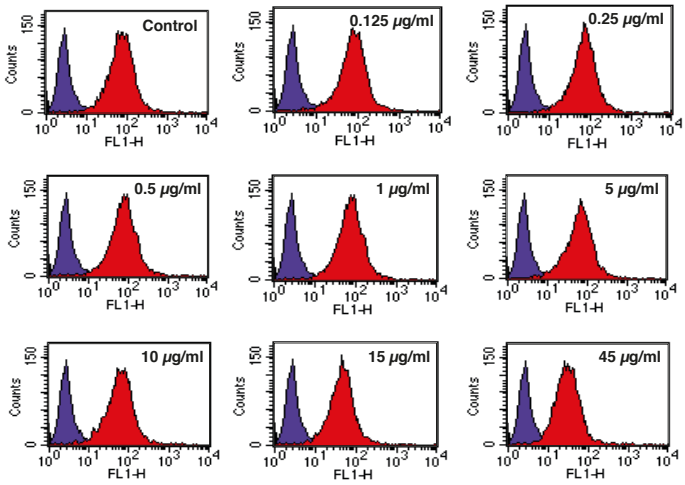

B)

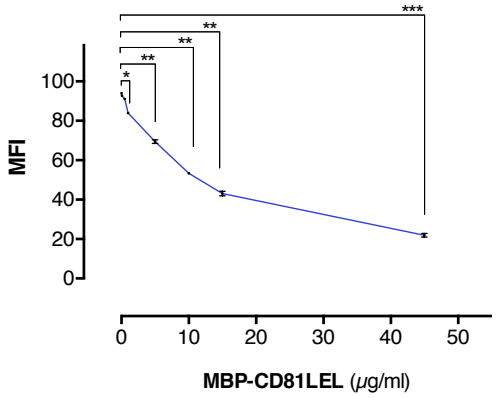

Figure 3.3-8 MBP-CD81 LEL Compete 293T in interaction with srE2^{322}-Fc

(A) Constant concentration (15 µg/ml) of purified srE2^{332}-Fc fusion (solid red histogram) and tPA-Fc (purple solid histogram) was incubated with detached 1x10^6 cells in 1ml DMEM per vial and in presence of MBP-CD81 LEL at the concentrations shown or in the absence of MBP-CD81 LEL (control) for 60 minutes at RT. Cells were probed for bound srE2^{332}-Fc with secondary anti-human Fc FITC conjugate serum (1 in 500) and analysed by flow cytometry. (B) Linear graph of histogram data showing gradual inhibitory response of labelled srE2^{332}-Fc interaction to 293T. tPA-Fc was used as negative control and the basal mean fluorescence intensity of each sample contain srE2^{322}-Fc was subtracted from corresponding tPA-Fc tag reading. T-test *: $p < 0.05$ (corrspnd to 1 µg/ml MBP-CD81), **: $p < 0.01$ (correspond to 5,10 and 15 µg/ml rMBP-CD81) and **: $p < 0.001$ (correspond to 45 µg/ml rMBP-CD81). Data are mean and SD of triplicate assay.

3.3.1.6 Studying of srE2^{332}-Fc binding to hepatoma cell lines

Binding of HCV to attachment factors on the liver cell surface is crucial for virus entry so the virus can enter into and replicate in the cytoplasm of the hepatocyte, thereby, sustaining infection (Zeisel *et al.*, 2011). Thus, it was important to test the interaction of srE2^{332}-Fc to surface factors present on hepatocytes. Huh7.0 and HepG2 cell lines, differentiated Hepatocellular carcinoma (HCC) liver cells, were chosen as the only available model target cell system to mimic the natural hepatocyte. Huh7.0 are the most common permissive cells used by researchers that are competent for HCV genome replication and persistent infectivity (Dash *et al.*, 1997; Yoo *et al.*, 1995). In addition, the Huh7 and HepG2 hepatoma cells are permissive for HCVpp and HCVcc cell entry studies (Coller *et al.*, 2009b; Narbus *et al.*, 2011).

3.3.1.6.1 Confocal testing of CD81 expression on Huh7.0 cells, HepG2 cells and 293T cells

To image CD81 on the hepatoma cell surface, cells were seeded in IBIDI slides at a density of 300 000 cells/ml and incubated at least for 24 hours before treatment. Next day, cells were fixed with 4% PFA in PBS prior and probed with anti-CD81 and anti-mouse Alexa Fluor 647 to examine the presence, localisation and arrangement of CD81 on cells. Visualised by confocal microscopy, strong staining was observed on the 293T cell surface indicating abundant expression of CD81. Also, Huh7.0 exhibited an overall peripheral cell surface staining with some notable unoccupied patches between fluorescence spots compared to the dense fluorescence expression observed on 293T cells. Thereby indicating higher expression of CD81 on 293T cells than Huh7.0. No significant fluorescence signal of Alexa Fluor 647 was identified on HepG2 cells treated with anti-CD81 except a few isolated fluorescent spots, which separated from each other leaving large areas of membrane unoccupied by CD81. Importantly, other researchers have found that that HepG2 cells express low levels or no CD81 under their experimental conditions (Bartosch *et al.*, 2003c; Cormier *et al.*, 2004b; Flint *et al.*, 2006;

Zhang *et al.*, 2004a). Our data is consistent with the view that HepG2 cells indeed has the ability to express CD81 but at exceedingly low levels (**Fig 3.3-9**).

A

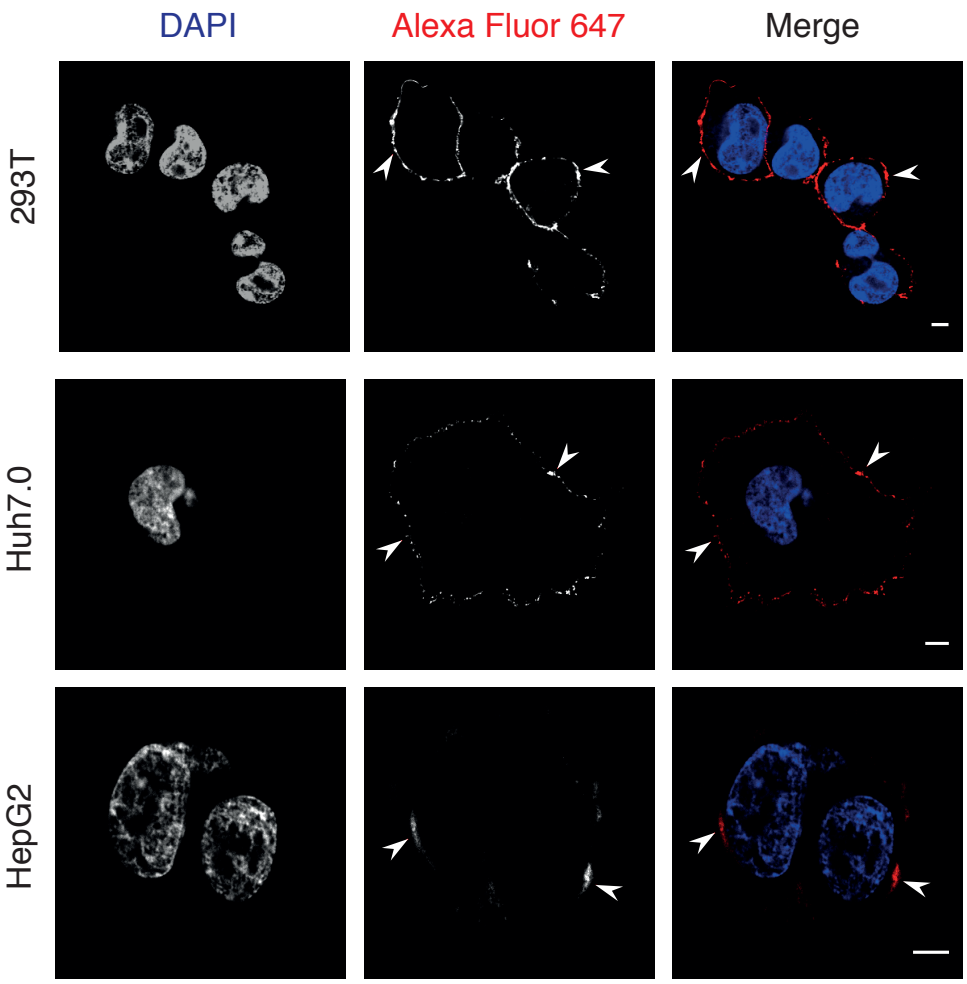

B)

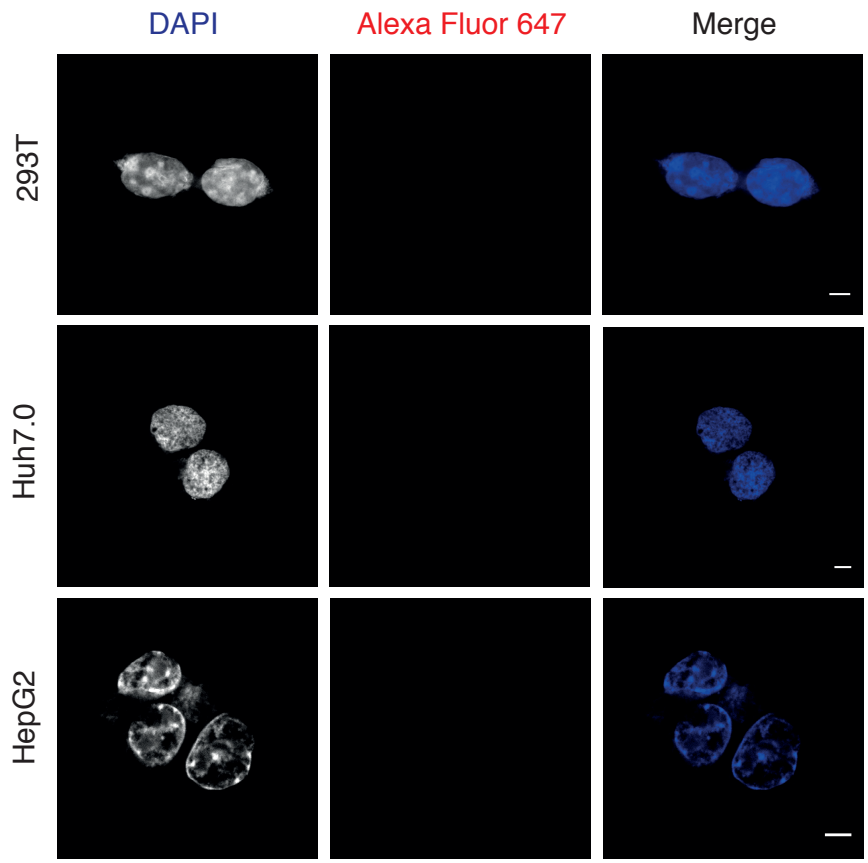

Figure 3.3-9 CD81 is expressed on Huh7.0 and 293T but at low levels on HepG2.

Immunofluorescence staining was done as discussed in section (2.3.3). In brief, Huh7.0 cells, HepG2 cells and 293T cells were cultured in 8-well IBIDI slides at density of 20,000 cells/well and incubated in 5% CO_2 at 37°C overnight. Cells were fixed with 4% PFA in PBS for 18 minutes at RT. After washing in PBS, cells were blocked with 5% BSA buffer. CD81 was detected by incubation cells in each µ-Slide well with 1.5 µg mouse anti-CD81 (5A6) antibody and reaction labelled with goat anti-mouse IgG Alexa Fluor 647 secondary (1 in 150) for 60 minutes (panel A). As a control background sample, cells were treated with irrelevant mouse anti-human IgG incubated with secondary antibody (panel B). Cells were counterstained with DAPI. IBIDI and examined by confocal microscopy. Merged nucleus (DAPI) and CD81 (Alexa Flour 647) are presented. Arrowheads indicate CD81 surface staining. Scale bar is 5 µM.

3.3.1.6.2 Flow cytometry- expression of CD81 on hepatoma cell lines

Both Huh7.0 and HepG2 cells grow as adherent cells attached to culture flasks and treating cells with trypsin allows the cells to detach. By contrast, treatment of these cells with EDTA alone is not sufficient to release the attached cells. However, trypsin may destroy cell surface markers required for HCV E2 binding. To overcome this problem and to develop a semi-quantitative $srE2^{332}$-Fc binding assay, we incubated trypsinised hepatoma cell lines in 5% CO_2 at 37°C for different times after detaching cells to allow regeneration and surface display of cell surface markers. Then, Anti-CD81-PE conjugate was added to cells, the cells were fixed and analysed by flow cytometry. Although Anti-CD81-PE binding could be detected on Huh7.0 cells and Huh7.5 cells immediately after lifting cells with trypsin (0 time point) (**Fig. 3.3-10A**), incubation of cells for 90 minutes and 6 hours post-trypsin showed a marked improvement in Anti-CD81-PE signal detection. High levels of CD81 expression on Huh7.0 and Huh7.5 cell lines were detected and the signal increased with time showing an optimum level around 90 minutes after trypsin addition. Thus, cells plated and incubated for 90 minutes show restored levels of receptor expression and this time interval was used for all flow cytometry experiments that involve Huh7 cells. In these experiments HepG2 cells showed detectable Anti-CD81-PE signals; indicating the presence of low levels of CD81receptors on the HepG2 cell surface (**Fig. 3.3-10B**). This finding differs from those of other researchers who found no detectable CD81 expression on HepG2 cells by flow cytometer analysis (Narbus *et al.*, 2011; Zhang *et al.*, 2004a). These differences may be due to the methodology of preparation or the use of different anti-CD81 sera. Significantly, the density of surface CD81 on HepG2 was about 64 % and 69% lower than the level of expression on Huh7.0 and Huh7.5 cells. Extended culture of hepatoma cells in suspension for 24 hours prior adding anti-CD81 sera revealed a 12-fold improvement in Anti-CD81 PE flourscence on Huh7 compared with the level of expression detected at 90 minutes post-trypsin addition (**Fig. 3.3-10A**); this indicates

continuous and high level CD81 expression and accumulation on Huh 7.0 cells forced to grow in suspension. HepG2 cells also displayed about 2-fold more receptor binding activity following extended post-trypsin culture (**Fig. 3.3-10B**). Though the levels are low by comparsion to Huh7 cells the results indicate that HepG2 cells express low levels of CD81 and not totally lacking CD81 expression. To confirm specific recognition of surface CD81, we incubated target cells with a serial dilution of anti CD81-PE conjugate after 90 minutes and 180 minutes post-trypsinisation of Huh7 and HepG2 cells respectively. Our data showed similar fluorescence detection on Huh7.0 and Huh7.5 cells (**Fig. 3.3-10C**). In contrast, HepG2 cells displayed low levels of CD81 (**Fig. 3.3-10C**).

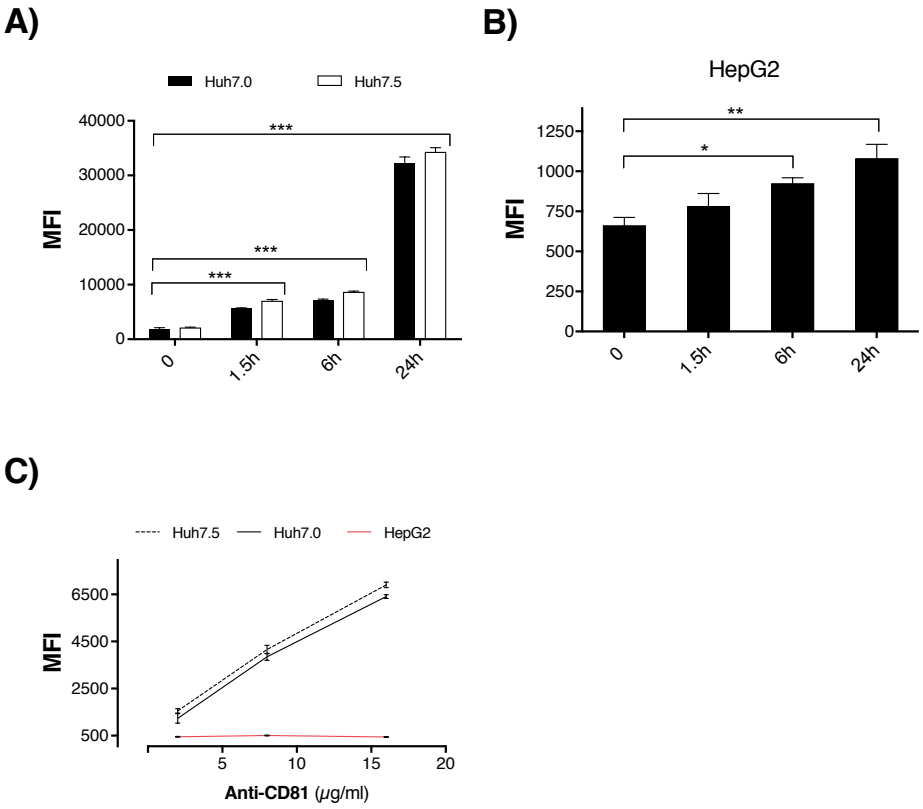

Figure 3.3-10 CD81 expressed highly on Huh7subclone and fairly on HepG2.
(A and B) Cells were lifted from flask with 0.05% Trypsin-EDTA and then washed. Cells suspended in 10% FBS containing DMEM or MEM media in falcon tube for Huh7.0 and HepG2 respectively and incubated at time point shown on in 5% CO2 at 37°C n incubated on SB3 rotator (Stuart) at 10 rpm. $1x10^6$ of cells in 1ml of media per sample test incubated with constant mouse anti C81-PE conjugate (1.5 µg /ml). Unbound anti-CD81sera was removed and sample was fixed with 0.5% PFA in PBS. T-test *: $p < 0.05$, **: $p < 0.01$ and **: $p < 0.001$. (C) Dose dependent response curve of trypsinised Huh7.0 and Huh7.5 incubated in falcone tube in 5% CO2 at 37°C for 90 minutes. HepG2 were incubated at same condition after trypsin addition for 180 minutes. $1x10^6$ of cells in 1ml of media per sample test incubated with mouse anti-C81 PE conjugate at different concentration shown. Unbound antibody was washed out followed with 0.5% PFA in PBS fixation. Fluorescence signal was measured by fortessa flow cytometer. For each sample, the mean fluorescence intensity is subtracted from result of irrelevant mouse anti-human IgG PE conjugate. Data values represent the mean of triplicate assays, error bars = SD.

3.3.1.6.3 Interaction analysis of srE2^{332}-Fc to Huh7.0 and HepG2

3.3.1.6.3.1 Microscopy of srE2^{332}-Fc binding to PFA-fixed hepatoma cells

In order to examine the binding properties of the srE2^{332}-Fc to hepatocytes, Huh7.0 and HepG2 were fixed with 4% PFA in PBS prior adding srE2^{322}-Fc. After 60 minutes of treating cells with srE2^{322}-Fc, goat anti-Human Fc-FITC was added to the reaction and subsequently visualised by confocal microscopy. High srE2^{322}-Fc specific FITC immunofluorescence staining was observed on both Huh7.0 and HpeG2 surface indicating presence of abundant srE2^{332}-Fc receptors on the hepatoma cell surface, which are competent for srE2^{332}-Fc binding (**Fig. 3.3-11**). Cells were also incubated with control tPA-Fc and labelled with secondary anti-Fc-FITC (**Fig. 3.3-11; Control**). Other samples were treated only with anti-Fc FITC for these probes confocal microscopy (not shown) showed no FITC signal indicating that binding to Huh7.0 and HepG2 cells is determined by the E2 component of srE2^{322}-Fc.

3.3.1.6.3.2 Flow cytometer analysis of srE2^{332}-Fc binding to hepatoma cells

After optimising a protocol to develop an effective flow cytometry based assay for Hepatoma cells treated with trypsin, we wished to confirm our confocal data of functional binding of srE2^{332}-Fc to hepatoma cell lines. We treated hepatoma cells with increasing doses of srE2^{332}-Fc at RT and probed the reaction with anti-human Fc-FITC. Our data confirm detection of srE2^{332}-Fc-dependent FITC-specific fluorescence and functional interaction of the HCV srE2^{332} domain to the surface of both Huh7.0 and HepG2 cells. The FITC fluorescence increased in proportion to srE2^{332}-Fc concentration indicating that the interaction of srE2-Fc is dose-dependent, saturable and receptor-mediated. Probing cells with ≤18.75 µg/ml of E2^{332}-Fc fusion showed a gradual increase in floursecence signal. Surprisingly, there was a marked and

reproducible increase in FITC fluorescence intensity at ≥ 37.5 µg/ml srE2^{332}-Fc which may reflect an abundance of a low capacity receptor or co-factor on Huh7.0 and HepG2 cells (**Fig. 3.3-12**). Moreover, cells were individually treated with control tPA or secondary anti Fc FITC antibodies (**Fig. 3.3-12; subtracted**) to exclude direct interaction of the Fc-region to the hepatoma cell surface and no binding was observed.

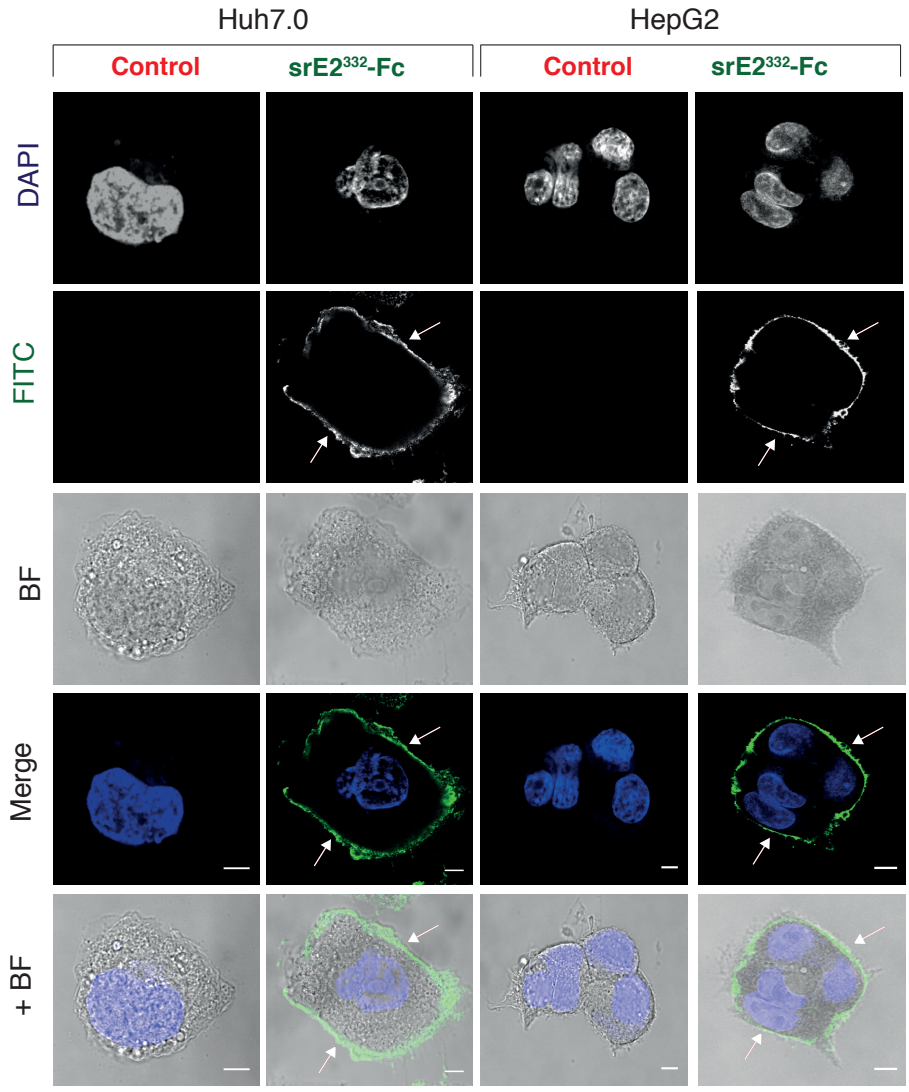

Figure 3.3-11 Functional binding of srE2^{332}-Fc to Huh7.0 and HepG2.
Lifting, growing and fixation of cells was performed as discussed in material and methodology (section 2.3.3). Cells in each well were incubated with of purified srE2^{332}-Fc (200 ng/µl) for 60 minutes at RT and bound fusion protein in each well was probed with secondary goat anti-human Fc FITC (1:50). Cells were counterstained with DAPI. IBIDI mounting media was applied to the slide followed by confocal analysis. As a control, cells were treated with the control tPA-Fc and probed with secondary conjugated antibody (control). Merged images of nucleus (DAPI) and srE2^{332}-Fc (FITC) or with bright field (+BF) are presented. Arrows indicate srE2^{332}-Fc staining on cell surface. Scale bar is 5 µM.

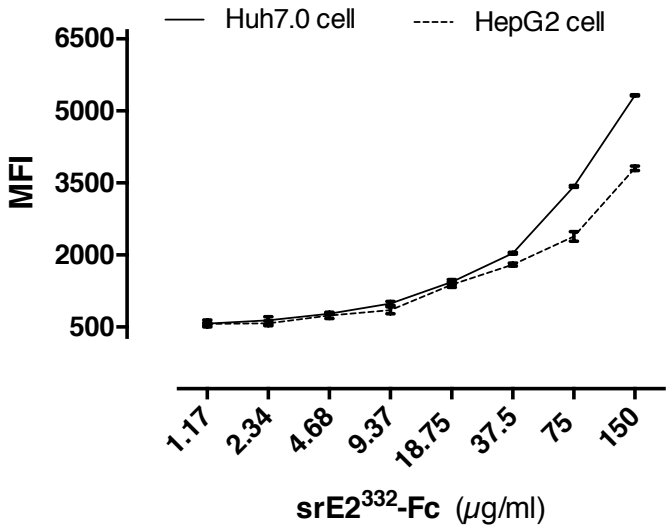

Figure 3.3-12 Dose-dependent binding of srE2^{332}-Fc to Huh7.0 and HepG2.

The method for sample preparation and FCM analysis was adapted from section (3.3.1.6.2). Target cells were treated with E2^{332}-Fc at the concentrations shown and probed for bound srE2^{332}-Fc with secondary goat anti-Human Fc FITC (1:500) and detected by flow cytometry. Control samples were incubated with tPA-Fc and secondary anti-human Fc FITC and basal MFI from these controls was subtracted from each of the data points shown. Data are mean and standard deviation from triplicate assays.

3.3.2 Comparison of truncated srE2-Fc forms interaction with 293T, Huh7.0 and HepG2

We wished to test the ability of different deleted E2 glycoprotien fusions (srE2^{295}-Fc, srE2^{278}-Fc, srE2^{265}-Fc and srE2^{195}-Fc) to bind to the human cell surface, and to compare the activity of the deleted forms with the full-length E2-Fc fusion. We therefore performed confocal and flow cytometer analysis to test binding to 293T cells and hepatoma cells.

3.3.2.1 Confocal analysis of binding to 293T

The srE2^{332}-Fc and its derivatives were incubated with cultured 293T cells already fixed with 4% PFA. Subsequently, the mixture was labelled with goat anti-FC FITC sera. A set of 293T cells were incubated with primary mouse anti-CD81 and secondary goat anti-mouse FITC conjugate to address the presence of the CD81 attachment factor on the 293T cell surfaces and the binding of srE2 deleted forms. The fluorescence intensity of secondary goat anti-human Fc FITC conjugate labelled srE2^{332}-Fc was detected on the outer surface of 293T in the form of abundant fluorescent dot complexes distributed on the outer membrane of the cells, indicating the functional binding of the srE2 full-length fusion, which is consistent with quantitative results obtained for the interaction of srE2^{322}-Fc to 293T cells by flow cytometry (3.3.1.2). Importantly, a FITC signal was detected on the 293T surface of the 293T treated with srE2^{295}-Fc, srE2^{278}-Fc and srE2^{265}-Fc and it was similar to the fluorescence appearance of srE2 full-length protein expression, which reflects the functional interaction of these E2 derivatives to the 293T surface. In addition, the fluorescence dots detected on cells treated with goat anti-mouse FITC conjugate (labelled mouse anti CD81) were similar to the appearance of the dots identified on the 293T surface upon incubation with antihuman-Fc FITC. This provides evidence that srE2^{295}-Fc, srE2^{278}-fc and srE2^{265}-Fc forms might interact with the CD81 receptor on 293T. Interestingly, cells incubated with srE2^{195}-Fc showed exceedingly weak fluorescence intensity of FITC

conjugate that located as a few dots, with substantial distance between them, over the outer membrane of 293T cells; Thus, the $E2^{195}$-Fc form binds poorly to PFA fixed 293T cells, which is likely due to poor interaction of $E2^{195}$ domain to the abundant CD81 on the 293T cell surface (**Fig.3.3-13**).

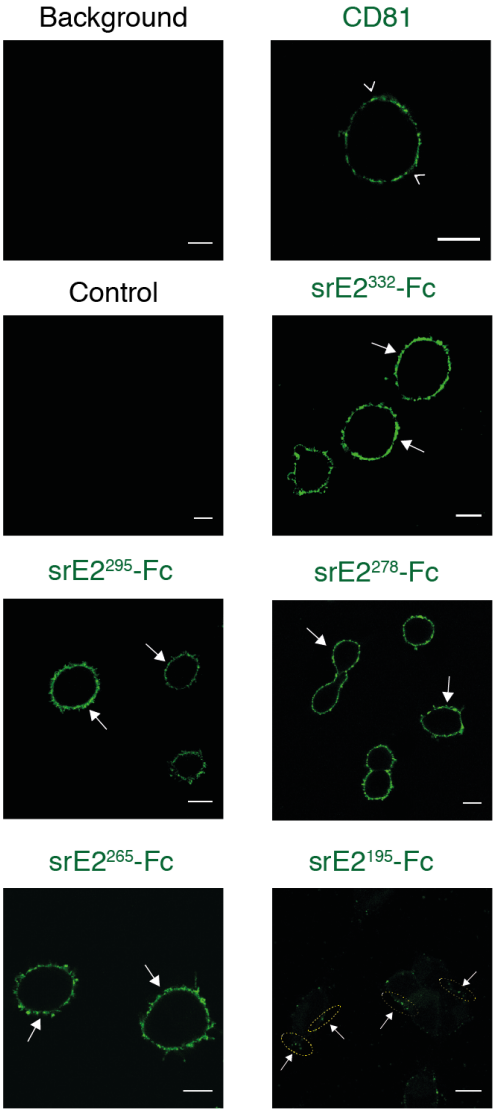

Figure 3.3-13 Binding of srE2^{332}-Fc and its derivatives to 293T.

The lifting, growing and fixation of cells methodology was performed according to material and method (section 2.3.3). Cells in each well were incubated with purified srE2^{332}-Fc (200 ng/µl) and the bound fusion protein probed with secondary goat anti-human Fc FITC (1:50). IBIDI mounting media was applied to µ-Slide wells and imaged by confocal microscopy. A set of cells were treated with tPA-Fc as negative control or not treated with srE2-Fc fusion as a background control. The various fusion proteins, srE2^{295}-Fc, srE2^{278}-Fc, srE2^{265}-Fc and srE2^{195}-Fc (FITC), are presented. Arrows indicate srE2^{332}-Fc staining on the cell surface. The scale bar is 5 µM.

3.3.2.2 Flow cytometer analysis of interaction of E2-Fc forms to 293T cells

To compare the reactivity of generated truncated glycoprotein forms to cell surface receptors, 293T cells were incubated with each deleted envelope fusion then labelled with secondary goat anti-Fc FITC conjugate and analysed by flow cytometry. FITC-specific fluorescence signals on cells treated with srE2^{295}-Fc and srE2^{278}-Fc and srE2^{265}-Fc detected and was consistent with the confocal data of PFA fixed 293T cell surface recognition by E2 deleted forms (**Fig. 3.3-14**). In terms of the comparison of the binding capacity to 293T cells, srE2^{332}-Fc displayed the most robust interaction with the cell surface, which makes it a competent HCV envelope fusion to conduct further host interaction studies. Relative to the full-length parental construct srE2^{332}-Fc, the truncated fusion proteins srE2^{295}-Fc, srE2^{278}-Fc, and srE2^{265}-Fc were mildly but progressively impaired for cell binding and were 9.97%, 19.61 % and 60.65% lower, respectively, than the binding activity of srE2^{332}-Fc. It is important to note that the envelope-specific FITC-fluorescence on cells treated with srE2^{195}-Fc was a fraction (97.52% lower) of that shown by srE2^{332}-Fc fusion and was consistent with the data achieved by confocal analysis (3.3.2.1). Thereby, providing evidence that the interaction of E2^{195} to the 293T cell surface is severely impaired. From this data I conclude that robust binding to cells requires the inclusion of E2 amino acids that are C-terminal to residue G^{195}.

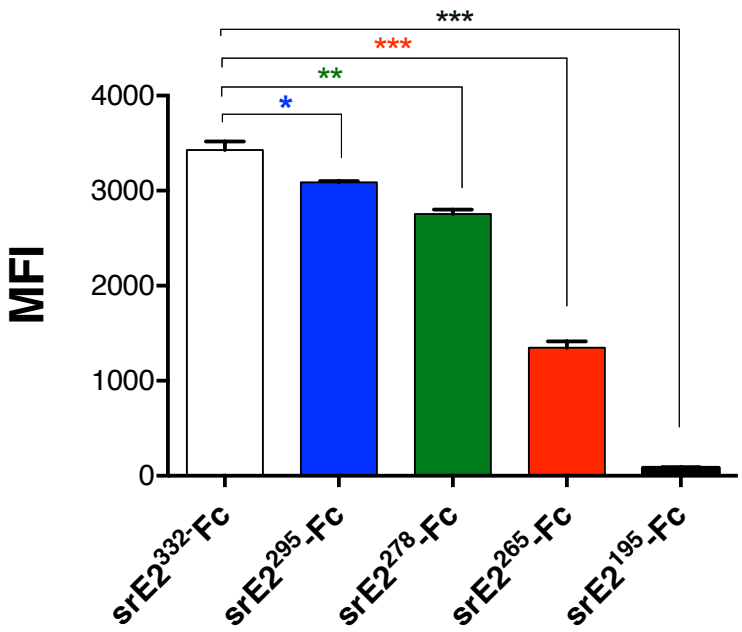

Figure 3.3-14 Different binding capacity of srE2^{332}-Fc derivatives for interaction to the 293T cell surface.

Detached 293T cells were treated with 25 µg/ml of each srE2 derivative and reaction was labelled with FITC-conjugated anti-human Fc goat secondary (1:500). MFI was measured using flow cytometery. The average background binding of the control protein tPA-Fc was subtracted from all data values shown; data values represent the mean of triplicate assays, error bars = SD. Upper large N-Zigzag line represents P-value between srE2^{332}-Fc fusion and each individual E2 derivative (srE2^{295}-Fc, srE2^{278}-Fc, srE2^{265}-Fc and srE2^{195}-Fc). T-test *: $p < 0.05$, **: $p < 0.01$ and ***: $p < 0.001$.

3.3.2.3 Confocal imaging of binding to Huh7.0 and HepG2 cells

We wished to analyse the binding ability and pattern of interaction of our soluble recombinant E2-derivatives to PFA fixed hepatoma cell lines. Immunofluorescence staining of goat anti-human Fc FITC-conjugate that bound to srE2^{295}-Fc, srE2^{278}-Fc and srE2^{265}-Fc was expressed on the outer surface of Huh7.0 and HepG2, indicating the functional binding of E2 glycoprotein deleted forms to hepatoma cells. In addition, the staining on the two cell types exhibits a very similar pattern on the outer cell surface and was similar to that of srE2^{332}-Fc interaction to PFA fixed hepatoma cell lines. This result may be evidence of high level expression of the cellular factors involved in HCV E2 binding to Huh7.0 and HepG2 cells. Interestingly, srE2^{195}-Fc FITC-specific fluorescence showed only a few distinctive circular shaped fluorescence bodies, which was higher in number on the surface of HepG2 cells than Huh7.0 cells. This finding differs from the fluorescence appearance of other E2 deleted forms interacting with hepatoma cells which may indicate the unique binding of E2^{195} peptide fusion to distinct and alternative factors on both Huh7.0 and HepG2 cells (**Fig. 3.3-15**).

A)

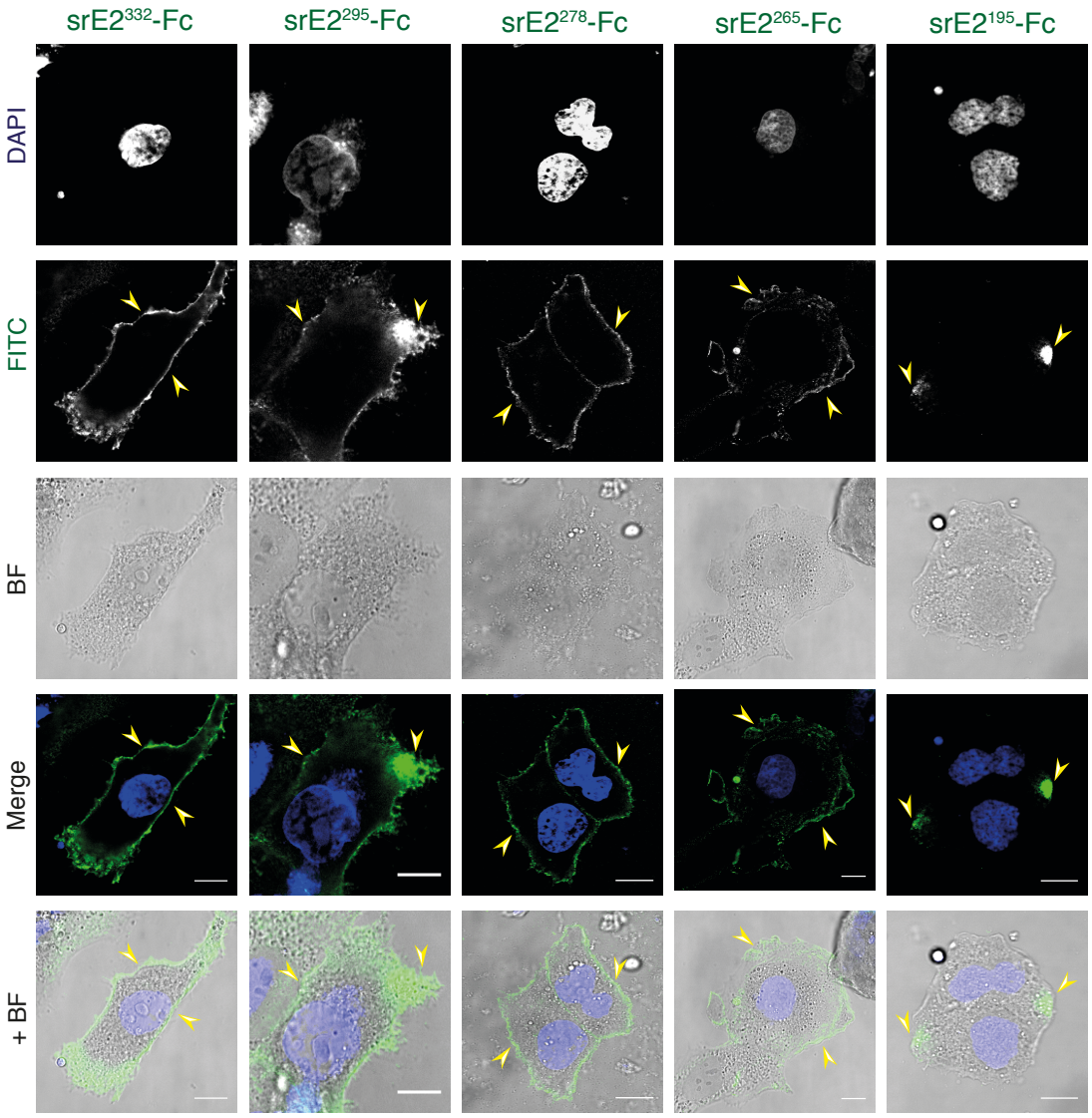
srE2332-Fc
srE2295-Fc
srE2278-Fc
srE2265-Fc
srE2195-Fc
DAPI
FITC
BF
Merge
+ BF

B)

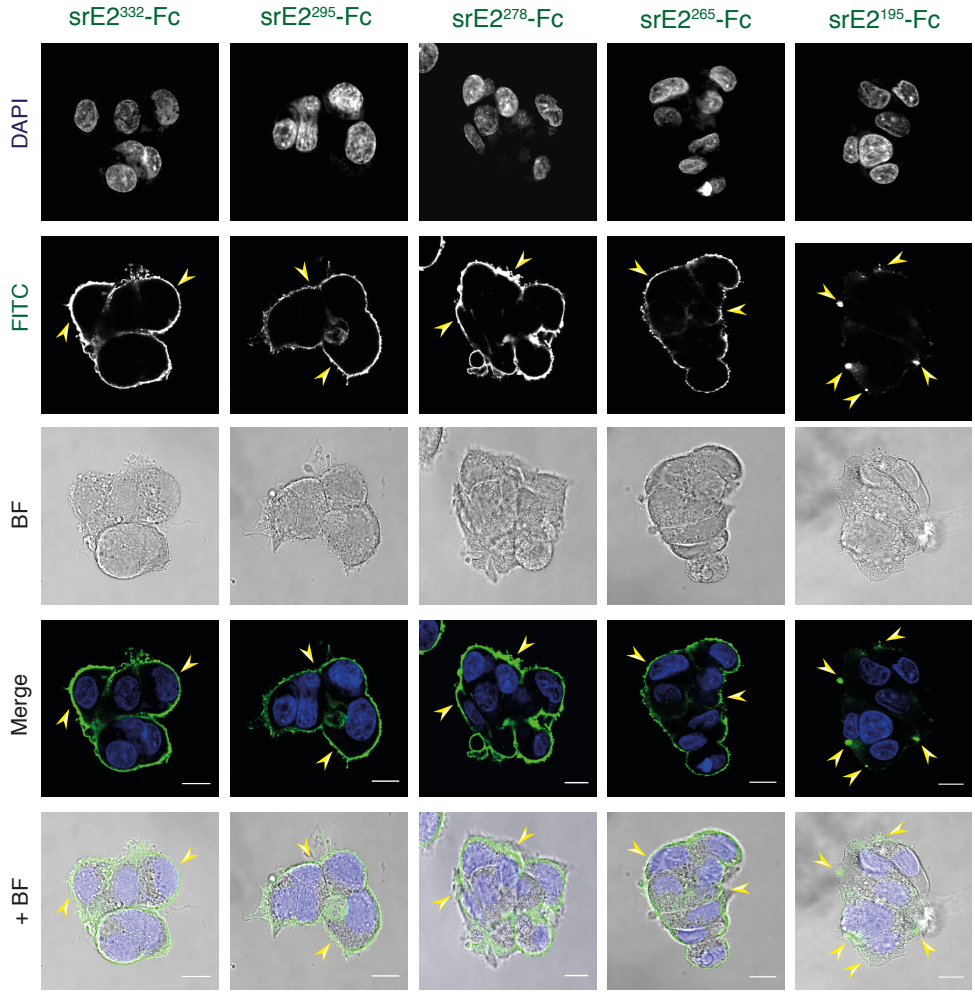

Figure 3.3-15 srE2-Fc derivatives interact with the surface of Huh7.0 and HepG2.

The lifting, growing and fixation of cells methodology was performed as discussed in material and methodology (section 2.3.3). Huh7.0 (Panel A) and HepG2 (Panel B) cells were treated with 200 ng/µl of purified recombinant E2 peptide derivatives (srE2^{295}-Fc, srE2^{278}-Fc, srE2^{265}-Fc and srE2^{195}-Fc) for 60 minutes at RT and bound fusion protein in each well was probed with secondary goat anti -human Fc FITC (1:50). Cells were counterstained with DAPI to stain DNA and imaged by confocal microscopy. Cells incubated with srE2^{332}-Fc were used as a positive control and with tPA-Fc as a negative control (not shown). Merged nuclear (DAPI) and srE2^{332}-Fc (FITC) or with bright field (+BF) are presented. Arrowheads indicate srE2-Fc derivatives staining on cell surface. The scale bar is 10 µM.

3.3.2.4 Flow cytometry- interaction of E2-Fc forms with hepatoma cell lines

We compared the srE2 interaction with hepatoma cells by incubating cells with each E2-Fc truncated fusion and labelled with FITC-conjugate to goat anti-human FC and measuring the fluorescence signal using flow cytometry. FITC-specific fluorescence on Huh7.0 and HepG2 surfaces in the presence of srE2-Fc deleted forms that express 295a.a, 278a.a and 265a.a sequences was detected, indicating interaction with surface attachment factors on these cells. Regarding the capacity for interaction with the cell surface, $srE2^{332}$-Fc exhibited high binding capacity to Huh7.0 followed by the closely related $srE2^{295}$-Fc and $srE2^{278}$-Fc, then $srE2^{265}$-Fc. Importantly, treating CD81 severely deficient-HepG2 showed a higher affinity interaction of $srE2^{278}$-Fc followed by the closer relative binding capacity of $srE2^{332}$-Fc, $srE2^{265}$-Fc and then $srE2^{295}$-Fc binding to HepG2 (**Fig. 3.3-16**). However, a relatively weak interaction was achieved with Huh7.0 for cells treated with $sE2^{195}$-Fc, and the mean fluorescence intensity of anti-Fc FITC detected on HepG2 cells was higher and consistent with data obtained from treating PFA fixed hepatoma cell line (section 3.3.2.2). From the accumulated data, I conclude that there are alternative attachment factors, other than CD81, that have the capacity to bind the $srE2^{195}$-Fc fusion.

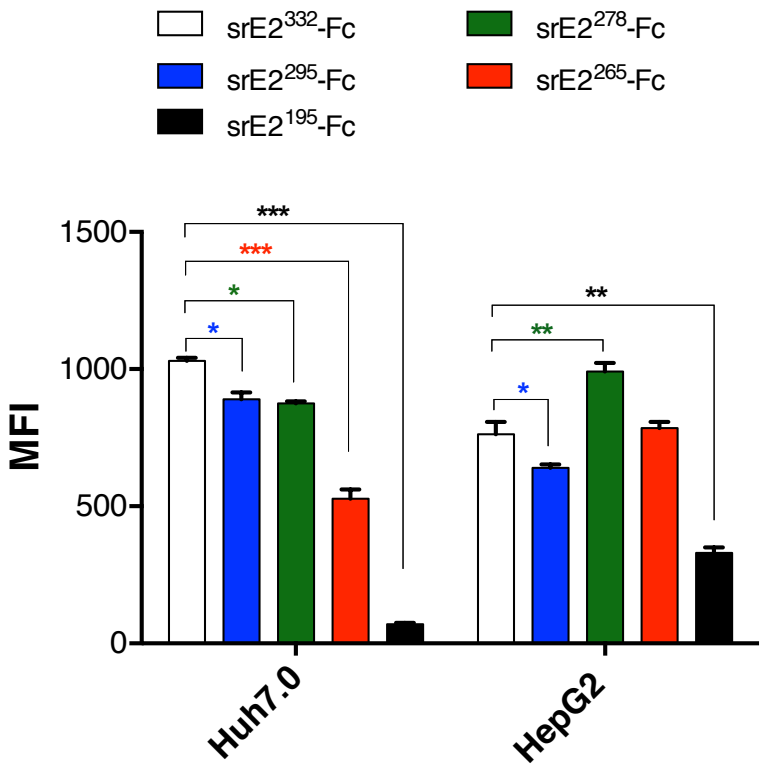

Figure 3.3-16 srE2^{295}-Fc, srE2^{278}-Fc, srE2^{265}-Fc and srE2^{195}-Fc fusions bind differently to Huh7.0 and HepG2 cells.

Hepatoma cells treated with 15 µg/ml E2 variants and the bound envelope was labelled with FITC-conjugated anti-human Fc goat secondary (1:500). MFI was measured by flow cytometery. The average background binding of the control protein tPA-Fc was subtracted from all data values shown; data values represent the mean of triplicate assays, error bars = SD. Upper large N-Zigzag line represents P-value between srE2^{332}-Fc fusion and each individual E2 derivative (srE2^{295}-Fc, srE2^{278}-Fc, srE2^{265}-Fc and srE2^{195}-Fc). T-test *: $p < 0.05$, **: $p < 0.01$ and ***: $p < 0.001$.

3.3.2.5 Analysing the binding of E2 derivatives to MBP-CD81 LEL

We wanted to analyse if our produced truncated residues of E2 envelope fusion could recognise the functional large extracellular loops of CD81 in the same manner as srE2^{332}-Fc, which successfully and specifically recognises the CD81 LEL-domain fused to a MBP fusion partner. To address this, we adapted the ELISA method described in section (3.3.1.4.4). ELISA plates coated with MBP-STOP showed no binding activity for the panel of E2 variants. By contrast, functional binding of labelled soluble E2^{295}-Fc, srE2^{278}-Fc, srE2^{265}-Fc with rMBP-CD81LEL fusion was observed (**Fig. 3.3-17**). The full-length srE2^{332}-Fc characteristically displayed more efficient low-dose binding to CD81-LEL and consistently saturated binding at lower concentrations than the other E2-derivatives. This was followed by the efficient binding of srE2^{295}-Fc and srE2^{278}-Fc to the CD81LEL, which demonstrated almost identical binding activity. Compared to srE2^{332}-Fc, srE2^{265}-Fc routinely bound to CD81 LEL with reduced efficiency and was approximately two to four times lower than the interaction affinity of srE2^{332}-Fc and both srE2^{295}-Fc and srE2^{278}-Fc, respectively. Interestingly, srE2^{195}-Fc was profoundly impaired in CD81 LEL binding **(Fig. 3.3-17**). Though srE2^{195}-Fc binding is severely impaired, this 195 amino acid region of E2 does contain motifs known to be important for binding to the CD81 receptor, (Drummer *et al.*, 2002; Kong *et al.*, 2013). This data reveals that while srE2^{265}-Fc is proficient for CD81 LEL binding as it includes most amino acid residues which were identified as the CD81 receptor binding site (Higginbottom *et al.*, 2000; Kong *et al.*, 2013), larger C-terminal deletions are not proficient for binding. Although the amino acid residues of E2 domains beyond residue 265 are not obligatory for CD81 LEL binding, our data suggest that they nevertheless contribute in a subtle manner to the efficiency of CD81 binding.

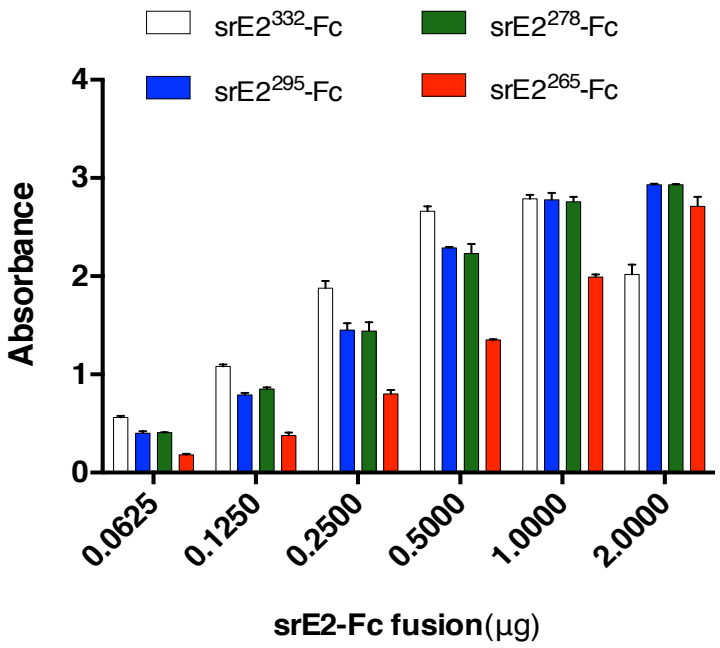

Figure 3.3-17 srE2^{295}-Fc, srE2^{278}-Fc and srE2^{265}-Fc fusions, but not srE2^{195}-Fc, bind rMBP-CD81LEL.

Purified E2 variants at the concentrations shown were added to ELISA plates coated with 1µg of MBP-CD81LEL fusion. The E2 glycoprotein binding activity was detected using anti-Human FC specific HRP conjugate secondary (1 in 5000). Absorbance of the HRP signal was measured at 450nm using ELISA plate reader. srE2^{195}-Fc binding was negative and the results was at the background level. MBP-STOP control samples were incubated with E2 variants to exclude cross-reaction to the MBP domain (not shown). The reading from the negative control tPA-Fc was subtracted from the data shown which represent the mean and standard deviation from three independent assays.

3.3.2.6 Effect of anti-CD81 Ab on binding of srE2-Fc variants to 293T cells

In order to examine the effect of anti-CD81 on the binding of srE2 deleted forms to cell-surface CD81, 293T cells were incubated with a serial dilution of mouse monoclonal anti-CD81 (5A6) unconjugated sera for 30 minutes at RT. A fixed concentration of srE2-Fc variant was added to the 293T and the reaction was labelled with goat anti-human FC- FITC secondary. MFI of FITC for cells incubated with anti-CD81 (0.5 µg/ml) showed a sharp reduction in the binding of srE2^{332}-Fc, srE2^{295}-Fc and srE2^{278}-Fc and reached an approximately 50% decrease upon addition of 4 µg/ml of anti-CD81 to 293T. srE2 ^{265}-Fc was least sensitive to anti-CD81 and retained approximately 76% binding activity for 293T cells. However, this data may demonstrate a higher capacity of srE2^{265}-Fc to bind alternative receptors compared with other E2-derivatives. Alternatively, the missing residues after A^{265}, may expose the CD81-binding sites leading to improved binding to CD81 and therefore greater resistance to competition from anti-CD81.

Despite inhibiting the binding to 293T cells, it is notable that at a certain point of anti-CD81 addition, FITC mean intensity indicated no additional antagonistic effects on srE2 fusions binding to 293T cells. This may indicate the presence of alternative limited factors other than CD81 that interact with the srE2 variants to facilitate cell surface binding (**Fig. 3.3-18**).

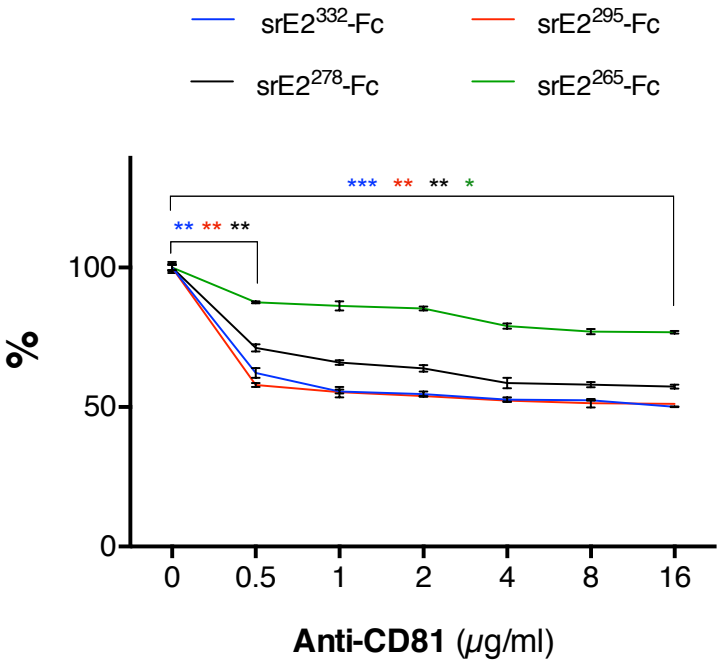

Figure 3.3-18 Anti-CD81 reduces binding of srE2 variants to 293T.
Mouse monoclonal anti-CD81 (5A6) sera at the concentrations shown was added to 293T cell for 30 minutes at RT. Then, a constant amount of the srE2-Fc variant (15 µg/ml, a minimum concentration leads to interaction with cell surface) was incubated with the 293T cells for 60 minutes at RT. Control cells were also incubated in absence of anti-CD81 sera (control). Cells were probed for bound glycoprotein with secondary anti-human-Fc-FITC conjugate serum (1 in 500). Samples were analysed by flow cytometery. The tPA-Fc fusion was used as a negative control and the basal mean fluoresce intensity from tPA-FC was subtracted from the corresponding srE2-Fc fusion data. Reduction in binding to 293T was calculated as percentage decrease according to native E2-Fc form binding in absence of anti-CD81 sera (% on Y axis). Data are mean and SD of triplicate assays. Lower small N-zigzag represents T-test for control sample and test sample (0.5 µg/ml). Upper large N-Zigzag line represents P-value between the control sample and test sample (16 µg/ml). T-test *: $p < 0.05$, **: $p < 0.01$ and ***: $p < 0.001$.

3.4 Cell surface interaction, localisation and internalisation of srE2^{332}-Fc fusions

As discussed previously, HCV attachment is the first step to occur before the virus gains access to the target cells and activates replication of its genome. Accumulated reports from cell culture studies reported that the concentration of a virus on the cell surface is likely initiated through interaction of the viral envelope glycoproteins (E1 and E2) with lipoproteins LDL, VLDL, and lipoprotein E (Chang *et al.*, 2007). Binding with GAGs is also reported and might enhance concentration of the virus on the cell surface. Subsequently, this is followed by multiple attachment steps that occur prior to effective virus entry; firstly, the envelope glycoprotein is bound by a four highly specific entry factors, i.e. CD81, SR-BI, CLDN1 and OCLN and most recently, NPC1L1. Then the virus gains entry by endocytosis in which a fusion process between the virus membrane and early endosome occurs (Dubuisson *et al.*, 2008; Meertens *et al.*, 2006; Sainz *et al.*, 2012; Takada *et al.*, 1997). The consequence of this process of attachment to the cell surface and fusion are not yet completely understood and even the critical virus proteins that participate in this process are not fully characterised. We hypothesized that the HCV envelope E2, in the absence of other virus structures, is sufficient to bind and co-localise with cell surface receptors and entry factors, and in particular with the CD81 receptor leading to internalisation into the cytosolic compartment of the target hepatocytes.

To address this hypothesis, we analysed if srE2^{332}-Fc, after initial binding to the host cell surface is efficient at promoting binding to cell surface factors and transfer across the cell membrane thereby mediating cytosolic entry.

3.4.1 Analysis of srE2^{332}-Fc ability to be localised on 293T surface

3.4.1.1 Time lapse immunofluorescence imaging of srE2^{332}-Fc incubated with live 293T

Our data show successful binding of srE2 peptide fusions to human cell lines. 293T was chosen as an initial and comparative model due to its high capacity surface interaction with srE2^{332}-Fc. One key step of our protocol included incubating cell lines with srE2^{332}-Fc fusion in 5% CO_2 and at 37°C environment (live treat) at different time lapses starting with 1 minute and maximising time up to 60 minutes. Unbound glycoproteins were washed out with 1% BSA in PBS followed by adding 4% PFA to fix the reaction event between srE2 peptide fusion and cell surface complexes. tPA-Fc fusion was incubated with cells for 60 minutes as a negative control and included mock cells which were not treated with probe (**Fig. 3.4-1, control**). srE2^{332}-Fc bound to cells was labelled with goat anti-Fc FITC conjugate and the reaction was imaged by confocal microscopy. In terms of the initial binding moment, the FITC signal was detected on the cell surface after 1 minute of treating 293T with soluble E2 peptide (**Fig. 3.4-1, 1 minutes**). Our finding indicates that srE2^{332}-Fc was able to recognise receptors on the 293T surface within 60 seconds, which indeed reflects its high binding capacity. After 5 minutes, FITC was distributed over the 293T surface (**Fig. 3.4-1, 5 minutes**), which means more binding of srE2^{332}-Fc fusion to cell surface. A more intense fluorescence signal was detected over the entire cell surface after 15 minutes of srE2^{332}-Fc incubation (**Fig. 3.4-1, 15 minute**), which suggests that the surface receptors were almost occupied with the E2^{332}-Fc fusion. Interestingly, the detection of prominent fluorescent spots in the form of discrete patches with obvious gaps over the 293T cell surface after 30 minutes of treating 293T cells was a sign that srE2^{332}-Fc fusion-cell surface complexes span the 293T cell membrane and lead to capping formation at the lateral side of the 293T cell (the region of cell-cell contact) (**Fig. 3.4-1, 30 minutes**). Importantly, fluorescent patch formation

increased over 45 minutes and aggregate to produce large well-defined capping structures (**Fig. 3.4-1, 45 minutes**). This may suggest that srE2^{332}-Fc and its associated cell surface factors accumulate overtime at specific site on cell surface. After all time lapses of incubating cells with srE2^{332}-Fc, spots remained on the outer surface of the cell and there was no sign for FITC fluorescence visualised into 293T cell cytoplasm. However, from the robust capacity interaction of srE2^{332}-Fc to attachment factors on 293T and detectable translocation over cell membrane, our finding demonstrates that 293T cells are not competent for internalisation of srE2^{332}-Fc. Live cells were treated with tPA-Fc (negative control) and showed no binding, co-localisation, or entry.

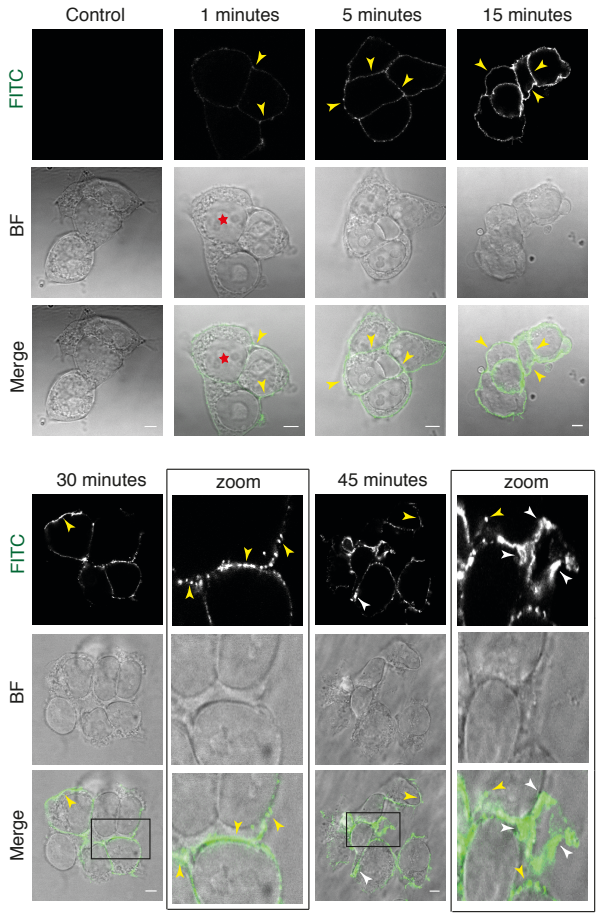

Figure 3.4-1 srE2^{332}-Fc is co-localised over 293T surface and is a component of produced capping structure complex.

srE2^{332}-Fc fusion (30 µg) was incubated overnight grown live cells (20 x10^3 cells/ single IBIDI well) in 5% CO_2 at 37°C for the time point shown. Media aspirated and treated 293T cells were fixed, blocked, washed and, bound glycoproteins probed with goat anti-human Fc FITC (1:150 in blocking solution) for 60 minutes and unbound secondary antibody washed away and the cells imaged by confocal microscopy. srE2^{332}-Fc (FITC) and merged with the corresponding BF image are shown. Control image represents 293T cells incubated with the control tPA-Fc fusion. Yellow arrowheads indicate fluorescent spots (discrete patches) and white arrowheads indicate capped structures on the cell membrane. The red star indicates nucleus. The boxed area is shown at greater magnification. Scale bar 5 µM.

3.4.1.2 Optimizing visualisation of srE2^{332}-Fc

The binding of soluble E2^{332} peptide fusion to surface factors and spanning over 293T are likely to be associated with folding changes of both srE2^{332}-Fc and host factors, which may result in masking some Fc domains fused to our E2 tag and reduced binding capacity of FITC conjugate anti-Fc sera. However, our applied protocol in section 3.4.1.1 showed good labelling for srE2^{332}-Fc upon incubation with live cells; it was important to exclude the possibility that this might have resulted from masking of the Fc domain during E2 fusion/receptor confirmation process and to confirm no entry of srE2^{322}-Fc into 293T cell cytoplasm. Therefore, we benefited from Fc features having 2 heavy domains through the incubation of 30µg E2 Fusion protein with 2x higher volume of routinely used anti-Fc FITC probes in DMEM containing 10% FBS for 60 minutes at RT with mixing samples using a rotor. This specific volume of substances was expected to allow more anti-Fc to target single srE2^{332}-Fc fusion, thus increasing probe fluorescence intensity during imaging. To avoid any precipitation that may have resulted from extra binding between E2 immunoadhesin and Anti-Fc FITC, the mixture was pelleted down at 6,000rpm for 3 minutes prior to adding it to the cell line. Then, srE2^{332}-Fc bound to anti-Fc FITC was incubated with live 293T at the same time points as was conducted in the earlier experiment (section 3.4.1.1). After live incubation, the cells were immediately fixed with 4% PFA and washed properly with 1% BSA to remove unbound full length E2 fusion bound to anti-Fc FITC. Our result showed fluorescence signal on incubated 293T cells for 15 minutes and proved that the binding of srE2^{332}-Fc to anti-Fc FITC conjugate prior to incubation does not affect the affinity interaction to 293T (**Fig. 3.4-2, 15 minutes**). At time lapses of 30 minutes, strong intensity of FITC probes was observed and expressed as fluorescence discrete patches distributed over the 293T cell surface which was evidence of the spanning stage of srE2^{332}-Fc and associated binding receptors in the form of discrete patches **Fig. 3.4-2, 30 minutes**). In addition, a fluorescence capping structure was detected on 293T, which was obviously large in size with apparent fluorescence intensity. It is

worth noting that such capping formation was not observed on 293T cells treated firstly with srE2^{332}-Fc and labelled with FITC conjugate after fixation with PFA, which is probably due to the fact of masking the Fc tag. This is consistent with the suggested view that HCV envelope-surface factors interactions leads to folding changes of E1-E2 which might be true as well for conformational changes of attachment factors on a cell surface (Dubuisson *et al.*, 2008). Longer time lapses of 60 minutes of incubation was characterised with continuing fluorescence discrete patches and capping structure formations with no significant evidence of srE2^{332}-Fc localised into 293T cell cytoplasm (**Fig. 3.4-2, 60 minutes**). Overall, this is a real indication of abundant attachment factors that bind srE2^{332}-Fc, which was co-localised over the cell membrane but these attachment factors are not enough for srE2^{332}-Fc internalisation due to the absence of a further entry factor.

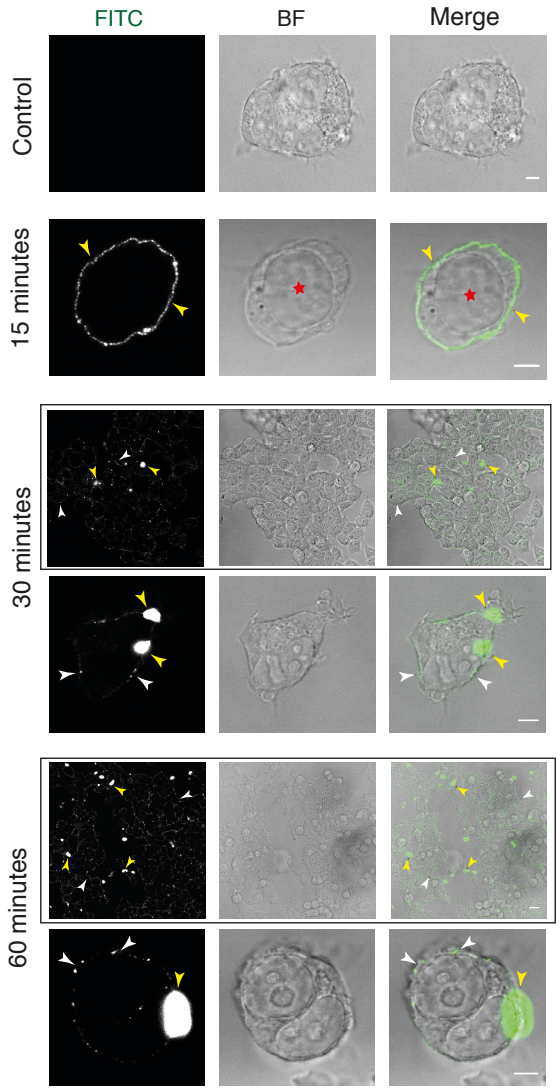

Figure 3.4-2 Capping formation reveals abundance of cellular factors that involve in localisation of srE2^{332}-Fc fusion on 293T.

srE2^{332}-Fc fusion (30 µg) bound goat anti-FC FITC conjugate was incubated with live cells in 5% CO_2 at 37°C for the time intervals shown. Treated 293T cells were fixed, washed and imaged by confocal microscopy (40x or 63x objectives). srE2^{332}-Fc (FITC) and the same image merged with the corresponding BF image are shown. Control image represents incubating 293Tcells with the control tPA-Fc fusion. White arrowheads indicate fluorescent spots (discrete patches) and yellow arrowheads indicate capping structure complex located on the cell membrane. The red star indicates nucleus. Scale bar 5 µM and 25 µM (boxed images).

3.4.2 Analysis of srE2^{322}-Fc localisation on Hepatoma cells

Live Huh7.0 and HepG2 cells were treated with full-length E2 fusion and incubated for different time points. Confocal imaging showed no detectable FITC fluorescence after 2 minutes of incubating Huh7.0 with srE2^{332}-Fc. An initial fluorescence was observed after 5 minutes of incubation and more fluorescence detected on the Huh7.0 cell surface after 10 minutes of incubation (**Fig. 3.4-3 A, 5 & 10 minutes**). Here, intense fluorescent covering of the cells might mean saturation of the Huh7.0 cell surface with srE2^{332}-Fc. Interestingly, prominent large fluorescence spots were visualised on Huh7.0 after 20 minutes and indicate cross-linking of srE2^{332}-Fc (**Fig. 3.4-3 A, 20 minutes**). The formation of discrete fluorescent patches and capping structures on the outer surface of the Huh7.0 plasma membrane was detected which may indicate lateral diffusion of srE2^{332}-Fc and its binding receptors and/or co-receptors on the plasma membrane into higher order complexes. At 30 minutes of incubation, obvious multiple fluorescent capping forms were seen in Huh7.0 cell cytoplasm with few fluorescence patches located on the plasma membrane (**Fig. 3.4-3 A, 30 minutes**). Extending incubation for 60 minutes demonstrated much more accumulation of fluorescence spots distributed throughout Huh7.0 cell cytoplasm, which indicate that srE2^{332}-Fc is successfully internalised into the cytoplasm (**Fig. 3.4-3 A, 60 minutes**). To further confirm localisation and entry of secreted E2 peptide fusion, we adapted the assay performed in section (3.4.1.2). Incubating srE2^{332}-Fc bound anti Fc-FITC with live Huh7.0 revealed obvious abundant fluorescence patches and capping forms in terms of number and size, which localised on the Huh7.0 cell membrane or crossed to the cell cytoplasm (**Fig. 3.4-3 B**).

In addition, a capping structure of significant size was detected and imaged in the cytosolic compartment of cells. This result may indicate that some Fc domains linked to full-length peptides are masked and could not be recognised when anti-Fc FITC was added after fixation of live Huh7.0. Moreover, these improvements in staining of srE2^{332}-Fc fusion when cells incubated with srE2^{332}-Fc bound anti Fc-FITC may suggest that srE2^{332}-Fc/cell surface factors

interaction leads to folding changes of srE2^{332}-Fc. This suggestion depends on the staining improvement and further investigation is required.

Overall, it provided extra evidence that binding and localisation with its associated surface factors leading to the delivery of srE2^{332}-Fc fusion into the cytosol of Huh7.0. It is worth noting that our srE2^{332}-Fc fusion was taken up by Huh7.0 cells 15-30 minutes after binding to the cell surface. This is closely consistent with the time points reported by (Coller *et al.*, 2009a; Schwarz *et al.*, 2009) in which HCVcc (JFH-1 and J6/JFH isolates) bound to Huh7.5 cells and were internalised within 23 minutes.

Treating live HepG2 cells with srE2^{332}-Fc showed a gradual increase of FITC-fluorescence on the HepG2 cells by 30 minutes of incubation and presented as small fluorescent complexes (**Fig. 3.4-4, 5-30 minutes**). This indicates the gradually slow binding of srE2 fusion to attachment factors on HepG2. Extending incubation by 45-60 minutes, resulted in the complete covering of the plasma membrane of HepG2 with FITC fluorescence in the form of discrete patches and this indicates more binding of srE2^{332}-Fc which is slowly localised over the HepG2 cell surface (**Fig. 3.4-4, 45-60 minutes**). Importantly, this hepatocyte was observed with no significant capping formation such as Huh7.0, and no signs of srE2^{332}-Fc entry into the HepG2 cell cytoplasm had been detected. This slow rate of HepG2 in the binding or localisation of srE2^{332}-Fc might be due to the density of suface expression of important factors mainly CD81 on HepG2 surface. All cells treated with the control probe (tPA-Fc fusion or with tPA-Fc bound anti-Fc FITC) showed no binding or cluster formation or entry into the cell cytoplasm.

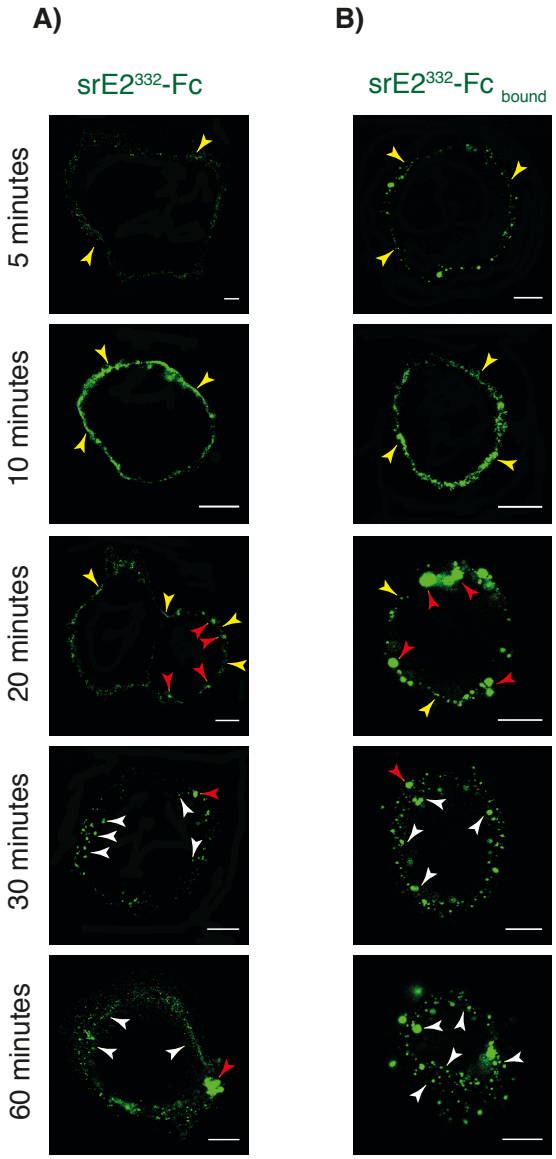

Figure 3.4-3 Incubating srE2^{332}-Fc with Huh7.0 cells results in capping of receptor complexes and translocalisation of the fusion protein into the cell cytoplasm.
Panel A: srE2^{332}-Fc fusion (30 µg) was incubated with overnight grown live cells in 5% CO_2 at 37°C for the time periods indicated. Images were analysed by confocal microscopy using 63x objective. Panel B: srE2^{332}-Fc (30 µg) bound goat anti-FC FITC conjugate was incubated with live cells in 5% CO_2 at 37°C for the time shown. tPA-Fc was used as a negative control (not shown). For both panels: yellow arrowheads indicate fluorescent spots and discrete patches and red arrowheads indicate capped structures located on the cell membrane and white arrowheads represent srE2^{332}-Fc entry. Scale bar 10 µM.

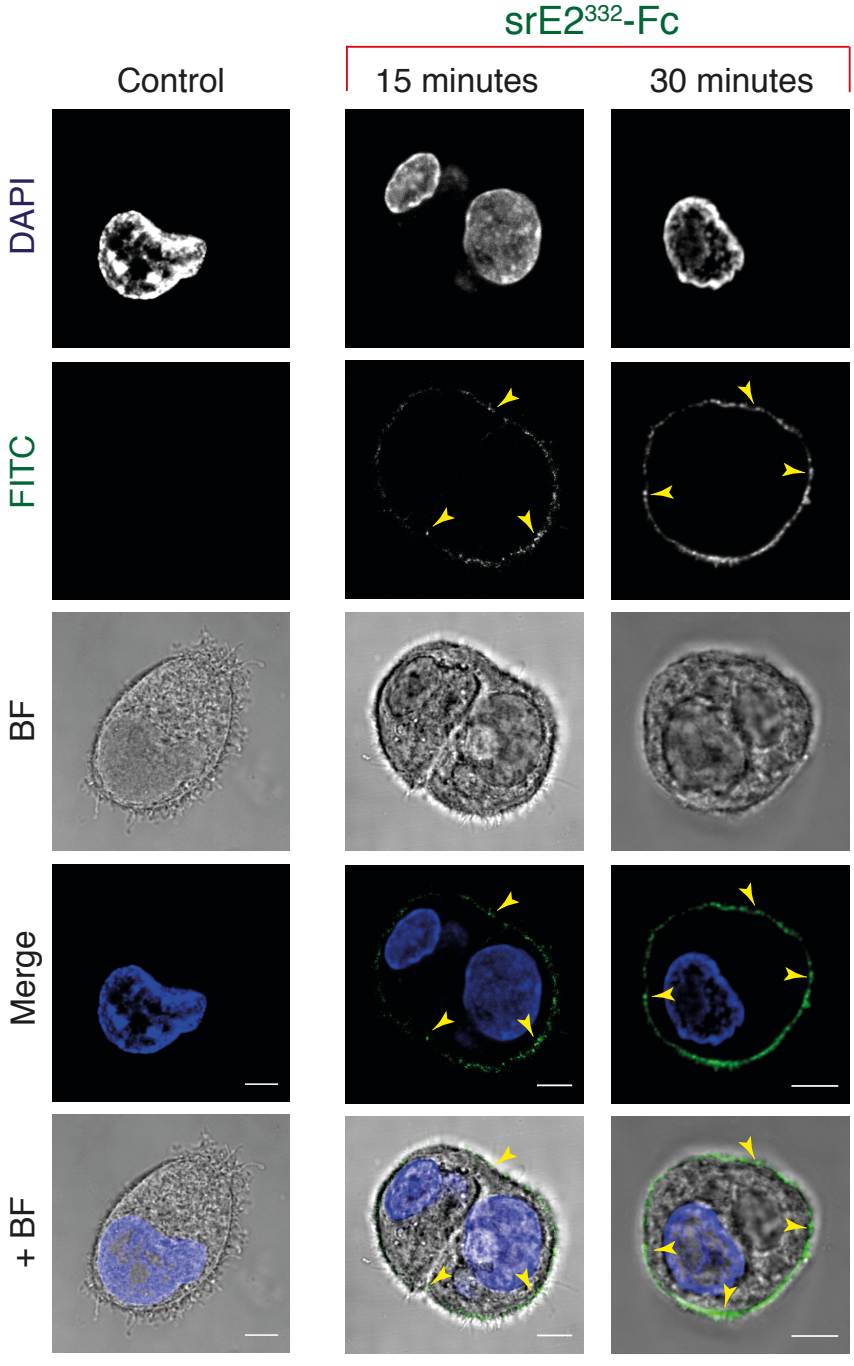
srE2^{332}-Fc
Control
15 minutes
30 minutes
DAPI
FITC
BF
Merge
+ BF

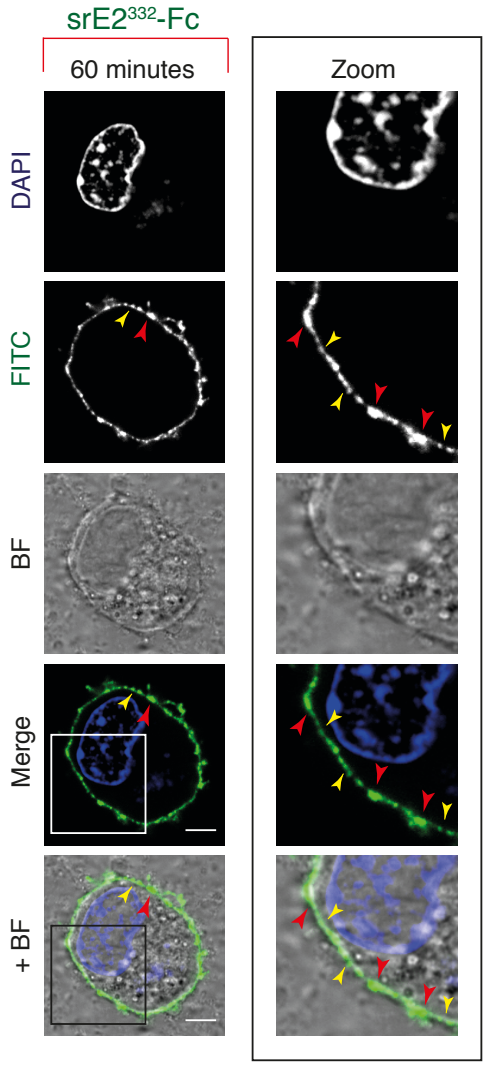

Figure 3.4-4 Live HepG2 cells treated with srE2^{332}-Fc show reduced rates of capping and no sign for entry.

srE2^{332}-Fc (30 µg) was incubated with live cells for 15, 30 and 60 minutes. Cells were analysed by confocal microscopy (63x objective). Nucleus (DAPI) and srE2^{332}-Fc (FITC) and images merged with the corresponding BF image are shown. Control image represent incubating HepG2 with tPA-Fc. Yellow arrowheads indicate fluorescent spots (discrete patches) and red arrowheads indicate capping structure located on the cell membrane. The boxed area is shown at greater magnification. Scale bar 5 µM.

3.4.3 Analysis of the expression of CLDN-1, SR-B1 and OCLN on 293T cells, Huh7.0 and HepG2 cell lines

HepG2 cells failed to localise and internalise srE2^{332}-Fc compared with the rapid internalisation observed with Huh7.0 cells. This might relate to the surface expression of single or multiple factors on HepG2 cells, which participate in the immediate binding to E2^{332} or activate other associated factors to efficiently localise and uptake srE2^{332}-Fc. Our previous data indicated that CD81 receptor expression on the HepG2 surface is exceedingly low and may be the reason for the failure of HepG2 cells to effectively internalise srE2^{332}-Fc. For greater understanding of this issue, it was important to test the expression of other surface attachment factors in particular CLDN-1, SR-B1 and OCLN on the HepG2 cell surface and to compare this with the levels of expression found on Huh7.0 and 293T cells. This will help to analyse possible correlations between the expression rate of these factors on HepG2 and the poor behaviour for srE2^{332}-Fc localisation and entry.

3.4.3.1 Confocal microscopy analysis of receptor expression

PFA fixed cell lines were incubated with primary mouse anti-CLDN1 (A-9), rabbit anti-SRB1 (ab36970) and goat anti-OCLN (Y-12) antibodies, which were then labelled with secondary goat anti-mouse Alexa Fluor 647 conjugate, goat anti-rabbit alexa Fluor 647 and anti-goat FITC, respectively. Confocal data showed the detection of 647-fluorescence conjugate that bound anti-CLDN1, indicating expression of CLDN-1 on Huh7.0, HepG2 and 293T (**Fig. 3.4-5**). On the Huh7.0 cell, CLDN-1 was observed as a scatter of small fluorescence domains with only a few complexes distributed around the outer cell membrane. In addition, we noticed a prominent larger complex at one side of each single cell, which seemed to be an accumulation of abundant CLDN-1 located laterally on the cell surface. A similar style of CLDN-1 localisation was observed on the HepG2 cell membrane. CLDN-1 was present as a few fluorescent spots on 293T cells, which may reflect a lower level of expression

for CLDN-1 on 293T cells compared with a higher expression rate on hepatoma cells.

In terms of SR-B1 expression, Alexa-Fluor-647 demonstrated abundant expression of SR-B1 on the surface of HepG2, moderate on Huh7.0 and exceedingly low level expression on 293T cells (**Fig. 3.4-6**). In terms of OCLN expression, FITC fluorescence was detected on the surfaces of hepatoma cell lines and 293T cells, which demonstrated expression of the tight-junction protein OCLN receptor on these cells (**Fig. 3.4-7**). The organisational style of OCLN was characterised as a fluorescence cluster accumulated at the lateral side of both hepatoma cell lines and 293T cells. High fluorescence intensity was observed on HepG2 cells, which may indicate abundant OCLN expression on HepG2 compared with moderate density expression on Huh7.0 and 293T. The pattern of OCLN staining on all cell lines may indicate expression of OCLN at cell-cell contact region. Treating cells with irrelevant primary antibodies which labelled with corresponding secondary conjugate or treating cells only with secondary conjugate were used as a negative control and confocal data showed no cross reactivity to cells.

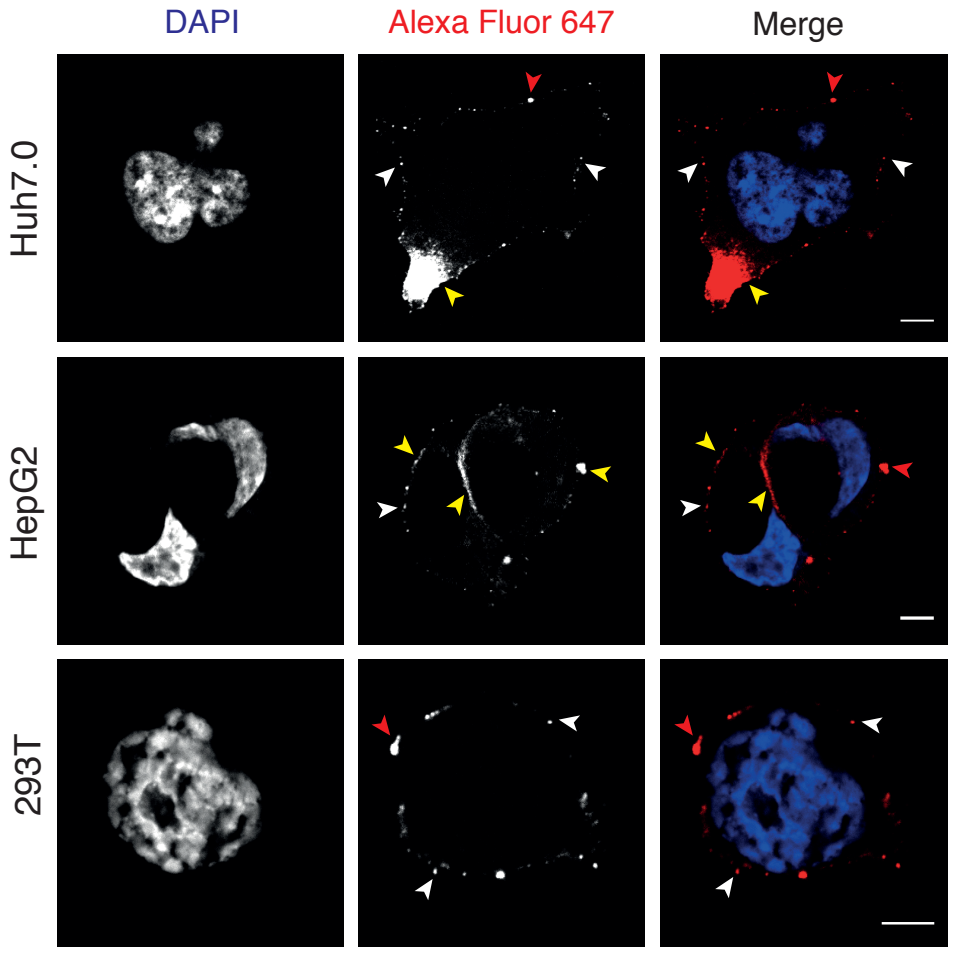

Figure 3.4-5 CLDN-1 receptor is expressed on HepG2, Huh7.0 and 293T cells.
The presence of CLDN-1 was detected by incubation cells in each µ-Slide well with 1.5 µg mouse anti-CLDN1 (A-9) for 60 minutes and the reaction labelled with goat anti-mouse alexa Fluor 647 conjugate (1 in 150) for 60 minutes. As a control background sample, cells were not treated with anti-CLDN1 or were treated with irrelevant mouse anti-human IgG and incubated with secondary antibody. Images were captured using confocal microscopy (63x scanning objective). Merged nucleolus (DAPI) and CLDN-1 (Alexa Fluor 647) are presented. CLDN-1 surface staining in the form of spots (white arrowheads), small complex (red arrowheads) and lateral prominent complexes or continuous linear complexes (yellow arrowheads) are shown. Scale bar is 5 µM.

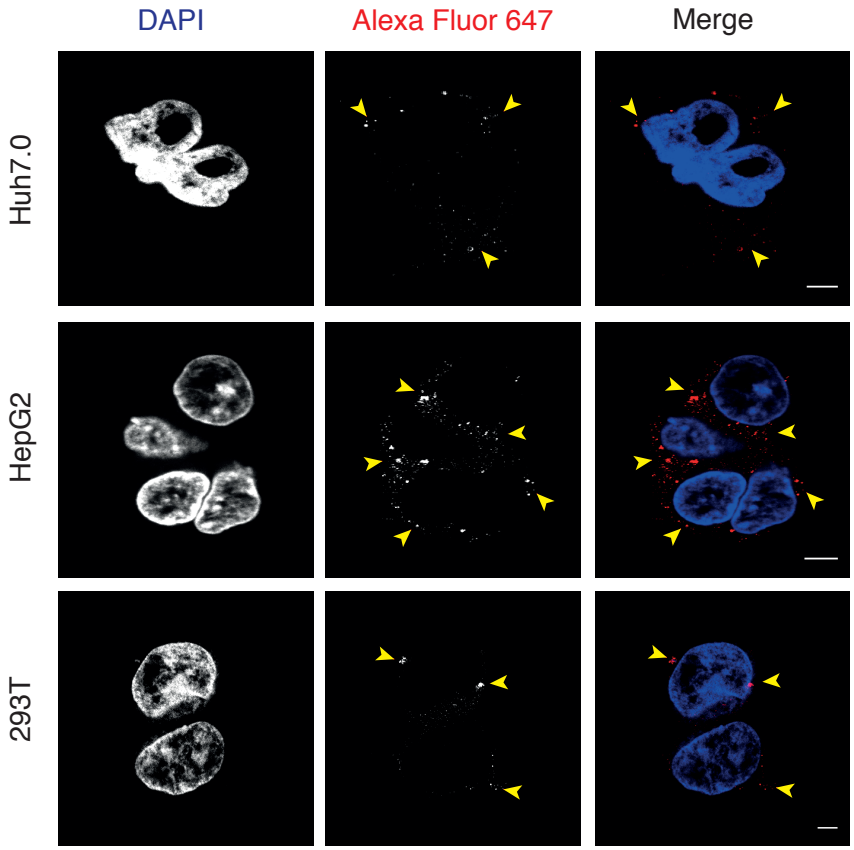

Figure 3.4-6 SR-B1 receptor expressed on HepG2, Huh7.0 and 293T cell surface. The presence of SR-B1 was detected by incubation cells in each µ-Slide well with 1:30 rabbit anti-SRB1 (ab36970) for 60 minutes and reaction probed with goat anti-rabbit Alexa Fluor 647 conjugate (1 in 75) for 60 minutes. As a control background sample, cells were not treated with anti-SR-B1 or were treated with irrelevant rabbit anti-human IgG and probed with secondary antibody. Images were captured using confocal microscopy (63x scanning objective). Merged nucleolus (DAPI) and SR-B1 (Alexa Fluor 647) are presented. Yellow arrowheads represent SR-B1 surface staining. Scale bar is 5 µM.

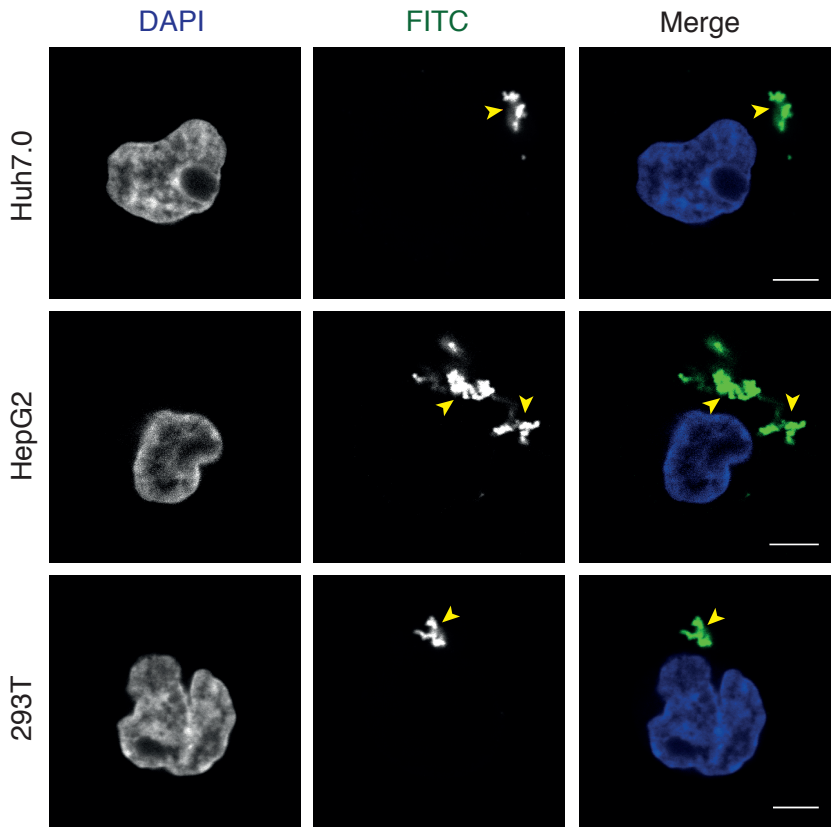

Figure 3.4-7 OCLN is expressed on Huh7.0, HepG2 and 293T.
OCLN expression was detected by incubating cells in each µ-Slide well with 1 µg goat anti-OCLN (Y-12) for 60 minutes and the reaction probed with secondary donkey anti-goat FITC (1 in 30) for 60 minutes. As a control background sample, cells were not treated with anti-occludin or were treated with irrelevant goat anti-human IgG and incubated with secondary antibody. Images were captured using confocal microscopy (63x scanning objective). Merged nucleus (DAPI) and OCLN (FITC) are presented. OCLN surface staining on the lateral side of the cell membrane is shown (yellow arrowhead). Scale bar is 5 µM.

3.4.3.2 Measurement of putative HCV receptors on cells by Flow cytometry

We wished to study the expression of receptors on hepatocyte and 293T using FCM analysis, which will add a quantitative comparison to our accumulated confocal data (section 3.4.3.1). Cells incubated with mouse anti-CLDN1 (A-9) or rabbit anti-SRB1 (H-180) or goat anti-OCLN (Y-12) antibodies at RT. The reaction was then labelled with secondary anti-mouse Alexa Fluor 647 conjugate, anti-rabbit Alexa Fluor 647 conjugate and anti-goat FITC, respectively. The fluorescence signal of conjugate on both hepatoma cell lines and 293T were measured (**Fig. 3.4-8**). The finding not only proved receptor expression but provides evidence of different expression rates by different cell types. The mean fluorescence signal of Alexa Fluor 647 conjugate of anti-mouse antibody detected on Huh7.0 and HepG2 were higher when compared with the small fluorescence value measured on 293T cells (**Fig. 3.4-8, CLDN-1**). This was consistent with the confocal data of Alexa Fluor 647 fluorescence intensity observed on PFA cells which in turn means a higher rate of claudin-1 expression on hepatocytes than 293T. The fluorescence level of FITC detected on 293T and Huh7.0 was high but was 3x higher on HepG2 indicating abundant expression of occludin on HepG2 (**Fig. 3.4-8, OCLN**). The fluorescence signal generated from Alexa Fluor 647 that bound anti-rabbit sera revealed the lowest expression of SR-B1 on the 293T surface, followed with moderate expression on Huh7.0. Interestingly, the highest expression of SR-B1 was detected on HepG2 with a value 6x higher than the expression level on Huh7.0 (**Fig. 3.4-8, SR-B1**). It seems that hepatoma cell lines vary in their expression level for surface receptors, in particular SR-B1 which has been extensively studied using HepG2 cell culture; this indicate that this cell expresses SR-B1 at a good level in comparison with other hepatoma cell lines (Rhainds *et al.*, 1999; Rhainds *et al.*, 2004; Rigotti *et al.*, 1995). The Huh7 subclone has been shown to express SR-B1 and from published data it is likely to be at a lower level of expression, as consistent with our observations (Sainz *et al.*, 2009). Incubation of irrelevant primary antibodies, labelled with

suitable secondary conjugates, were used as negative control probes and always showed negative fluorescence detection. Overall, these initial data accumulated from confocal and flow cytometry analysis showed that the slow rate of localisation and lack of efficient entry of srE2^{332}-Fc in HepG2 cells is unlikely related to these attachment factors expression and strengthen our argument that high CD81 density might support internalisation of full-length E2.

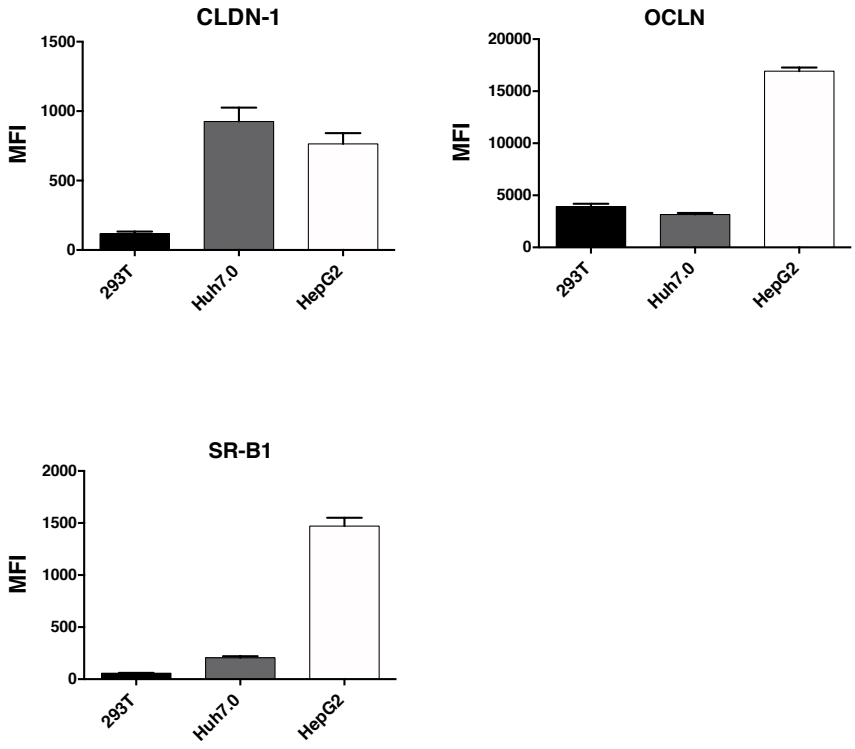

Figure 3.4-8 Hepatoma cells and 293T showed different levels of CLDN-1, OCLN and SR-B1 expression.

For CLDN-1, OCLN and SR-B1 expression, primary 1.5 µg/ml mouse anti-CLDN1 (A-9), 2 µg/ml goat anti-OCLN (Y-12) and 6 µg/ml rabbit anti-SRB1(H-180) sera, respectively, were incubated with $1x10^6$ cells and the reactions probed with secondary anti-mouse Alexa Fluor 647 conjugate (1:1000), donkey anti-goat FITC (1:500) and anti-rabbit Alexa Fluor 647 conjugate (1:1000), respectively. Fluorescence signals were measured by flow cytometery. The background fluorescence obtained from irrelevant anti-sera was deducted from each of the data points shown. Data values represent the mean of triplicate assays, error bars = SD.

3.4.4 Longer Incubation of srE2^{332}-Fc with live cell Lines

3.4.4.1 Six hours of treating cells with srE2^{332}-Fc

Live cell lines were incubated with srE2^{332}-Fc bound anti-Fc FITC for a time period longer than 60 minutes (with experimental steps adapted from section 3.4.1.2). The aim of increasing the time of incubation to six hours is to test whether time is a factor that could result in the obvious localisation or entry of srE2^{332}-Fc in HepG2. In addition, although 293T cells express high levels of CD81 incubation with srE2^{332}-Fc and resulted in the formation of capped structures on cells; it is Important to test if longer incubation of srE2^{332} with 293T cells results in initiation of E2 envelope entry. Huh7.0 cells were also incubated with srE2^{332}-Fc for extended periods of time. After six hours of incubating srE2^{332}-Fc with HepG2, intense FITC-fluorescence spots, which varied in size, were observed on the majority of HepG2 cells surfaces and some cells showed localisation of few residual fusion proteins into the cytoplasm at the area close to the inner side of the cell membrane (**Fig. 3.4-9**). We think that E2 internalisation after a long time of incubation is consistent with the low level of CD81 expressed on HepG2 cell surfaces, and that there is even entry evidence of srE2^{332}-Fc; however, it is still not efficient in terms of the time duration required for entry and number of cells that successfully internalise srE2^{332}-Fc. This finding indicates that the binding capacity of E2^{332}-Fc to surface attachment factors and capping in the presence of exceedingly low levels of CD81 still existed. This stresses the importance of efficient CD81 expression for inducing rapid localisation and entry into the cytosolic compartment in HepG2-CD81 cells. On the other hand, competent Huh7.0 showed continuous localisation and entry of srE2^{332}-Fc into the cytoplasm of each single cell (**Fig. 3.4-10**). Our finding hypothesised that there is an association between the level of CD81 expression and speed rate of E2^{332} fusion co-localisation and entry into the hepatoma derived cell line. On the vast majority of 293T cells incubated with srE2^{332}-Fc bound anti Fc FITC for 6 hours, fluorescence staining was detected on the cell surface, mainly in the form of one large capping structure on each single cell (**Fig. 3.4-11**). This

finding indicates that srE2^{332}-Fc fusion has a high capacity to bind surface factors on 293T cells and is localised over the cell surface. In addition, the lack of efficient srE2^{332}-Fc entry into 293T resulted in more condensation of E2 fusion on the cell membrane, resulting in very large capped structures. It was interesting that abundant CD81 on 293T failed to rescue efficient E2^{332} Fc fusion entry, which might relate to undefined extra specific features, found on hepatocytes and not 293T cells. As a negative control, incubating cell lines with tPA-Fc bound anti-Fc FITC showed no fluorescence detection and no cross reactivity to hepatoma or 293T cells.

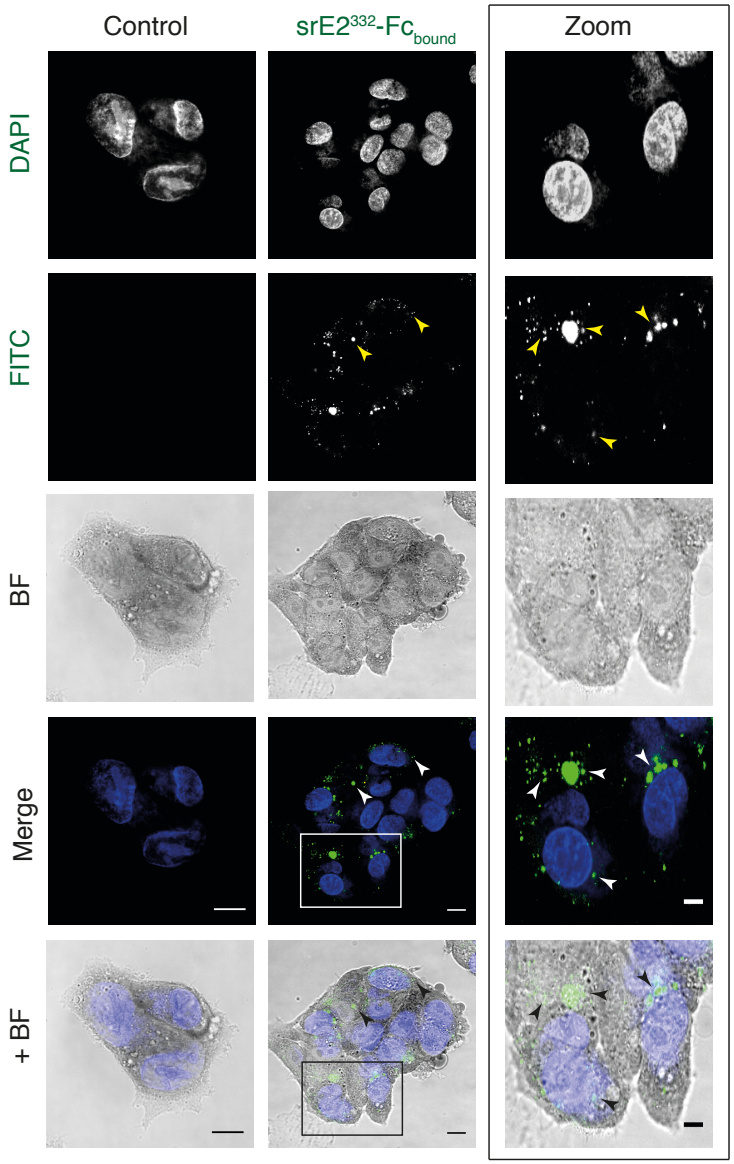

Figure 3.4-9 Six hours of incubating HepG2 with srE2^{332}-Fc results in capping formation with little fusion protein entry.
Nucleus (DAPI) and srE2^{332}-Fc (FITC) +/- same image merged with the corresponding BF image are shown. The control image represents incubating HepG2 with tPA-Fc fusion. Arrowheads indicate fluorescent capping structures located mainly on the cell membrane with exceedingly few spots in the cytoplasm. The boxed area is shown at greater magnification to the right. srE2^{332}-Fc$_{bound}$ stand for E2 peptide fusion bound goat anti-human Fc-FITC. Scale bar 10 μM and 5 μM for boxed area.

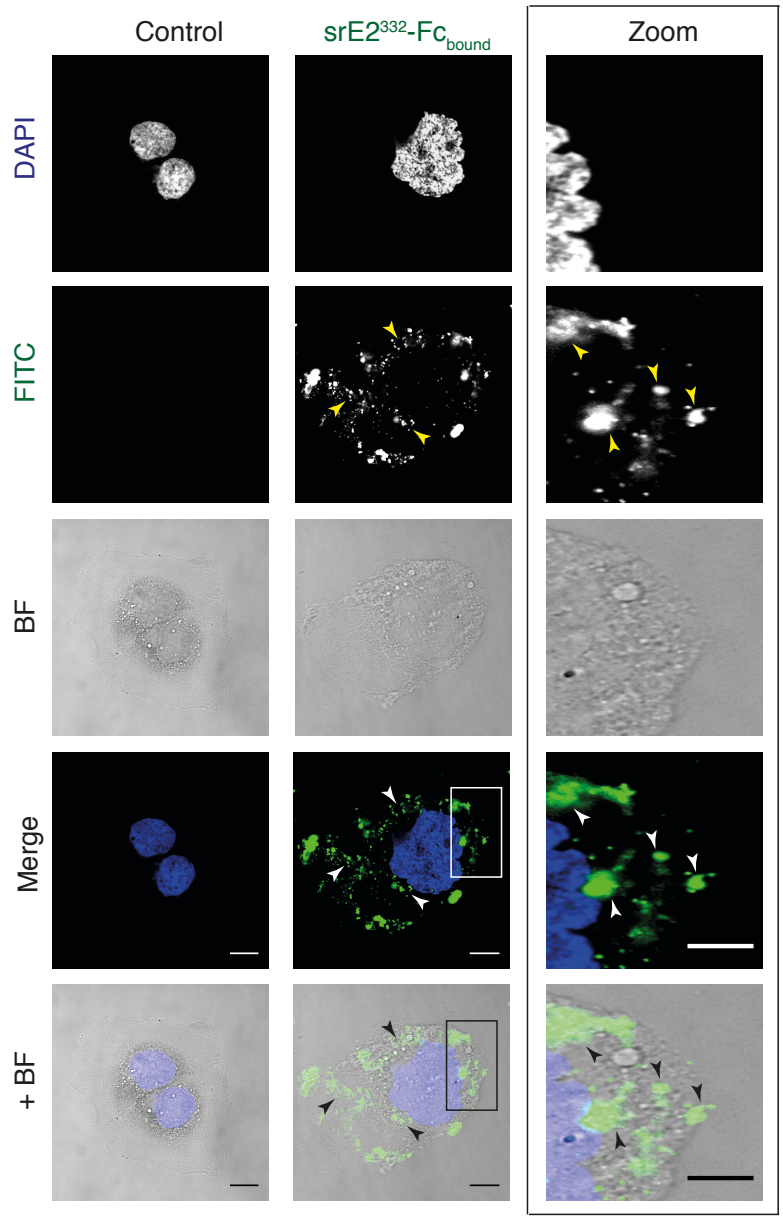

Figure 3.4-10 high level of srE2^{332}-Fc entry into cytoplasm of single Huh7.0 over six hours of incubation.

Nucleus (DAPI) and srE2^{332}-Fc (FITC) +/- same image merged with the corresponding BF image are shown. The control image represents incubating Huh7.0 with tPA-Fc fusion. Arrowheads indicate fluorescent srE2^{332}-Fc located in the cytoplasm. The boxed area is shown on the right at greater magnification. srE2^{332}-Fc$_{bound}$ stand for E2 peptide fusion bound goat anti human Fc FITC. Scale bar 10 μM and 5 μM for boxed area.

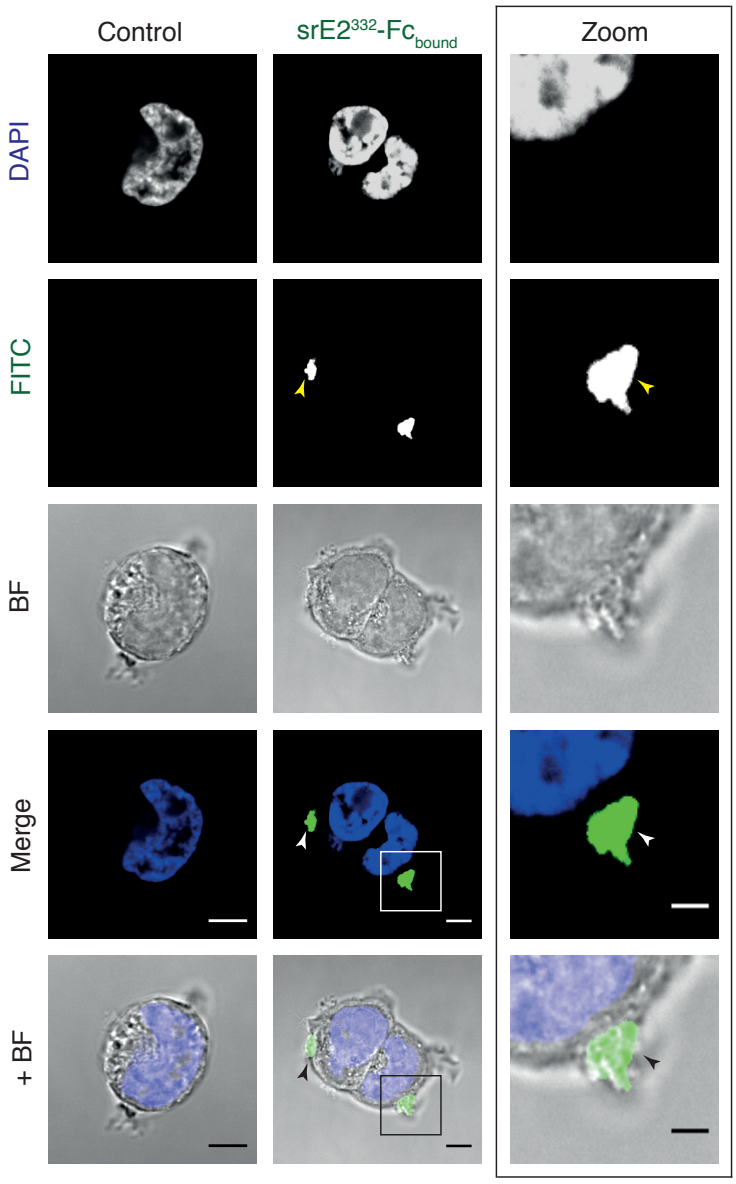

Figure 3.4-11 Incubating srE2^{332}-Fc with 293T for 6 hours does not lead to efficient entry.

Nucleus (DAPI) and srE2^{332}-Fc (FITC) +/- same image merged with the corresponding BF image are shown. The control image represents incubating 293T with tPA-Fc fusion. Arrowheads indicate fluorescent srE2^{332}-Fc fusions accumulated laterally on outside of the cell membrane. The boxed area is shown at greater magnification. srE2^{332}-Fc$_{bound}$ stand for E2 peptide fusion bound goat anti-human Fc FITC. Scale bar 5 μM and 2.5 μM for boxed area.

3.4.4.2 Z-stack- cells treated 24 hours with srE2^{332}-Fc

To confirm our specific observation of E2^{332} peptide fusion capping and entry, many sections through an individual cell already incubated with srE2^{332}-Fc fusion for 24 hours were created according to thickness by moving the microscope focus up and down through a detected amount of cell thickness (Z-Stack). Image slices were accumulated to generate a 3D structure by using the image J processing technique. To reduce exposure of fluorescence in this experiment in order to provide clearer details about the location of srE2^{332}-Fc complex, whether on the cell surface or within cell cytoplasm, anti-Fc conjugated FITC was added to the cell lines after PFA fixation. Huh7.0 combined slices confirmed observation of FITC-fluorescence in the hepatocyte cytoplasm; indicating srE2^{332}-Fc entry into the cell (**Fig. 3.4-12, Panel Huh7.0**). Importantly, large srE2^{332}-Fc-specific fluorescent complexes were a distinctive feature of the srE2^{332}-Fc that had located to Huh7.0 cell cytoplasm. We noticed that longer incubation of soluble E2^{332} -Fc with Huh7.0 resulted in its cytoplasmic accumulation in a package and located close to the nucleus. A further finding was that the cytoplasm of new dividing Huh7.0 cytoplasm contains srE2^{332}-Fc. srE2^{332}-Fc were detected as a few small fluorescent intracellular complexes distributed into the cytoplasm of HepG2 with the majority of bigger srE2^{332}-Fc Fusion complexes located on and close to the inner side of the cell membrane (**Fig. 3.4-12, Panel HepG2**). Analysing Z-slices for 293T cells showed fluorescence localisation and capping generation, which were composed of srE2^{332}-Fc bound with cellular factors, at a specific area close to the sites of filopodia formation (**Fig. 3.4-12, Panel 293T**). Moreover, obvious florescence complexes distributed on the 293T cell outer surface and podia were detected. Z-stack analysis confirmed no FITC detected in 293T cellular cytoplasm and 293T cells do not compete for efficient srE2 ^{332}-Fc entry.

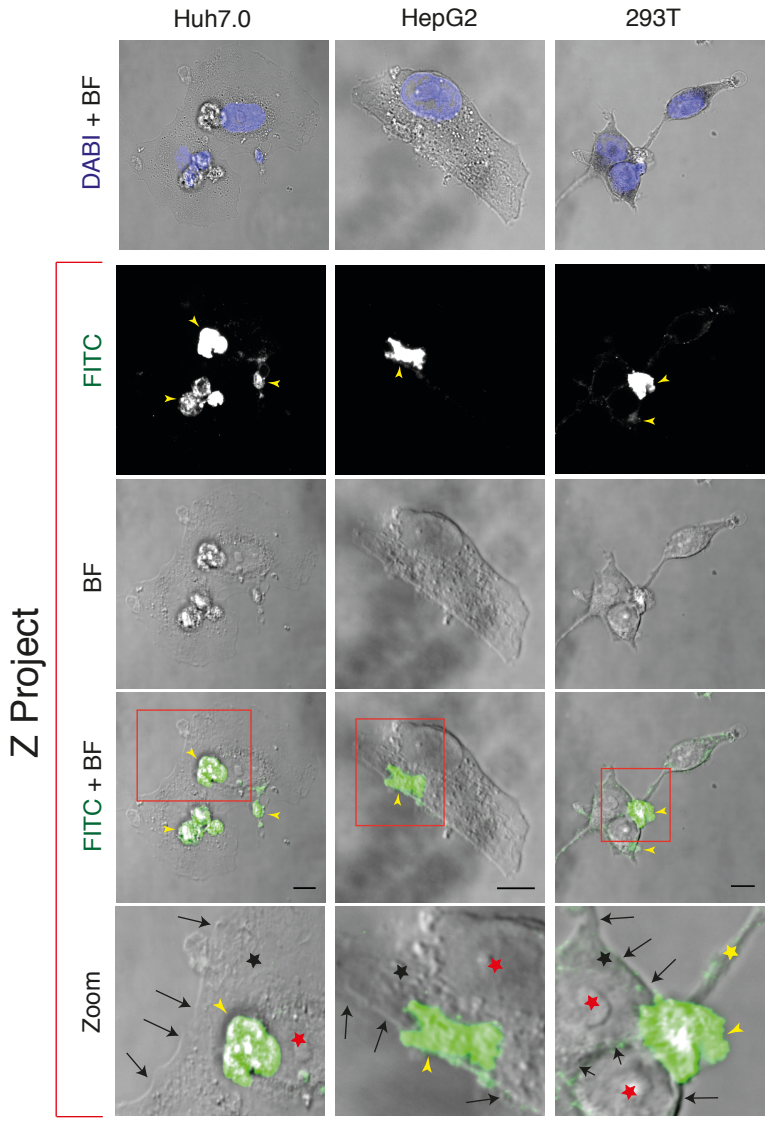

Figure 3.4-12 Z-stacking analysis of cell lines incubated for 24hrs with srE2^{332}-Fc fusion.

The full methodology of the procedure for treating cells and preparation of the slide for confocal imaging were adapted from section (3.4.1.1). Nucleus (DAPI) image is merged with the corresponding BF image and is presented as a 2D image. The sum of combined stacks imaged along the Z-axis for FITC staining (srE2^{332}-Fc) and BF series are presented as grouped Z-project. The boxed area is shown at greater magnification. Yellow arrowheads indicate srE2^{332}-Fc staining. Black arrows indicate cell surface, yellow stars indicate cytoplasm and the red star indicates nucleus. Zoom images show srE2^{332}-Fc localisation at the centre of Huh7.0 cytoplasm, intact to the outer and inner side of the HepG2 cell membrane of HepG2 and accumulation on the 293T membrane near the podia site. Scale bar 10 µM.

3.4.5 Testing incorporation of CD81 and CLDN-1 in spanning mechanism with srE2^{332}-Fc

CD81 and its CLDN-1 co-factor are primary post-binding entry receptors for HCV (Evans *et al.*, 2007; Liu *et al.*, 2009; Pileri *et al.*, 1998). A recently published report for an association between CD81 and its partner CLDN-1 during HCV entry (Farquhar *et al.*, 2012). In this work, we wished to determine whether srE2^{332}-Fc localisation over the cell surface involved CD81 and CLDN-1 receptors. Antibodies against CD81 and CLDN-1 were used to label corresponding receptors after 60 minutes of incubating srE2^{332}-Fc bound anti-Fc FITC with live cell lines. The reason behind choosing this time point was that, according to our previously accumulated data, 60 minutes was sufficient time for co-localisation of srE2^{332}-Fc on the cell surface and for capping structure formation. In addition, to prevent interference of E2^{332}-Fc binding by the primary antibody the antibody was added to the cells following treatment with srE2^{332}-Fc and the PFA fixation step. The reaction was then labelled with secondary conjugated antibody and analysed using confocal microscopy.

3.4.5.1 Cells labelled with primary anti-CD81 antibody

Live 293T cells were treated with tPA-Fc (negative control) or not treated (mock cells) for 60 minutes at 37°C. After PFA fixation, cells treated with anti-CD81 showed Alexa 647 spots on the 293T cell surface and indicated the expression of CD81 receptors and its normal distribution over 293T cell surfaces (**Fig. 3.4-13 A**). After 60 minutes of srE2^{332}-Fc incubation with live 293T cells, capping structure showed an overlay of both Alexa 647 and FITC fluorescence on the surface (**Fig. 3.4-13 B**). This is an indication that CD81 receptors spanned over the cell in association with srE2^{332}-Fc and is a key component for capping complex formation. It is important to note that no Alexa 647 fluorescence spots were detected in the cytoplasm of 293T cells, which demonstrates again that CD81 is not internalised, but remained in association with the capped structures containing srE2^{332}-Fc on the plasma membrane of 293T cells. On both mock cells and negative control cells, Alexa Fluor 647 dye

was recognised as fluorescent spots on Huh7.0 cell surface showing normal distribution of CD81 over the Huh7.0 cell (**Fig. 3.4-14 A**). Incubating srE2^{332}-Fc with Huh7.0 for 60 minutes was associated mostly with Alexa Fluor 647 fluorescence detection and an overlay with the FITC fluorescence image reveals capped structures on the cell surface and importantly within the Huh7.0 cytoplasm (**Fig. 3.4-14 B**). This finding demonstrates the involvement of the CD81 receptor in binding, localising and entry of srE2^{332}-Fc into the Huh7.0 cell cytoplasm.

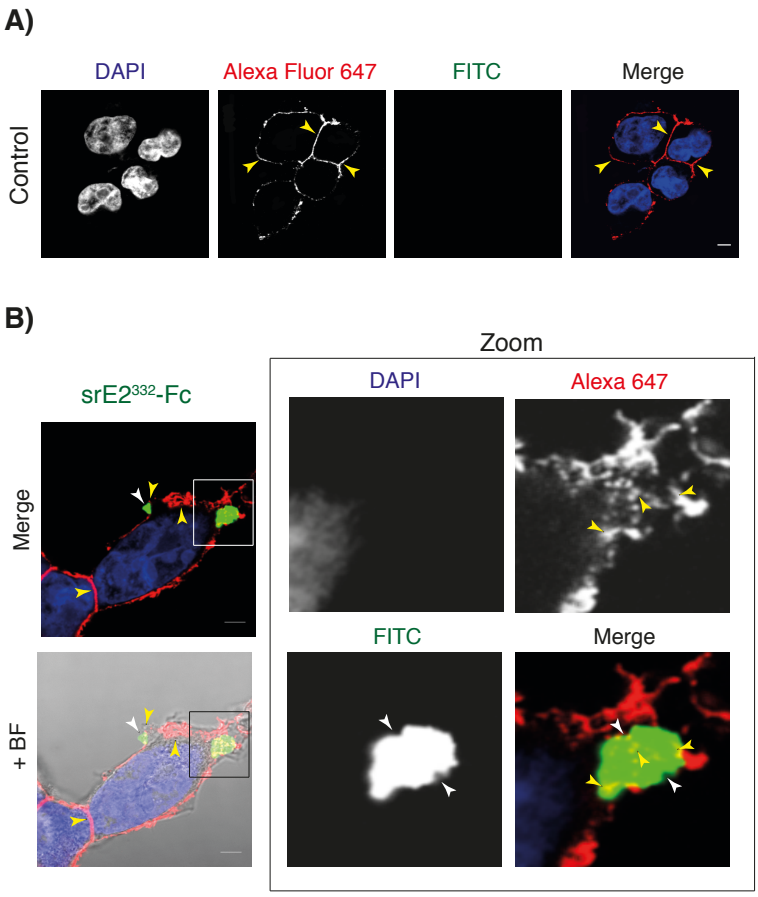

Figure 3.4-13 CD81 involve in srE2^{332}-Fc localisation and capping formation on surface of 293T cells.

Live 293T in each single µ-Slide well were treated with 30 µg srE2^{332}-Fc or tPA-Fc (control) bound goat anti-Fc FITC sera in DMEM/FBS media for 60 minutes in 5% CO_2 at 37°C. Unbound peptide fusion was washed out and cells were fixed with 4% PFA in PBS for 18 minutes at RT. 0.1% Triton X-100 in PBS was added for 5 minutes and was followed by washing with 2 mM glycine/PBS for 5 minutes at RT. Blocking solution (5% BSA in PBS) was incubated with cells for 60 minutes at RT and followed by media aspiration. CD81 presence was detected by incubating cells in each µ-Slide well with 1.5 µg mouse anti-CD81 (5A6) antibody and reaction labelled with goat anti-mouse IgG Alexa Fluor 647 secondary (1 in 150) for 60 minutes followed by the washing step. Dilute DAPI counterstaining solution was added to the well slide. IBIDI mounting media was applied to cells in wells followed by confocal analysis (63x scanning objective). Merged nucleus (DAPI), CD81 (Alexa Fluor 647) and srE2^{332}-Fc (FITC) +/- 293T cell (BF) are presented. Yellow arrowheads indicate CD81 presence on the cell surface (panel A and B) and white arrowheads indicate srE2^{332}-Fc fusion staining located on the cell surface (panel B). Boxed area is shown at greater magnification. Scale bar is 5 µM.

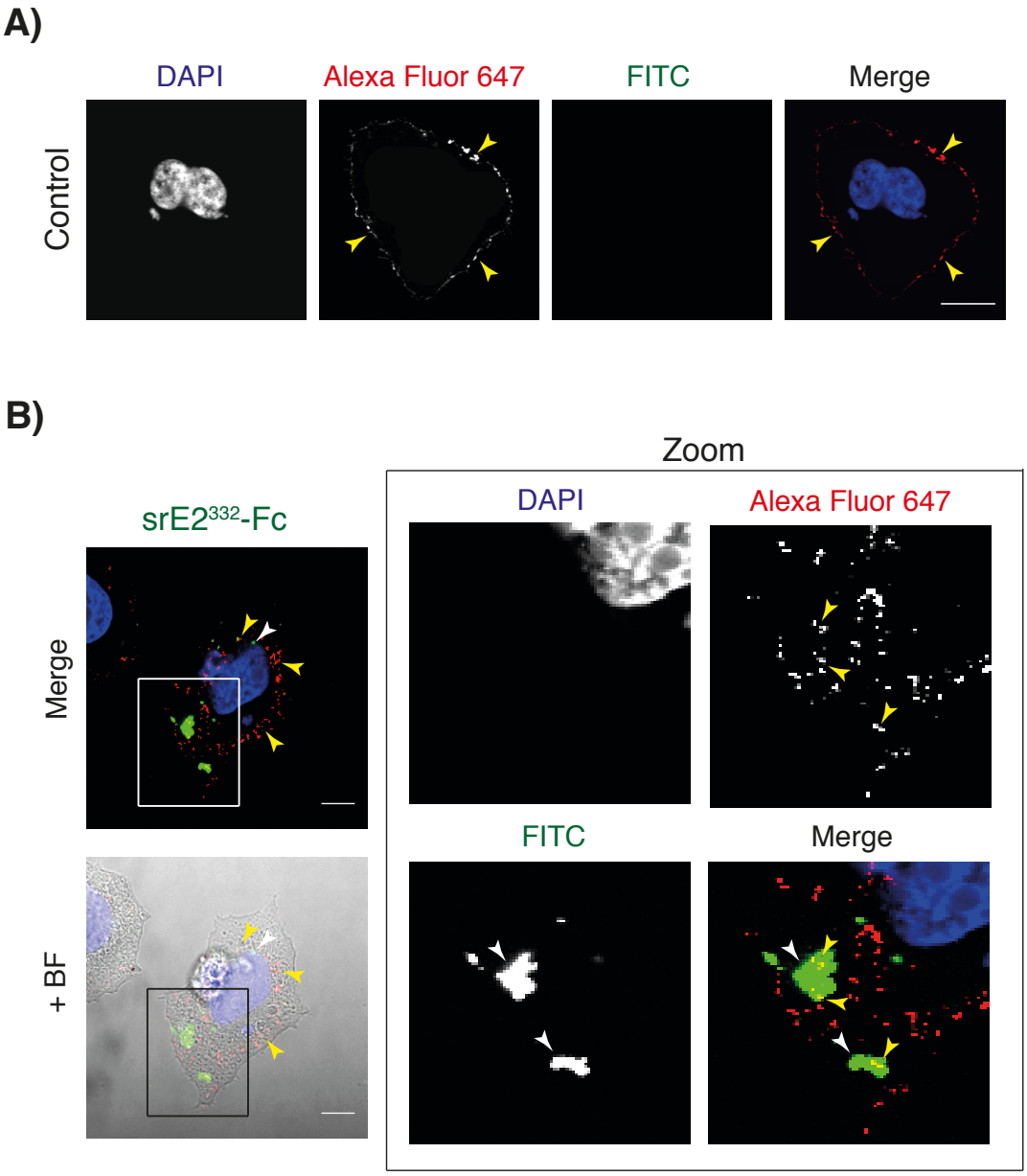

Figure 3.4-14 CD81 expressed on Huh7.0 cell associate with localisation and entry of srE2^{332}-Fc.

The methodology was performed as discussed for treating 293T with srE2^{332}-Fc fusion and labelling with anti-CD81 sera (section 3.4.5.1). Merged nucleus (DAPI), CD81 (Alexa Fluor 647) and srE2^{332}-Fc (FITC) +/- Huh7.0 (BF) are presented. Yellow arrowheads indicate CD81 expressed on the cell surface (panel A) or distributed into the cytoplasm (panel B). White arrowheads indicate srE2^{332}-Fc fusion staining located into the cytoplasm. Boxed area is shown at greater magnification. Scale bar is 10 μM.

3.4.5.2 293T and Huh7.0 probed with anti-CLDN1

Mouse anti-CLDN1 sera was able to recognise CLDN-1 on 293T cells and the CLDN-1 was distributed over the cell membrane with some CLDN-1 tending to be accumulated in lateral clusters facing the inner side of the cytoplasm but still extending to the membrane of the cell (**Fig. 3.4-15 A**). After 60 minutes of treating 293T with srE2^{332}-Fc bound anti-Fc FITC, Alexa Fluor 647 spots were detected on the outer surface of 293T cells and some spots co-localised with the FITC fluorescence capped structures (**Fig. 3.4-15 B**). This finding confirms that the CLDN-1 receptor is another component shared in capping formation. There was no sign of the accumulation of Alexa Fluor 647 fluorescence into 293T cells meaning no internalisation of CLDN-1 when srE2^{332}-Fc is present on the cell surface. In addition, the site of the capping complex was detected at a site close to an intense Alexa Fluor 647 complex, similar to that observed on control 293T cells.

Regarding to the Huh7.0 cells, Alexa 647 staining was detected on untreated cells with srE2^{332}-Fc or treated with tPA-Fc for 60 minutes (**Fig. 3.4-16 A**). The staining distribution pattern of CLDN-1 on Huh7.0 as much accumulated complexes located at the lateral side of the cell surface and facing the cytoplasm side of cells with some CLDN-1 located on the cell surface. After 60 minutes of incubation, a merged view detected close association of FITC and Alexa 647 fluorescence, indicating the association of srE2^{332}-Fc in capped complexes with CLDN-1 in the Huh7.0 cell cytoplasm (**Fig. 3.4-16 B**). Overall, this indicates that CLDN-1 involves in the co-localisation of srE2^{332}-Fc and its internalisation into Huh7.0 cell lines.

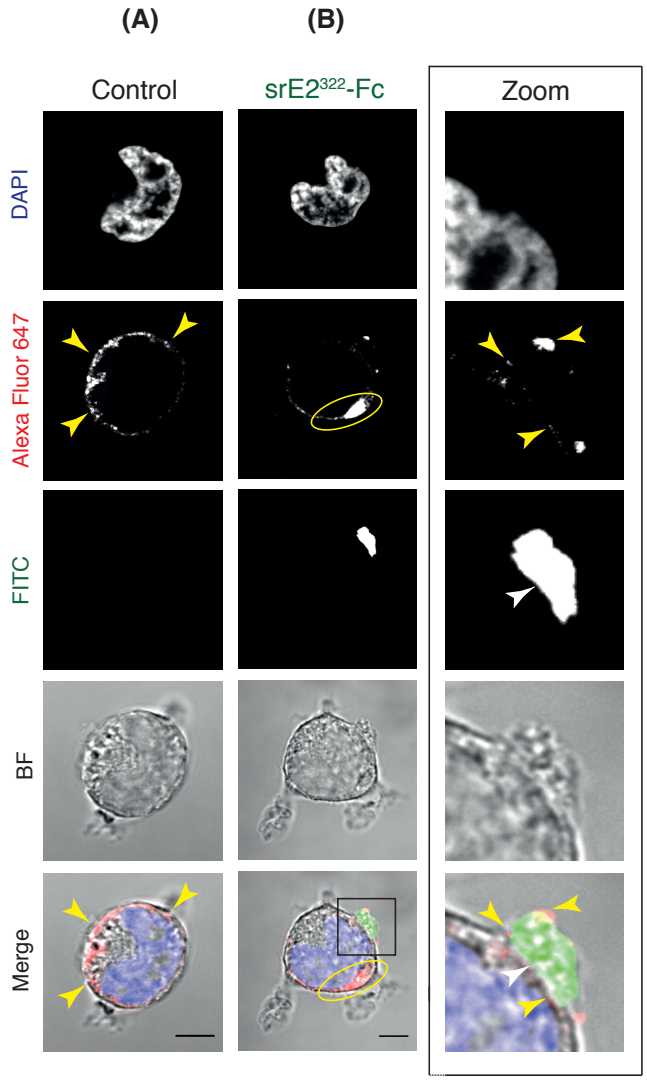

Figure 3.4-15 Co-localisation of CLDN-1 with srE2^{332}-Fc on the 293T cell surface. Live 293T in each single µ-Slide well were treated with 30 µg srE2^{332}-Fc or tPA-Fc (control) bound goat anti-Fc FITC sera in DMEM/FBS media for 60 minutes in 5% CO_2 at 37°C. Unbound peptide fusion was washed out and cells were fixed with 4% PFA in PBS for 18 minutes at RT. 0.1% Triton X-100 in PBS was added for 5 minutes followed by washing with 2 mM glycine / PBS for 5 minutes at RT. Blocking solution (5% BSA in PBS) was incubated with cells for 60 minutes at RT followed by media aspiration. CLDN-1 presence was detected by incubating cells in each µ-Slide well with 1.5 µg mouse anti-CLDN1 (A-9) antibody and the reaction labelled with of goat anti-mouse IgG Alexa Fluor 647 secondary (1 in 150) for 60 minutes followed by the washing step. Dilute DAPI counterstaining solution was added to the well slide. IBIDI mounting media was applied to cells in wells followed by confocal analysis (63x scanning objective). Merged nucleus (DAPI), CLDN-1 (Alexa Fluor 647), srE2^{332}-Fc (FITC) and 293T (BF) are presented. Yellow arrowheads indicate CLDN-1 presence on the cell surface (panel A and B) and white arrowheads indicate srE2^{332}-Fc fusion staining (capping structure) which is located on the cell surface (panel B). The yellow circle represents CLDN-1 complexes near the site of srE2^{332}-Fc capping structure on the 293T cell membrane. Boxed area is shown at greater magnification. Scale bar is 5 µM.

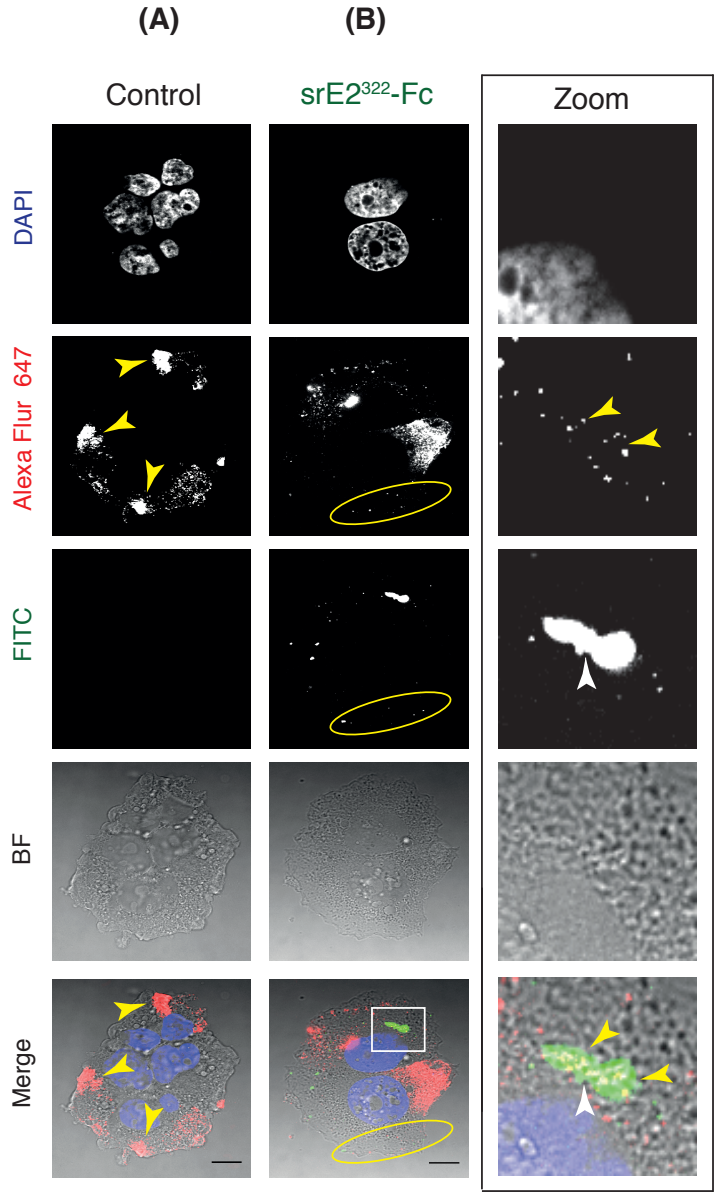

Figure 3.4-16 CLDN-1 receptor involved into entry of srE2^{332}-Fc into Huh7.0.
The methodology was performed as discussed for treating 293T with srE2^{332}-Fc fusion and labelling with anti-CLDN1 sera (section 3.4.5.2). Merged nucleus (DAPI), CLDN-1 (Alexa Fluor 647) and srE2^{332}-Fc (FITC) +/- Huh7.0 (BF) are presented. White arrowheads indicate CLDN-1 on the surface of the control cell (panel A) and into the cytoplasm (panel B). Yellow arrowheads indicate srE2^{332}-Fc fusion staining located into the cytoplasm (panel B). The yellow circle represents close association and overlay of CLDN-1 and srE2^{332}-Fc on Huh7.0 cell membrane. Boxed area is shown at greater magnification. Scale bar is 10 μM.

3.4.6 Analysing ability of E2 variants to interact and localise over live 293T

We previously showed that full length srE2^{332}-Fc has the highest capacity to bind to the 293T cell surface and rMBP-CD81 LEL, followed by binding of srE^{295}-Fc and srE^{278}-Fc and then by proficient srE2^{265}-Fc. In addition, srE2^{195}-Fc was demonstrated to have severely impaired binding capacity. Thus, we wished to study the ability of soluble E2 variants to bind and form capping structures on cells with abundant CD81 such as 293T cells. The experimental procedure was conducted according to section (3.4.1.1) with three time points of incubation with 293T (10, 25 and 60 minutes).

We observed FITC fluorescence spots on 293T cells treated with srE2 ^{295}-Fc or srE2^{278}-Fc for 10 minutes and this supports our previous findings, which indicate functional binding of both E2 derivatives to attachment factors on 293T surfaces (**Fig. 3.4-17 A & B, 10 minutes**). Incubation for a further 15 minutes was associated with more fluorescence spots observed on 293T cells and this correlates with more binding of both E2 deleted forms to 293T cells (**Fig. 3.4-17 A & B, 25 minutes**). Extending the reaction for 35 minutes was associated with more intense fluorescence spots in the form of discrete patches and some capping which was compatible with the normal organisation of CD81 on the 293T cell surface and may indicate binding to the CD81 receptor (**Fig. 3.4-17 A & B, 60 minutes**). In comparison with srE2^{332}-Fc (section 3.4.1.1), these deleted forms seemed to exhibit similar behaviour in spanning and forming capped structures but at a slower rate as srE2^{332}-Fc occupied almost all the sites on the 293T cell surface after 15 minutes of live incubation, while both srE2^{295}-Fc and srE2^{278}-Fc fusions did not achieve the same result and 25 minutes of live incubation showed the best time point for occupying almost the entire 293T surface area (not all) for both derivatives. This is consistent with our previous finding that srE2^{295}-Fc and srE2^{278}-Fc have a good capacity to bind CD81 (but not compete with binding capacity of srE2^{332}-Fc), which probably takes part in the spanning and localisation of HCV E2 but at a slower rate of process. Treating 293T cells with srE2^{265}-Fc showed

obvious large fluorescence aggregates at 10 minutes compared with smaller abundant spots detected on the 293T surface incubated with srE2^{295}-Fc and srE2^{278}-Fc fusion at the same time point (**Fig. 3.4-17 C, 10 minutes**). In addition, fluorescence signals were not distributed completely over the cell membrane upon extending incubation up to 60 minutes and did not fit with the known distribution style of abundant CD81 on cell membranes (**Fig. 3.4-17 C, 25 & 60 minutes**). However, we cannot exclude the binding of srE2^{265}-Fc fusion to some CD81 on 293T surfaces. This is consistent with our finding in which srE2^{265}-Fc was the smallest E2 form to be sensitive to anti-CD81 added to 293T (section 3.3.2.6). This probably demonstrates that srE2^{265}-Fc has a higher capacity to bind other receptors than CD81 when initially incubated with 293T. Incubating 293T with largest deleted C-terminal srE2^{195}-Fc fusion for 10 minutes and 25 minutes showed no fluorescence spots on the cell surface (**Fig. 3.4-17 D, 10 & 25 minutes**). Few scattered fluorescence spots with significant large uncovered area on 293T surface were observed over 60 minutes of fusion incubation (**Fig. 3.4-17 D, 60 minutes**). This finding explains the weak interaction of E2^{195}-Fc fusion to attachment factors on 293T and might associate as well with specific binding to unknown rarely expressed alternative receptors. Overall, despite the different finding obtained using our deleted forms, this again confirms the presence of extra residues on srE2^{332}-Fc which seem critical for super spanning and capping formation over 293T which probably requires strong interaction to the CD81 receptor to drive this process. Non of the srE2 variants enter into 293T cytoplasm.

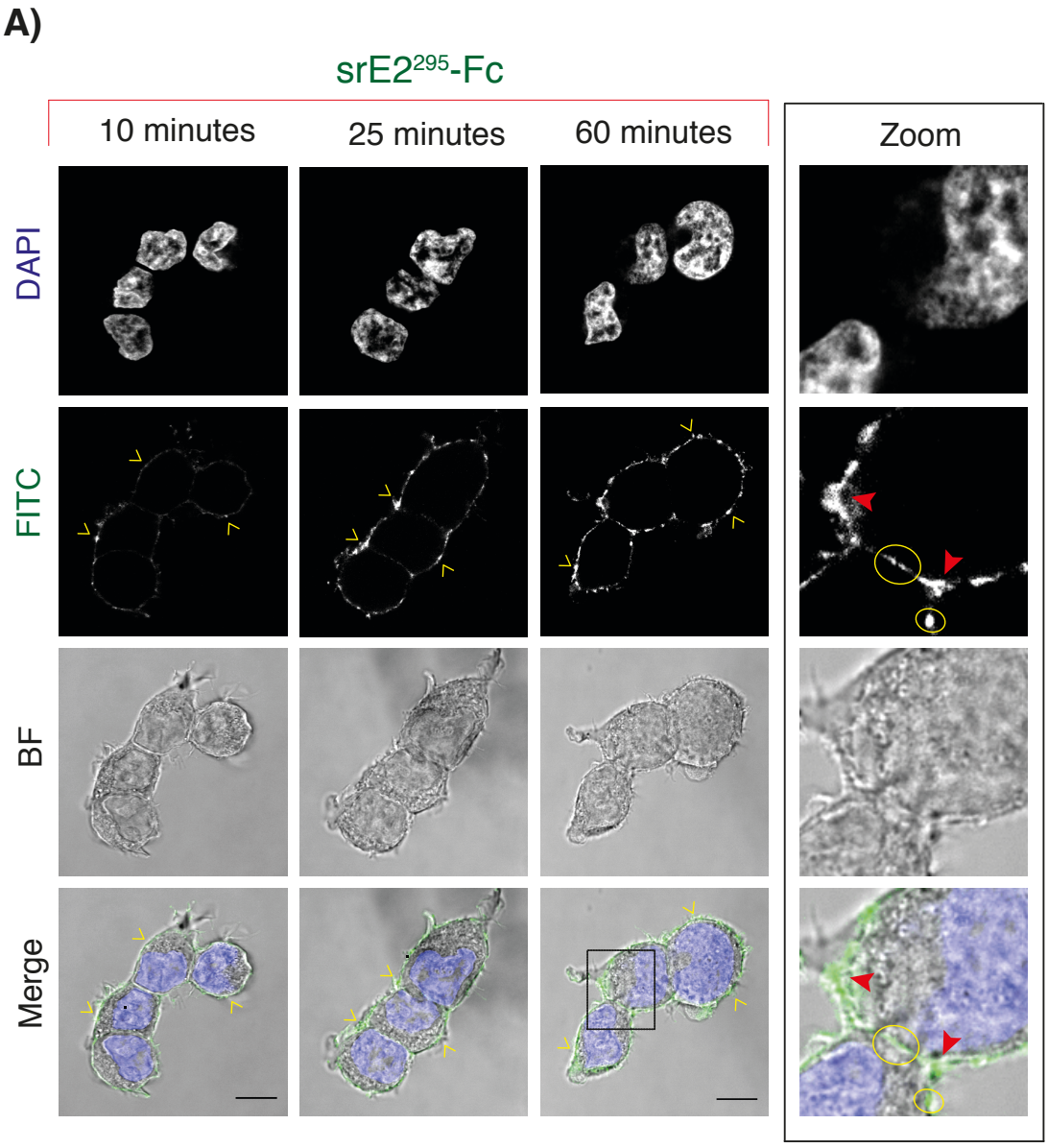
A)
srE2295-Fc
10 minutes
25 minutes
60 minutes
Zoom
DAPI
FITC
BF
Merge

B)

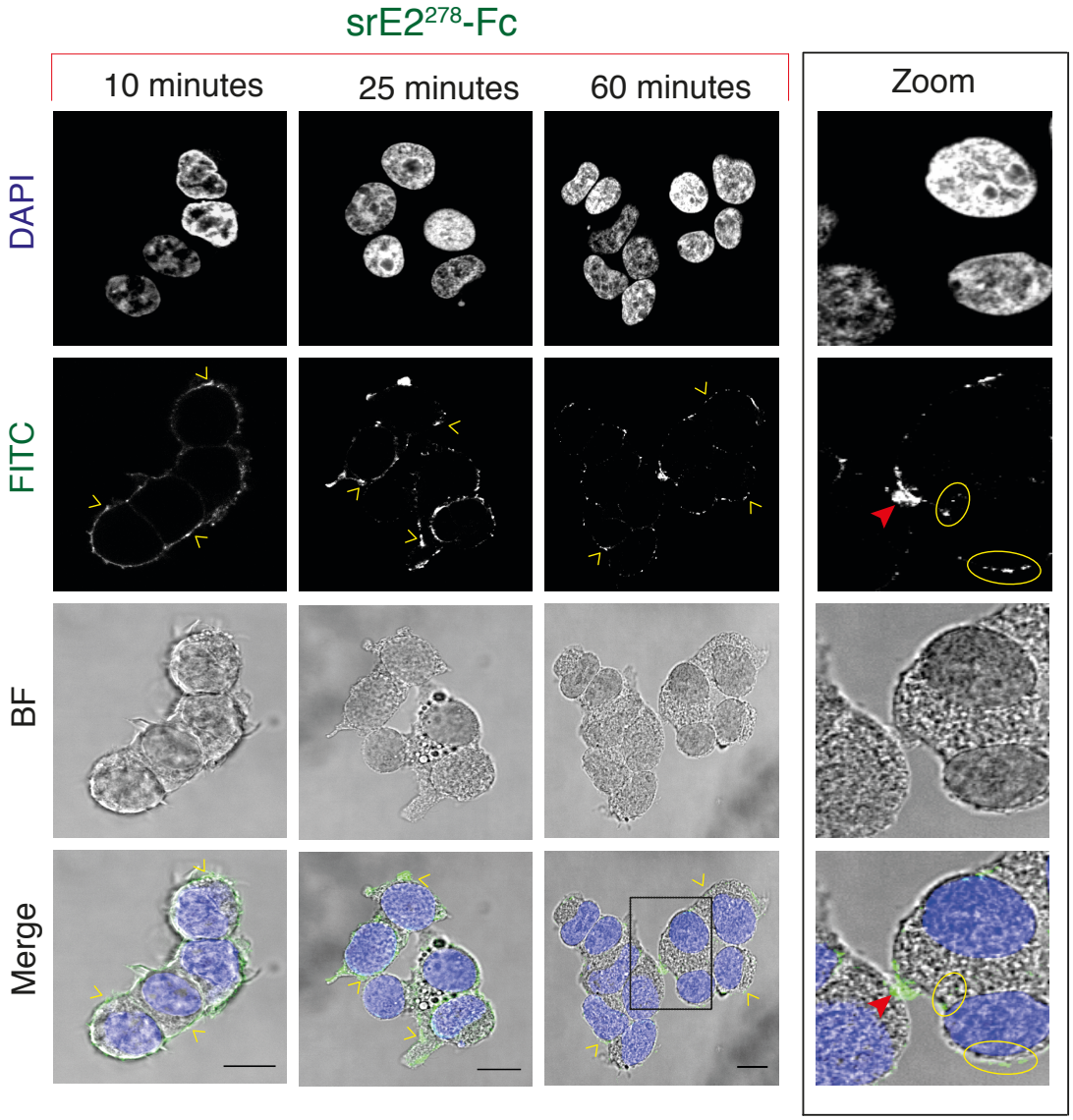
srE2278-Fc
10 minutes
25 minutes
60 minutes
Zoom
DAPI
FITC
BF
Merge

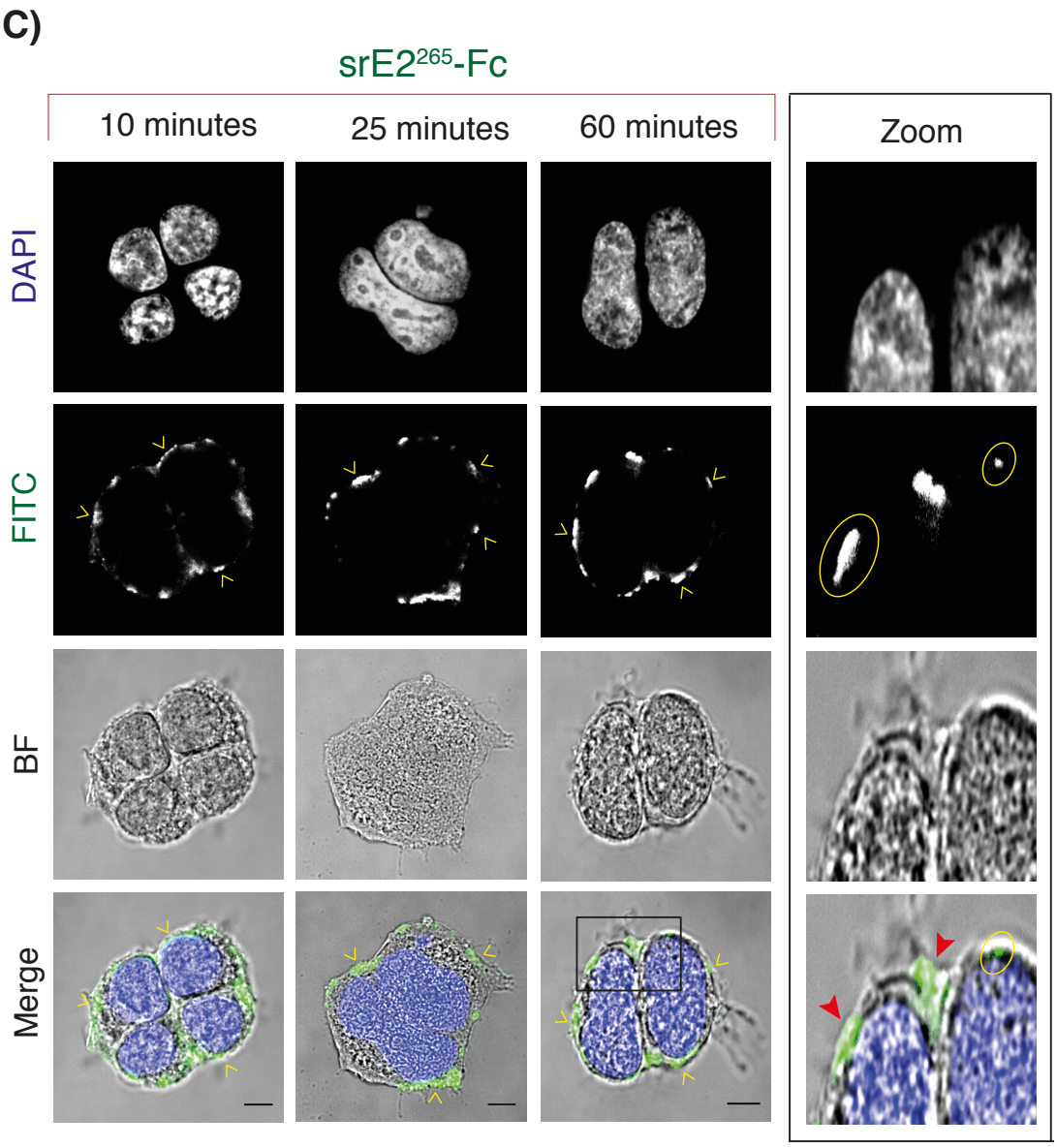
C)
srE2265-Fc
10 minutes
25 minutes
60 minutes
Zoom
DAPI
FITC
BF
Merge

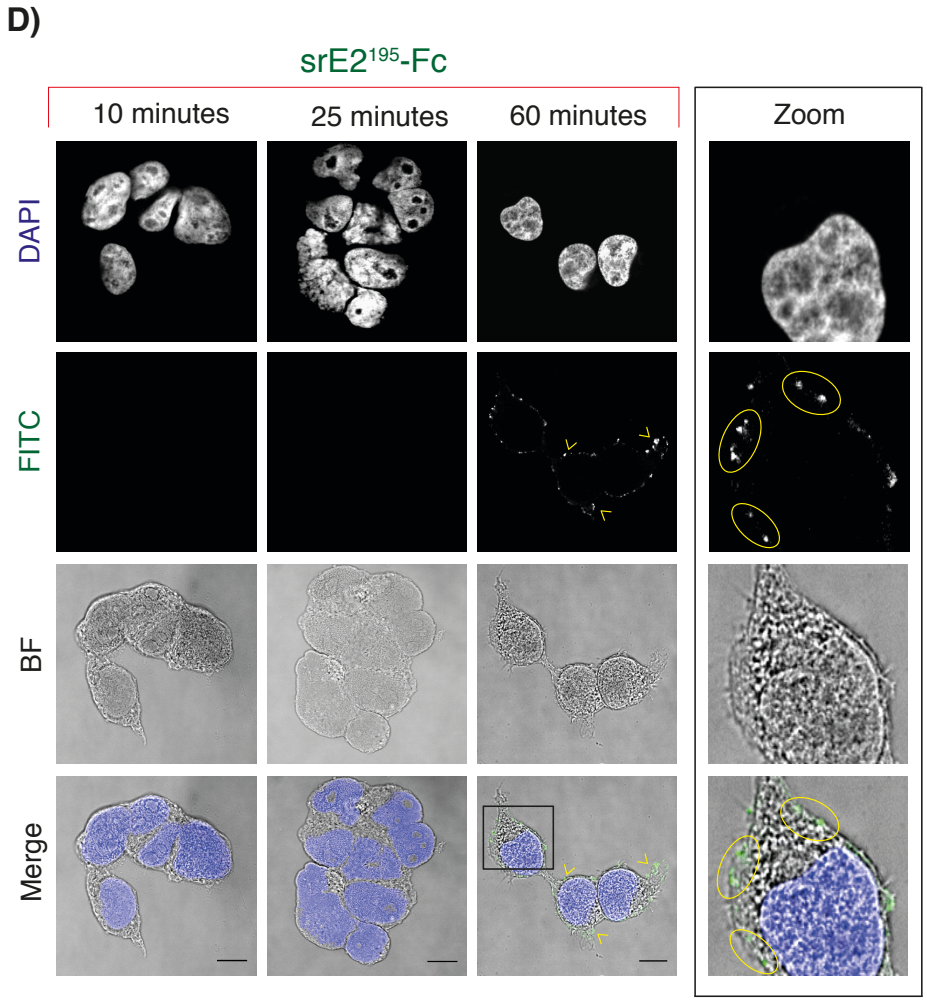

Figure 3.4-17 Incubation of srE2-Fc variants with live 293T cells up to 60 minutes. The method was conducted as described in section (3.4.1.1). Four panels show live incubation of 293T with srE2^{295}-Fc (A), srE2^{278}-Fc (B), srE2^{265}-Fc (C) and srE2^{195}-Fc (D). Nucleus (DAPI) and srE2 variant fusion (FITC) and the same image merged with the corresponding BF image are shown. tPA-Fc fusion was used as the negative control (not shown). Yellow arrowheads and circles indicate fluorescent spots (discrete patches) and red arrowheads indicate capping structure located on the cell membrane. The boxed area is shown at greater magnification. Scale bar 10 μM for all images except panel images related to srE2^{265}-Fc (5 μM).

3.5 Transfecting HepG2 with CD81 resulted in a fast rate of srE2^{332}-Fc entry

Our accumulated data has already demonstrated that HepG2 express few CD81 receptors and is not efficient for srE2^{332}-Fc internalisation. Therefore, we hypothesised that there will be an association between ectopic CD81 expression and an efficient entry of E2^{332}-Fc in hepatoma cell lines. Thus, we transfected HepG2 with pcDNA3.1-CD81 plasmid and then incubated srE2^{332}-Fc with the engineered cells for binding and entry analysis.

3.5.1 Test expression of CD81 on HepG2 cell surface

Both native HepG2 and CD81-HepG2 cells were fixed with 4% PFA, then labelled with mouse anti-CD81 (5A6) sera and secondary anti-mouse Alexa Fluor 647 conjugate. Confocal imaging of transfected cells with CD81 factor showed fluorescence signal distribution of secondary conjugate that label primary anti-CD81 indicating successful expression of ectopic CD81 factor over HepG2 cell surface. On the other hand, very weak Alexa Fluor 647 fluorescence was detected on parental HepG2 indicating exceedingly limited expression of CD81 on the cell surface as expected (**Fig. 3.5-1**). Flow cytometry was conducted to test the level of CD81 expression on the cell surface. Our data showed a high PE conjugate signal on CD81-HepG2 indicating further evidence of the functional recognition of CD81 epitope by anti-CD81 antibody. Weak fluorescence intensity of PE was measured on native HeG2. All this confirmed the successful CD81 transfection process of correctly folded and high rate of CD81 expression on the HepG2 cell surface (**Fig. 3.5-2**). Both confocal assay and Flow cytometer analysis showed a negative result for the control used (irrelevant primary mouse anti-human IgG and irrelevant mouse anti-human IgG-PE conjugate) and no cross reactivity was detected.

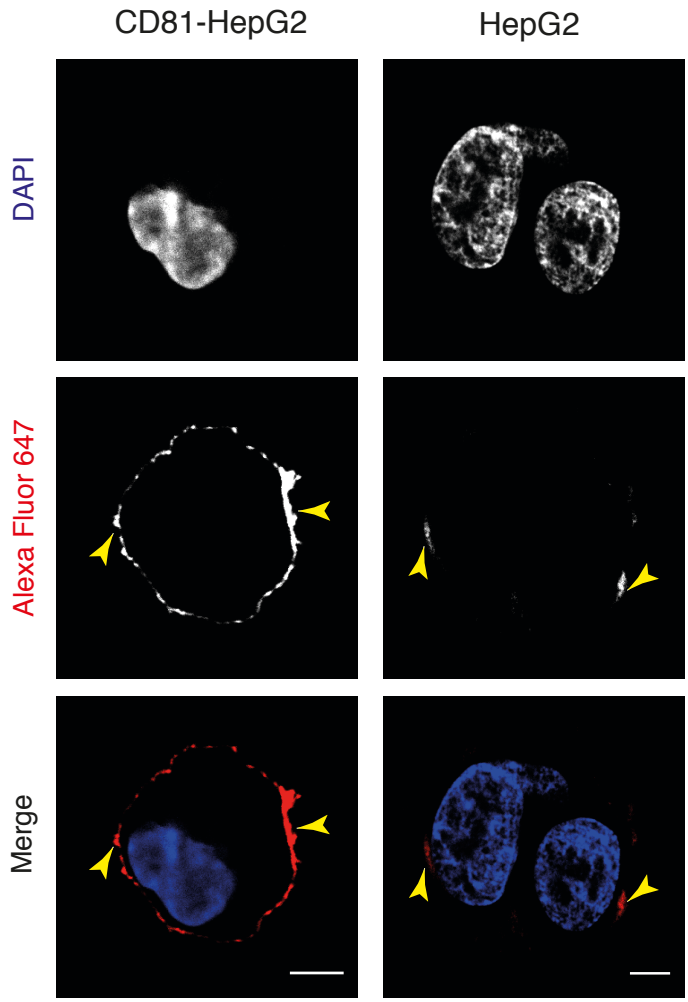

Figure 3.5-1 Ectopic expression of CD81 on HeG2 transfected with CD81 plasmid.

As a control background sample, cells were not treated with mouse anti-CD81 or irrelevant mouse anti-human IgG and are incubated with secondary anti-mouse IgG Alexa Fluor 647 conjugate (data not shown). Merged nucleus (DAPI) and CD81 (Alexa Fluor 647) are presented. Arrowheads indicate CD81 surface staining. Scale bar is 5 μM.

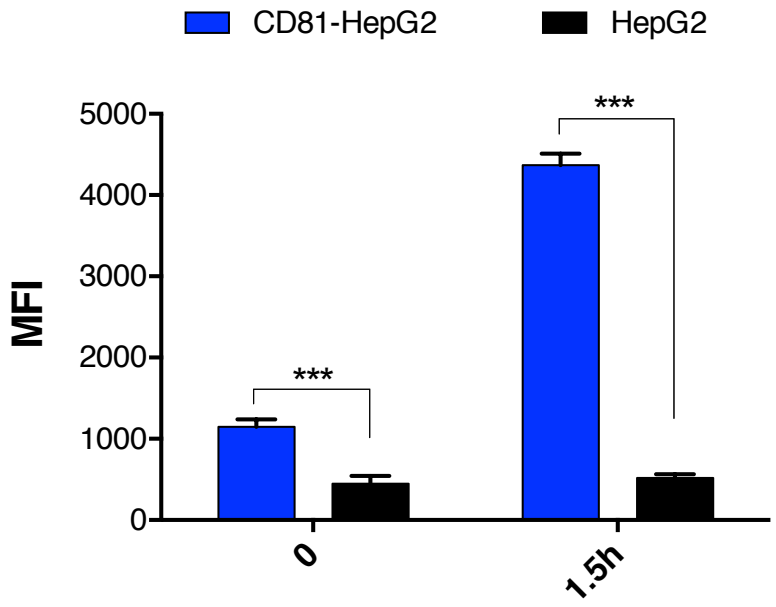

Figure 3.5-2 High level of CD81 present on CD81-HepG2.

Time points shown on the x-axis of graph indicate the incubation period of cells in a falcon tube post 0.05% Trypsin-EDTA treatment before adding primary mouse anti CD81-PE conjugate (1 µg/ml). The fluorescence signal was measured by fortessa flow cytometer. For each sample, the MFI is subtracted from the result of irrelevant mouse anti-human IgG PE conjugate. Data values represent the mean of triplicate assays, error bars = SD. T-test ***: $p < 0.001$.

3.5.2 Binding analysis of srE2^{332}-Fc to CD81-HepG2

We wanted to ensure that E2^{332}-Fc recognised the cell surface of the HepG2 transfected cell and to compare binding capacity with parental HepG2 and Huh7.0 cells. Immunofluorescence analysis showed FITC fluorescence detection, which was distributed over the whole outer surface of CD81-HepG2 and was similar to the visualising of the fluorescence signal on native HepG2. Our finding confirms that srE2^{332}-Fc still recognises surface factors on engineered HepG2 cells and achieving similar florescence distribution. This might initially mean no disruption for other attachment factors expression or organisation upon transfection of plasmid DNA into HepG2 (**Fig. 3.5-3**). To compare the capacity of binding level in the presence of high level CD81 expression, we conducted flow cytometer analysis through incubating cells with srE2^{332}-Fc and labelling with anti-Fc FITC conjugate. Our data showed significant high fluorescence intensity of anti-Fc FITC that was measured on CD81-HepG2 and was 2 times the fluorescence intensity measured on both native HepG2 and Huh7.0 (**Fig. 3.5-4**). This confirmed that pronounced increase in plasma membrane-associated CD81 on HepG2-CD81 cells was accompanied by a concomitant increase in srE2^{332}-Fc binding activity consistent with an increase in available cell surface binding sites for HCV E2.

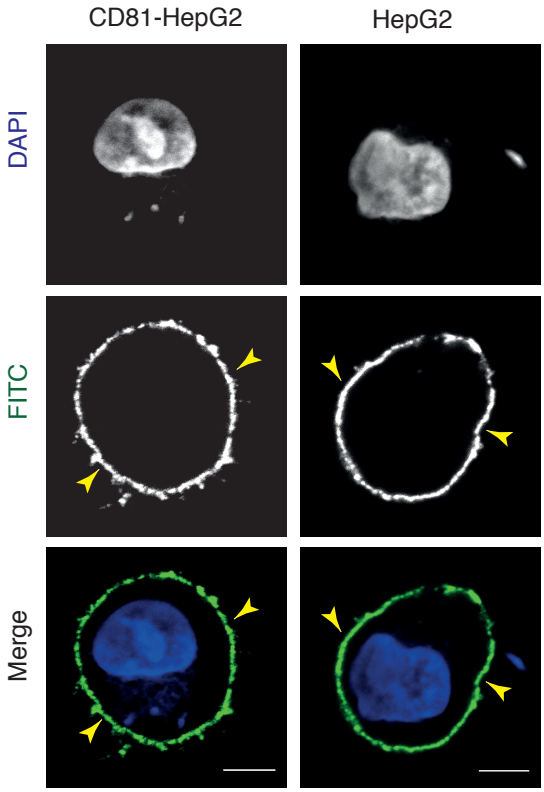

Figure 3.5-3 srE2^{332}-Fc bind CD81-HepG2 cell surface.

CD81-HepG2 was incubated with purified srE2^{332}-Fc (20 µg) and labelled with secondary goat anti-human Fc FITC (1:50). As a control, a set of cells were treated with tPA-Fc or not treated with srE2^{332}-Fc and probed with secondary conjugated antibody (data not shown). Merged nucleus (DAPI) and srE2^{332}-Fc (FITC) are presented. Arrows indicate srE2^{332}-Fc staining on the cell surface. Scale bar is 5 µM.

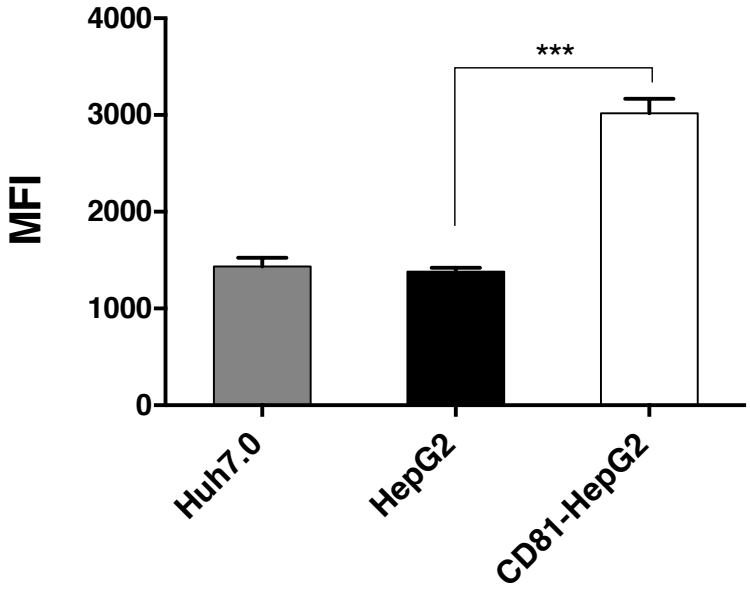

Figure 3.5-4 High capacity interaction of srE2^{332}-Fc to CD81-HepG2.
Target cells were treated with 18µg/ml E2^{332}-Fc and probed with secondary goat anti-human Fc FITC (1:500). Samples were incubated with tPA-Fc (control) or only with secondary anti-human Fc FITC and MFI from the control samples was subtracted from each of the reading points shown. Data are mean and standard deviation from three triplicate assays. T-test ***: $p < 0.001$.

3.5.3 Studying E2-Fc derivatives interaction to CD81-HepG2

We wanted to analyse the binding of E2 variants to CD81-HepG2 and compare it with interaction capacity of parental HepG2. Different FITC fluorescence intensity was detected on native HepG2 incubated with E2 deleted forms which indicated a high interaction rate of srE2^{278}-Fc followed with srE2^{295}-Fc and srE2^{265}-Fc fusions. This means that srE2^{278}-Fc has more capacity to bind different surface receptors on HepG2 surface than srE2^{295}-Fc and srE2^{265}-Fc. Interestingly, the fluorescence intensity measured on CD81-HepG2 treated with srE2^{332}-Fc, srE2^{295}-Fc and srE2^{278}-Fc forms showed an increase by 45%, 51% and 30%, respectively, compared with binding to native HeG2. Moreover, srE2^{332}-Fc was the best glycoprotein fusion in terms of binding to the CD81-HepG2 surface which again confirmed the critical importance of full extra amino acids sequences present on full-length E2 after residue S^{295}. FITC fluorescence showed no significant increase on CD81-HepG2 cells treated with srE2^{265}-Fc compared with native HepG2 cells indicating probably higher capacity to bind other receptors on the Hepatoma surface than CD81. This finding might indicate more important amino acids located between residue no. 265 and residue no. 332 on the E2 envelope which has more capacity to bind primary CD81 receptors even if there are other competing receptors on CD81-HepG2 cells. Importantly, an approximate 60% decrease in anti-Fc FITC mean fluorescence on CD81-HepG2 was detected when srE2^{195}-Fc was incubated compared with the interaction to the native HepG2 surface. This confirms that srE2^{195}-Fc is exceedingly impaired or shows no interaction with CD81 on transfected HepG2 cells (**Fig. 3.5-5**).

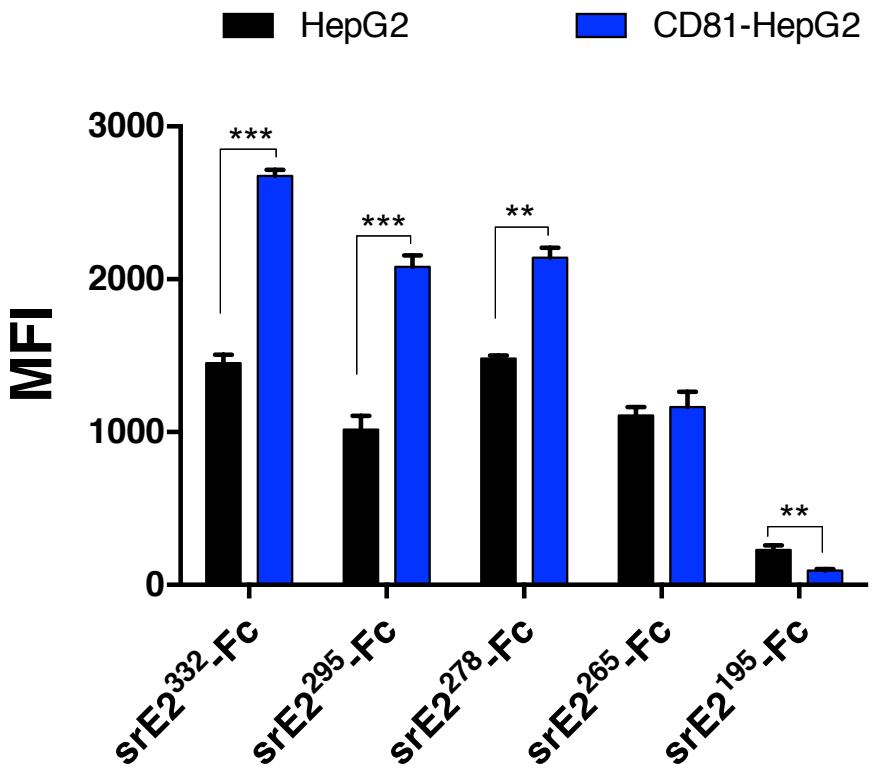

Figure 3.5-5 Comparison interaction of E2 variants to CD81-HepG2.
Target cells were treated with 20 µg/ml srE2^{332}-Fc or its variants and then probed with secondary goat anti-Human Fc FITC (1:500). Samples were incubated with tPA-Fc (control) or only with secondary anti-human Fc FITC and basal MFI from the control samples was subtracted from each of the reading points shown. Data are mean and standard deviation from triplicate assays. T-test **: $p < 0.01$ and ***: $p < 0.001$.

3.5.4 Expression of CLDN-1, OCLN and SR-B1 on CD81-HepG2

Our accumulated data previously showed expression of CLDN-1, OCLN and SR-B1 receptors on the surface of native HepG2. Here, we performed confocal and FCM analysis to ensure that engineered CD81-HepG2 cells still show the presence of these factors at comparable levels with parental HepG2 and that high levels of CD81 transfection does not mask these receptors. Confocal imaging showed Alexa Flour 647 fluorescence signals on the outer surface of transfected HepG2 incubated with mouse anti-CLDN (A-9). This indicates expression of CLDN-1 which approximately covers the whole outer membrane of the cells (**Fig. 3.5-6A**). In addition, cells incubated with rabbit anti-SR-B1 (ab36970) showed a distribution of Alexa Fluor 647 staining over CD81-HepG2 which demonstrates expression of SR-B1 (**Fig. 3.5-6B**). FITC fluorescence was detected on cells treated with goat anti-OCLN which shows OCLN expression on CD81-HepG2 cell (**Fig. 3.5-6C**). FCM data provided us with more information about the level of factor expression and surprisingly the mean fluorescence of Alexa Fluor 647 that label mouse anti-CLDN1 sera was approximately three times higher than the fluorescence intensity detected on native HepG2. This finding indicates that transfecting HepG2 with CD81 plasmid may be associated with enhanced CLDN-1 expression from a moderate level to a more pronounced level. Low CLDN-1 expression on 293T and moderate expression on Huh7.0 was detected. Moreover, FCM analysis showed similar FITC and rabbit Alexa Fluor 647 fluorescence intensity which label antibody bound to goat anti-OCLN (Y-12) and rabbit anti-SRB 1(H-180) sera, respectively. This indicates a similar high level expression of OCLN and SR-B1 receptors on parental and CD81 transfected HepG2 (**Fig. 3.5-7**). Overall, it seems that transfecting HepG2 cells with CD81 has no negative impact on the functional expression of important identified receptors for HCV E2.

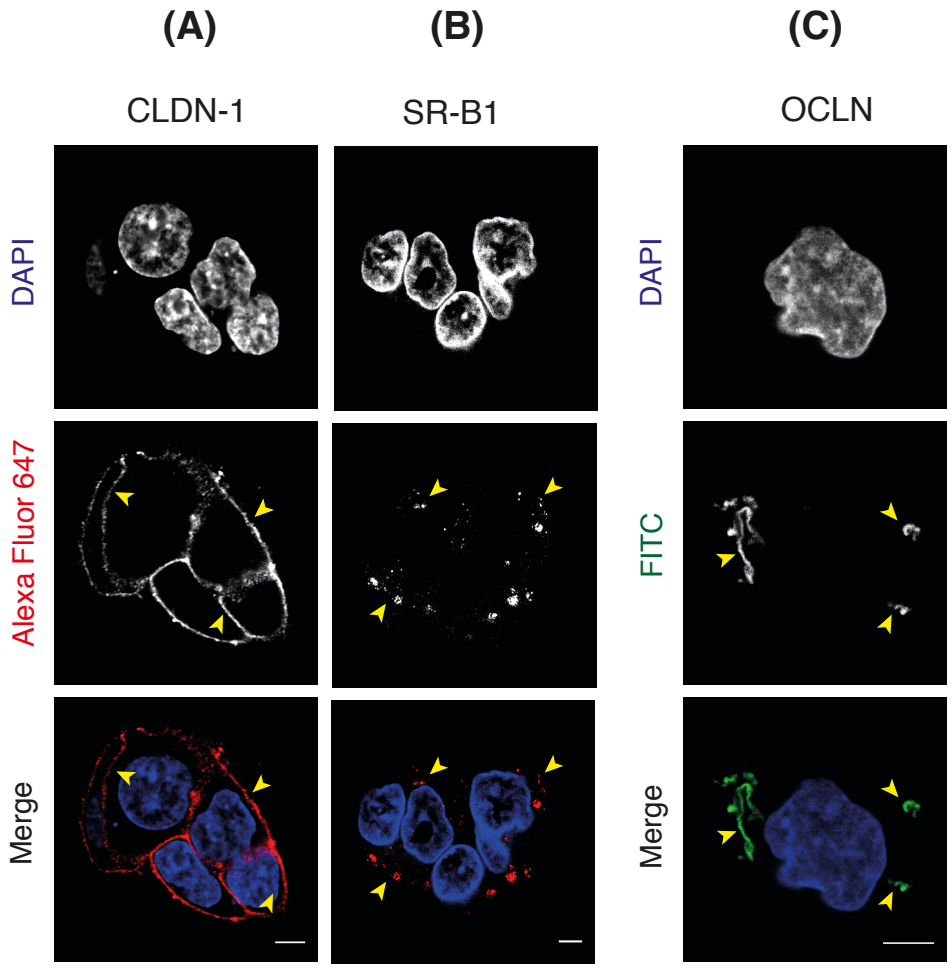

Figure 3.5-6 confocal analysis- CLDN-1, SR-B1 and OCLN are expressed on CD81-HepG2.

CLDN-1 presence (panel A) was detected with 1.5 µg mouse anti-CLDN1 (A-9) in each µ-Slide well and the reaction labelled with secondary goat anti-mouse Alexa Fluor 647 conjugate (1 in 150). SR-B1 expression (panel B) was detected in each µ-Slide well with 1:30 rabbit anti-SRB1 (ab36970) and the reaction labelled with secondary goat anti-rabbit Alexa Fluor 647 (1 in 75). OCLN expression (panel C) was detected by incubating cells in each µ-Slide well with 1 µg goat anti-OCLN (Y-12) and the reaction labelled with secondary donkey anti-goat FITC (1 in 30). As a control background sample, cells were not treated with anti-receptor or were incubated with irrelevant anti-human IgG and labelled with secondary antibody. Merged nucleus (DAPI) and CLDN-1 or SR-B1 (Alexa Fluor 647) or OCLN (FITC) are presented. Arrowheads indicate fluorescence staining of the surface receptor. Scale bar is 5 µM.

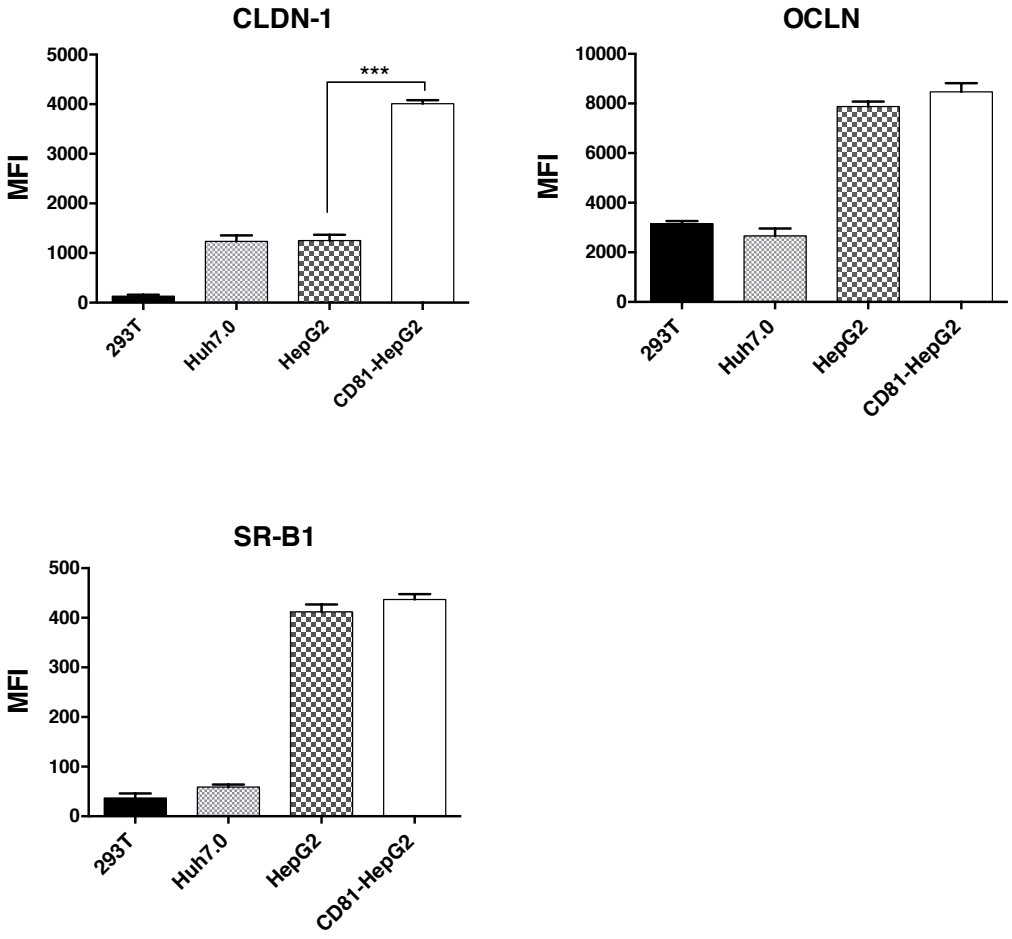

Figure 3.5-7 FCM- CLDN-1, OCLN and SR-B1 expressed on CD81-HepG2.

For CLDN-1, OCLN and SR-B1 expression, primary 1.5 µg/ml mouse anti-CLDN1 (A-9), 2 µg/ml goat anti-OCLN (Y-12) and 6 µg/ml rabbit anti-SRB1(H-180) sera, respectively, was added to the cells and labelled with secondary goat anti-mouse alexa fluor 647 conjugate (1:1000), Donkey anti-goat FITC (1:500) and anti-rabbit Alexa Fluor 647 conjugate (1:1000), respectively. The fluorescence signal was measured by fortessa flow cytometer. For each sample, the MFI is subtracted from the result of irrelevant anti-sera. Data values represent the mean of triplicate assays, error bars = SD. T-test ***: $p < 0.001$.

3.5.5 srE2^{332}-Fc entry into CD81-HepG2 cells

We wanted to address if the presence of abundant CD81 on HepG2 improve live binding and entry of srE2^{332}-Fc. To conduct this analysis, we adapted the method carried out in section (3.4.1.1). Our data showed that after incubating srE2^{332}-Fc with hepatoma cells for 15 minutes, a remarkably strong and rapid fluorescence intensity of anti-Fc FITC conjugate was detected on the whole outer surface of CD81-HepG2. In contrast, few fluorescence spots were distributed over parental HepG2 cell surfaces. This indicates existence of the association between the high-level expression of CD81 factors and the efficient binding capacity of E2 peptide fusion to transfected HepG2 (**Fig. 3.5-8A**). Extending incubation of E2^{332}-Fc for an additional 15 minutes was accompanied with few fluorescence complexes detected on the cell membrane of CD81-HepG2. In addition, most detected complexes were observed close to the inner side of the cell membrane and extended throughout the cell cytoplasm. This mean that srE2^{332}-Fc already underwent localisation over the cell surface and was involved with attachment factors in forming capping complexes, which was taken up successfully by the CD81-HepG2 cell. On the other hand, imaging of native HepG2 showed increase FITC fluorescence spots on the outer surface of the cells and confirms the sign of slow localisation as the spots were observed close to each other (**Fig. 3.5-8B**). This late slow process of capping formation and entry is clearly related to the limited expression of CD81 receptors on native HepG2 surfaces compared to the fast process of srE2^{332}-Fc entry into CD81-HepG2. Treating cells with full-length E2 for 60 minutes confirmed continuous srE2^{332}-Fc entry, represented by a high rate of fluorescence spots localised into the cytoplasm of CD81-HepG2. As expected, fluorescence intensity on native HepG2 at the 60-minute time point showed the distribution of more srE2^{332}-Fc on the outer surface with no obvious fluorescence spots detected in the cytoplasm (**Fig. 3.5-8C**). Data obtained from the comparison reaction of E2^{332}-Fc interaction with both CD81-HepG2 and native HepG2 indicated the real impact of high level CD81 expression on speeding up binding and induction of efficient envelope E2

protein entry. As a positive control, srE2^{332}-Fc, incubated with Huh7.0 for 15 minutes, showed high capacity of binding to the cell surface. Over 30 minutes of incubation, srE2^{332}-Fc was observed as large fluorescence capping complexes located on the cell membrane and in Huh7.0 cytoplasm which confirms capping complex formation and an entry of srE2^{332}-Fc. Extending incubation for an extra 30 minutes showed abundant E2^{332}-Fc localisation around the site of the nucleus. This means that the CD81-HepG2 cell is a competitive model to uptake srE2^{332}-Fc in a similar behaviour performed by Huh7.0 cells, and that this competitive feature is due to the expression of a high density of CD81 on the HepG2 cell, which is critical for the efficient entry of full-length E2 Fusion.

A) 15 minutes

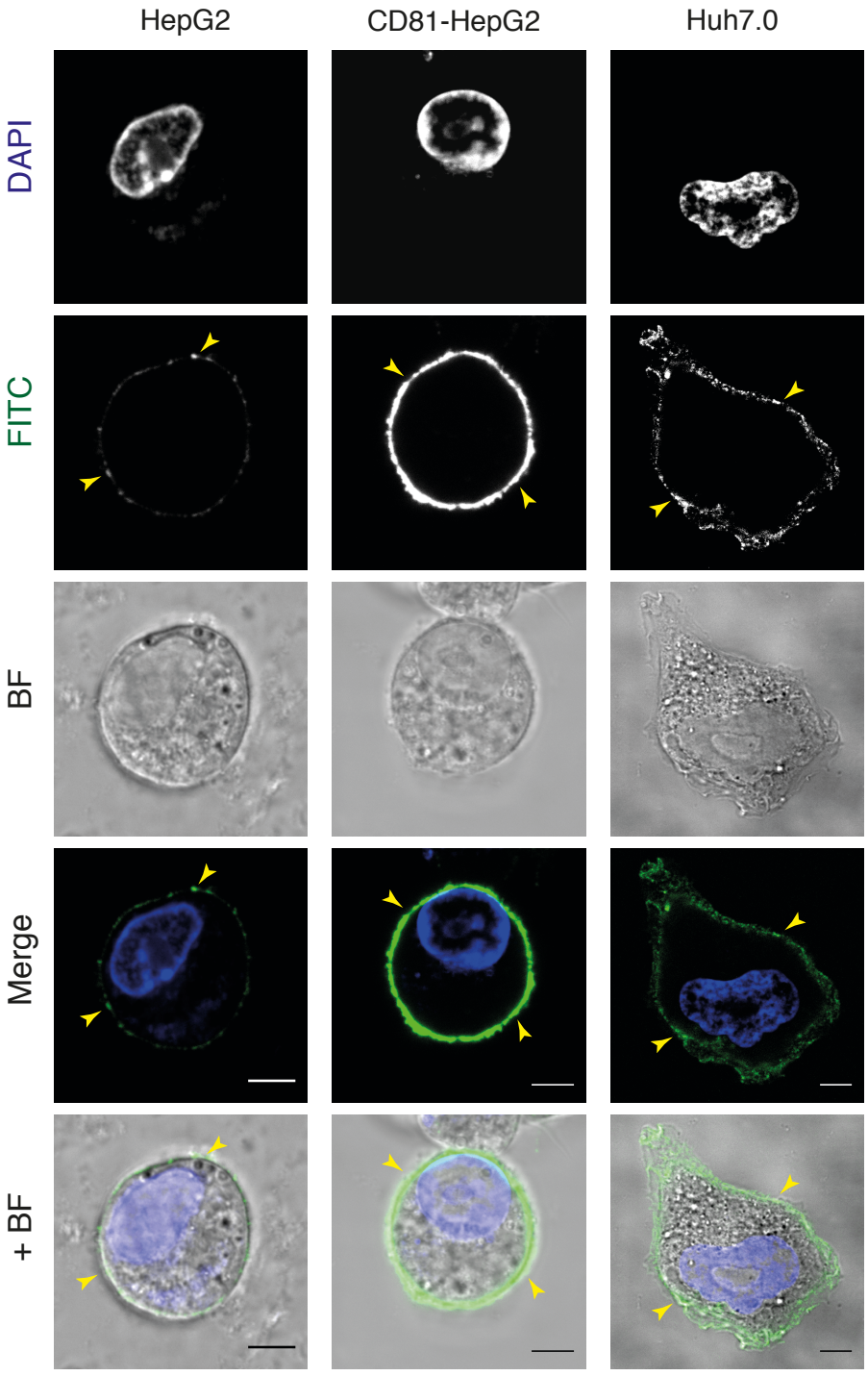

B) 30 minutes

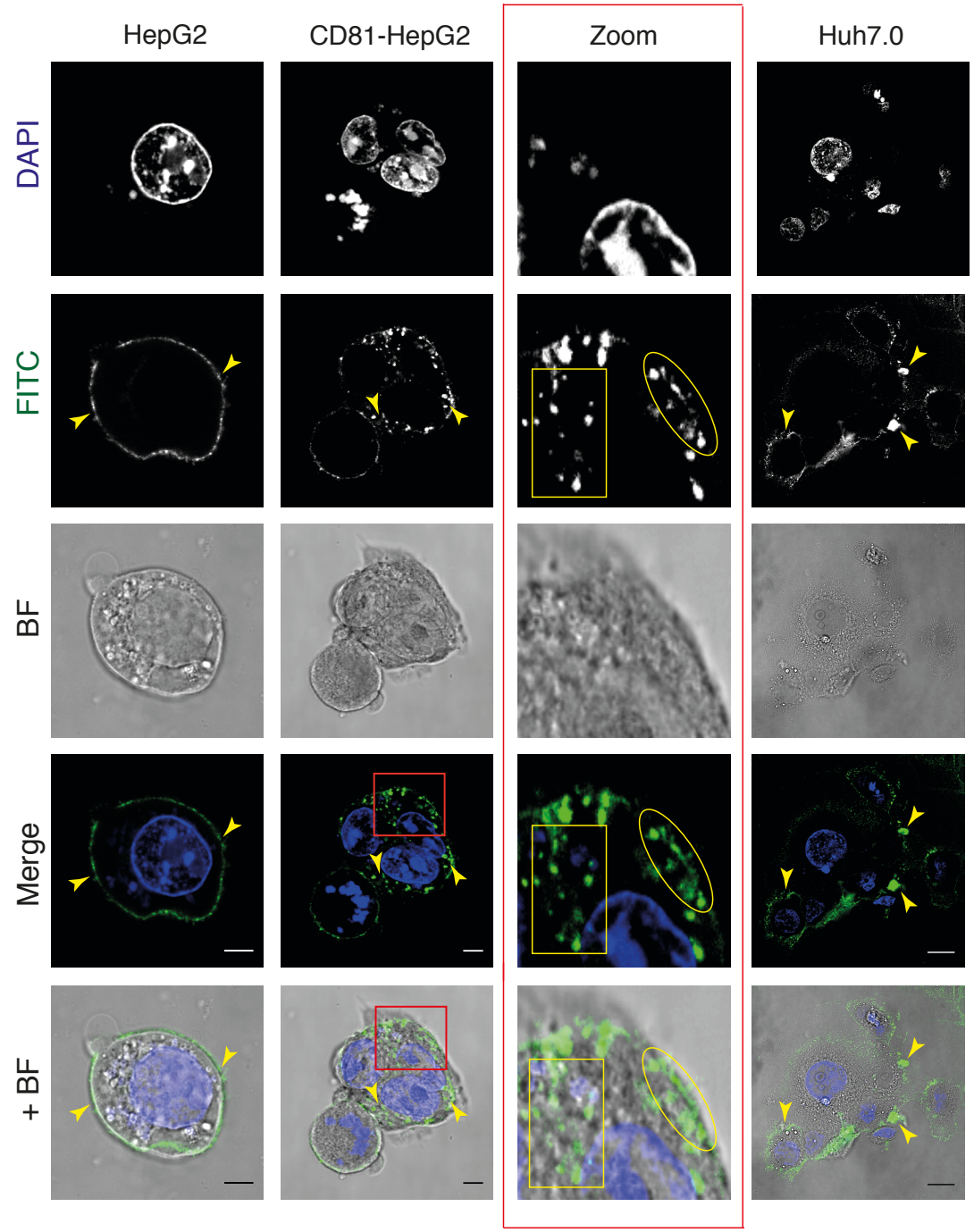

C) 60 minutes

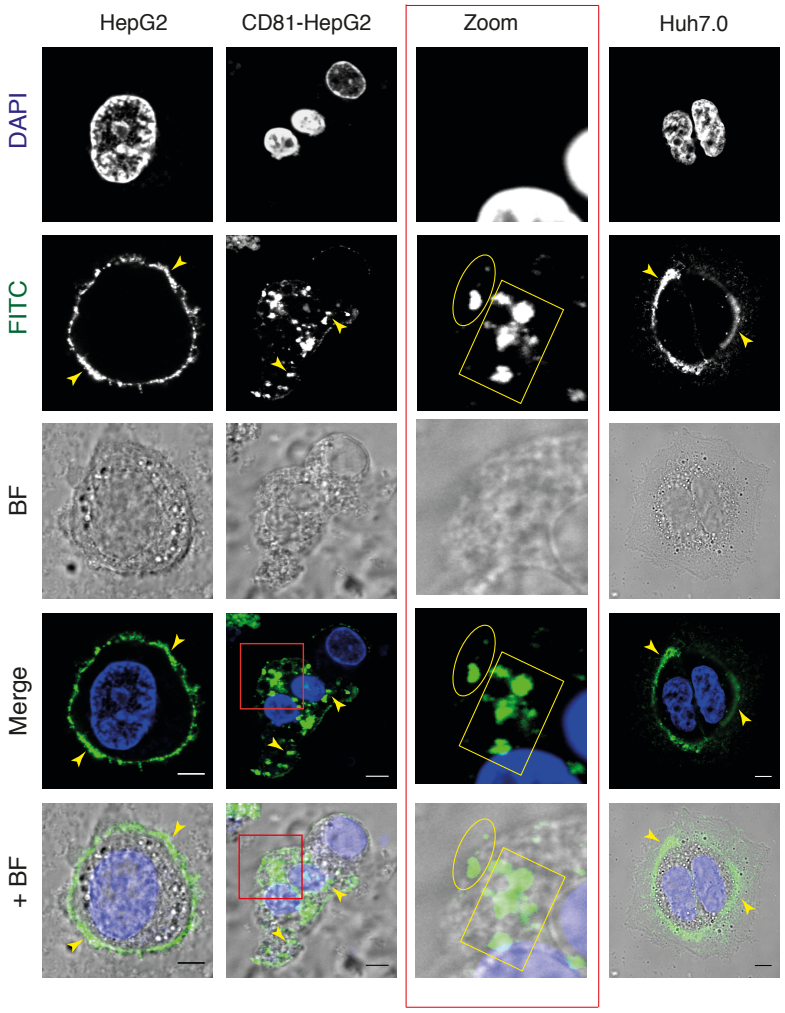

Figure 3.5-8 Live CD81-HepG2 interact remarkably with srE2^{332}-Fc and induce its internalisation.

srE2^{332}-Fc incubated with hepatoma cells for 15 minutes (panel A), 30 minutes (Panel B) and 60 minutes (panel C). Nucleus (DAPI) and srE2^{332}-Fc (FITC) and images merged with the corresponding BF image are shown. tPA-Fc was used as a negative control (not shown). Yellow arrowheads represent srE2^{332}-Fc staining on the cell membrane and into the cytoplasm. The red boxed area is shown at greater magnification. The yellow circle indicates large complexes (capping structure) on or near the inner side of the cell membrane and yellow rectangles indicate the same structures crossing the central area of the cytoplasm. Scale bar 5 μM for all images except panel images related to incubated Huh7.0 for 30 minutes (20 μM).

3.6 srE2^{332}-Fc is internalised into hepatoma cells by clathrin-mediated endocytosis process

After achieving the efficient entry of srE2^{332}-Fc into Huh7.0 and CD81-HepG2, we wanted to study if our srE2^{332}-Fc is internalised into the cytosolic compartment of target cells by the endocytosis pathway. Many reports have already suggested that entry of HCVpp and HCVcc is commonly via a clathrin mediated endocytosis mechanism. Their evidence showed HCV entry, which triggers fusion of the virus with structures in the cytoplasm, most probably endosome or liposome and was dependent on acidic pH (Blanchard *et al.*, 2006; Hsu *et al.*, 2003; Lavillette *et al.*, 2006; Matsuda *et al.*, 2014). To asses this mechanism, we used mouse anti-heavy chain clathrin (MA1065) antibody as a marker to locate clathrin in the cytoplasm of the cells and goat anti-human Fc FITC to locate srE^{322}-Fc. Subsequently, by confocal microscopy we studied whether clathrin and srE2^{332}-Fc associated together in the cell cytoplasm.

3.6.1 Analysing clathrin expression into hepatoma cell lines

We aimed to test the presence and organisation of clathrin into untreated Huh7.0, native HepG2 and CD81-HepG2. All cells were fixed with PFA, permeabilised and incubated with mouse anti-clathrin antibody, then labelled with secondary anti-mouse Alexa Flour 647 conjugate and imaged by confocal microscopy. Our data showed fluorescence spots distributed in the middle of the cytoplasm of all hepatoma cell lines. In addition, there was little fluorescence staining localised onto the cell membrane indicating that clathrin might mostly accumulate in the centre of the cellular cytoplasm rather than closer to the outer hepatoma cell membrane (**Fig. 3.6-1**). Irrelevant mouse anti-human IgG (control probe) were incubated with hepatoma cells and showed no cross reactivity to any cytoplasmic or surface clathrin and the results were always negative.

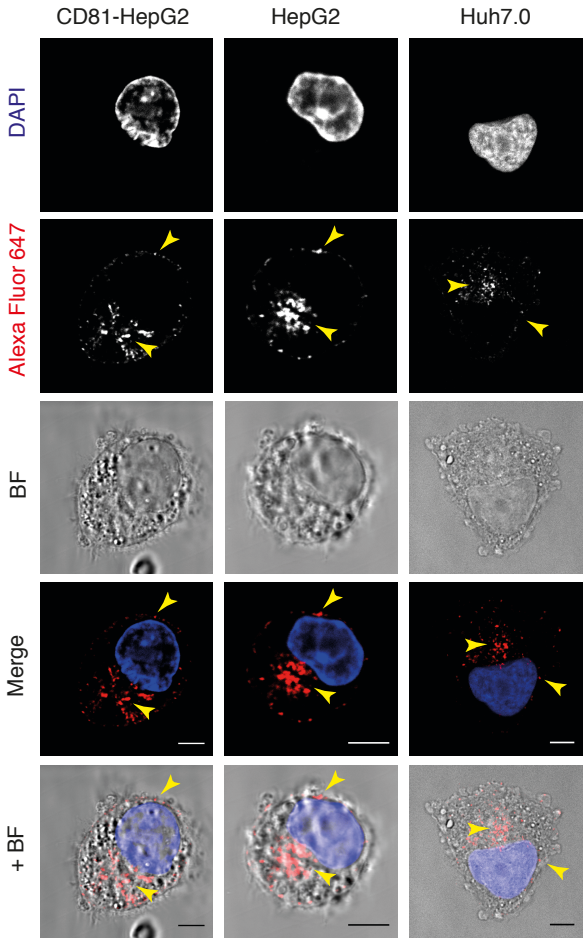

Figure 3.6-1 Clathrin located mainly into middle site of hepatoma cell cytoplasm.

Clathrin presence was detected with 1µg mouse anti- heavy chain clathrin antibody (MA1065) for 60 minutes at RT, and the reaction labelled with goat anti-mouse IgG Alexa Fluor 647 secondary (1 in 150) for 60 minutes at RT. As a control background sample, the cells were not treated with anti-clathrin or incubated with irrelevant mouse anti-human IgG and labelled with secondary antibody. Merged nucleus (DAPI) and clathrin (Alexa Flour 647) +/- the same image merged with the corresponding BF are shown. Arrowheads indicate clathrin intact to the surface and in the cytoplasmic compartment. Scale bar is 5 µM.

3.6.2 Study the association of clathrin with srE2^{332}-Fc incubated over 90 minutes

All hepatoma-derived cells were incubated with srE2^{332}-Fc at 37°C in 5% CO_2 over 3 time points: 15, 30 and 90 minutes and then fixed with PFA. Permeabilisation solution containing 0.1% Triton X-100 in PBS was added to the cells followed by the washing step. To prevent masking of target epitopes which might possibly happen upon labelling of both markers (srE2^{332}-Fc or clathrin), hepatoma cells were first incubated with anti-clathrin sera then labelled with secondary anti-mouse Alexa Fluro 647 conjugate. Finally, cells were treated with anti-Fc FITC to label bound srE2^{332}-Fc. Over 15 minutes of incubation, CD81 transfected HepG2 showed expression of Alexa Fluro 647 fluorescence spots close to the cell surface and abundantly distributed around the inner side of the plasma membrane of the cell (**Fig. 3.6-2A, 15 mins.**). This finding indicates the re-arrangement of clathrin in the cytoplasm and localisation toward the CD81-HepG2 cell outer border. Importantly, an overlay of FITC fluorescence and Alexa Fluor 647 fluorescence at the cell membrane was observed, indicating that localisation of clathrin around the cell membrane was probably triggered by the binding of srE2^{332}-Fc to the cell surface. The exact process of clathrin re-organisation when srE2^{332}-Fc interacts with cell surface has not been identified yet. Treating CD81-HepG2 cells for 30 minutes showed more Alexa Fluor 647 fluorescence spots merged with FITC fluorescent spots at the cell membrane and in the cytosolic compartment of cell which means that entry of srE2^{332}-Fc is associated with clathrin localisation (**Fig. 3.6-2A, 30 mins.**). Surprisingly, as srE2^{332}-Fc was already internalised at this time point, fluorescence staining was detected mostly in the cytoplasm with few fluorescence spots present at the cell membrane of CD81-HepG2. This might mean that clathrin that does not associate with srE2^{332}-Fc is re-localised again to its normal location at the centre of the cell cytoplasm. In addition, the number of clathrin spots detected upon incubating cells with srE2^{332}-Fc was astonishing compared with untreated cells, likely meaning that the clathrin exposed more of its heavy chain during its re-localisation in the

cytoplasm and migration to the cell membrane which were easily targeted by anti-clathrin sera.

Extending incubation with cells for an extra 90 minutes resulted in the detection of variable-sized vesicles decorated with FITC fluorescent at the cell membrane and in the cytoplasm. Importantly, we were able to detect Alexa Fluor 647 spots located on the outer border of these vesicles (**Fig. 3.6-2A, 90 mins.**). It is worth saying that in other repeated experiments after 30 minutes of incubation, we did notice that these vesicles coated with srE2^{332}-Fc and clathrin were located exactly at the cell membrane of cells which means that the formation of this circle structure happened post binding of srE2^{332}-Fc to the cell surface and before entry into the cytoplasm. It is difficult to explain how and why this vesicle is formed. We speculate that this might be a sign of clathrin coated vesicles formation, which carries srE2^{332}-Fc from the cell membrane to the cytoplasm and fuses it with the membrane of cell organelles, in particular the endosome. An alternative explanation is that the vast majority of bound srE2^{332}-Fc that had entered into the clathrin-enriched zones of the cell cytoplasm by 90 minutes frequently appeared to be in cytoplasmic vacuoles which associated with clathrin and differed widely in size typical of early and late endosomes. At the moment, it is difficult to discriminate clathrin coated pits from clathrin containing endosome. In contrast, however, the binding and entry process upon incubating srE2^{332}-Fc with parental HepG2 is slow: incubating cells for 15 minutes and 30 minutes demonstrated the re-localisation of clathrin which organised as a cluster near the cell membrane at the site of srE2^{332}-Fc binding (**Fig. 3.6-2B, 15 & 30 mins.**). After 90 minutes of incubation, we noticed association of both srE2^{332}-Fc and clathrin that interacted with the HepG2 cell membrane in a vesicle structure and tended to be similar to clathrin coated vesicles detected in CD81-HepG2 cytoplasm at the incubation points of 30 minutes (**Fig. 3.6-2B, 90 mins.**). In addition, exceedingly few E2^{332}-Fc fusions which entered the cytoplasm were combined with clathrin. However, no efficient entry of E2^{332}-Fc fusion was achieved using HepG2, and it is more likely that clathrin responded to the post binding srE2^{332}-Fc event or post localisation of capping complexes. This might indicate that

binding of srE2^{332}-Fc to surface factors on HepG2 cells might be enough to recruit clathrin to the cell surface. Clathrin failed to undergo the wide spread association into punctate aggregations with membrane bound srE2^{332}-Fc that were already observed in HepG2-CD81 may be because of the low density of some factors required for srE2^{332}-Fc clustering (possibly CD81). Thus, the rate of srE2^{332}-Fc entry in HepG2 cells was severely impaired. Huh7.0 cells incubated for 90 minutes with srE2^{332}-Fc exhibited a similar pattern of staining to that observed for HepG2-CD81 cells, and the internalised srE2^{332}-Fc was again present in clathrin-enriched regions of the cytoplasm (**Fig. 3.6-2C**).

A)

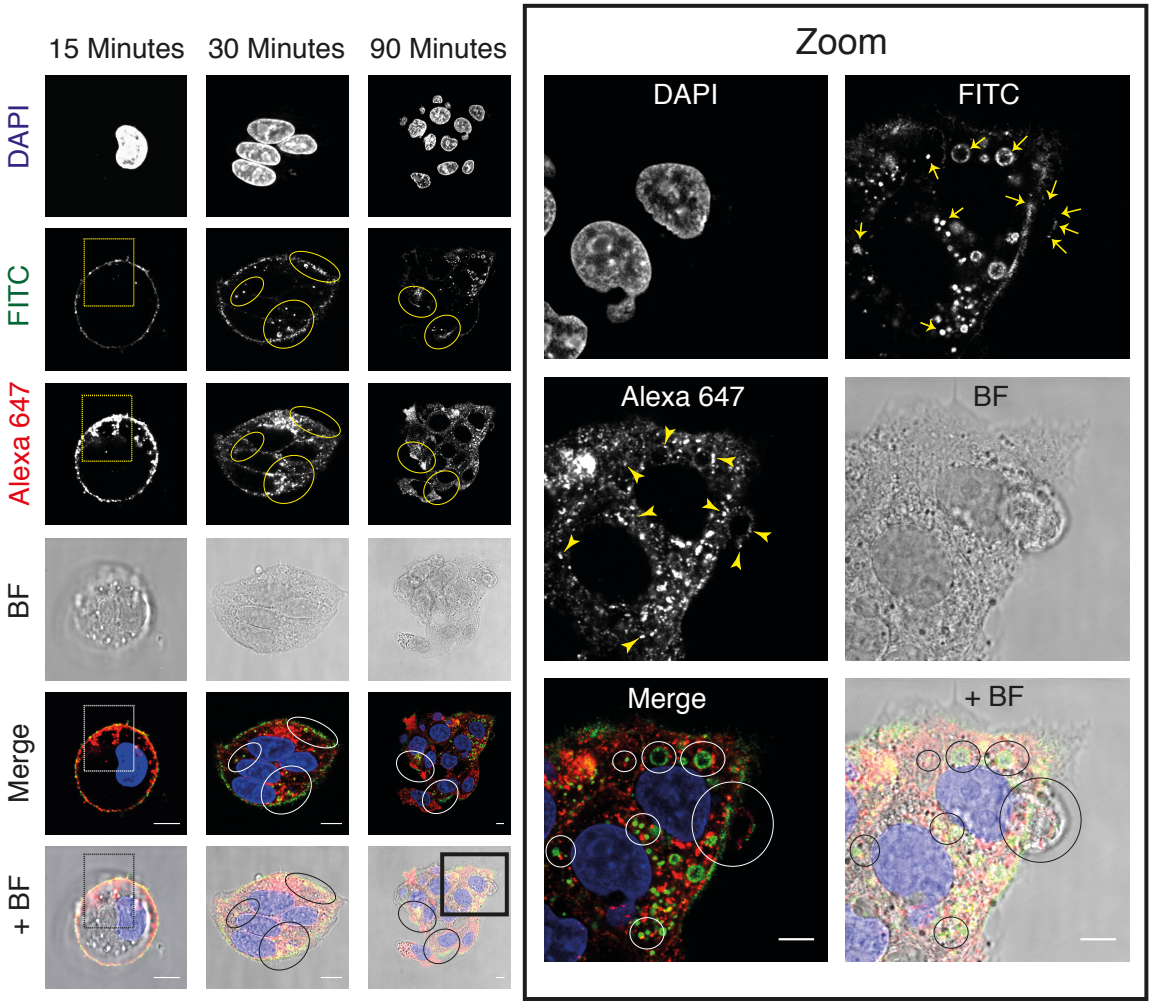
15 Minutes
30 Minutes
90 Minutes
DAPI
FITC
Alexa 647
BF
Merge
+ BF
Zoom
DAPI
FITC
Alexa 647
BF
Merge
+ BF

B)

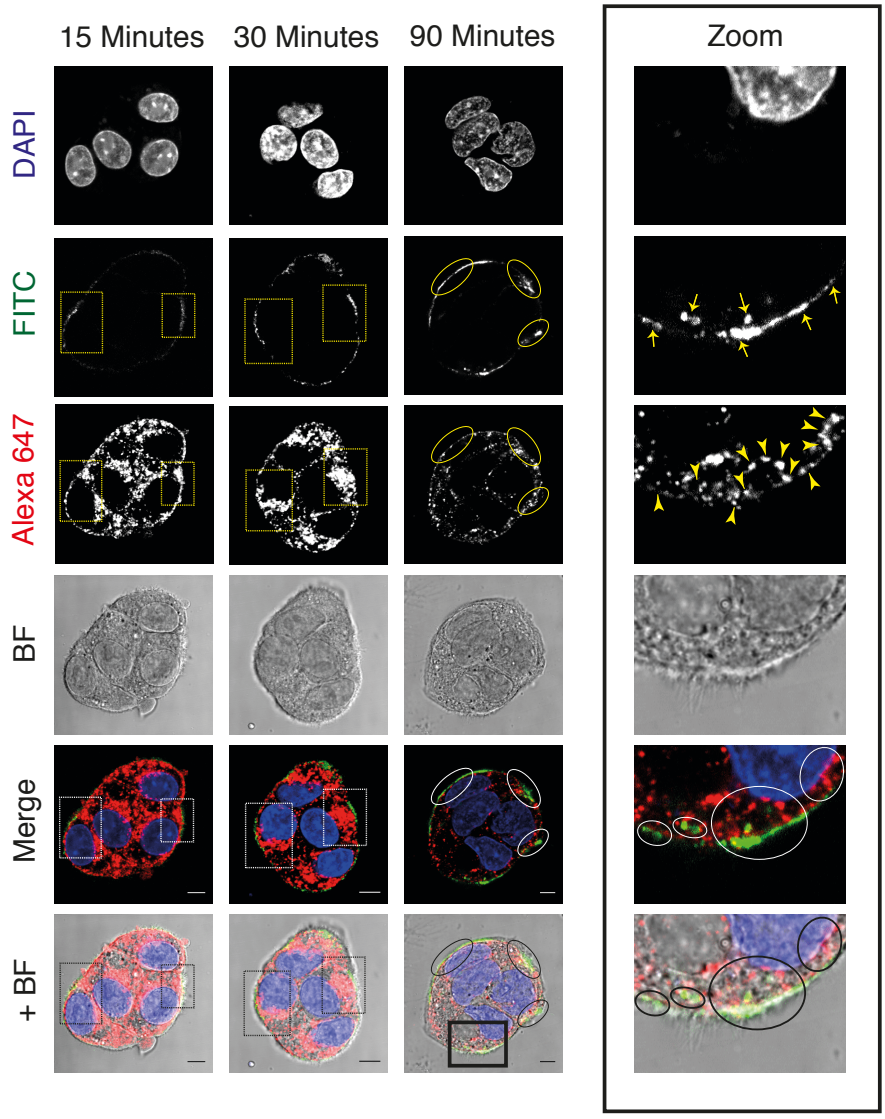
15 Minutes
30 Minutes
90 Minutes
Zoom
DAPI
FITC
Alexa 647
BF
Merge
+ BF

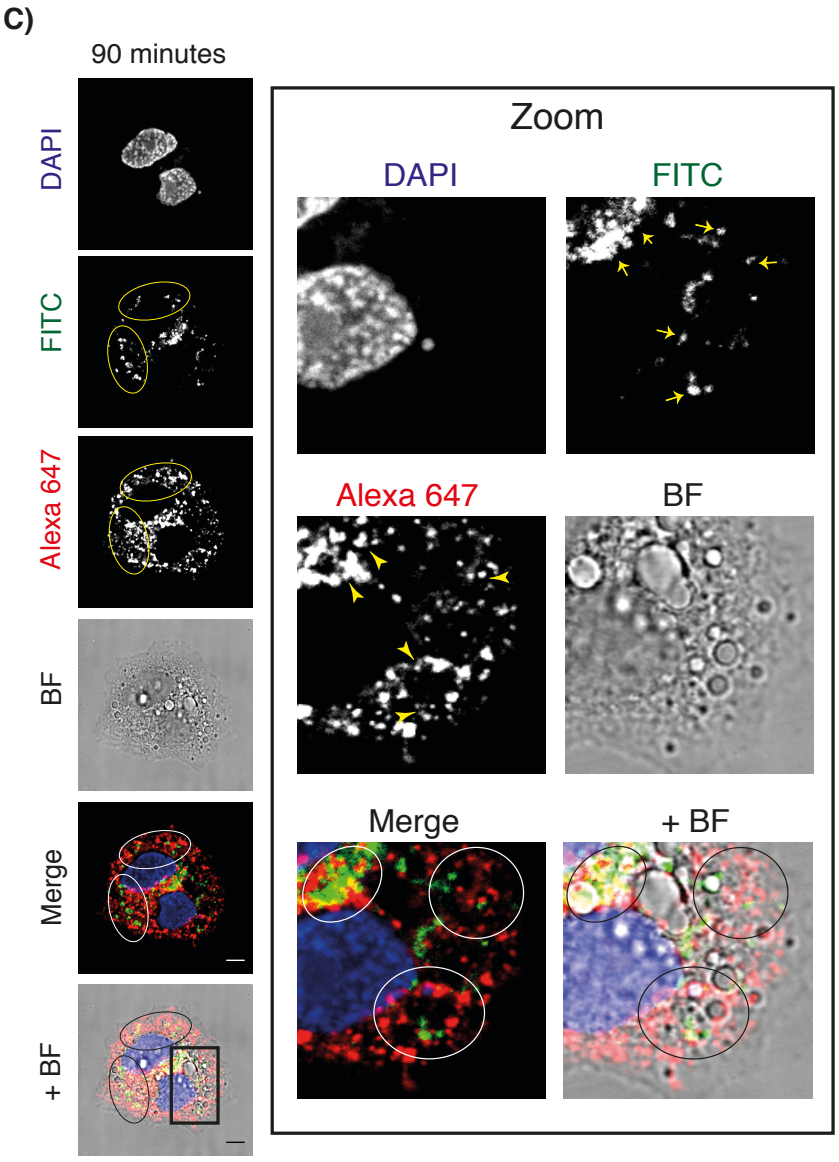

Figure 3.6-2 Entry of srE2^{332}-Fc in hepatoma cell is by a clathrin dependent endocytotic mechanism.

CD81-HepG2 (panel A), HepG2 (panel B) and Huh7.0 (panel C) were treated with srE2^{332}-Fc at the time point shown and incubated in 5% CO_2 at 37°C. Following this, they were fixed with 4% PFA in PBS for 18 minutes at RT. After washing in PBS, cells were permeabilised with 0.1% Triton X-100 in PBS and then washed with 2 mM glycine/PBS. The blocking step with 5% BSA in PBS was conducted for 60 minutes. Clathrin presence was detected by incubating cells in each well with 1µg mouse anti-heavy chain clathrin antibody (MA1065) for 60 minutes, followed by the washing step and bound clathrin was labelled with goat anti-mouse IgG alexa 647 secondary (1 in 150) for 60 minutes. After washing unbound protein, goat anti-Fc FITC (1:30) was added. Cells were counterstained with DAPI, mounted and imaged by confocal microscope. As a control background sample, cells were treated with tPA-Fc or no Fc fusion and then labelled with secondary antibody. Merged nucleus (DAPI), clathrin (Alexa Flour 647) and srE2^{332}-Fc and images merged with the corresponding BF image are shown. Rectangles indicate condensation of clathrin staining at the area close/intact to the cell membrane and

showed overlaying with surface srE2^{332}-Fc staining. Circles indicate an overlay area of clathrin staining with srE2^{332}-Fc staining at the cell surface and into the cytoplasm. The black boxed area is shown at greater magnification and showed detected vesicle decorated with srE2^{332}-Fc (Arrows), clathrin coat (arrowheads) and their overlay (white and black circles). Scale bar is 5 μM.

3.6.3 Study of the association of clathrin with srE2^{332}-Fc incubated for 48 hours with cell lines

We wished to determine whether longer incubation of srE2^{332}-Fc fusions still associate with clathrin into cell cytoplasm. The incubation of CD81-HepG2 for 48 hours with srE2^{332}-Fc showed obvious large cytoplasmic vacuoles decorated with srE2^{332}-Fc fusions and clathrin (**Fig. 3.6-3A**). These vacuoles were obviously larger in size than those previously detected after 90 minutes of incubation (**Fig. 3.6-2**). Each vacuole was well stained with srE2^{332}-Fc and clathrin, which likely means that the small vesicles (which might be endosomes) which were observed after entry of srE2^{332}-Fc at an earlier time point of incubation (30-90 minutes) are fused to each other to form larger vacuoles and indicates that there is a continuum for this fusion. One can speculate that may be an artificial structural formation due to the absence of other HCV components such as envelope E1 or core; their presence might be important to induce functional defined fusion and move the virus to the next step of its life cycle.

On the other hand, incubation with native HepG2 showed srE2^{332}-Fc fusion staining joined with clathrin. Interestingly, the circular structures decorated with both clathrin and srE2^{332}-Fc fusion were still detected, primarily close to the cell membrane with few located into the cytoplasm, indicating poor entry of srE2^{332}-Fc fusion which again points out a correlation between CD81 density rate and efficient envelope E2 entry (**Fig. 3.6-3B**). Huh7.0 showed more entry and localisation with clathrin (**Fig. 3.6-3**). Taken together, our data indicate that although HepG2 cells are poorly competent for srE2^{332}-Fc internalisation, clathrin nevertheless relocates from the cell cytoplasm to the plasma membrane in response to srE2^{332}-Fc binding. In addition, the relocated clathrin in the absence of enough CD81 fails to promote subsequent efficient internalisation of srE2^{332}-Fc. In contrast, clathrin in CD81 positive Huh7.0 and CD81-HepG2 is redistributed from a dispersed cytoplasmic distribution to the plasma membrane region and in particular to membrane clusters in response to srE2^{332}-Fc binding, resulting in efficient srE2^{332}-Fc internalisation in a

process closely associated with clathrin presence. Incubating hepatoma cells with tPA-Fc or only anti-clathrin sera showed no effect on clathrin organisation indicating that the effect on clathrin re-organisation is not due to Fc tag or anti-clathrin sera but specific to the srE2^{332} tag binding effect.

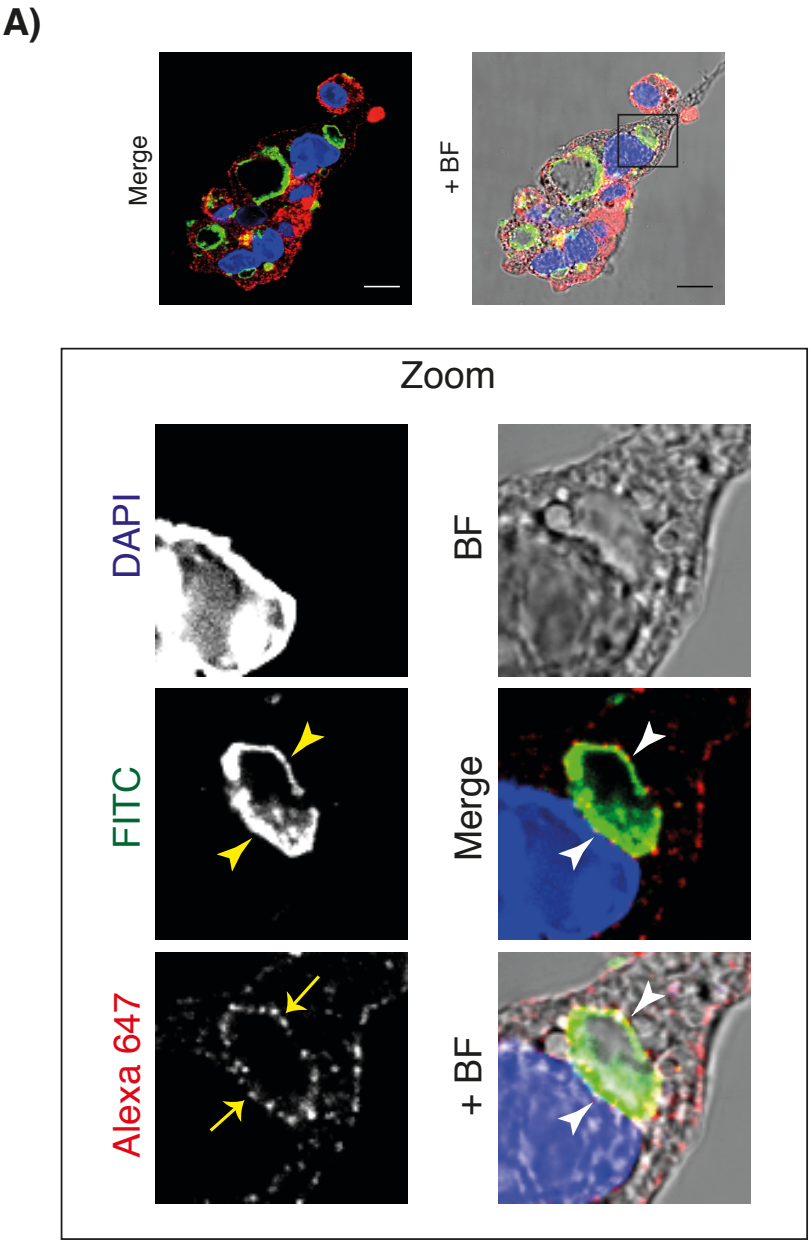
A)
Merge
+ BF
Zoom
DAPI
BF
FITC
Merge
Alexa 647
+ BF

B)

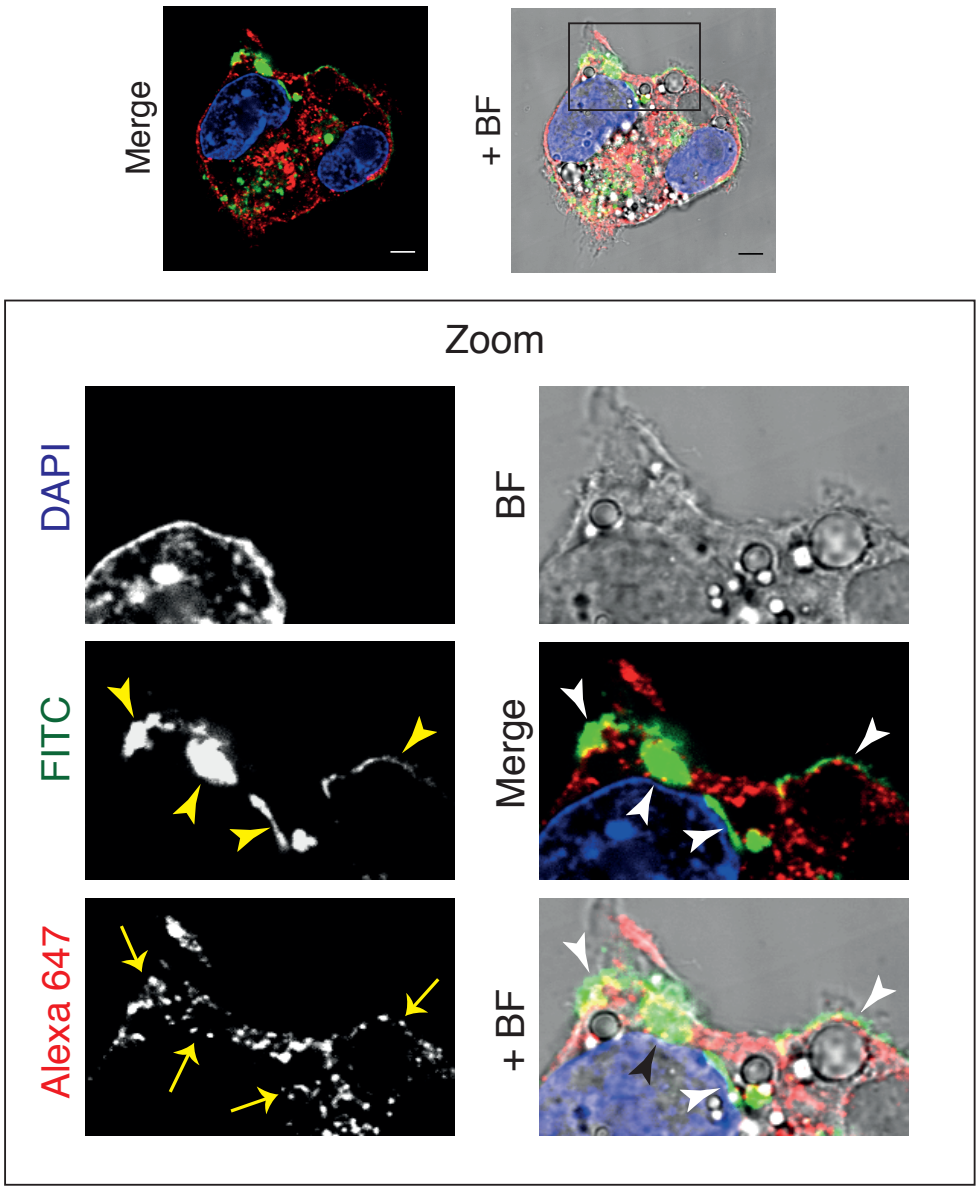

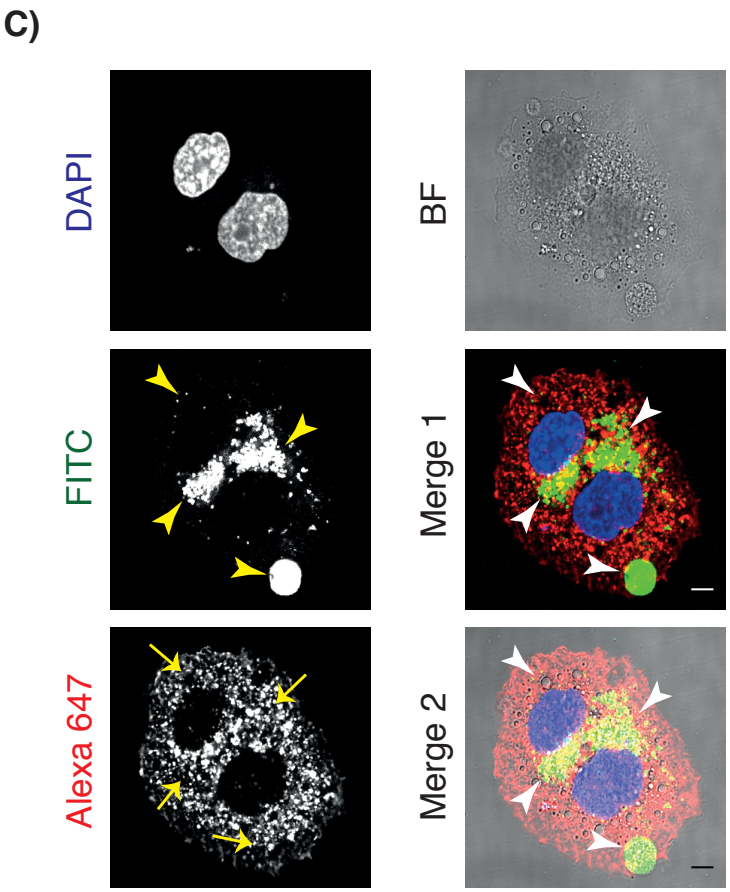

Figure 3.6-3 longer incubation (48 hours) of srE2^{332}-Fc fusion revealed continuous fusion process in association with clathrin.

CD81-HepG2 (panel A), HepG2 (panel B) and Huh7.0 (panel C) were treated with 25 µg srE2^{332}-Fc in each single slide well and labelled with goat anti-Fc FITC (1:30). Clathrin presence was detected with 1 µg mouse anti-heavy chain clathrin antibody (MA1065) and bound clathrin was labelled with goat anti mouse IgG alexa 647 secondary (1 in 150). As a control, cells were treated with tPA-Fc (data not shown). Merged nucleus (DAPI), clathrin (Alexa Flour 647) and srE2^{332}-Fc +/- same image merged with the corresponding BF are shown. The black boxed area is shown at greater magnification. Panel (A) shows vacuole into CD81-HepG2 cytoplasm decorated with srE2^{332}-Fc (yellow arrowheads) and clathrin coats staining (yellow arrows). Panel (B) represents parental HepG2 with clathrin coat vesicles located on and close to the cell membrane (arrows) and its associated srE2^{332}-Fc fusion (yellow arrowheads). Panel (C) shows Huh7.0 with srE2^{332}-Fc staining located at the middle of the cytoplasm and around the nucleus (yellow arrowheads) in association with clathrin (yellow arrows). For all panels, white arrowheads indicate the merged pointed area. Scale bar 10 µM for panel A and 5 µM for panel B and C.

3.6.4 srE2^{332}-Fc entry is markedly reduced by Dynasore

Dynasore is a small inhibitory protein which targets the viral entry step through blocking the GTPase activity of Dynamin (Mues *et al.*, 2015). Dynamin is a multi-domain protein. One of these domains contains the GTP binding site and is important for GTPase hydrolysis activity. Three types are reported: Dynamin-1 specifically present in neuronal tissue; Dynamin-2 has an ubiquitous distribution in various tissue; and Dynamin-3 is expressed in brain, lung, heart and testicular and ovarian tissues (Deol *et al.*, 2000; Rahn *et al.*, 2011). Dynamin plays a key role in the clathrin mediated endocytosis pathway through forming a spiral ring around the neck domain of clathrin coated vesicles which attach to the cell membrane, and upon its GTPase hydrolysis, it pinches off the vesicle from the membrane to the cytoplasm (Hinshaw, 2000; Mettlen *et al.*, 2009). Moreover, dynamin-actin filament binding was demonstrated to play a role in the reorganisation of the actin assembly (Gu *et al.*, 2010). Entry of Herpes simplex viruses (HSV-1 and HSV-2) into keratinocytes of human and murine origin, papillomavirus (HPV16) into human HEK 293T, and VSV into hela cells are all examples of clathrin dependent endocytosis and their entry was reported to be disrupted when cells were incubated with dynasore (Abban *et al.*, 2008; Johannsdottir *et al.*, 2009; Mues *et al.*, 2015; Rahn *et al.*, 2011). Dynamin mutation (K^{44}A) on Madin-Darby bovine kidney (MDBK) cells abolishes the infectivity of the pestivirus bovine viral diarrhoea virus (BVDV) (Cherne *et al.*, 2006). In addition, the infectivity rate of HCVpp (Gt1a H77 strain) and HCVcc (J6/JFH strain) entry into Huh7.5 was decreased by dynamin 2 inhibitor-dynasore (Farquhar *et al.*, 2012; Liu *et al.*, 2009). All demonstrate that these viruses entry are via dynamin-dependant endocytosis.

Thus, we sought to evaluate the impact of dynasore added to Huh7.0 and CD81-HepG2 at the time of srE2^{332}-Fc post binding and pre-entry steps. In brief, to allow binding and reduce the chance of srE2^{332}-Fc fusion entry, cells were incubated with an envelope fusion at 4°C for 25 minutes, which is the predicted optimum time for full-length E2 fusion-cell surface interaction. Control

0.25% DMSO buffer or dynasore were added to treated cells and incubated for an additional 45 minutes at 37°C for temperature-dependent srE2^{332}-Fc entry and srE2^{332}-Fc was labelled with goat anti-human Fc FITC. Our data showed FITC signals were detected abundantly across the cytoplasmic compartment of Huh7.0 and CD81-HpeG2 treated with a control buffer (no dynasore) whereas signals detected on the cell membrane of Huh7.0 and CD81-HepG2 treated with Dynasor showed no significant florescence staining in the cytoplasm (**Fig. 3.6-4**). Therefore, it is likely that the presence of dynasore inhibits the entry of surface-bound srE2^{332}-Fc by blocking dynamin-dependent endocytosis. This thought to happen through disruption of the GTPas activity of dynamin and prevents fission of newly formed clathrin coated vesicles from the cell membrane, stopping their trafficking to the endosome. This data reflects the importance of dynamin as an essential factor for the endocytosis of HCV envelope E2.

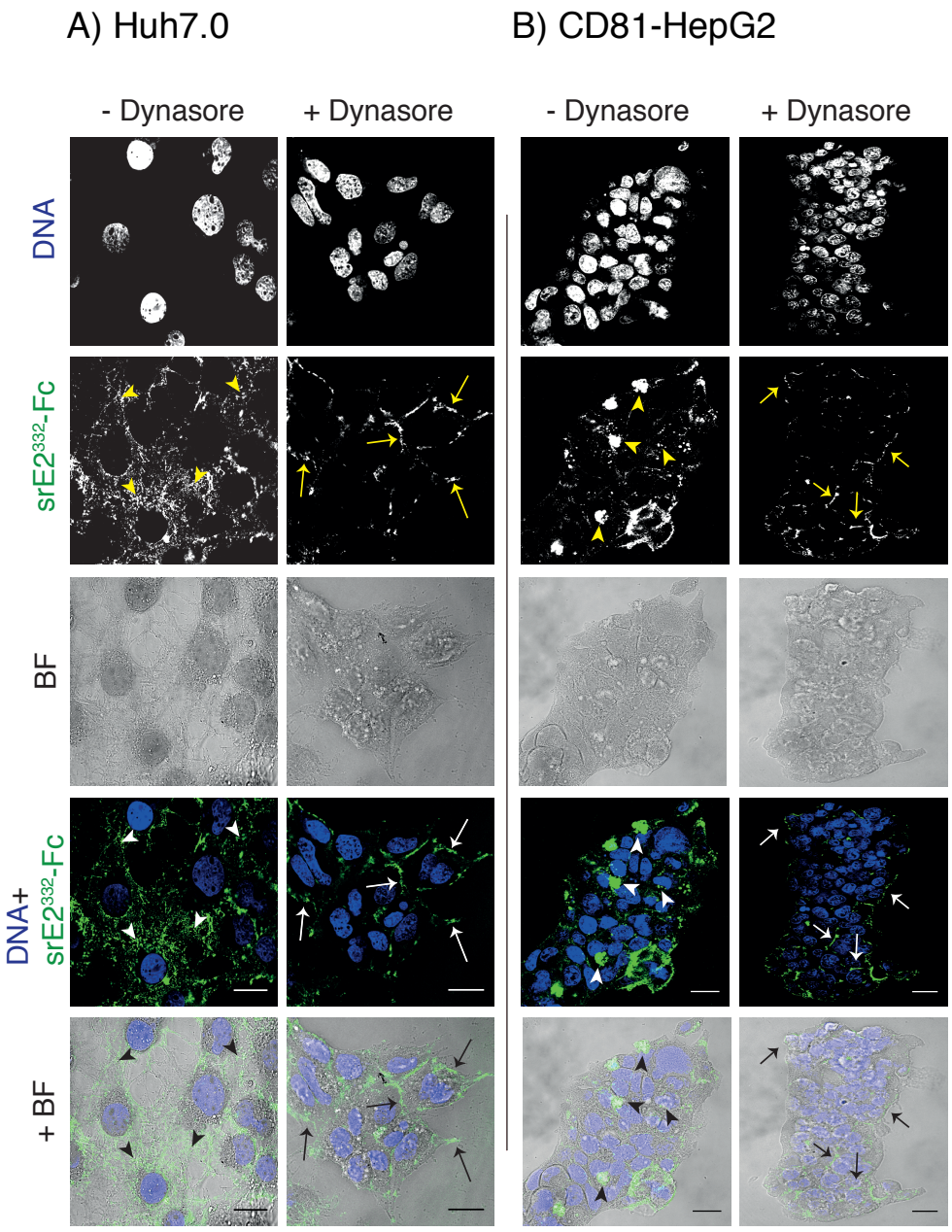

Figure 3.6-4 srE2^{332}-Fc entry into Huh7.0 and CD81-HepG2 is disrupted by dynasore.

The grown cells overnight (20x10^3 per µ-IBIDI slide) were first pre-treated with 15 µg srE2^{332}-Fc for 25 minutes at 4°C (referred to as the period that is required for binding to cell surface at cold condition). Subsequently, unbound envelope fusions were removed by washing cells 3x with serum free media. 40 µM Dynasore hydrate (D7693) with 0.25% dimethyl sulfoxide (DMSO) and serum-free medium or 0.25% DMSO with serum-free media (control) were added to the treated cells and incubated for 45 minutes in 5% CO_2 at 37°C. The cells were washed 3x to remove dynasore or control buffer and were fixed with 4% PFA in PBS for 18 minutes at RT.

Cells were washed 1x and incubated with 0.1% Triton X-100 in PBS for 3 minutes, incubated with 2 mM glycine/PBS for 5 minutes and washed out 3x with PBS. Cells were blocked with 5% BSA in PBS for 60 minutes at RT. After triplicate washing with 0.1% BSA in PBS, secondary goat anti-human Fc FITC (1:150 in blocking solution) was added for 60 minutes. Unbound secondary sera was washed with 0.1% BSA in PBS (3x). Cells were co-stained with DAPI. IBIDI mounting media applied to cells in wells was followed by confocal analysis. Nucleus (DAPI) and srE2^{332}-Fc (FITC) and images merged with the corresponding BF image are shown. Control (-Dynasore) and sample images (+ve dynasore) for treated Huh7.0 (panel A) and CD81-HepG2 (panel B) are presented. Arrows indicate srE2^{332}-Fc staining which accumulated into the cytoplasm of cells treated with control buffer. Arrowheads indicate srE2^{332}-Fc staining on the cell membrane of cells incubated with dynasore (no significant cytoplasmic staining was observed). Scale bar 20 μM.

3.7 srE2^{332}-Fc is internalised into IPSCs

The hepatoma cell lines, HepG2 and Huh7, differ radically in surface marker expression and permissiveness for HCV infection and are not typical of untransformed human hepatocytes. We therefore examined the ability of human pluripotent stem cell (hPSCs) derived hepatocytes (also called induced pluripotent stem cells, IPSCs) to bind and internalise srE2^{332}-Fc. Human hepatocytes were derived from hPSC by small-molecule-driven differentiation. The hepatocytes formed dense monolayers and exhibited key hepatic attributes including glycogen storage, serum protein generation, and cytochrome P450 expression (Siller *et al.*, 2015).

Incubating fixed IPSCs with mouse anti-CD81 and probing with anti-mouse Alexa Fluor 488 demonstrated fluorescence expression, distributed over almost the entire cell surface **(Fig. 3.7-1A).** This indicates that hepatocyte monolayers displayed CD81 abundantly. Strikingly, treating live IPSCs with srE2^{332}-Fc for 30 or 60 minutes in 5% CO_2 at 37°C followed by labelling with anti-Fc FITC after the cells were fixed revealed the detection of FITC signals on the cell surface and in the cytoplasmic compartment **(Fig. 3.7-1B)**. These results demonstrate that induced pluripotent stem cells bound copious amounts of srE2^{332}-Fc and internalised the srE2^{332}-Fc fusion, which was observed in small granular speckles after 30 minutes of incubation and enlarged speckles after 60 minutes of incubation. The sizes of the spherical vacuoles were up to 11 μm in diameter and were generally consistent with early endosomes appearance; this possibly means the srE2^{332}-Fc reached the fusion process too. Thus, the rapid internalisation of srE2^{332}-Fc in the complete absence of all other viral protein is observed in induced pluripotent stem cells and is not peculiar to transformed hepatoma cell lines.

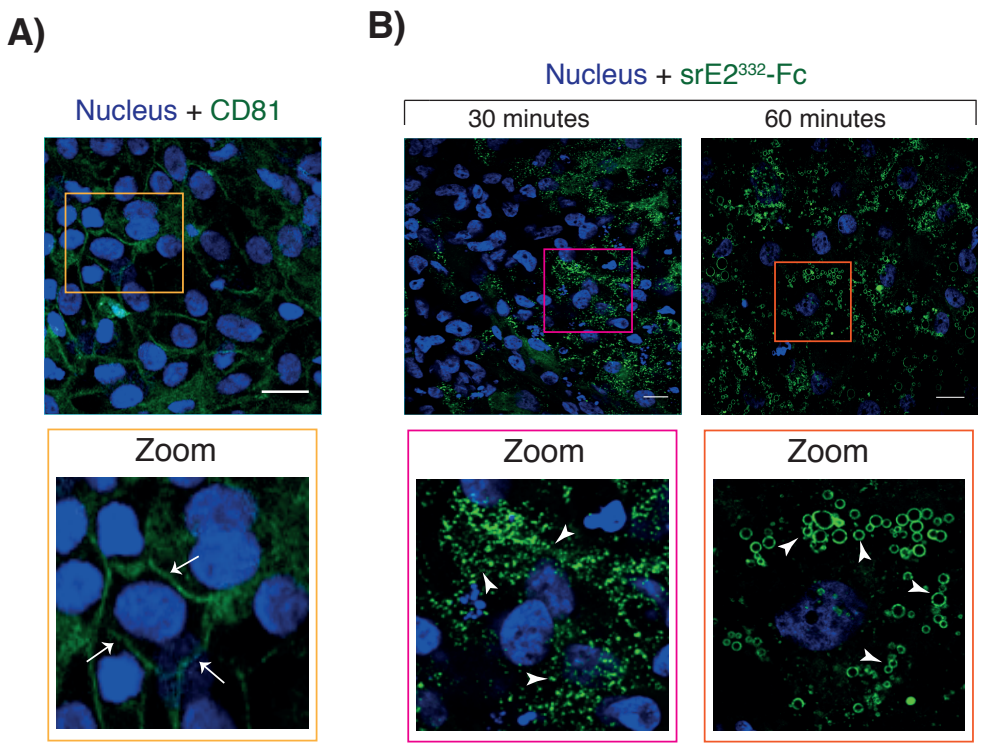

Figure 3.7-1 IPSCs express CD81 and uptake srE2^{332}-Fc.
The methodology of growing monolayers cells was done by Dr. Gareth's laboratory. Panel (A) staining protocol: cells were incubated with PFA, rinsed 2x in PBS and then incubated with 5% BSA in PBS solution at RT. CD81 presence was detected by incubating cells in each µ-Slide well with 1.5 µg mouse anti-CD81 (5A6) followed by 3x wash in washing buffer (0.1% BSA in PBS). The reaction was labelled with goat anti-mouse Alexa Fluor 488 conjugate (1 in 150) for 60 minutes and the cells were then rinsed 3x in washing buffer. Panel (B) staining protocol: srE2^{332}-Fc (30 µg) were added to cells in 5% CO_2 at 37°C for 30 or 60 minutes. Unbound antibody was removed and cells were fixed with 4% PFA/PBS solution for 18 minutes at RT. 0.1% Triton X-100/PBS solution was added followed by the washing step 2x in PBS. Then, cells were incubated with 2 mM glycine/PBS for 5 minutes followed by a wash 2x in fresh PBS solution. Cells were incubated with blocking solution (5% BSA/PBS) for 60 minutes at RT followed by the removal of extra blocking solution. The reaction was probed with goat anti-human FC FITC (1 in 150) and incubated for 60 minutes followed by 3x wash in washing solution (0.1% BSA/PBS). For both A and B panels, DAPI staining (nucleus) and Alexa Fluor 488 and FITC staining (CD81 or srE2^{332}-Fc fusion respectively) are shown as a merged image. tPA-Fc was used as a negative control (not shown). The boxed area is shown at greater magnification. Arrows indicate expression of CD81 staining on the surface of IPSCs. Arrowheads indicate srE2^{332}-Fc staining located in the cell cytoplasm and circular vacuoles decorated with srE2^{332}-Fc after envelope fusion incubation as shown. Panel (A) represents expression of surface CD81 and panel (B) represents entry of srE2^{332}-Fc into IPSCs. Images were caught using 40x scanning objective. Scale bar 50 µM. Practical work was done by Dr. Gareth Sullivan and his group (University of Oslo, Norway) using our reagents and following our methodology guidelines.

.

3.8 Discussion

3.8.1 The efficient expression of E2 immunoadhesin form by DS2ES

Our knowledge of HCV entry into cells has been increased by the development of pseudotyped virus-like particles and HCV culture systems. However, interpretation of the data obtained have been complicated by the disparate nature of these biological systems, variations in the infectivity of such systems at different laboratories, the use of laboratory-adapted HCV isolates, the range of cell types employed, and the diversity of the markers used to detect and quantify infection. To overcome some of these issues, in this study, we have developed a set of HCV E2-derived immunoadhesins for use as direct biochemical probes for E2 function and cell-receptor binding activity. It has been reported that the expression of HCV envelope glycoproteins in mammalian systems tends to increase the risk of production of large proportions of misfolded and disulfide linked aggregated proteins due to related to unknown host and virus factors (Choukhi *et al.*, 1998; Deleersnyder *et al.*, 1997; Flint *et al.*, 2000). In many cases, the mammalian expression of secreted E2 (GT1a) involves truncation at residues Gly^{285}, Gly^{321} and Lys^{332} (corresponding to $E2_{668}$, $E2_{704}$ and $E2_{715}$), which leads to the development of misfolded E2 aggregates. These are considered merely poor, functional dead-end products, in terms of the weak recognition of conformational structures and disulfide binding proteins, and the associated achievement of low yields (Forns *et al.*, 2000a; Lavanchy, 1999; Michalak *et al.*, 1997). Indeed, these sites of truncation are behind the widely applied truncation of the GT1a envelope E2 at residue Glu^{278}, which has been associated with the production of the best, most correctly folded $E2_{661}$ mammalian protein (Choukhi *et al.*, 1999; Lucas *et al.*, 2003). Forns *et al.* (2000a) have concluded that when E2 is truncated at Glu^{278}, efficient surface expression is achieved in Huh7 cells that display correct folding features. This is compared with poor surface-expression results achieved with (full-length) E2 truncation at Lys^{332}. In addition, some

researchers report that small fractions of E1 and E2 complexes can be detected in the cell lysate of transfected mammalian cells and associated with low protein yield, which creates issues when seeking to study HCV envelope proteins with sufficient reagents (Dubuisson *et al.*, 1994). It is likely that, where the expression of HCV envelope E2 is concerned, some researchers have avoided extending E2 truncation beyond Glu^{278} due to the aforementioned difficulties associated with E2 expression.

It is important to ensure that the glycoproteins produced undergo the correct conformational pathway so that accurate understandings of the functional characterisation of HCV envelopes can be achieved. Our results indicate that the drosophila expression system, which does not seem to have been applied to a great extent in the study of HCV envelopes, is a suitable model that can be used to increase the efficiency of HCV E2 glycoprotein expression. This is due to the retention of biological activities and high levels of expressed protein (indistinguishable from those produced by mammalian cell lines) which are associated with the model. Additionally, immunoadhesin of the heavy-chain Fc dimers that link all E2 derivatives in both reduced denatured conditions and non-reduced native conditions has been found to enable the Fc domain to retain its binding affinity. This suggests that insect cells support the production of highly natural, conserved conformational proteins, as indicated previously by colleagues investigating the expression of human antibodies and other proteins (Flajnik, 1994; Kirkpatrick *et al.*, 1995). Most importantly, monoclonal anti-E2 (15B10) recognised our linear soluble E2 epitopes successfully and immobilised native E2 forms. HCV patient sera containing anti-HCV E2 were also found to recognise immobilised $srE2^{332}$-HAH6 fusion, which indicates that E2 follows the proper folding and maturation pathways in insect cell systems, when fused with Fc or HAH6 domains. After 24 hours of $CuSO_4$ induction, we noted fast expression rates for $srE2^{332}$-Fc fusion (and variants $srE2^{295}$-Fc, $srE2^{278}$-Fc, $srE2^{265}$-Fc and $srE2^{195}$-Fc) into S2 media, while cell lines were still at the transient stage, as well as massive levels of E2 expression after the selection of stable cell lines. These findings are likely to be due to virus-related and host-related factors. The lack of C-terminal hydrophobic regions in our

HCV E2 sequence supported the secretion of the E2 into culture media. This is consistent with the results of previous studies, which have found that C-terminal domains have ER-retention signals and are associated with the localisation of expressed E1 and E2 into the ER of mammalian cells. Absences of C-terminal domains of envelopes lead to the detection of the secreted product in media (Cocquerel *et al.*, 1998; Duvet *et al.*, 1998b; Ralston *et al.*, 1993). Moreover, we cannot ignore that the fast rates of solubility for $E2^{332}$-Fc (and its derived variants) and the high yields of the final products were related to advantages associated with drosophila S2 cells, which involve Metallothionein promotor (pMT) that can process approximately 1000 gene copies in a single stable S2 cell, when selected with Hygromycin B (Angelichio *et al.*, 1991; Santos *et al.*, 2007). Our findings correspond with those of other researchers, in terms of the achievement of high levels of expressed proteins in drosophila cells such as hepatitis B surface antigens (HBsAg) (Jorge *et al.*, 2008), heavy-chain Fc proteins (Kirkpatrick *et al.*, 1995), human interlukin-2 (IL-2) (Shin *et al.*, 2003) and recombinant rabies virus glycoproteins (rRVGP) (Yokomizo *et al.*, 2007). Furthermore, the strong affinity of protein A with properly folded Fc helped the large-scale purification of srE2-Fc-derived fusions.

One published report has demonstrated that $E2_{661}$-HA expressed on the surface of transfected 293T cells and lacking TMD can be recognised successfully by Mab anti-E2 (H2) and anti-E2 (H33), and can interact with recombinant CD81 LEL. This finding indicates that an absence of TMD might help to reduce misfolding in E2 production (Flint *et al.*, 1999a; Flint *et al.*, 1999b). This can be applied not only to functional secreted proteins that carry the same point of truncation (srE2^{278}-Fc) but also to other forms that carry a truncation point beyond Glu^{278} (srE2^{295}-Fc and srE2^{332}-Fc) or before Glu^{278} (srE2^{265}-Fc and srE2^{195}-Fc). Some scientists have reported that transient expression in 293T cells results in high proportions of soluble $E2_{661}$ products in aggregated forms that are unable to recognise native CD81 receptors and related monoclonal antibodies, unless processed using high-pressure liquid

chromatography (HPLC) to form monomeric proteins (Flint *et al.*, 2000). In our study, native srE2^{332}-Fc, srE2^{295}-Fc, srE2^{278}-Fc and srE2^{265}-Fc did not undergo such a significant phenomenon, and all were able to bind conformational-dependent monoclonal anti-E2, rMBP-MBP-CD81 LEL and native CD81 factors in 293T cells without the need for HPLC processing. This reveals that E2 in drosophila cells tends to follow what could be considered the optimum conformational pathway, being secreted in a form that probably mimics native single E2 on the virus surface. Based on this accumulated evidence, we recommend the *Drosophila melanogaster* Schneider 2 cell expression system (DS2ES) for the expression of secreted, highly glycosylated HCV E2 due to the proper protein processing and biological activity associated with this method.

3.8.2 srE2^{332} peptide fusion recognise native CD81 and rCD81 LEL

Our chimeric immunoadhesin protein accurately reflected the cell and receptor binding properties of native HCV E2. srE2^{332}-Fc fusion was highly efficient for binding to a variety of human cell types, including fibroblast-derived cells, hepatoma cells and lymphoma cell lines. Moreover, the binding of srE2^{332}-Fc to 293T cells was dose-dependent and saturable, reflecting specific binding to surface factors on 293T cells. The expression of abundant CD81 on the surface of 293T was observed, and srE2^{332}-Fc binding was antagonised by the monoclonal anti-CD81 mouse antibody (5A6) at 37°C, which means that srE2^{332}-Fc fusion recognises native CD81 receptors on the surface of 293T cells, in the absence of blocking anti-CD81 sera. A similar approach has already been taken by Pileri *et al.* (1998), who found that recombinant E2$_{661}$ forms expressed in CHO cells can bind CD81 receptors successfully on Epstein-Barr virus (EBV)-associated B-cell lymphomas. In addition, the treatment of EBV-B cells with rE2$_{661}$ at 4^{o}C, after which anti-CD81 antibodies were added (clone JS-81, Pharmingen) led to inhibition E2$_{661}$ binding to cells. Although the use of anti-CD81 led to a noticeable antagonistic effect on

srE2^{332}-Fc fusion results, we could not inhibit total surface binding. This result might indicate that HCV binding to 293T cells occurs through the interaction of full-length srE2 with additional limited cell-surface molecules (other than CD81). Additionally, it was found that, in ELISA, both the anti-CD81 antibody and srE2^{332}-Fc (which corresponds to E2$_{715}$) bound to the large extracellular loop of immobilised recombinant MBP-CD81 LEL, which is consistent with other researchers' findings, in which the C-terminal LEL (or EC2) of human CD81 was fused with Thioredoxin (TRX- CD81 EC2) and bound to the recombinant E2$_{661}$ form (Pileri *et al.*, 1998). Our results are supported further by Flint *et al.* (1999b) and Higginbottom *et al.*'s (2000) findings, in which the soluble E2$_{661}$ form recognised the recombinant glutathione-S-transferase (GST)-CD81 LEL protein. Significantly, as measured by flow cytometry, the binding of srE2^{332}-Fc to cells was blocked in a dose-responsive manner in competition binding assays with soluble CD81 LEL at 37°C. Taken together, the data indicate that the immunoadhesion of srE2^{332}-Fc faithfully replicates the immunological features and known CD8-binding properties of HCV E2. This proves that our full-length E2^{332}-Fc (native E2$_{715}$) behave in such a way that is similar to the published truncated E2$_{661,}$ in terms of its binding capacity to CD81 LEL and various cell lines of human origin.

3.8.3 Increased efficiency in binding with srE2^{332}-Fc than with srE2^{265}-Fc fusion

Recent structural and functional studies have mapped the E2 amino acids that are required for interaction with CD81, and it has been found that these E2 residues form part of a discontinuous CD81-binding motif (Khan *et al.*, 2014; Kong *et al.*, 2013). Significantly, our deletion constructs retain the known CD81-binding residues, with the exception of srE2^{195}-Fc fusion, which carries a large C-terminal deletion that extends into the CD81-binding region and removes the amino acid residues Y^{230}, H^{234} and Y^{235} that have been reported to be involved in interactions with the LEL of CD81 (Rothwang *et al.*, 2008). To date, srE2^{265}-Fc (which corresponds to E2$_{648}$) has been shown to retain all of

the amino acids present in the recently solved crystal structure of the core HCV E2 protein. The extra amino acids that are involved in the full-length srE2^{332}-Fc fusion protein (which lack only the E2 transmembrane spanning domain) and the deletion derivatives terminating at amino acid residues 278 and 295, (which have relatively small deleted C-terminal regions) have not yet been shown to be involved in CD81 binding. It is notable that, among the E2 derivatives utilised here, differences were found in the ability of E2 immunoadhesins to bind to 293T cell immobilised CD81 LEL. We observed routinely that srE2^{332}-Fc was the most efficient in binding to cells and to the LEL domain of CD81, followed by srE2^{295}-Fc and srE2^{275}-Fc. Where cell and CD81 LEL binding are concerned, srE2^{265}-Fc was found to be less efficient in which the large C-terminal deletion in the srE2^{265}-Fc derivative resulted in a protein that was less efficient in binding assays than srE2^{332}-Fc. This was most apparent at low protein concentrations. The E2 core structure defines a CD81-binding region that includes a large, discontinuous contact motif, comprised of amino acids that are brought into proximity by the E2 fold. The E2 amino-acid residues revealed to be important for CD81 binding by structural analysis are all contained within the E2 sequences present in srE2^{265}-Fc. Why, then, is srE2^{332}-Fc more efficient than srE2^{265}-Fc in binding to cells or to immobilised CD81 LEL? HCV E2 is known to bind to a variety of cell surface factors that act to enhance HCV binding and internalisation, and it may well be that srE2^{265}-Fc lacks the relevant co-factor binding sites found in the C-terminal regions in E2. In addition, residues more C-terminal than amino acid 265 may contribute directly to CD81 interaction, thereby enhancing the affinity with CD81. Alternatively, the C-terminal region may contribute to the binding reaction by helping to present the CD81-binding domain of E2 in an optimum form for interaction with CD81. Currently, we cannot exclude the possibility that regions of E2 distal to residue 265,simply improve the solubility of the longer srE2-Fc constructs thereby improving the availability of the recombinant proteins for CD81 binding. Interestingly, 293T cell-specific binding by srE2^{332}-Fc could not be outcompeted fully by competition with excess exogenous recombinant CD81 LEL, indicating that either the LEL binds poorly to E2, relative to the

native plasma membrane displayed in CD81, or that receptors other than CD81 play important roles in primary recognition of, and attachment to, the surfaces of cells.

Although 293T cells bind to srE2-immunoadhesins, these cells do not support HCV or virus pseudoparticle entry (Bartosch *et al.*, 2003b). We compared the pattern for E2 binding, therefore, with that for human hepatoma cells. In our study, fluorescence imaging and flow cytometry indicated that, as described previously, Huh7.0 cells express an abundance of cell-surface CD81, and these cells are known to be permissive of HCV entry. Contrastingly, like others, we have found that HepG2 cells display exceedingly low levels of cell-surface CD81, and these cells are known to be poorly permissive of the entry of free virus particles (Zhang *et al.*, 2004a; Zhong *et al.*, 2005). Despite these marked differences in CD81 expression and sensitivity to HCV infection, both these hepatoma cell lines were found to bind copious amounts of srE2^{332}-Fc. Our data demonstrate that, while HepG2 cells display a paucity of CD81, they are competent, nevertheless, in terms of binding E2. Here, the amount of E2 bound exceeds the CD81 that is available, which is consistent with the view that E2 is competent for binding directly to cell surface receptors other than CD81, and that this involve attachment of full length srE2^{332}-Fc and therefore HCV to cells. In contrast with the binding of other E2 forms to hepatoma cells, we observed that srE2^{332}-Fc was the most efficient in binding to Huh7.0 cells, followed by srE2^{295}-Fc and srE2^{275}-Fc. Additionally, srE2^{265}-Fc is less efficient in cell binding, behaving similarly in Huh7.0 cells as in 293T cells. This result is consistent with the view that large, deleted C-terminal srE2^{265}-Fc has a low binding capacity with CD81 receptors and that presence of residues beyond R^{265} are important in enhancing the attachment of a virus to a CD81 receptor. In addition, our data demonstrate that HepG2 cells bind copious amounts of the srE2^{295}-Fc, srE2^{278}-Fc and srE2^{265}-Fc probes. Flow cytometry showed that srE2^{278}-Fc was the most efficient in binding the HepG2 cell surface, which was followed by srE2^{332}-Fc and srE2^{265}-Fc, and then srE2^{295}-Fc. These differences in the capacity to bind the HepG2 cell surface are associated with the low

expression of CD81, and can be expected consistently, as there are many alternative attachment factors with different binding capacities for binding with various regions in HCV E2. Although the impaired binding of larger C-terminal deletion srE2^{195}-Fc to hepatoma cells that either do or do not express CD81 was demonstrated, binding to HepG2 was found to be better than binding to other cells. It is likely that first 195 residues sequence of the N-terminal of E2 has a higher capacity to bind alternative receptors than CD81, which are probably expressed more on HeG2 cell lines than on Huh7.0 cell lines.

3.8.4 Efficient srE2^{332}-Fc binding to HepG2 cells can be achieved via CD81 expression

Notably, the ectopic expression of CD81 on HepG2 cells increases the surface display of CD81 and, consistent with the increased density of cell surface receptors, augments the binding of srE2^{332}-Fc to cells. Additionally, in contrast with the binding pattern for srE2 forms to HepG2 cells, a flow cytometry examination confirmed a change in the affinity binding of E2 forms to these cells. srE2^{332}-Fc showed the highest efficient interactions with CD81-HepG2, followed by the identical binding of srE2^{295}-Fc and srE2^{278}-Fc. The binding capacity of srE2^{265}-Fc, however, did not seem to be improved much in the presence of abundant CD81 on the cell surface. This follows the view put forth that the full-length srE2-Fc form contains all the necessary amino acids to initiate a high capacity to bind CD81 whereas srE2^{265}-Fc is less efficient in binding CD81 and may have a high capacity to bind other receptors (or factors). Importantly, our results demonstrate that the binding capacity of the srE2^{195}-Fc form with CD81-HepG2 is up to two times less than the capacity with HepG2 cells. This might be due to the masking of the target surface factor on the cell surface; nevertheless, it is an important indicator that the binding of the large deletion srE2^{195}-Fc form to the CD81 receptor is severely impaired.

3.8.5 srE2^{332}-Fc induces receptor clustering in Hepatocytes and is internalised in a rate-limited manner determined by receptor density

An important observation from our studies is that in the complete absence of all other viral protein, E2 is sufficient not only for binding to cells, but also for rapid endocytosis-mediated internalisation into cells. Resonant with the distinct entry tropism of HCV and E2-pseudotyped virus-like particles, target cells differ markedly in their permissiveness of srE2^{332}-Fc internalisation. The HCV-permissive Huh 7.0 cell line, which expresses copious amounts of CD81, claudin-1 and occludin, permits rapid binding and rapid internalisation of srE2^{332}-Fc, which is present in clathrin-enriched regions of the cytoplasm. By comparison, 293T cells display CD81 and are competent for srE2^{332}-Fc binding, but do not support the rapid internalisation of E2, even after extensive incubation (6 hours). Instead, the E2-immunoadhesin remains associated with the cell surface, where it coalesces into large CD81- and claudin-1-associated aggregates after 60 minutes of incubation. Exceedingly little, if any, srE2^{332}-Fc is translocated to the interior of the cell following longer incubation (24–48 hours). It is worth noting that we witnessed a correlation between the greater capacity of the srE2-Fc form to bind 293T cells, and the speed of spanning over cell membranes and capping formation (predicted event post-binding and pre-entry of viral envelope) by confocal microscopy. Our data has confirmed that srE2^{332}-Fc fusion is the fastest form to be localised and has a significant capping structure, which may related to the high binding capacity between sE2^{332}-Fc and abundant surface CD81. srE2^{265}-Fc, on the other hand, was the slowest form in relation to such localisation and capping formation. This result is consistent with a lower binding capacity to bind MBP-CD81 LEL and CD81 on 293T cells. Furthermore, srE2^{265}-Fc had the lowest sensitivity to anti-CD81 added to 293T cells. Overall, these data suggest that, despite the surface expression of CD81 and the detectable expression of claudin-1, SR-B1 and occludin, either 293T cells lack a critical factor required for the rapid internalisation of E2 (and, by inference, HCV) or, alternatively the relative

densities of these various factors are not ideal for E2 internalisation. Contrastingly, HepG2 cells retain the ability to bind to srE2^{332}-Fc and to express high levels of claudin-1, occludin and SR-B1; they have, however, exceedingly low levels of surface-displayed CD81. Distinctively, HepG2 cells fail to internalise srE2^{332}-Fc efficiently even after periods of extended incubation (up to 24 hours), which contrasts with the entry manner into Huh7.0. Notably, the srE2^{332}-Fc internalisation phenotype can be dramatically rescued in HepG2 cells via ectopic CD81 expression, suggesting that, while other cell surface markers are sufficient for E2 binding, these markers are unable to support rapid E2 internalisation in the absence of adequate CD81.

We have also demonstrated that the entry of srE2^{332}-Fc into CD81-HepG2 cells involves clathrin-mediated endocytosis. Within a time period of less than 30 minutes of cell incubation, srE2^{332}-Fc can be observed as being attached to cell surface receptors and as being present in cytoplasmic vesicles (or vacuoles). Patches of srE2^{332}-Fc on the plasma membrane surface are frequently associated with areas on the cytoplasmic face of the membrane that are enriched with clathrin. Moreover, internalised srE2^{332}-Fc is present in vacuoles associated with CD81 in which clathrin frequently occurs. It is worth noting that treating Huh-7.0 and CD81-HepG2 cells with dynasore (a dynamin inhibitor) markedly inhibits the entry of surface-bound srE2^{332}-Fc, which, in all likelihood, is due to the dynamin GTPase activity, that is required for the fission of clathrin-coated vesicles with cell cytoplasm, being blocked. It is also probable that this entry inhibition involves a reduction in CD81 uptake. Farquhar *et al.* (2012) reported that treating Huh7.5 cells with antibody target receptors or with HCVpp increases the endocytosis of CD81 and claudin-1, while treating Huh7.5 cells with dynasore inhibits the entry of CD81 and claudin-1. This is consistent with our results regarding the accumulation of srE2^{332}-Fc, CD81 and claudin-1 in the cytoplasm of Huh7.0 cells, which, indeed, reflects their role in endocytosis of srE2^{332}-Fc fusion. Overall, the results that we obtained by using the srE2^{332}-Fc probe accord with earlier

studies, in which the poor HCV entry phenotype of HepG2 cells has been shown to be ameliorated by the expression of CD81.

3.8.6 Initial evidence regarding srE2^{332}-Fc incorporation in endosomal fusions

Our findings demonstrate that mature IPSCs generated initially from hPSCs can mimic transformed hepatoma cells, in terms of the binding and uptake of srE2^{332}-Fc – a process which added further functional value to the E2 peptide that we produced. In our data, small vacuoles associated with srE2^{332}-Fc were detected in the cytoplasm of CD81-HepG2 and IPSCs, when incubated live with srE2^{332}-Fc (20–30 minutes). Obviously enlarged vacuoles were detected after a further 30 minutes of incubation, thus giving an appearance identical to that of early endosomes. Extensive incubation of CD81-HepG2 with srE2^{332}-Fc (24 hours) led to a pronounced increase in the size of vacuoles, which formed tubular-like shapes. There was no sign of spherical vacuoles after longer time of incubation. This probably means that the spherical endosomes underwent further rapid fusion, leading to the formation of these giant endosomes. Indeed, our observations are comparable with Skjeldal *et al.*'s (2012) findings, in which the ectopic expression of cytoplasmic tails in Ii (MHC-class II-associated chaperone invariant chain), Rab5 and EEA1 in Madine-Darby canine kidney cells (MDCK cells) led to a prolonged endosomal process, which was associated with bigger endosomes of up to 10 μm in diameter (our srE2^{332}-Fc incubation with IPSCs for 60 minutes led to endosomes that measured up to 11 μm in diameter). In Skjedal *et al.*'s study, these large early endosomes also underwent a fast fusion process lasting a matter of seconds. If this style of fusion holds true for our CD81-HepG2 model, it might mean that our srE2^{332} peptide fusion is involved in recruiting high rates of Ii, Rab5 or EEA1, thus inducing the process of early-endosome fusion via an undefined endosomal mechanism. We stress the need here for further investigations to validate this scenario.

3.8.7 The proximal heptad region and the stem residues of E2

Our recombinant full-length $E2^{332}$-Fc contained membrane proximal heptad, located repeatedly at residues 292–316. Drummer and Poumbourios (2004) report that mutation introduced at conserved residues using six HCV genotypes (at L^{292}, S^{295}, L^{306} and L^{309}) significantly affects E1E2 heterodimer formation and prevents HCVpp entry into Huh7. In addition, they found that these mutants retain an affinity for rCD81 LEL binding and are neutralised by the antibody targeting E2 at residues 1–278. The mutation of E2 at residues P^{293} and P^{300} was shown to have no effect upon E1-E2 heterodimerisation or upon interaction with rCD81 LEL, while its mutation at P^{300} but not P^{293} totally blocked the entry of HCVpp into Huh7. Stem residues located at 317–332 (in accordance with our recombinant sequence) have been reported to confirm the heptad repeat region and enhance the heterodimerisation of E1-E2 (Molenkamp *et al.*, 2003). However these published results rely on an analysis of generated full-length E1 and E2, which involves the presence of TMD and different experimental conditions. The presence of both the proximal heptad region and stem residues in our secreted $E2^{332}$-Fc was associated with highly efficient binding with CD81, surface spanning with host factors on cell the membrane and entry into Huh7 cells. These findings suggest the importance of these regions to the optimum presentation of the E2 envelope.

The detailed roles of each HCV receptor and entry co-factor and the precise route of HCV entry are beginning to be resolved. Parallels have been drawn here with the sophisticated entry process of coxsackievirus B (CVB) into polarised human-gut epithelia (Coyne & Bergelson, 2006; Coyne *et al.*, 2007). In brief, CVB binds initially to CD55, which permits the lateral translocation of the CD55/CVB complex to the tight junction, where CVB binds coxsackievirus and adenovirus receptors (CAR) and undergoes internalisation (Coyne & Bergelson, 2006; Coyne *et al.*, 2007). Current models suggest that a similar process may underlie the rapid internalisation of HCV particles, where HCV docks with cell surface CD81, which allows the translocation of the virus particle over the membrane surface to sites where the recruitment of additional

entry factors such as claudin-1 and the tight-junction protein occludin can occur. The viral E2 protein can be said, therefore, to orchestrate the assembly of a multimeric complex that is competent for endocytosis and for translocation into cells. Importantly, our data reveal that at low CD81 densities, E2 remains competent for cell-surface binding, presumably due to interactions with other co-factors within the binding and entry pathway. Our results indicate that it is unlikely that there is a strict order of binding to cell surface factors, in which E2 binds initially to CD81 which was detected on the surface of low expressing CD81 HepG2 cells; instead, E2 may be capable of binding at multiple distinct receptor sites, subsequently recruiting the pertinent co-factors required for endocytosis and translocation across the plasma membrane. However, a lack of one or more factors in the binding and entry pathway, or, alternatively, the insufficient density of a particular factor (such as CD81) on the plasma membrane can impair the assembly of an endocytosis-competent entry complex, thus affecting the rate of E2-orchestrated uptake (and, therefore, virus particle entry) severely.

Our panel of E2-derived immunoadhesins provides a valuable set of tools with which to probe and dissect the HCV E2-dependent entry process at a molecular level. Taken together, amino-acid sequences and the structurally resolved core of HCV E2 play an important role in facilitating the binding of E2 to cells. To date, research has found that HCV entry can be achieved in the presence of both functional E1-E2 proteins, as produced via HCVpp and HCVcc systems. Importantly, our data reveal that, in the complete absence of TMD and all other viral proteins (including E1), E2 is not only competent in cell binding; it is also capable of orchestrating receptor-mediated endocytosis in human hepatoma cells. Moreover, the internalisation of E2 is highly dependent on the relative densities of the receptors and co-receptors in target cells. We have found no evidence for primary binding to CD81 and the subsequent recruitment of co-receptors. Instead, our data are consistent with the view that the primary cell-surface binding of E2 can occur at distinctly CD81-independent binding sites; a full complement of receptors (including CD81) is

required, however, to assemble a translocation-competent entry complex. Further molecular dissection of the E2-directed entry process is likely to yield information of value for the design of therapeutic strategies to antagonise HCV entry into human cells.

Chapter 4 srE2^{195}-Fc fusion bind alternative surface factor and enhance binding of srE2^{332}-Fc and other variants

4.1 Brief overview

Our flow cytometer data showed that the C-terminally deleted E2 construct srE2^{195}-Fc has residual binding to human cell lines with an indication of higher binding capacity to HepG2 than Huh7.0 and 293T. Importantly as mentioned earlier, binding of srE2^{195}-Fc to CD81-HeG2 showed a reduction in binding compared with the interaction with wild-type HepG2 cells suggesting that srE2^{195}-Fc is unlikely to be binding to CD81 on the surface of transfected HepG2 cells (**Fig. 4.1-1**). This finding was consistent with data that showed no binding of srE2^{195}-Fc to recombinant LEL of CD81 (section 3.3.2.5). In addition, interaction with PFA fixed cell lines demonstrated srE2^{195}-Fc binding to a different and low distribution surface factor compared to highly binding expression factors that bind srE2^{332}-Fc and other variants (section 3.3.2.1 and 2.3.2.3). On the other hand, initial confocal imaging and flow cytometry data of known HCV binding receptors (CD81, CLDN-1, SR-B1 and OCLN) in terms of surface organization and expression level suggested that srE2^{195}-Fc binds to an alternative attachment factor on these cell lines (sections 3.3.1.6.1, 3.4.3, 3.5.1 and 3.5.4). Previous data demonstrated that srE2^{195}-Fc requires at least 60 minutes of incubation with 293T cells for binding to occur. Whereas, other forms of srE2 show high level binding to 293T cells within a 15 minute incubation period (section 3.4.6). We hypothesize that correctly folded srE2^{195}-Fc binds to a factor other than the 4 main putative HCV receptors and that the large deletion in srE2^{195}-Fc has exposed a novel previously unrecognised receptor binding motif. The following sections test this hypothesis.

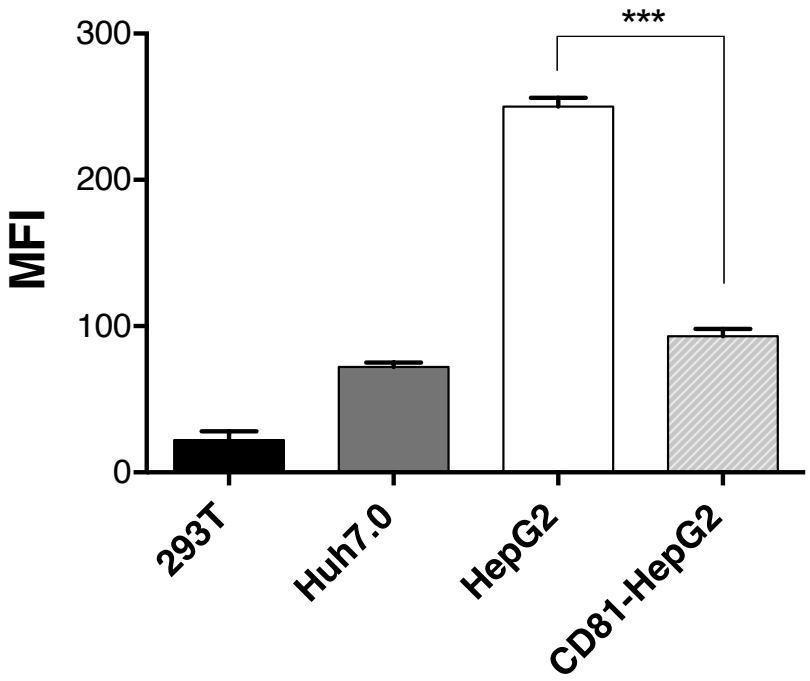

Figure 4.1-1 Differential binding of srE2^{195}-Fc to human cell lines.

Each type of detached cells as indicated (X-axis) at density of 1x10^6 in FBS-free medium were treated with 15 μg/ml srE2^{195}-Fc and labeled with FITC-conjugated anti-human Fc goat secondary (1:500). MFI of FITC staining (Y-axis) was measured using flow cytometry. The average background binding of the control protein tPA-Fc was subtracted from all data values shown; data values represent the mean of triplicate assays, error bars = SD. T-test ***: $p < 0.001$.

4.2 Antibody engagement with CD81 enhances interaction of srE2^{195}-Fc to cells

4.2.1 Flow cytometry-Anti CD81 and binding capacity of srE2^{195}-Fc

To analyse the effect of anti-CD81 on binding of srE2^{195}-Fc to surface factors, human cells were incubated with serial dilutions of mouse monoclonal anti-CD81 (5A6) unconjugated sera for 30 minutes at RT. After washing, a constant concentration of srE2^{195}-Fc fusion was added to cells and reaction was labelled with secondary goat anti-human FC-FITC. Flow cytometry showed that FITC signal of 293T samples incubated with 0.2 μg/ml of anti-CD81 was markedly increased 381% compared to the FITC signal of 293T cells incubated in the absence of anti-CD81 (control). It was notable that adding higher concentration of anti-CD81 sera showed more gradual enhancement in FITC intensity and responded in a dose dependent manner. The reaction was saturated by adding 3.2 μg/ml of anti-CD81 sera. These data indicate that binding of srE2^{195}-Fc to the 293T cell surface is promoted by engagement of the CD81 receptor by antibody (**Fig. 4.2-1 A & B**). A further experiment was conducted using hepatoma cell lines. Data demonstrated that adding 0.4 μg/ml anti-CD81 to cells improved FITC signals by approximately 335% (HepG2) and 200% (Huh7.0) and 103% (CD81-HepG2) over that detected on control cells with no anti-CD81 (**Fig. 4.2-1 C**). Incubating Huh7.0 and HepG2 with >0.4 μg/ml anti-CD81 enhanced binding of srE2^{195}-Fc in a dose dependent manner. It is worth noting that FITC intensity measured on CD81-HepG2 cells treated with anti-CD81 showed lower enhancement in binding than srE2^{195}-Fc binding to treated parental HepG2; this effect on binding capacity was saturated by adding just 0.4 μg/ml anti-CD81. It was consistent with transient transfection of CD81 on HepG2 cell surface possibly masking srE2^{195}-Fc binding to alternative factors. The improvement of srE2^{195}-Fc binding due to anti-CD81 indicates that srE2^{195}-Fc fusion interacts with another factor. Our finding here demonstrated that engagement of CD81

receptor by anti-CD81 (5A6) on target cell surface may be associated with direct or indirect releasing or promote exposing of alternative factor which has higher capacity to bind srE2^{195} -Fc fusion.

Additional experiments were conducted by incubating 293T with low concentrations of anti-CD81 (0.4 μg/ml to 1 x10^{6} cells) and at time point lower and longer than 30 minutes to study the effect on interaction of srE2^{332}-Fc and srE2^{195}-Fc fusions. Treating 293T cells for just 5 minutes with anti-CD81 showed that the interaction of srE2^{195}-Fc was 13-fold higher on anti-CD81 treated cells compared to untreated 293T cells (**Fig. 4.2-2**). Extending anti-CD81 incubation to 30, 60 and 180 minutes improved srE2^{195}-Fc interaction by 19-fold, 26.5-fold and 36.9-fold respectively. In contrast, incubation of anti-CD81 for 5 minutes improved binding of srE2^{332}-Fc fusion by 2.6-fold and extending 293T incubation with anti-CD81 for 30 minutes and 60 minutes was associated with a decrease in binding by 2.3-fold and 1.7-fold which was still higher than the interaction with untreated cells (control). 120 to 180 minutes of anti-CD81 incubation demonstrated a decrease in binding capacity of srE2^{332}-Fc fusion to 293T which is possibly the minimum time (120 minutes) required for 0.4 μg/ml anti-CD81 (5A6) sera to block binding of full length envelope E2 fusion to CD81 receptor. Surprisingly, through 90-180 minutes of antibody incubation period, both interaction of srE2^{195}-Fc and srE2^{332}-Fc showed closer interaction values to 293T which possibly indicates that both srE2^{332}-Fc (which involve harboring first 195 a.a. extend downstream N-terminus of E2) and srE2^{195}-Fc fusions bind similar alternative factor which is not CD81 receptor.

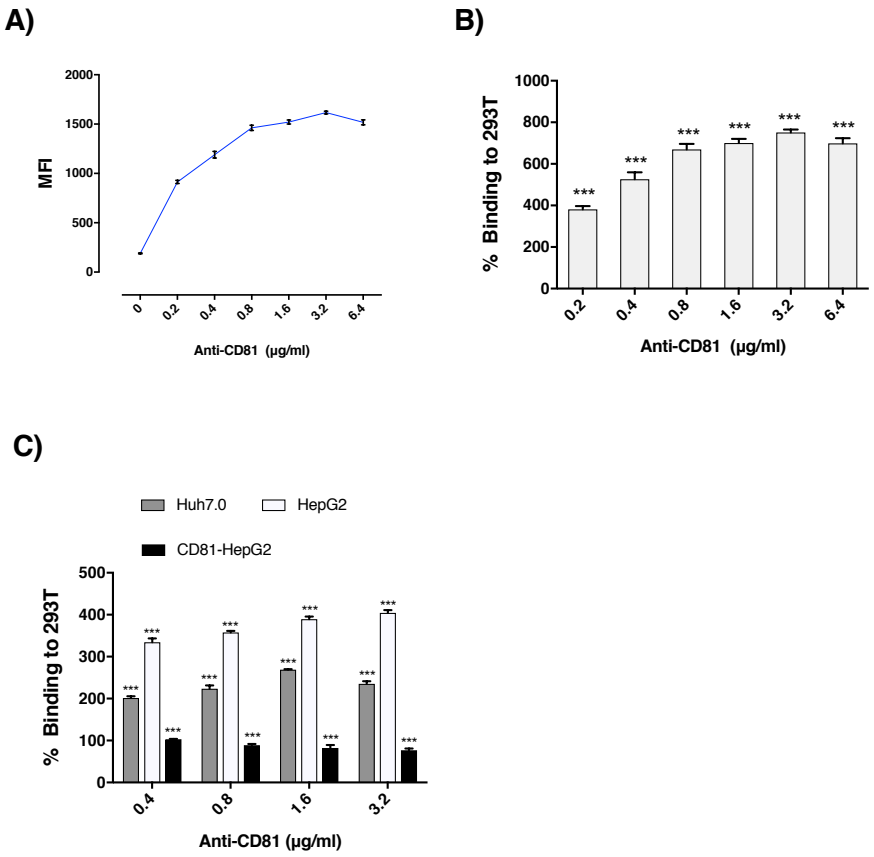

Figure 4.2-1 Adding anti-CD81 to 293T and hepatoma cells associated with improvement of srE2^{195}-Fc binding capacity.

Mouse Anti-CD81 (5A6) serum at a different concentration as indicated (X-axis) was added to each sample containing 1x10^6 cells in 1ml medium and incubated for 30 minutes at RT. Unbound anti-CD81 were washed out and pellet cells were resuspended in medium containing purified srE2^{195}-Fc (25 µg/ml) and incubated for 60 minutes at RT. Cells were pelleted down and the cell pellets were dissolved into fresh DMEM (for 293T and Huh7.0) or MEM (for HepG2 and CD81-HeG2) and probed with FITC-conjugated goat anti-human-Fc goat secondary (1:500). Unbound secondary antibodies were washed out and cell pellets were resuspended in 1ml of 0.5% PFA/PBS solution. FITC signals (Y-axis) were measured using a fortessa machine. Sets of cells were incubated only with srE2^{195}-Fc (no pre-treatment with anti-CD81) and used as control samples. Sets of samples were probed with tPA-Fc (negative control) and basal mean fluorescence intensity from control was subtracted from each of the data points shown. Graph (A) shows the binding capacity of srE2^{195}-Fc to 293T in the presence of different concentration of anti-CD81 (Zero anti-CD81 on X-axis indicates native interaction of srE2^{195}-Fc to 293T in the absence of antibody). Graph (B) is another presentation of data in the graph (A). It shows a rate of increased binding of srE2^{195}-Fc to pre-treated cells with anti-CD81 by percentage (Y-axis) compared with results of control native binding to untreated cells (normalised to zero, not shown). Graph (C) shows interaction rate of srE2^{195}-Fc in percentage (Y-axis) to hepatoma cells, which were pre-treated with anti-CD81 at the concentration shown (X-axis) compared with native srE2^{195}-Fc interaction (normalised to zero, not shown). Data values represent the mean of triplicate assays, error bars = SD. P-value was calculated between MFI of the control sample and each individual pre-treated sample with anti-CD81 serum. T-test **: $p < 0.01$ and ***: $p < 0.001$.

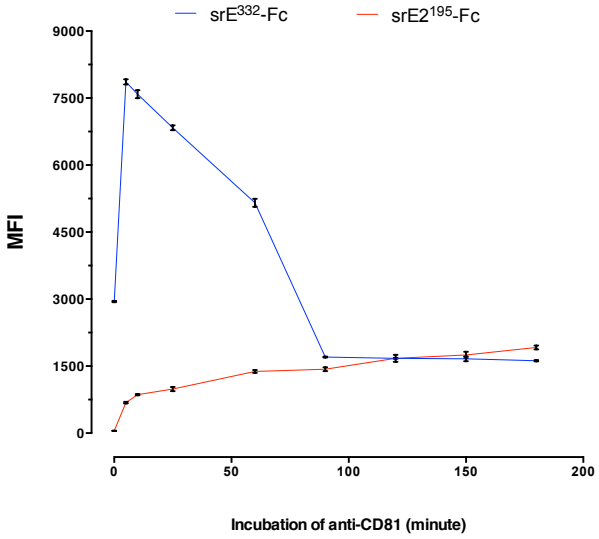

Figure 4.2-2 Engagement of CD81 on 293T leads to enhancement srE2^{195}-Fc binding and inhibition of srE2^{332}-Fc binding.

Cells were probed with 0.4 µg/ml mouse Anti-CD81 (5A6) serum and incubated at time point 5, 10, 25, 60, 90, 120, 150 and 180 minutes as indicated on the X-axis. Zero minute indicates incubation of srE2-Fc fusion with cells untreated with anti-CD81 serum. Cells were pelleted down and probed with srE2-Fc fusion (25 µg/ml) and incubated for 60 minutes at RT. Cells were pelleted down and were dissolved into fresh DMEM containing FITC-conjugated anti-human Fc goat secondary (1:500). The FITC signal was measured using a fortessa machine. Mean fluorescence intensity (MFI), as indicated on Y-axis, of samples containing tPA-Fc (negative control) was subtracted from each of the data points shown. The graph shows the binding capacity of srE2^{332}-Fc and srE2^{195}-Fc to incubated 293T in absence or presence and anti-CD81 over the time period. Data values represent the mean of triplicate assays, error bars = SD.

4.2.2 Confocal analysis of srE2^{195}-Fc binding post-anti CD81 treatment

We wished to test whether adding anti-CD81 sera to live 293T and Huh7.0 cells could discriminate binding of srE2^{195}-Fc to a factor other than CD81 through imaging. To conduct this analysis, cell lines were incubated with anti-CD81 for different times up to 60 minutes in 5% CO_2 at 37°C. Then, cells were fixed with 4% PFA in PBS solution and a constant volume of srE2^{195}-Fc fusion was added to cells for 60 minutes at RT. Binding of anti-CD81 to cell surface was labeled with secondary anti-mouse Alexa 647 and bound srE2^{195}-Fc fusion was probed with goat anti-human Fc FITC. Control cell lines were incubated with srE2^{195}-Fc for 60 minutes without the prior step of adding anti-CD81. Confocal imaging of control samples showed few FITC signals distributed over individual 293T cell surface with large areas of membrane devoid of FITC-specific stain (**Fig. 4.2-3, panel of control**). On control Huh7.0 Cell, FITC detection was characterised as a fluorescence concentrate located at one side of cell membrane (**Fig. 4.2-4, panel of control**). Its worth noting that incubation of control cells with srE2^{195}-Fc for less than 60 minutes resulted in undetectable or very limited FITC signals on the cell membrane of both 293T and Huh7.0 cells (data not shown). Taken together the data reveal a limited binding capacity of srE2^{195}-Fc on 293T and Huh7.0 cell membranes; suggesting that srE2^{195}-Fc binds a limiting factor on cells. Interestingly, 293T cells treated with anti-CD81 for 10 minutes showed detection of Alexa Fluor 647 stain over cell surface and some regions on cell membrane that were not stained indicating that CD81 receptors underwent spanning over cell surface upon interaction with anti-CD81 sera (**Fig. 4.2-3, 10 mins.**). Extending reaction for longer time showed larger Alexa Fluor 647 spots coalescing on the cell surface; indicating the formation of a CD81 capped structure. Most importantly, during capping of CD81 receptors, a prominent large area of membrane not covered with Alexa 647 was occupied instead with abundant FITC-specific signals revealing that srE2^{195}-Fc was binding to a CD81-independent surface receptor (**Fig. 4.2-3, 20 mins.**). Extending time of incubation up to 30 minutes

showed larger FITC spots (**Fig. 4.2-3, 30 mins.**), which end up with capping formation located at one side of cells after 40 and 60 minutes of antibody incubation (**Fig. 4.2-3, 40 & 60mins.**). This indicates that 293T cells treated with anti-CD81 expose a novel antigen that has the capacity to bind to the first 195 a.a of the E2 N-terminal domain. As we added srE2^{195}-Fc after the PFA fixation step, the attachment factor for srE2^{195}-Fc is likely associated and masked by CD81 in the absence of anti-CD81. Furthermore, some srE2^{195}-Fc-specific FITC-staining detected on 293T merged with Alexa 647 stain. From the accumulated data it is likely that the alternative factor can co-localise or interact with CD81 on the cell surface. Thus, confocal imaging demonstrated that most of the binding of srE2^{195}-Fc is due to factors other than CD81.

Incubation of Huh7.0 with anti-CD81 demonstrated similar behaviour to that which occurred on 293T cells, in terms of the recognition of CD81-independent binding sites by srE2^{195}-Fc and the discrete localisation of these sites away from regions of CD81 staining. Again this pattern of staining was observed on cells following antibody-dependent capping of CD81 (**Fig. 4.2-4**). Huh7.0 cells pre-incubated with anti-CD81 for 20 minutes showed srE2^{195}-Fc staining that occupied most of the surface area on Huh7 with little co-localisation with CD81 staining (**Fig. 4.2-4, 20 & 30 mins.**). In addition, srE2^{195}-Fc-specific staining revealed areas of plasma membrane comprising high incidence of different sizes of circular invaginations decorated with Alexa Fluor 647 and FITC stains. Expanded areas on cells were noticed and stained with FITC conjugate, which bound to srE2^{195}-Fc. Interestingly, extending time of incubation with anti-CD81 up to 60 minutes resulted in formation of bigger size of invaginations (vacuoles) that were budded into the cytoplasm and were still adherent to inner side of plasma membrane (**Fig. 4.2-4, 40 & 60 mins)**.

Further experiments were conducted and involved treating live Huh7.0 and HepG2 with anti-CD81 for 30 minutes and followed with live incubation with srE2^{195}-Fc for 60 minutes in 5%CO_2 at 37°C and then fixed. Imaging analysis of Huh7.0 showed similar result mentioned previously (**Fig 4.2-5 A**). Moreover, some localisation of srE2^{195}-Fc fusions into central compartment of cytoplasm

was observed. Imaging of HepG2 demonstrated formation of invaginations at cell membrane, which were decorated with srE2^{195}-Fc (**Fig 4.2-5 B**). In addition, few CD81 receptors were detected in HepG2 cytoplasm and mostly these were not merged with srE2^{195}-Fc. This is in agreement with flow cytometry data in which adding anti-CD81 to HepG2 which expresss a low level of CD81 resulted in marked increase of srE2^{195}-Fc binding.

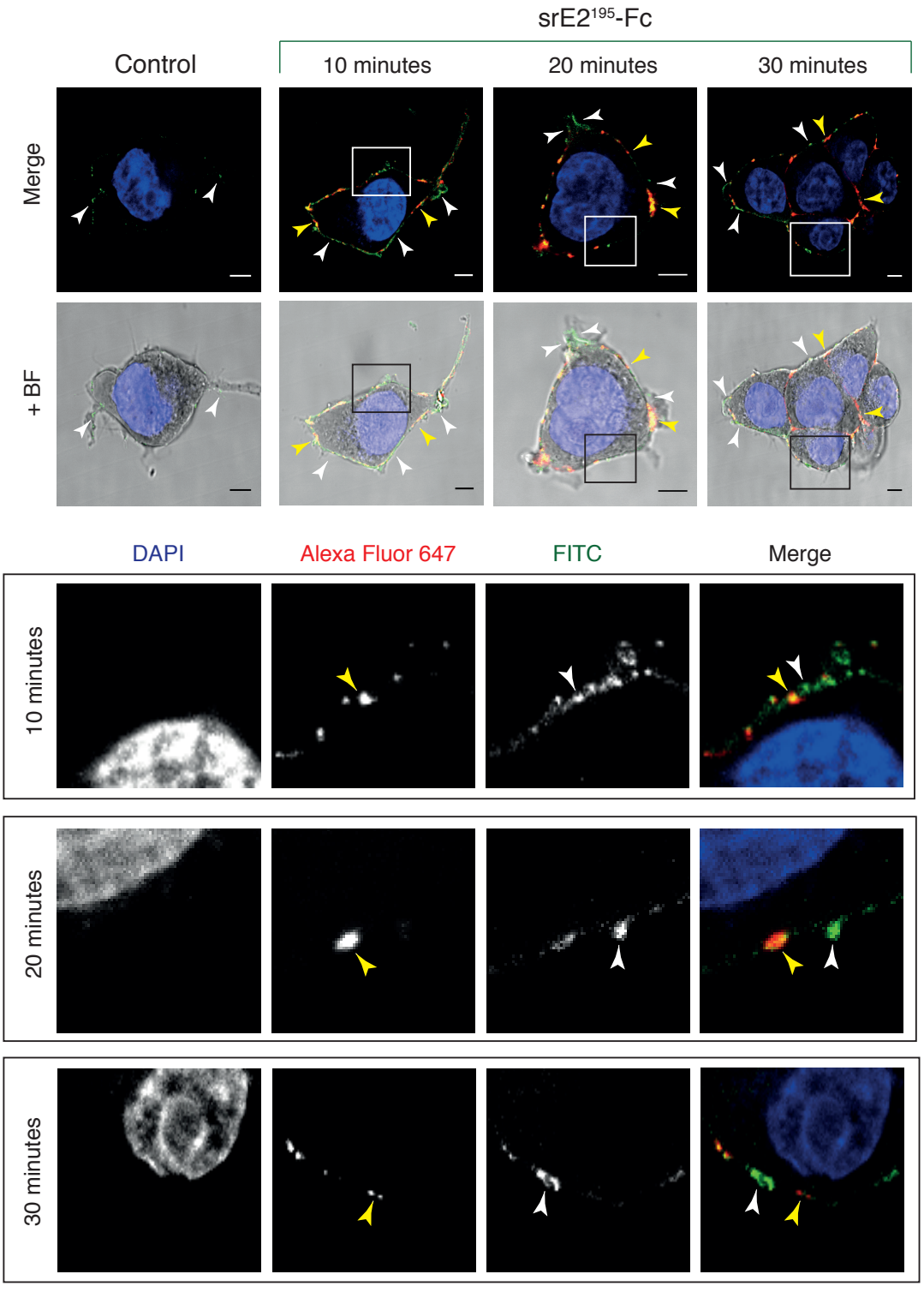
srE2195-Fc
Control
10 minutes
20 minutes
30 minutes
Merge
+ BF
DAPI
Alexa Fluor 647
FITC
Merge
10 minutes
20 minutes
30 minutes

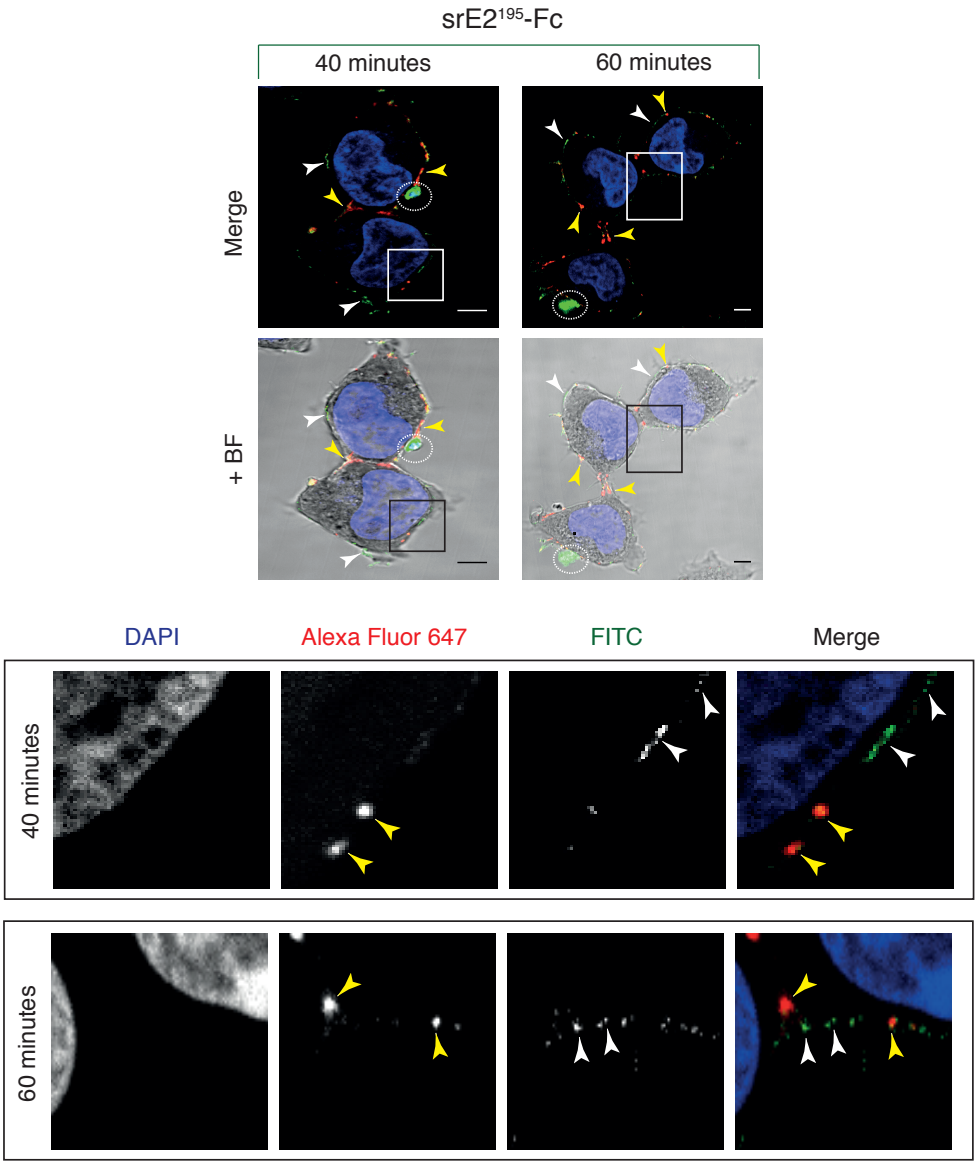

Figure 4.2-3 Incubation of 293T with anti-CD81 resulted in exposure of alternative factor which bind highly srE2^{195}-Fc

Live 293T in each well were treated with 1.5 µg mouse anti-CD81 (5A6) antibody and incubated in 5% CO_2 at 37°C for time points shown (Panels 10, 20, 30, 40 and 60 minutes). Unbound antibody was washed out. The cells were fixed, permeabilised, blocked and washed. srE2^{195}-Fc (30 µg) was added to each µ-slide well and incubated for 60 minutes at RT. Unbound fusions were washed out 3x in washing buffer. Presence of anti-CD81 bound to the cells was detected by incubation with goat anti-mouse IgG Alexa Fluor 647 secondary (1 in 150) for 60 minutes. Unbound proteins were removed by washing 3x in washing solution. Reaction was probed with goat anti-human FC FITC (3 in 150) in each single well and incubated for 60 minutes followed with 3x wash in washing buffer. Cells were counterstained with DAPI and imaged by confocal microscope. Live 293T (panel of control) incubated with srE2^{195}-Fc for 60 minutes at 37°C in 5% CO_2, fixed, probed with goat anti-FC FITC,

counterstained with DAPI and mounted. Merged nucleus (DAPI), CD81 (Alexa Fluor 647) and srE2^{195}-Fc (FITC) +/- 293T the cell (BF) are presented. Panel of control represents live 293T incubated with srE2^{195}-Fc for 60 minutes at 37°C in 5% CO_2. Yellow arrowheads indicate CD81 and white arrowheads indicate srE2^{195}-Fc staining located on the cell surface. The boxed area is shown at greater magnification. Scale bar is 5 μM.

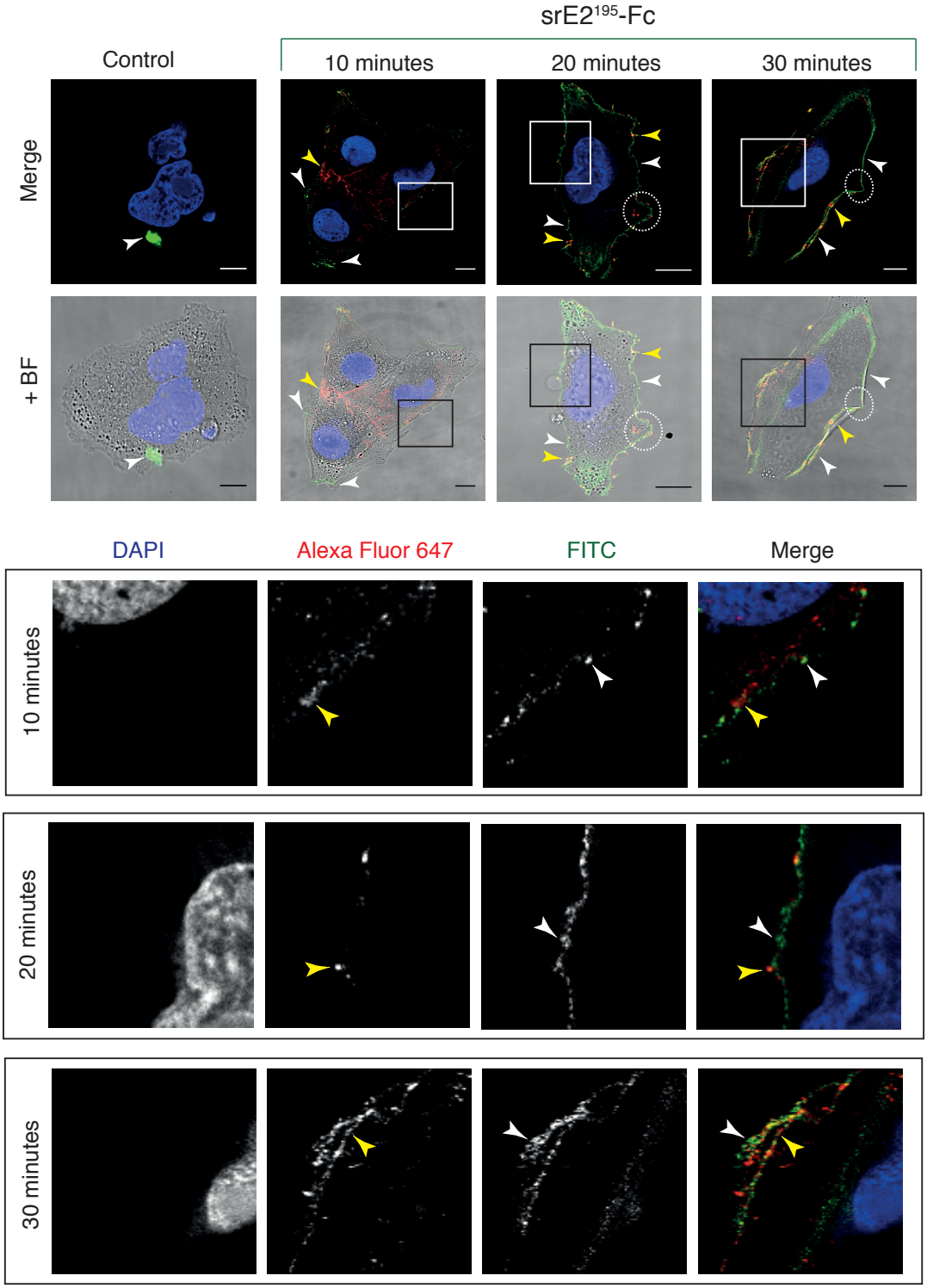
srE2195-Fc
Control
10 minutes
20 minutes
30 minutes
Merge
+ BF
DAPI
Alexa Fluor 647
FITC
Merge
10 minutes
20 minutes
30 minutes

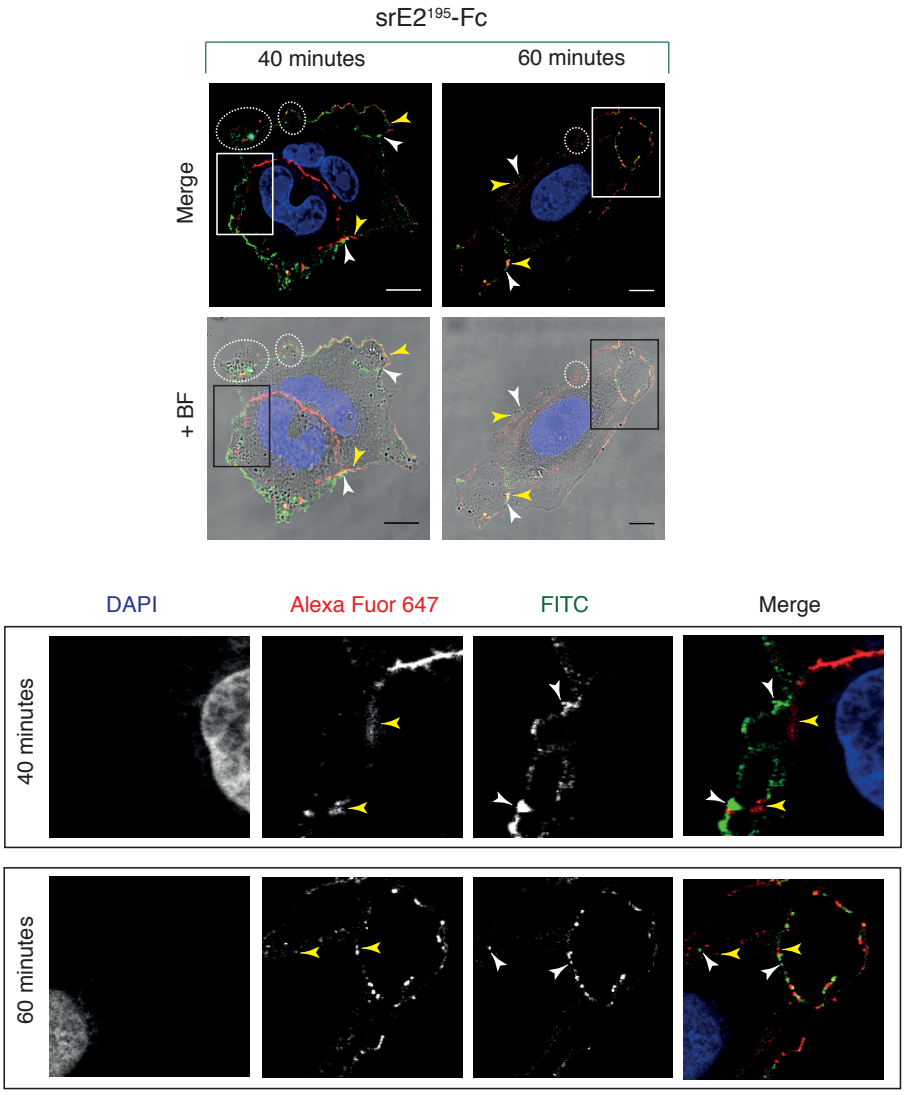

Figure 4.2-4 An alternative factor than CD81 was recognised by srE2^{195}-Fc on Huh7.0 pre-treated with anti-CD81

The method of treating the live cells and immunofluorescence steps in order is done exactly as discussed for 293T (legend of figure 4.2-3) using Huh7.0 as the cell line. Merged nucleus (DAPI), CD81 (Alexa Fluor 647) and srE2^{195}-Fc (FITC) and images merged with the corresponding BF image are presented. Live Huh7.0 (control panel) incubated with srE2^{195}-Fc fusion for 60 minutes at 37°C in 5% CO_2. Yellow arrowheads indicate CD81 and white arrowheads indicate srE2^{195}-Fc fusion staining located on the cell surface or in the cytoplasm. The white oval shape represents the cell surface expansions and formation of circular shapes that contain CD81 and srE^{195}-Fc staining. Boxed area is shown at greater magnification. Scale bar is 5 μM.

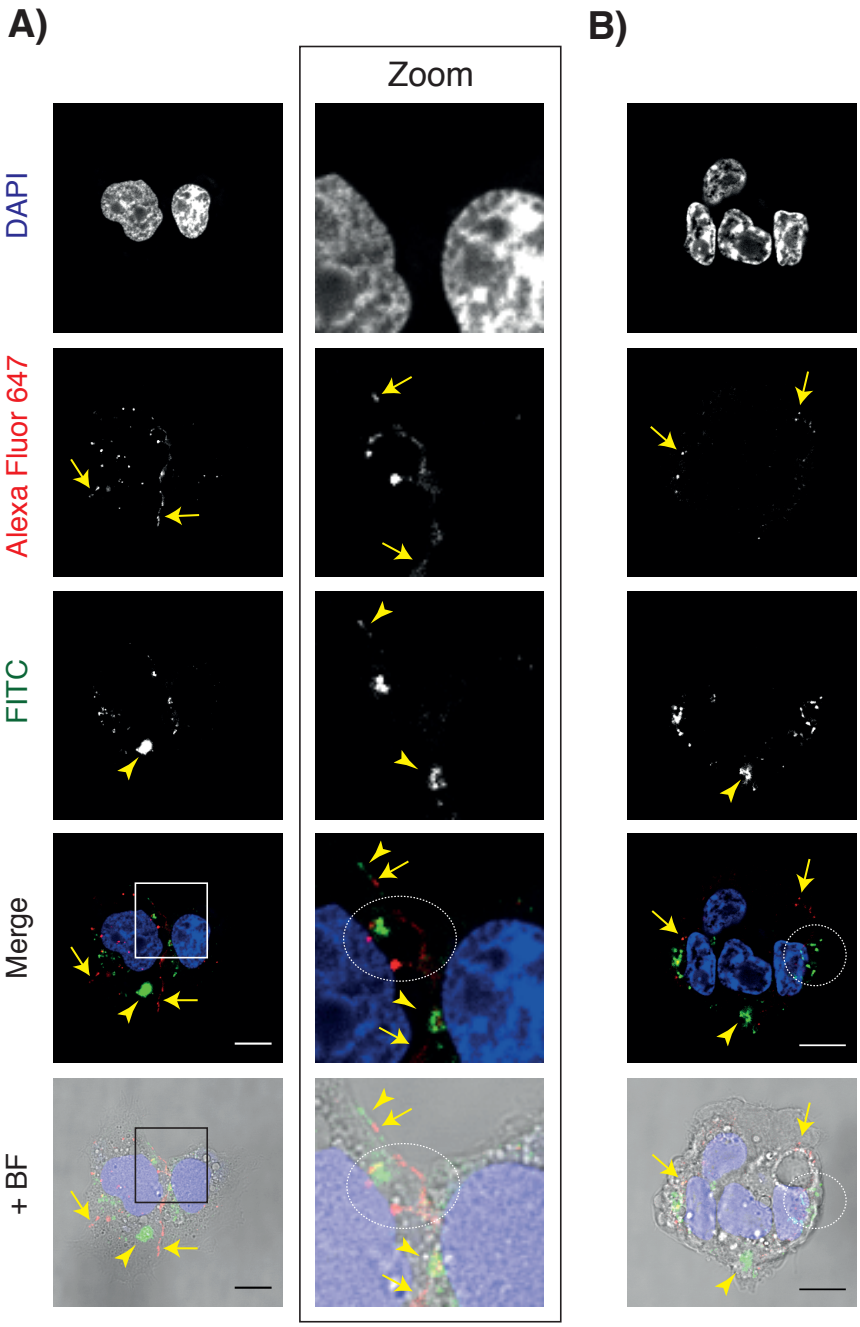
A)
B)
Zoom
DAPI
Alexa Fluor 647
FITC
Merge
+ BF

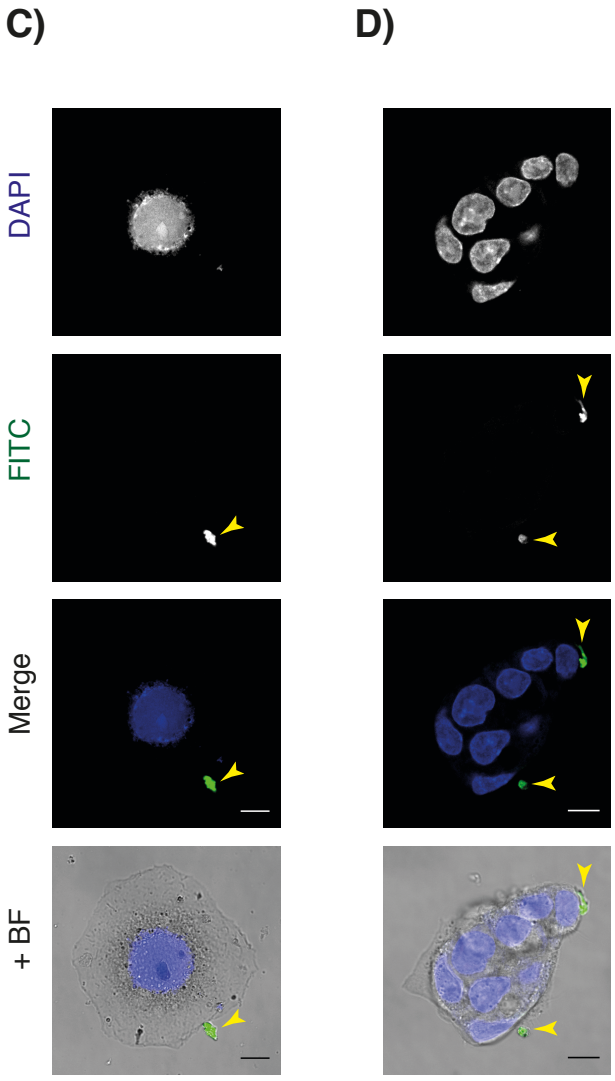

Figure 4.2-5 Live incubation of anti-CD81 then srE2^{195}-Fc leads to co-localisation of srE2^{195}-Fc bound alternative factors into hepatocyte cytoplasm.

Mouse anti-CD81 (5A6) antibody (1.5µg) was added to live Huh7.0 (panel A) or HepG2 (panel B) in 5% CO_2 at 37°C for 30 minutes. Unbound antibody was removed and the cells were treated with srE2^{195}-Fc (30 µg) at the same condition for 60 minutes. Unbound fusions were washed out. The cells were fixed, permeabilised, blocked and washed. Bound anti-CD81 to the cells presence was detected by incubation with goat anti-mouse IgG Alexa Fluor 647 secondary (1 in 150) for 60 minutes. Unbound proteins were aspirated by washing 3x in the washing solution. The reaction was probed with goat anti-human FC FITC (3 in 150) in each single well and incubated for 60 minutes followed with 3x wash in washing solution (0.1% BSA/PBS). Cells were counterstained with DAPI, mounted and imaged by confocal microscope. Merged nucleus (DAPI), CD81 (Alexa Fluor 647) and srE2^{195}-Fc (FITC) +/- hepatocyte (BF) are presented. As a control sample, live Huh7.0 (panel C) or HepG2 (panel D)

incubated with srE2^{195}-Fc for 60 minutes at 37°C in 5% CO_2. Yellow arrows indicate CD81 and yellow arrowheads indicate srE2^{195}-Fc staining located on the cell surface or in the cytoplasm. The white oval shape represents invaginations formed at the cell membrane and contain CD81 and srE^{195}-Fc staining. Boxed area is shown at greater magnification. Scale bar is 10 μM.

4.3 CLDN-1 engagement associated with promoting binding capacity of srE2^{195}-Fc

4.3.1 Flow cytometry- binding of srE2^{195}-Fc in presence of anti-CLDN1

The 293T and hepatoma derived cell lines were incubated with a constant volume of mouse anti-CLDN1 for 50 minutes. Then, srE2^{195}-Fc fusion was incubated with these cells and labelled with anti-human Fc FITC. Flow cytometry showed a significant increase (1037%) in detection of srE2^{195}-Fc-specific FITC intensity on antibody-treated HepG2 cells compared to untreated cells (**Fig. 4.3.1 A**). This result was evidence of the presence of an alternative factor on parental HepG2 cells, which has a greater interaction with srE2^{195}-Fc following CLDN-1 engagement by anti-CLDN1. It is important to note that CD81-HepG2 cells have a significantly higher expression of CLDN-1 than the parental HepG2 cells or wild-type Huh7.0 cells (section 3.5.4) and adding anti-CLDN1 still resulted in an increase in srE2^{195}-Fc binding to cells (107%) compared with binding in absence of anti-CLDN1 but was approximately decreased by 10X compared to binding by incubating parental HepG2 with anti-CLDN1 (**Fig. 4.3-1 A**). This was expected because expression of CD81 was associated with reduction in binding of srE2^{195}-Fc to its target factor on the cell surface. This may indicate masking of srE2^{195}-Fc fusion's alternative factor by both high levels of CD81 and CLDN-1 receptors, which may prevent exposing alternative factors to srE2^{195}-Fc. Incubation of anti-CLDN1 with 293T cells that naturally express lower levels of CLDN-1 and Huh7.0 that express moderate CLDN-1 level resulted in increased binding of srE2^{195}-Fc by 258% and 578% respectively compared to cells untreated with anti-CLDN1 (**Fig. 4.3-1 A**). It is a consistent finding that this large deleted c-terminal E2 form binds to an alternative higher binding capacity factor than CLDN-1 and CD81 receptors. It is likely that srE2^{195}-Fc has no direct contact with CLDN-1 receptor. We compared binding of other srE2-Fc variants after incubating anti-CLDN1 with 293T for 50 minutes. This demonstrated that blocking expressed CLDN-1

receptor on 293T did not reduce capacity of binding of srE2^{332}-Fc, srE2 ^{295}-Fc, srE2^{278}-Fc, srE2^{265}-Fc and srE2^{195}-Fc, but instead promoted the binding of srE2-Fc variants by approximately 175%, 133%, 118%, 236% and 266% respectively (**Fig. 4.3-1 B**). We cannot exclude that blocking CLDN-1 may give more chance for E2-Fc variants (except srE2^{195}-Fc fusion) to bind CD81; close rate of improvement in binding rate of srE2^{265}-Fc and srE2^{195}-Fc fusions possibly suggested similar binding toward unknown surface factor, which is not CD81 and CLDN-1. However as already reported by (Evans *et al.*, 2007; Liu *et al.*, 2009; Yang *et al.*, 2008) there is an important association between CLDN-1 expression and HCV entry; our confocal results show close localisation of srE2^{332}-Fc with CLDN-1 (section 4.3.2) and the available data using anti-CLDN1 are consistent with other researcher findings in that no direct binding between all E2 variants involving srE2^{195}-Fc and CLDN-1 has been confirmed.

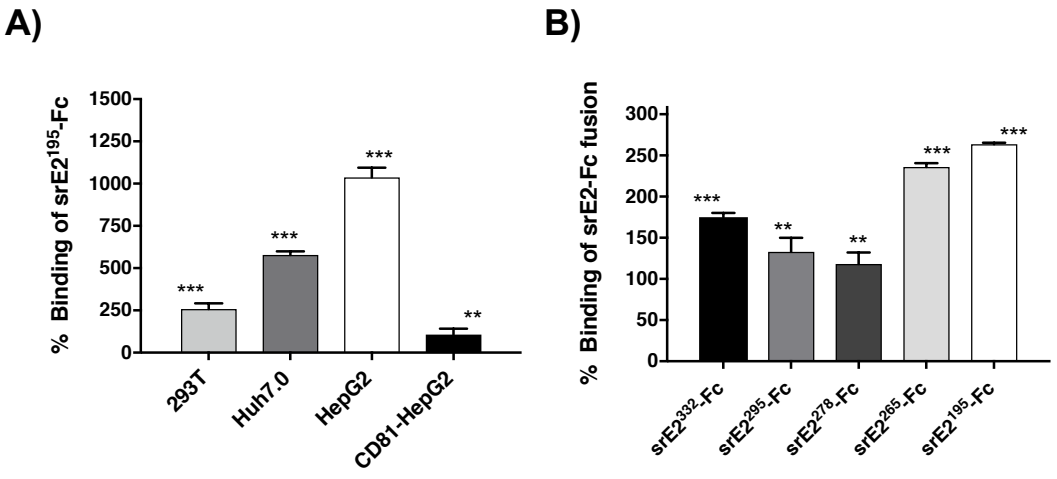

Figure 4.3-1 Enhancement binding of srE2^{195}-Fc and other E2-Fc forms to the cells pre-incubated with anti-CLDN1.

3µg/ml (panel A) or 2 µg/ml (panel B) mouse Anti-CLDN1 (A-9) serum was added to each sample containing 1x10^6 cells and incubated for 50 minutes at RT. Unbound anti-CLDN1 was washed out 2x in PBS solution and pellet cells were resuspended in medium contained 25 µg/ml purified srE2-Fc fusion and incubated for 60 minutes at RT. The reaction was probed with FITC-conjugated anti-human Fc goat secondary (1:500). Unbound secondary antibodies were washed out and the cells were fixed. FITC signal was measured using a fortessa machine. In addition, set of cells were incubated only with srE2^{195}-Fc and probed with FITC-conjugated anti-human Fc goat secondary (1:500) and represent native binding capacity of srE2^{195}-Fc with cells (not involve pre-treatment with anti-CLDN1). Some set of samples (negative control) was probed with tPA-Fc and basal MFI from this control was subtracted from each of the data points shown. Panel (A) shows the interaction rate of srE2^{195}-Fc in percentage (Y-axis) to hepatoma cells and 293T cells pre-treated with anti-CLDN1 (X-axis) compared with native srE2^{195}-Fc interaction (normalised to zero, not shown). Panel (B) represents the percentage of increase in srE2-Fc derivatives binding capacity to pre-treated 293T with anti-CLDN1 (X-axis) compared with native corresponding E2 forms interaction (normalised to zero, not shown). Data values represent the mean of triplicate assays, error bars = SD. P-values were calculated between MFI of the control sample and each individual pre-treated sample with anti-CLDN1 serum. T-test **: $p < 0.01$ and ***: $P < 0.001$

4.3.2 Confocal analysis of srE2^{195}-Fc binding in presence of anti-CLDN1

We wanted to locate the binding site for srE2^{195}-Fc on cells treated with anti-CLDN-1 and test if these sites co-localise with CLDN-1 receptors by confocal imaging. We selected HepG2 cells as they possess high natural binding of srE2^{195}-Fc in comparison to 293T and Huh7.0 cells (section 4.1). In addition, HepG2 cells express exceedingly low levels of CD81 and using HepG2 will confirm that improvement in srE2^{195}-Fc binding to cells pre-incubated with anti-CLDN1 is not related to cross binding to CD81 receptor. One experiment was conducted on PFA fixed HepG2 and CD81-HepG2 cells (**Fig. 4.3-2**). After PFA fixation, cells were incubated with mouse anti-CLDN1 sera at RT, and then srE2^{195}-Fc fusion was added. Appropriate secondary anti-mouse Alexa Fluor 647 and goat anti-FC FITC was incubated with cells for 60 minutes. Confocal imaging showed Alexa Fluor 647 signals expressed moderately on HepG2 cells but highly on the CD81-HpG2 cell surface; indicating a higher expression of CLDN-1 on HepG2 cells transfected with CD81 than parental HepG2 cells. Moreover, srE2^{195}-Fc-specific FITC signals were detected on both cell lines and concentrated on the lateral side of the cell surface and located close to a concentration of claudin receptors. On HepG2 both Alexa Fluor 647 and the limited FITC signal showed no overlap, which demonstrates that there is no direct binding between CLDN-1 receptors distributed over the cell surface and bound srE2^{195}-Fc. The vast majority of stained CLDN-1 on CD81-HepG2 cells showed no overlap with srE2^{195}-Fc staining, marginal overlay between both Alexa Flour 647 and FITC signal was detected on CD81-HepG2 cells. This is unlikely to be real srE2^{195}-Fc/CLDN-1 interaction but might due to higher expression of CLDN-1 receptors associated with expression of CD81 on HepG2 cells which may occupy an area close to the binding site for srE2^{195}-Fc. Our accumulated data previously demonstrated that upon expression of abundant CD81 on HepG2 cell surface, srE2^{195}-Fc showed a reduction in binding comparing with binding capacity to the parental HepG2 cell surface

(section 4.1). All this supports that the binding site for srE2^{195}-Fc fusion was masked by both abundant CD81 and CLDN-1 expression.

In a further separate experiment, we incubated live HepG2 with srE2^{195}-Fc for 60 minutes and then the reaction was labelled with secondary anti-human Fc Texas red conjugate to analyse the ability of fusion protein to localise over the cell surface (**Fig 4.3-3**). Our data showed specific binding to a concentrated-like structure and no sign for srE2^{195}-Fc distribution over the cell surface. Extending incubation to 24 hours showed two forms of detection of Texas red signal on the surface of both HepG2 and CD81-HepG2: concentrated signal at one side of the cell membrane; and a short continuous signal line at other side of the cell. This finding indicates the limited spanning degree of srE2^{195}-Fc that binds certain attachment factors on the cells' surfaces. Achieving such observations 24 hours post addition of srE2^{195}-Fc indicates its low capacity in binding to live factors on the cell surface and slow spanning srE2^{195}-Fc fusion.

A novel experiment was conducted by incubating live HepG2 with anti-CLDN1 up to 60 minutes in 5% CO_2 at 37°C and then fixing with PFA (**Fig. 4.3-4**). srE2^{195}-Fc was added to the cells for 60 minutes at RT. Bound anti-CLDN1 on the cell surface was probed with secondary anti-mouse Alexa Fluor 647, and srE2^{195}-Fc that bound to the cells was probed with goat anti-human Fc FITC. Moreover, control cell lines were incubated with srE2^{195}-Fc for 60 minutes without the prior step of adding anti-CLDN1. As expected, confocal imaging of the control sample showed few FITC signals located as a single concentrate over HepG2 the cells with very large area uncovered with FITC stain indicating limited binding sites for srE2^{195}-Fc over untreated HepG2 with anti-CLDN1 (**Fig. 4.3-4, panel of control**). It is worth noting that incubation of control cells with srE2^{195}-Fc for less than 60 minutes demonstrated undetectable or limited FITC signals on the cell membrane of HepG2 the cells, and this reminded us of the similar behaviour of this fusion on 293T cells (section 3.4.6); all may indicate natural weak binding capacity of srE2^{195}-Fc to factor on the cell surface. Importantly, HepG2 cells treated with anti-CLDN1 for 10 and 20 minutes showed detection of Alexa Fluor 647 stain which did not cover most

the area on the cell membrane and instead an accumulation in the form of many concentrates over HepG2 cell membrane were observed (**Fig. 4.3-4, panels 10 & 20 mins)**; this indicates that CLDN-1 receptors underwent localisation over the cell surface after interaction with anti-CLDN1 serum. Incubating the cells with anti-CLDN1 for 30 minutes showed detection of Alexa Fluor 647 spots into cytosolic compartment of HepG2; it was an indication of CLDN-1 entry. Moreover, 40 and 60 minutes of cell incubation with anti-CLDN1 was associated with difficulty in tracking Alexa Fluor 647 signals and this is might due to folding of CLDN-1 in a way that masks the recognisable epitope on anti-CLDN1 (**Fig. 4.3-4, panels 40 & 60 mins)**. More interestingly, during spanning events of CLDN-1 receptors, a prominent large uncovered area with anti-CLDN1 were occupied with abundant FITC signals in spots or discrete patches and distributed around the HepG2 cell surface after 10 and 20 minutes of antibody incubation (**Fig. 4.3-4, panels 10 & 20 mins)**. Extending time of incubation up to 30 minutes showed larger FITC spots in the form of capping structures, and no overlay with anti-CLDN1 fluorescence was detected (**Fig. 4.3-4, panel 30 mins)**. All were located in the cytoplasm of the HepG2 cells. After 40 and 60 minutes of antibody incubation, larger FITC complexes were detected in the cytoplasm (**Fig. 4.3-4, panels 40 & 60 mins)**, indicating that alternative factors for srE2^{195}-Fc fusion were taken up and accumulated in the cytoplasm of HepG2 after CLDN-1 engagement (**Fig. 4.3-4**).

A further experiment was conducted and involved treating live HepG2 with anti-CLDN1 for 30 minutes followed by live incubation with srE2^{195}-Fc for 60 minutes in 5% CO_2 at 37°C and then fixation (**Fig. 4.3-5**). Imaging analysis of HepG2 showed the biniding of srE2^{195}-Fc with areas on the cell surface which were not occupied with CLDN-1 (**Fig. 4.3-5 A**). Moreover, obvious localisation of srE2^{195}-Fc into a central compartment of the cytoplasm was observed which in turn means localisation of srE2^{195}-Fc's alternative factor. As mentioned in the previous experiment, our anti-CLDN1 was not able to recognise CLDN-1 after 30 minutes of incubation which was probably due to folding of CLDN-1.

The possiable explantion for this event is that live engagement of CLDN-1 by anti-CLDN1 resulted in association with other surface and intra-cellular factors; this may involves folding changes of CLDN-1 and in some way masks the target epitopes on anti-CLDN1. So, goat anti-mouse IgG Alexa Fluor 647 secondary failed to recognise anti-CLDN1 due to folding changes of CLDN-1.

Overall, this indicates that HepG2 cells express functional factors which have the capacity to bind to the first 195 a.a. of E2 N-terminal domain and might be re-localised over the cell surface during the spanning event of CLDN-1. As we added srE2^{195}-Fc after the PFA fixation step, alternative attachment factor for srE2^{195}-Fc is likely associated directly or indirectly with post-CLDN-1 stimulation. However, at certain incubation times, detection of srE2^{195}-Fc was at site near the CLDN-1 site, the vast majority of FITC staining detected on HepG2 was not merged with Alexa Fluor 647 stain, and from our accumulated data so far it is more likely that the expected alternative factor may occupy a region near site of CLDN-1 concentrates expression. At this moment, we cannot confirm if that binding site for srE2^{195}-Fc, which was detected on PFA-fixed the cells or live cells not treated with anti-CLDN1 is the same alternative factor detected on the cells with engaged CLDN-1. Nevertheless, confocal imaging proved that most binding of srE2^{195}-Fc is towards an alternative factor than CLDN-1. In addition, CLDN-1 receptors seem imprtant for entry of this alternative factor.

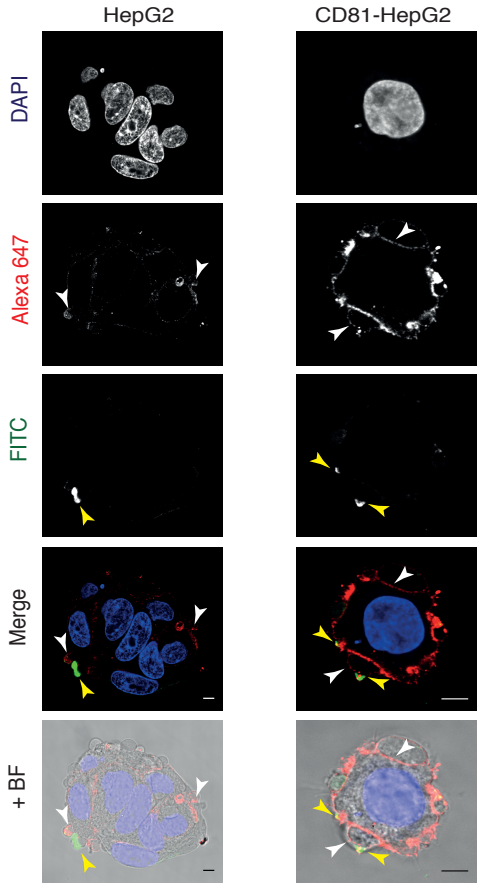

Figure 4.3-2 No merge between srE2^{195}-Fc and CLDN-1 on hepatoma cells.
CLDN-1 presence was detected by incubating the cells in each µ-slide well with 1.5 µg mouse anti-CLDN1 (A-9) and followed with 3x wash in washing buffer (0.1% BSA in PBS). Cells were incubated with 25 µg srE2^{195}-Fc in each well for 60 minutes at RT and rinsed 3x in washing buffer. The bound anti-CLDN1 was labelled with of goat anti-mouse Alexa Fluor 647 conjugate (1 in 150) for 60 minutes and the cells were then rinsed 3x in washing buffer. The bound fusion was labelled with goat anti-human Fc FITC in blocking buffer (1:50) and rinsed 3x in washing buffer. Cells were counterstained with with DAPI, mounted and imaged by confocal micrscope. Merged nucleus (DAPI), CLDN-1 (Alexa Fluor 647) and srE2^{195}-Fc (FITC) +/- HepG2 or CD81-HepG2 the cells (BF) are presented. Yellow arrowheads indicate srE2^{195}-Fc staining and white arrowheads indicate distributed surface CLDN-1. Scale bar is 5 µM.

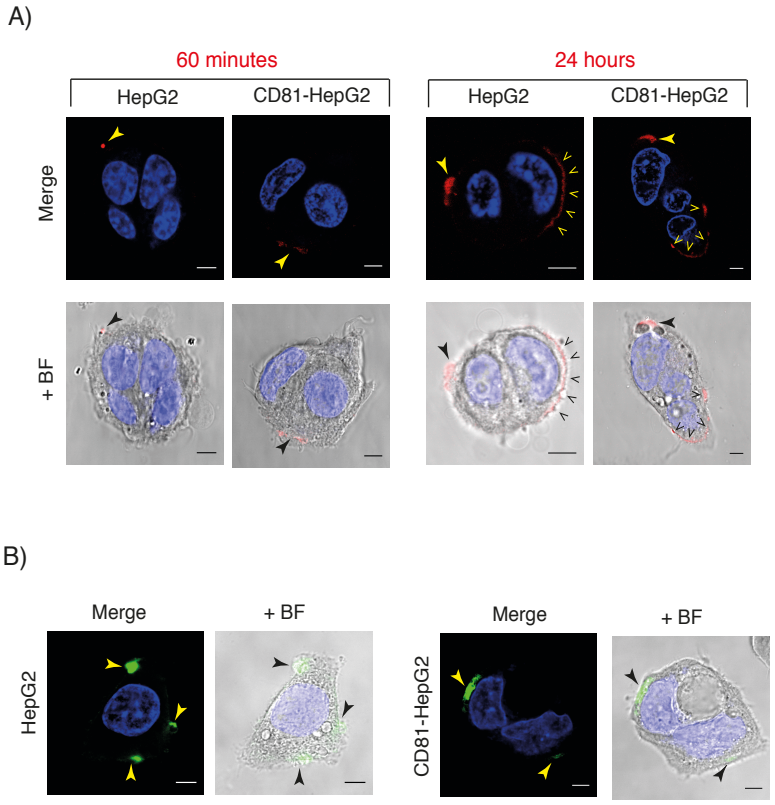

Figure 4.3-3 low binding capacity and slow localisation of srE2^{195}-Fc on live HepG2 and CD81-HepG2.

Panel (A): Live HepG2 or CD81-HepG2 was treated with 25 µg srE2^{195}-Fc in each well and incubated in 5% CO_2 at 37°C for the time point shown. Unbound protein was washed out. The cells were fixed, permeabilised, blocked and washed. The reaction was probed with rabbit anti-human FC Texas Red in 5% BSA/PBS solution (1 in 50) and incubated for 60 minutes followed with 3x wash in washing buffer. Panel (B): control the cells were fixed with 4% PFA/PBS solution, blocked with 5% BSA/PBS solution, incubated with 25µg srE2^{195}-Fc in each well for 60 minutes at RT, rinsed 3x in washing buffer, probed with goat anti-human Fc FITC in blocking buffer (1:50), and rinsed 3x in washing buffer. Samples (panels A and B) were counterstained with Dilute DAPI solution. IBIDI mounting media applied to the cells in wells followed by confocal analysis. Merged nucleus (DAPI) and srE2^{195}-Fc (Texas Red or FITC) +/- HepG2 or CD81-HepG2 the cell (BF) are presented. Closed arrowheads in panel (A) and (B) indicate srE2^{195}-Fc binding to a concentrate located at the lateral side of the cells. Open arrowheads in panel (A) indicate srE2^{195}-Fc interaction to scatter binding site/spanning over the cells. Scale bar is 5 µM.

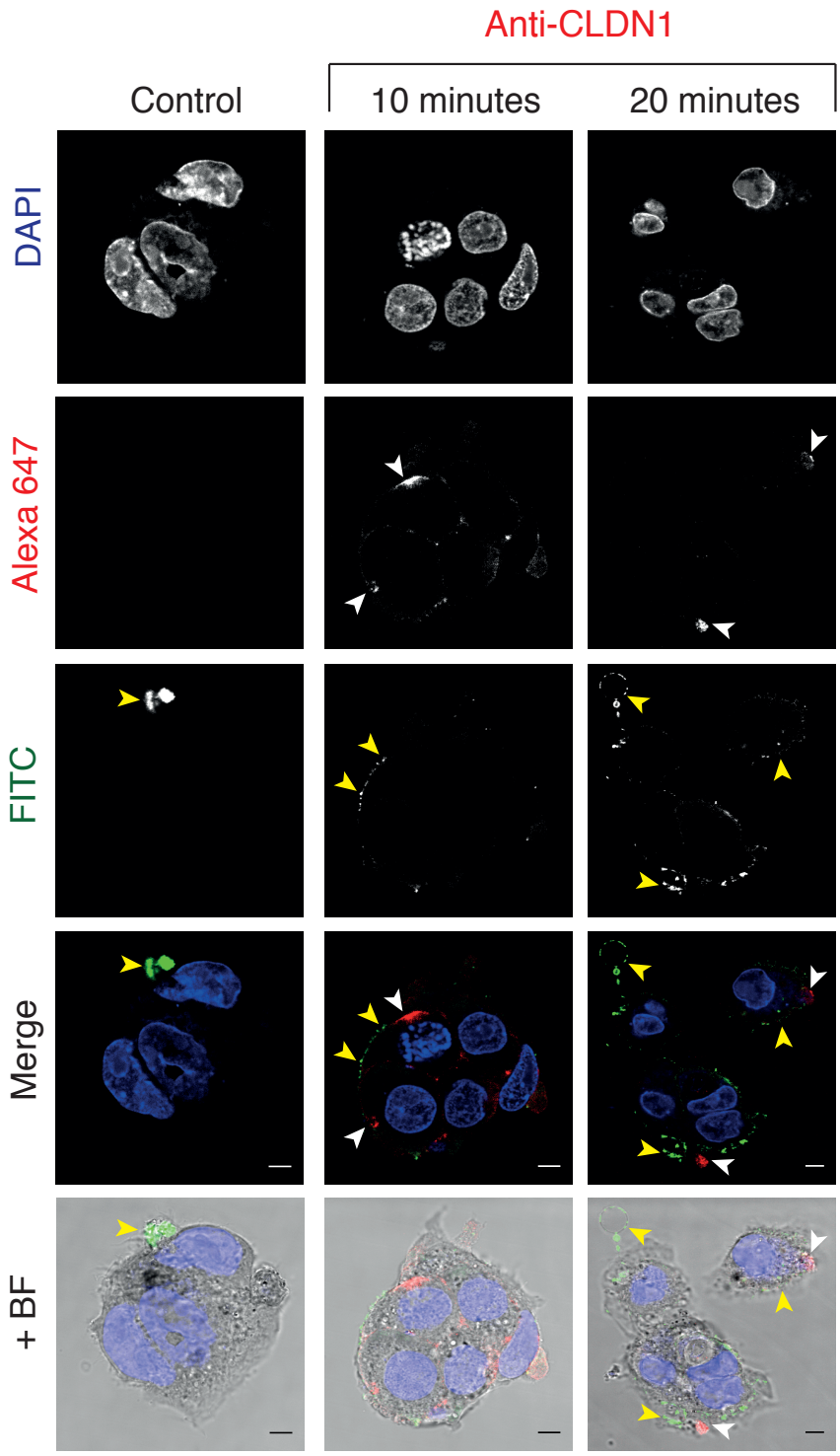
Anti-CLDN1
Control
10 minutes
20 minutes
DAPI
Alexa 647
FITC
Merge
+ BF

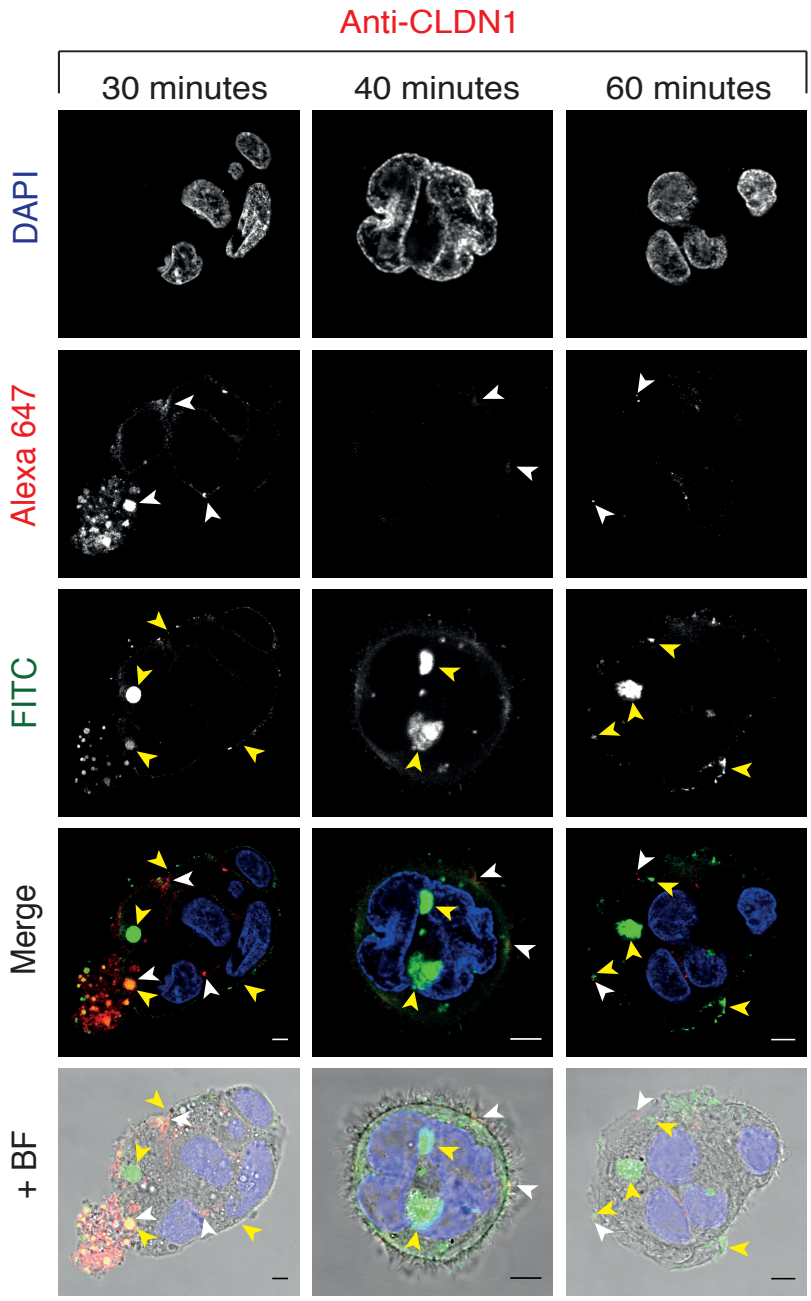

Figure 4.3-4 Pre-treated live HepG2 with anti-CLDN1 demonstrate binding, spanning and entry of alternative factor binding for srE2^{195}-Fc.

Mouse anti-CLDN1 A-9 antibody (1.5 µg) in MEM media containing 10% FBS was added to live HepG2 and incubated in 5% CO_2 at 37°C for different time points shown (Panels 10, 20, 30, 40 and 60 minutes). Unbound antibody was washed out. The cells were fixed, permeabilised, blocked and washed. srE2^{195}-Fc (30 µg) were added to each well and incubated for 60 minutes at RT. Unbound fusions were rinsed 3x in washing solution (0.1% BSA/PBS). Bound anti-CLDN1 was detected by incubation with goat anti-mouse IgG Alexa Fluor 647 secondary (1 in 150) for 60 minutes. Unbound proteins were aspirated and the cells were rinsed 3x in washing solution. The reaction was probed with goat anti-human FC FITC (3

in 150) and incubated for 60 minutes followed with 3x wash in washing solution. Cells were counterstained with with DAPI, mounted and imaged by confocal micrscope. Merged nucleus (DAPI), CLDN-1 (Alexa Fluor 647) and srE2^{195}-Fc (FITC) +/- HepG2 the cell (BF) are presented. Live HepG2 (panel of control) incubated with srE2^{195}-Fc for 60 minutes at 37°C in 5% CO_2, fixed, probed with goat anti-FC FITC, counterstained with DAPI and mounted. White arrowheads indicate CLDN-1 and yellow arrowheads indicate srE2^{195}-Fc staining located on the cell surface or in cytoplasm. Scale bar is 5 μM.

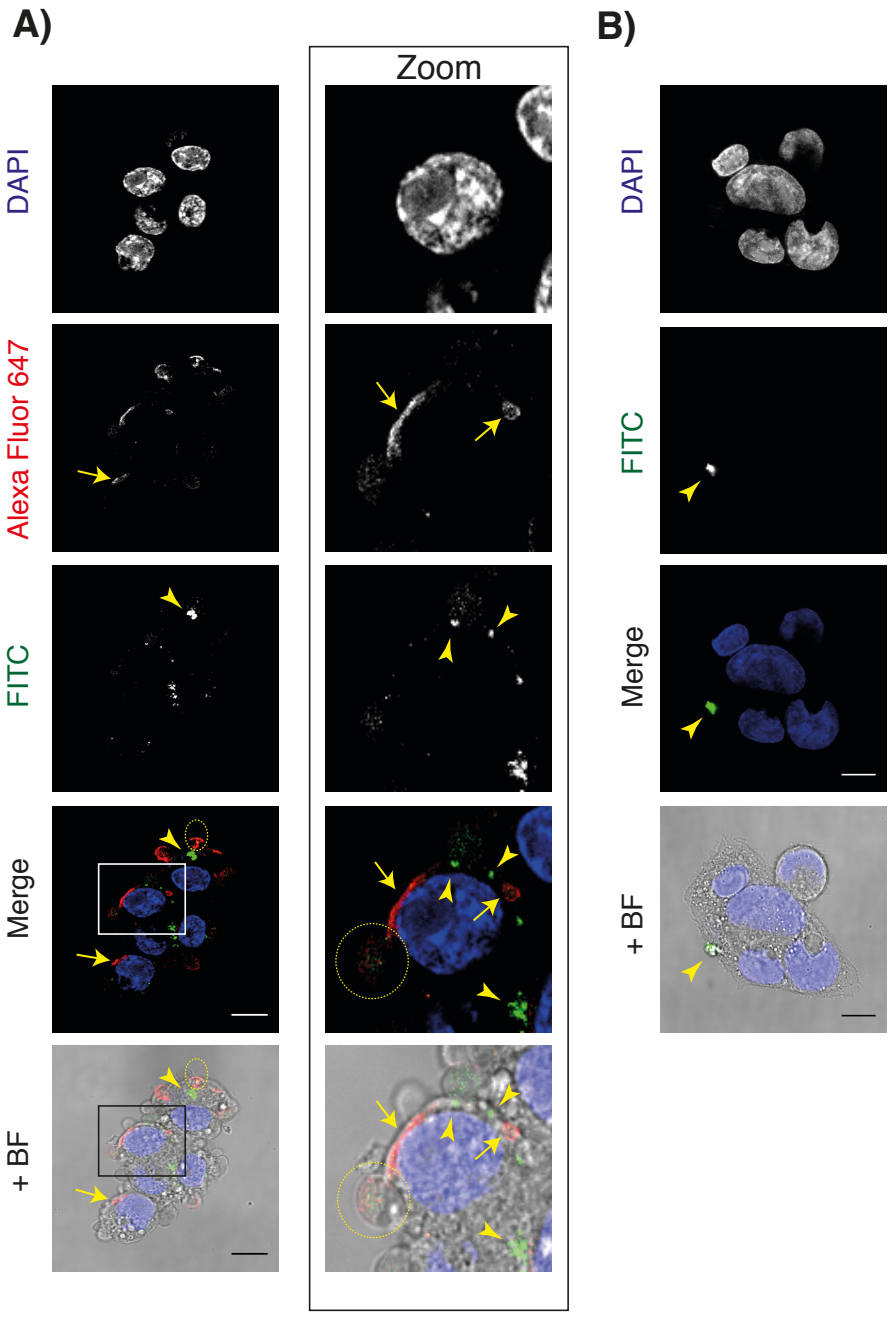

Figure 4.3-5 Live incubation of anti-CLDN1 then srE2^{195}-Fc leads to co-localisation of srE2^{195}-Fc bound alternative factors into the HepG2 cytoplasm.

Mouse anti-CLDN1 A-9 antibody (1.5 µg) was added to live HepG2 (Panel A) in 5% CO_2 at 37°C for 30 minutes. Unbound antibody was removed and the cells were treated with srE2^{195}-Fc (30 µg) at the same condition for 60 minutes. Unbound fusions were washed out. The cells were fixed, permeabilised, blocked and washed. Bound anti-CLDN1 was detected by incubation with goat anti-mouse IgG Alexa Fluor 647 secondary (1 in 150) for 60 minutes. Unbound proteins were aspirated by washing 3x in washing solution. The reaction was probed with goat anti-human FC FITC (3 in 150) and incubated for 60 minutes followed with 3x wash in washing solution (0.1% BSA/PBS). Cells were counterstained with with DAPI, mounted and

imaged by confocal micrscope. Merged nucleus (DAPI), CLDN1 (Alexa Fluor 647) and srE2^{195}-Fc (FITC) +/- hepatocyte (BF) are presented. As control sample, live HepG2 (panel B) incubated with srE2^{195}-Fc fusion for 60 minutes at 37°C in 5% $CO_{2.}$ Yellow arrows indicate CLDN-1 and yellow arrowheads indicate srE2^{195}-Fc fusion staining located on the cell surface or in cytoplasm. Yellow oval shapes represent invaginations formed at the cell membrane and contain CLDN-1 and srE^{195}-Fc staining. Boxed area is shown at greater magnification. Scale bar is 10 μM.

4.4 Engagement of SRB1 enhance binding of srE2^{195}-Fc

4.4.1 Flow cytometry-interaction of srE2^{195}-Fc to the cells with blocked SR-B1

For analysing the effect of anti-SRB1 on the binding of srE2^{195}-Fc to surface factors, human cells were incubated with rabbit anti-SRB1 (H-180) unconjugated serum for 30 minutes at RT. After the washing step, a constant concentration of srE2^{195}-Fc was added to the cells and the reaction was labelled with secondary goat anti-human FC FITC secondary. Data demonstrated that adding anti-SRB1 to the cells was associated with improving FITC signals by approximately 319% (293T) 746% (Huh7.0) and 472% (HepG2) and 107% (CD81-HepG2) higher than FITC detected on untreated cells (**Fig 4.4-1**).

It is worth noting that binding of srE2^{195}-Fc to pre-treated CD81-HepG2 with anti-SRB1 was 77% less than binding to pre-treated parental HepG2; this is again suggestive that transient transfection of HepG2 with CD81 possibly masks some alternative factors associated with srE2^{195}-Fc fusion binding. Data of significant improvement of srE2^{195}-Fc binding after engagement of SR-B1 on 293T which naturally expressed fewest SR-B1 receptors among other cell lines (section 3.4.3.2) indicates that srE2^{195}-Fc fusion possiably does not bind little expressed SR-B1 but interacts with other alternative factor. In addition, enhanced of srE2^{195}-Fc binding capacity to Huh7.0 was higher than that of HepG2 and previously we and other researchers (Rhainds *et al.*, 2004; Sainz *et al.*, 2009) showed that HepG2 the cells express high levels of SR-B1 compared with low rate expression on the surface of Huh7.0. Scarselli *et al.* (2002) identified HVR1 of E2 which includes 27 amino acids located at the N domain (corresponding to our srE2$^{1-27}$ peptide fusion), which was the specific binding site for SR-B1 on HepG2 cells, and deleting HVR1 of soluble GT1a E2$_{661}$ (corresponding to our srE2^{278} peptide) resulted in decreased binding to HepG2 by 30% in comparison with unmodified srE2$_{661}$ interaction. Our srE2^{195}-

Fc still had 168 a.a. extended downstream HVR1 and such high improvement in binding of srE2^{195}-Fc during blocking low rate or high rate SR-B1 receptors on 293T and Huh7.0 suggests that is mostly due to binding to alternative factors than SR-B1 only.

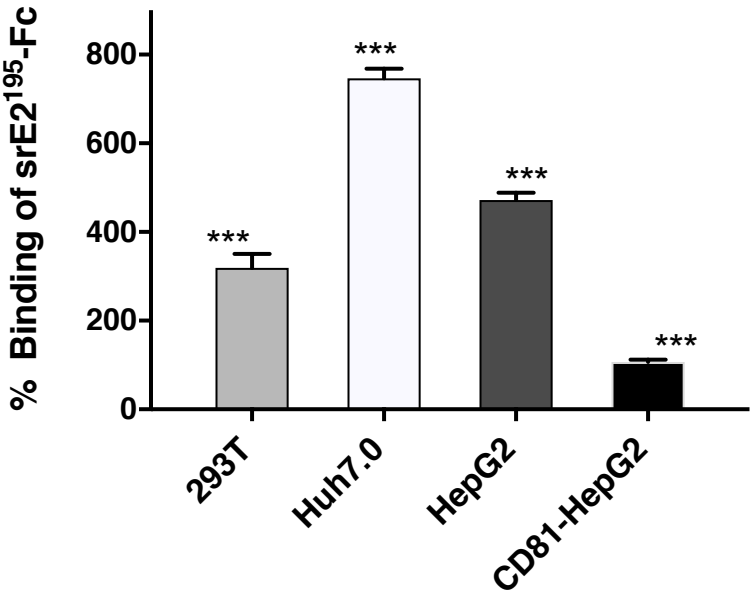

Figure 0-1 Enhancement binding of srE2^{195}-Fc to the cells when SR-B1 is engaged.

3 µg/ml rabbit Anti-SRB1 (H-180) serum was added to each sample containing 1x10^{6} of cells in 1ml FBS-free medium and incubated for 30 minutes at RT. Unbound anti-SRB1 was washed out and pellet cells were resuspended in medium containing 25 µg/ml purified srE2^{195}-Fc and incubated for 60 minutes at RT. Cells were pelleted down and the cell pellet was dissolved in fresh medium and probed with FITC-conjugated anti-human Fc goat secondary (1 in 500). Unbound secondary antibodies were washed out and the cells were fixed. FITC signals were measured using a fortessa machine. A set of the cells was incubated only with srE2^{195}-Fc (no pre-treatment with anti-SRB1) and used as control samples. A set of samples (negative control) was probed with tPA-Fc (negative control) and basal mean fluorescence intensity from control was subtracted from each of the data points shown. The graph represents calculated percentage of increase in srE2^{195}-Fc fusion binding capacity (Y-axis) to pre-treated cells with anti-SRB1 (X-axis) in comparison with native fusion interaction cells (normalised to zero, not shown). Data values represent the mean of triplicate assays, error bars = SD. P-value was calculated between MFI of the control sample and each individual pre-treated sample with anti-SRB1 serum. T-test ***: $p < 0.001$.

4.4.2 Microscopy - srE2^{195}-Fc binding in presence of the anti-SRB1

Rich SR-B1-expressing HepG2 cells were chosen as a model to image the effect of adding anti-SRB1 on interaction capacity of srE2^{195}-Fc to the cell surface and to analyse if such antibody addition may lead to srE2^{195}-Fc/SR-B1 overlay. One experiment was performed on PFA-fixed HepG2 (**Fig. 4.4-2**). In brief, after PFA fixation step, the cells were incubated at RT with rabbit anti-SRB1 serum (target SR-B1 and B2 of human origin at epitope mapped within the extracellular domain at amino acids 230-280) and then srE2^{195}-Fc was added. Secondary anti-rabbit Alexa Fluor 647 and goat anti-FC FITC was incubated with the cells for 60 minutes. Grouped Z imaging showed Alexa Fluor 647 signals expressed abundantly over HepG2 cell surface, indicating high expression of SR-B1 on HepG2 and was consistent with previous findings obtained by flow cytometry analysis (section 3.4.3.2). Moreover, FITC signals were detected on the cell surface as a concentrate and located close to the site of SR-B1 receptors. No overlay was observed between abundant Alexa Fluor 647 signals and limited FITC signal, which demonstrate no favourable direct binding between SR-B1 receptors organised mostly over the cell surface and limited srE2^{195}-Fc staining when the cells were treated with anti-SRB1.

A further experiment was conducted incubating live HepG2 with rabbit anti-SRB1 for 30 minutes in 5% CO_2 at 37°C and then fixed with PFA (**Fig. 4.4-3 A**). Then, srE2^{195}-Fc was added to the cells for 60 minutes at RT. Bound anti-SRB1 to the cell surface was probed with secondary anti-rabbit Alexa Fluor 647 and srE2^{195}-Fc that bound to the cells was probed with goat anti-human Fc FITC. Moreover, the control cell sample for this experiment involved probing with anti-SRB1 and srE2^{195}-Fc after fixation of HepG2. As expected and previously achieved, confocal imaging of the control sample showed restricted binding site for srE2^{195}-Fc with no overlay with rich SR-B1 expressed on the HeG2 cell surface (**Fig. 4.4-3 C**). Importantly, live treatment of HepG2 with anti-SRB1 showed low detection of Alexa Fluor 647 staining on the cell membrane and prominent different sized vacuoles which in the cytoplasm

which were observed to be in contact with the cell membrane and outer border of the nucleus (**Fig. 4.4-3 A**). In addition, these vacuoles were abundantly decorated with Alexa Fluor stains; this indicates that interaction of SR-B1 with antibody resulted in receptor localisation over the cell surface and induced entry. FITC signals were markedly expressed over the HepG2 cell surface in the form of spots or discrete patches with some overlays with Alexa Fluor signals (**Fig. 4.4-3 A**). In addition, FITC signals decorated the cell membrane border of vacuoles with few overlays with Alexa Fluor 647 in the cytoplasm. This finding demonstrates the g interaction of srE2^{195}-Fc to an alternative binding site on the outer surface during spanning and entry of SR-B1.

An additional experiment was conducted involving the addition of anti-SRB1 to live cells for 30 minutes followed by adding srE2^{195}-Fc for 60 minutes before PFA fixation (**Fig. 4.4-3 B**). Similar results were achieved in terms of significant enhancement of srE2^{195}-Fc interaction to HepG2 surface with no marked entry, abundant cytoplasmic localisation of SR-B1 with fair level observed on the cell surface, and prominent vacuoles decorated with srE2^{195}-Fc fusion (membranous joining border) and SR-B1. Overall, this supports the suggestion of the presence of alternative factors which have a higher binding capacity for srE2^{195}-Fc post targeting SR-B1 with a specific antibody and different conditions of experiments proved that srE2^{195}-Fc has higher interaction fractions to a surface factor other than SR-B1.

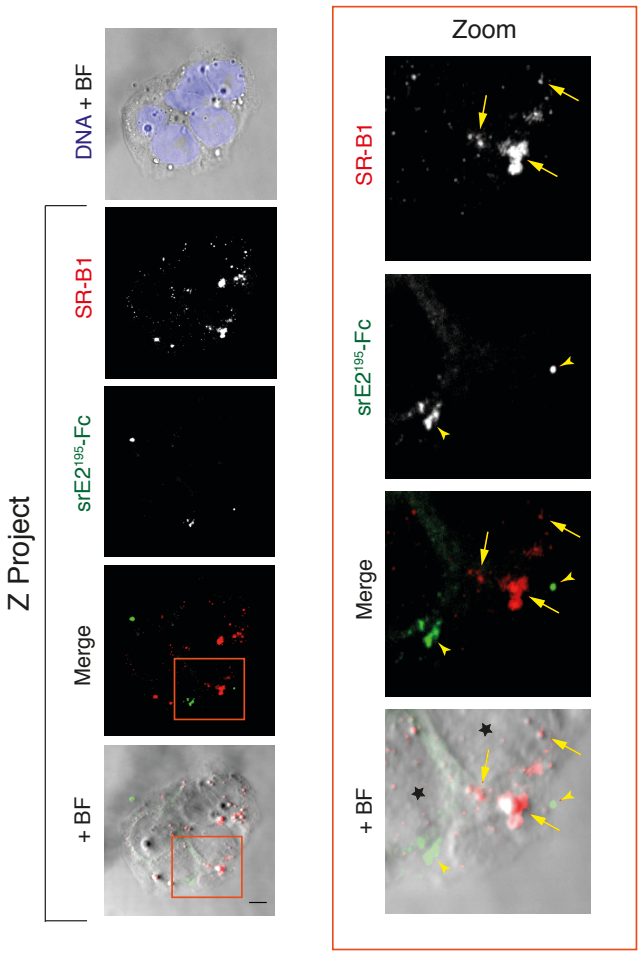

Figure 0-2 No overlay between srE2^{195}-Fc and SR-B1.

SR-B1 presence was detected by incubating the cells in each µ-slide well with 1:30 rabbit anti-SR-B1 (ab36970) and followed with 3x wash in washing buffer (0.1% BSA in PBS). Cells were incubated with 25 µg srE2^{195}-Fc in each well for 60 minutes at RT and rinsed 3x in washing buffer. The bound anti-SRB1 was labelled with goat anti-rabbit Alexa Fluor 647 conjugate (1 in 75) for 60 minutes and the cells then were rinsed 3x in washing buffer. The bound fusion was labelled with goat anti-human Fc FITC in blocking buffer (1:50), rinsed 3x in washing buffer. Cells were counterstained with with DAPI, mounted and imaged by confocal micrscope. Nucleus (DAPI) image was merged with the corresponding BF image. The sum of combined stacks was imaged along the Z-axis for FITC staining (srE2^{195}-Fc), SR-B1 staining (Alexa Fluor 647) -/+ BF series is presented as a grouped Z project. The boxed area is shown at greater magnification. Yellow arrowheads indicate srE2^{195}-Fc staining. Yellow arrows indicate SR-B1 staining and black stars indicate nucleus. The layers of the zoom panel show srE2^{195}-Fc binding to the cells at site not merged with SR-B1. Scale bar 5µM.

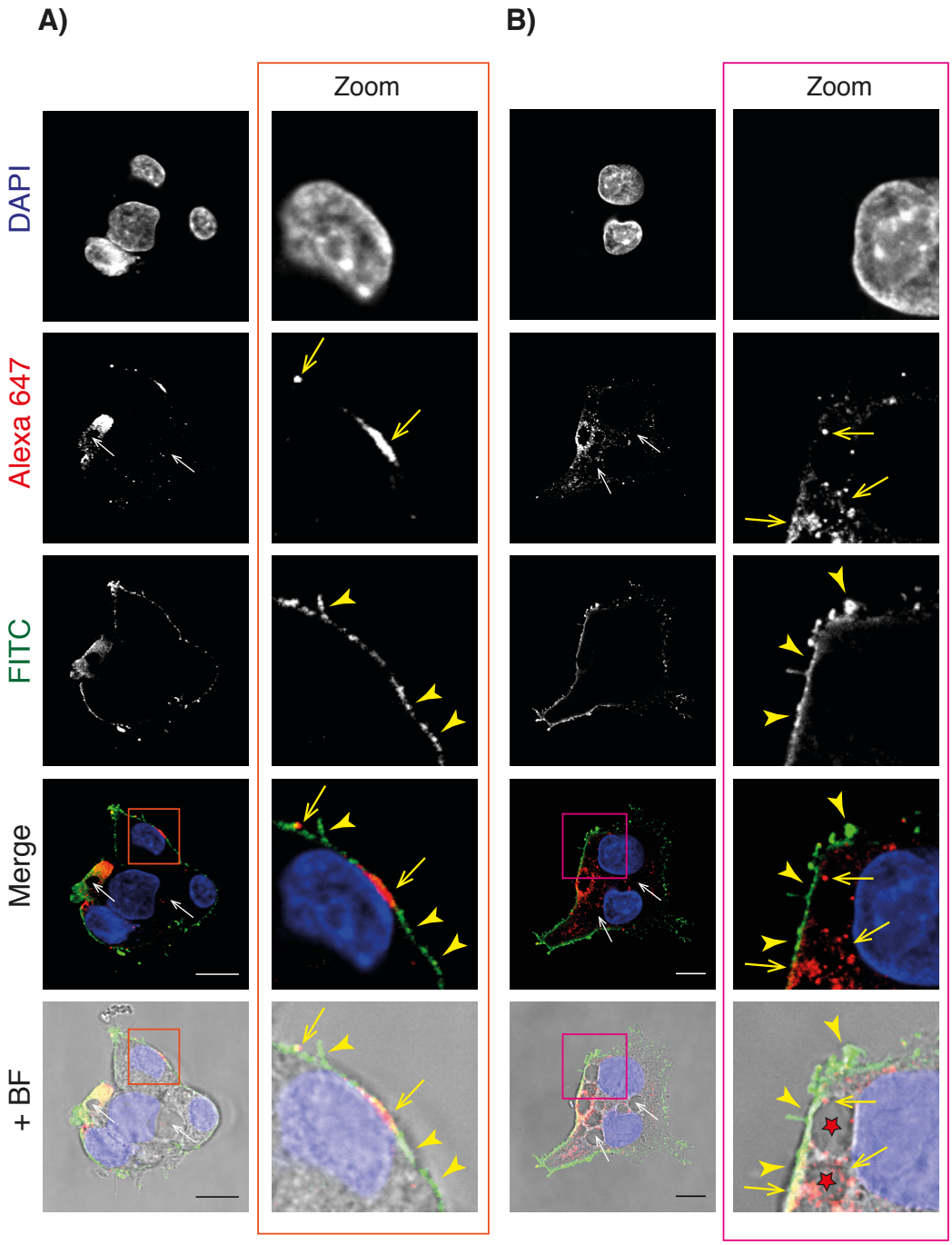
A)
B)
Zoom
Zoom
DAPI
Alexa 647
FITC
Merge
+ BF

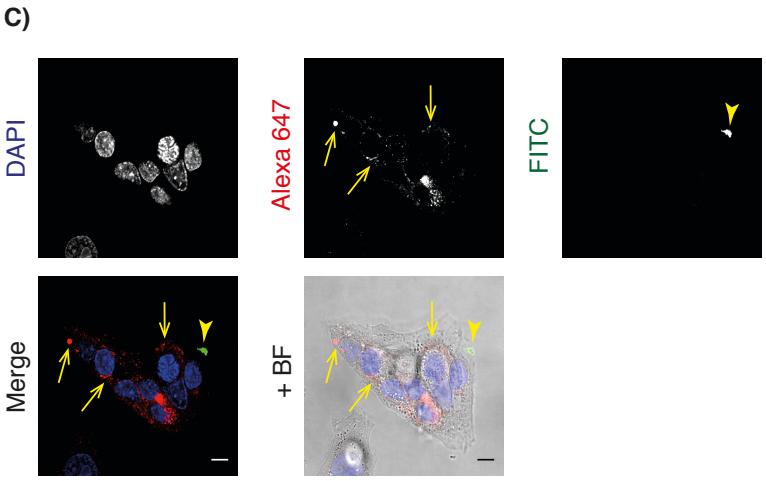

Figure 0-3 Pre-treated live HepG2 with anti-SRB1 demonstrated enhanced binding of srE2^{195}-Fc to the cell factor than SR-B1.

Panel (A) methodology: rabbit anti-SR-B1 (ab36970) at dilution of 1:30 was added to live HepG2 and incubated in 5% CO_2 at 37°C for 60 minutes. Unbound antibody was washed out. The cells were fixed, permeabilised, blocked and washed. srE2^{195}-Fc (30 µg) was added to each well and incubated for 60 minutes at RT followed with 3x washing steps. Goat anti-rabbit Alexa Fluor 647 conjugate (1 in 75) were added to each well and incubated for 60 minutes at RT. Unbound antibodies were rinsed 3x in washing buffer. Bound srE2^{195}-Fc to the cells presence was detected by incubation with goat anti-human FC FITC (3 in 150) and incubated 60 minutes followed with 3x wash in washing solution. Panel (B) methodology is similar to panel (A) methodology with the following modification: live incubation of rabbit anti-SR-B1 (ab36970) for 30 minutes and live incubation srE2^{195}-Fc fusion for 40 minutes before PFA fixation. Panel (C) methodology is similar to panel (A) methodology with the following modification: HepG2 the cells were fixed and incubated with rabbit anti-SR-B1 (ab36970) for 60 minutes then with srE2^{195}-Fc for 60 minutes. For all experiments: cells were counterstained with with DAPI, mounted and imaged by confocal micrscope. Merged nucleus (DAPI), SR-B1 (Alexa Fluor 647) and srE2^{195}-Fc (FITC) +/- HepG2 the cell (BF) are presented. Panel (A) represents interaction of srE2^{195}-Fc after fixing HepG2 cells, which were pre-treated with anti-SRB1. Panel (B) represent binding of srE2^{195}-Fc to live HepG2-bound anti-SRB1. Panel (C) is a control sample and demonstrates native binding of srE2^{195}-Fc to fixed HepG2, which includes labelling with anti-SRB1 after PFA fixation. The boxed area is shown at greater magnification. Yellow arrowheads indicate srE2^{195}-Fc staining, yellow arrows represent SR-B1 staining and white arrows (or red stars) indicate vacuoles decorated with SR-B1. Scale bar is 10 µM.

4.5 Engagement of OCLN leads to improvement of srE2^{195}-Fc binding capacity

4.5.1 Flow cytometry-interaction of srE2^{195}-Fc in presence of anti-OCLN

293T and hepatoma cells (Huh7.0, HepG2, and CD81-HeG2) were incubated with goat anti-OCLN (Y-12) unconjugated serum for 30 minutes at RT. srE2^{195}-Fc was added to the cells and then labelled with secondary goat anti-human FC FITC. Data demonstrated that adding anti-OCLN to the cells was associated with promoting FITC signals by approximately 339% (293T), 626% (Huh7.0), 475% (HepG2), and 97% (CD81-HepG2) than FITC detected on corresponding cells which were not incubated with anti-serum (**Fig 4.5-1**). Despite a different OCLN rate on the cell surface (3x higher on HepG2 comparing with 293T and Huh7.0), which was shown previously (section 3.4.3.2), FITC intensity measured on Huh7.0 was higher than on HepG2 treated with anti-OCLN. Although treated CD81-HepG2 with anti-OCLN showed enhancement in interaction with srE2^{195}-Fc, it was approximately 80% less than the binding capacity achieved with HepG2. This again suggests that abundant CD81 expressed on the surface of HepG2 results in masking the binding site for srE2^{195}-Fc.

We speculated that the binding of anti-OCLN antibody to OCLN receptors might lead to better exposure of srE2^{195}-Fc to other known HCV receptors. A study reported that silencing OCLN on Huh7 and on CLDN-1 expressing 293T did not affect expression rate and distributions of CD81, SR-B1 and CLDN-1. In addition, the same study indicated no differences between wild or OCLN-knockdown Huh7 in clathrin-mediated endocytosis of VSV (Benedicto *et al.*, 2008; Benedicto *et al.*, 2009). This means no direct effect of OCLN on HCV receptors or on the early stage of HCV entry and its critical role is at a later stage of entry (possibly the fusion process). This is probably in agreement with our findings in which transfecting HepG2 cells with CD81 was associated with increased CLDN-1 expression and no difference in the expression rate of SR-

B1 and OCLN between CD81-HepG2 and native HepG2 (section 3.5.4). Based on our work, we think that srE2^{195}-Fc has binding capacity to different factors and receptors than CD81, CLDN-1, SR-B1 and OCLN.

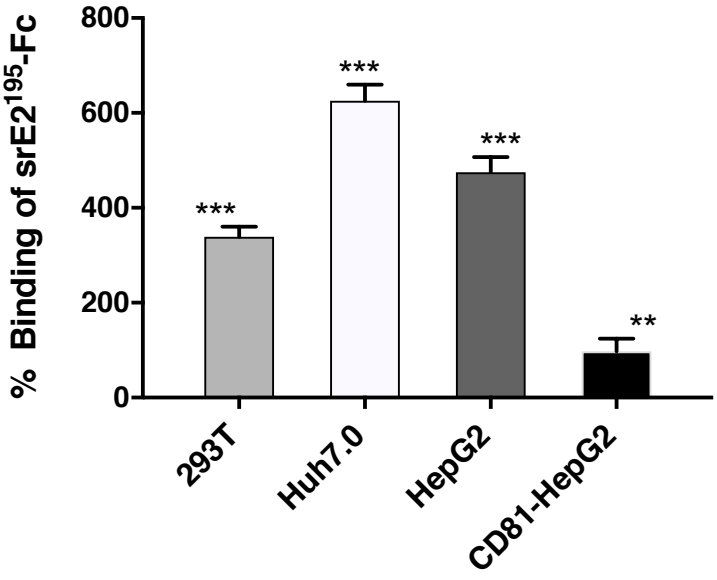

Figure 4.5-1 Enhancement binding of srE2^{195}-Fc to the cells pre-treated with anti-OCLN.

2 µg/ml goat anti-OCLN Y-12 serum was added to each sample containing 1x10^6 cells in 1ml medium and incubated for 30 minutes at RT. Unbound anti-OCLN was washed out and the cell pellet resuspended in FBS-free medium containing 25 µg/ml purified srE2^{195}-Fc fusion and incubated for 60 minutes at RT. Cells were pelleted down and the cell pellet was dissolved in fresh media and probed with FITC-conjugated anti-human Fc goat secondary (1:500). Unbound secondary antibodies were washed out and the cells were fixed. FITC signal were measured using a fortessa machine. A set of the cells was incubated with srE2^{195}-Fc (no pre-treatment with anti-OCLN) and used as a control sample. A set of samples (negative control) was probed with tPA-Fc (negative control) and basal mean fluorescence intensity from negative control was subtracted from each of the data points shown. The graph represents calculated percentage of increase in srE2^{195}-Fc binding capacity (Y-axis) to cells pre-treated with anti-OCLN (X-axis) in comparison to native fusion interaction cells (normalised to zero, not shown). Data values represent the mean of triplicate assays, error bars = SD. P-value was calculated between MFI of the control sample and each individual pre-treated sample with anti-OCLN serum. T-test **: $p < 0.01$.

4.5.2 Microscopy- srE2^{195}-Fc binding in presence of anti-OCLN

Expression style of OCLN which was visualised by goat anti-OCLN (Y-12) and interaction pattern of srE2^{195}-Fc to PFA fixed the cell lines was in the form of a single lateral fluorescent concentrate as mentioned previously (section 3.4.3.1), which suggested a possible merge between OCLN and srE2^{195}-Fc. We wished to probe PFA fixed HepG2 with anti-OCLN and srE2^{195}-Fc and analyse if srE2^{195}-Fc interaction merge with the OCLN site or not. Confocal imaging revealed an exact single fluorescence merge between Alexa Fluor 647 conjugated anti-OCLN and FITC conjugated anti-Fc serum on each single HepG2 (**Fig. 4.5-2 C**). This indicates an overlay (possibly interaction) between srE2^{195}-Fc and OCLN receptor.

A further experiment was conducted by incubating live HepG2 with goat anti-OCLN for 30 minutes in 5% CO_2 at 37°C and then fixing with PFA (**Fig. 4.5-2 A**). srE2^{195}-Fc fusion was added to the cells for 60 minutes at RT. Bound anti-OCLN to the cell surface was probed with secondary anti-goat Alexa Fluor 647, and srE2^{195}-Fc fusion that bound to the cells was probed with goat anti-human Fc FITC. Surprisingly, live treatment of HepG2 with anti-OCLN showed abundant Alexa Fluor 647 stain distributed over the cell membrane and in an overlay with FITC. It demonstrates that binding of specific antibody targeting OCLN, which is naturally organised in the form of individual lateral concentrate, resulted in localisation of OCLN on the cell surface and importantly showed an interaction of srE2^{195}-Fc to spanned OCLN. In addition, Alexa Fluor 647 did not completely occupy the whole HepG2 the cell surface which demonstrates the absence of OCLN in these areas. Rich FITC staining with no overlay with Alexa Fluor 647 staining was detected in these OCLN-free regions which means binding of srE2^{195}-Fc to additional alternative factors than OCLN receptor. Detection of fluorescent vacuoles like shape was observed at the inner side of the cell membrane and in the central part of the HepG2 cytoplasm decorated densely with srE2^{195}-Fc, and little with OCLN. Imaging of srE2^{195}-Fc fusions in HeG2 cell cytoplasm indicates internalisation

of srE2^{195}-Fc which detected after incubating HepG2 with anti-OCLN. An additional experiment was conducted involving the addition of anti-OCLN to live the cells for 30 minutes followed by adding srE2^{195}-Fc for 60 minutes before PFA fixation step (**Fig. 4.5-2 B**). Similar results were achieved in terms of OCLN spanning which merged with srE2^{195}-Fc, dense srE2^{195}-Fc interaction to surface area not expressing OCLN, and the presence of membranous and cytoplasmic vacuoles decorated with srE2^{195}-Fc and OCLN. Overall, engagement of OCLN on HepG2 resulted in srE2^{195}-Fc fusion interaction with unknown alternative factors and is closely associated with OCLN receptor (possibly real interaction).

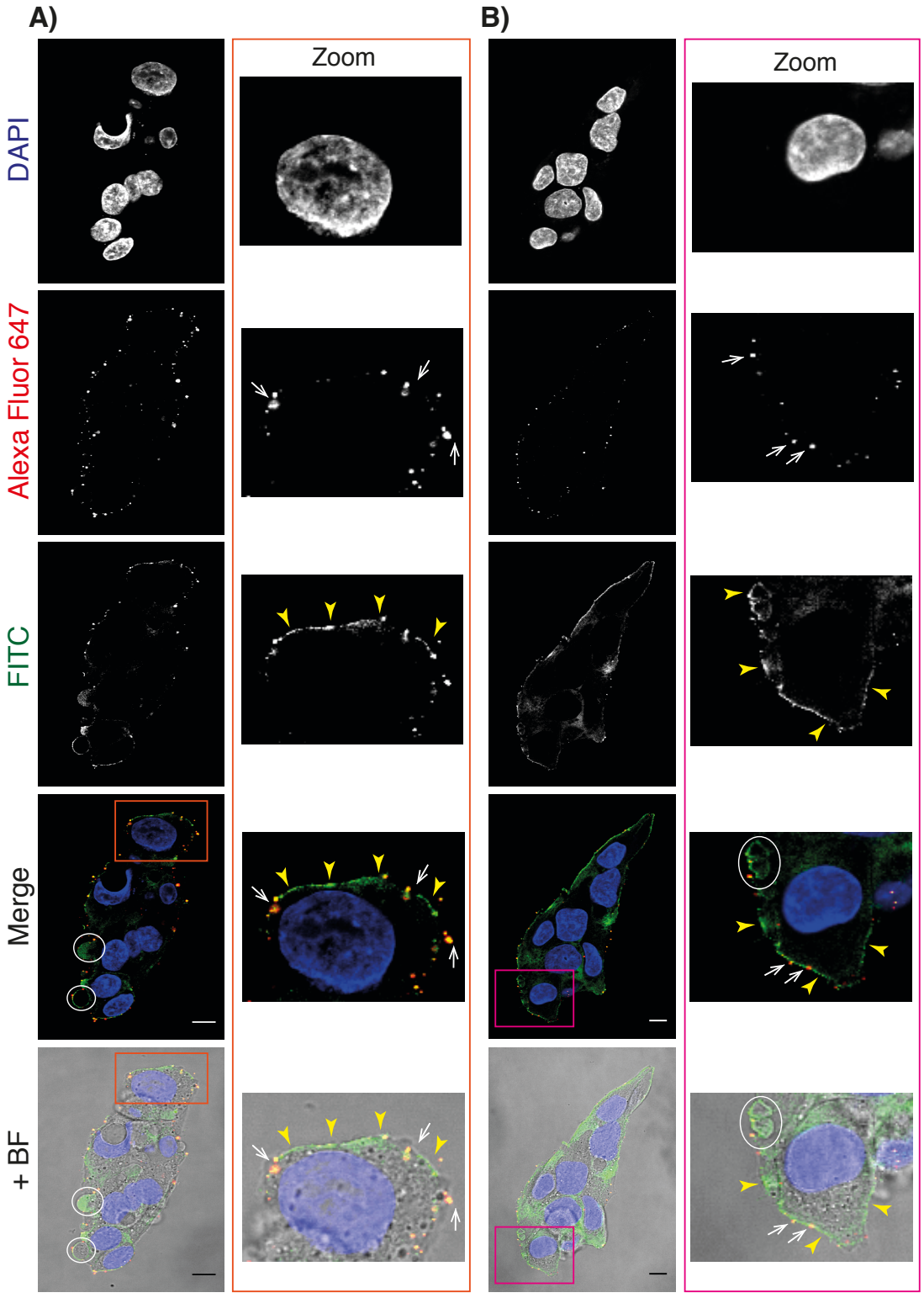
A)
B)
Zoom
Zoom
DAPI
Alexa Fluor 647
FITC
Merge
+ BF

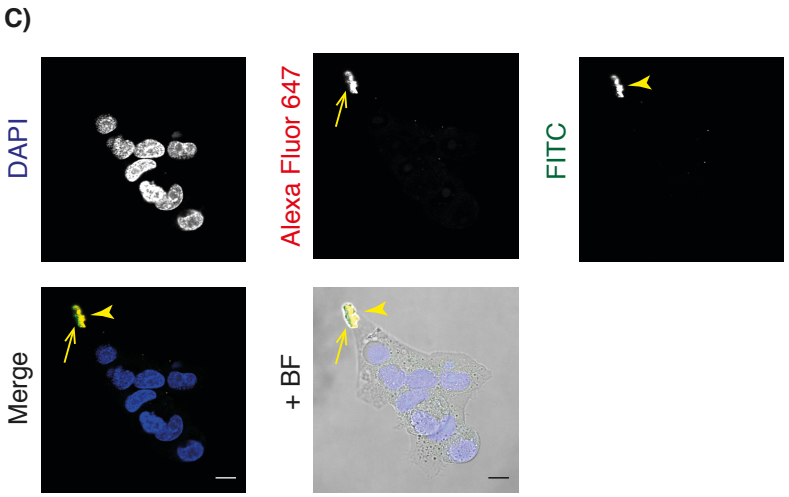

Figure 4.5-2 Pre-treated live HepG2 with anti-OCLN demonstrated enhanced binding of srE2^{195}-Fc to the cell membrane apart from OCLN.

Panel (A) methodology: 1.2 µg goat anti-OCLN (Y-12) was added to live HepG2 per well and incubated in 5% CO_2 at 37°C for 60 minutes. Unbound antibody was washed out. The cells were fixed, permeabilised, blocked and washed. srE2^{195}-Fc (30 µg) was added to each well and incubated for 60 minutes at RT followed with 3x washing steps. Donkey anti-goat IgG Alexa Fluor 647 conjugate (1 in 75) was added to each well and incubated for 60 minutes at RT. Unbound antibodies were rinsed 3x in washing buffer. srE2^{195}-Fc bound to the cells was detected by incubation with goat anti-human FC FITC (3 in 150) and incubated for 60 minutes followed with 3x wash in washing solution. Panel (B) methodology is similar to panel (A) with the following modification: live incubation of goat anti-OCLN (Y-12) for 30 minutes and live incubation srE2^{195}-Fc for 40 minutes before PFA fixation. Panel (C) methodology is similar to panel (A) with the following modification: HepG2 the cells were fixed and incubated with goat anti-OCLN (Y-12) for 60 minutes then with srE2^{195}-Fc for 60 minutes. For all experiments, Cells were counterstained with with DAPI, mounted and imaged by confocal micrscope. Merged nucleus (DAPI), OCLN (Alexa Fluor 647) and srE2^{195}-Fc (FITC) +/- HepG2 the cell (BF) are presented. Panel (A) represents interaction of srE2^{195}-Fc after fixing the HepG2 cells which were pre-treated with anti-OCLN. Panel (B) represents binding of srE2^{195}-Fc to live HepG2-bound anti-OCLN. Panel (C) is a control sample and demonstrates native binding of srE2^{195}-Fc to fixed HepG2 which include labelling with anti-OCLN after PFA fixation. The boxed area is shown at greater magnification. Yellow arrowheads indicate srE2^{195}-Fc staining and white arrows show overlay of occludin and srE2^{195}-Fc staining. White circle represents vacuole decorated with srE2^{195}-Fc and OCLN. Scale bar is 10 µM.

4.6 Further improvement in the binding of srE2-Fc forms when the cells pre-bound srE2^{195}-Fc

4.6.1 Interaction analysis of srE2^{332}-Fc to the cells pre-incubated with srE2^{195}-Fc

We wanted to test whether binding of srE2^{195}-Fc to 293T has any effect on the interaction of srE2^{332}-Fc. An assay was conducted by treating 293T with srE2^{195}-Fc followed with proper washing to remove unbound protein. Then, 293T cells were incubated with srE2^{332}-Fc and probed with goat anti-human Fc FITC conjugate. The FITC signal of 293T cells incubated with 30 µg/ml of srE2^{195}-Fc was increased approximately three folds compared to FITC signal of srE2^{332}-Fc on 293T cell not pre-treated with srE2^{195}-Fc (**Fig. 4.6-1 A**). It is notable that both the srE2^{332} peptide and the srE2^{195} peptide are fused with the functional Fc domain and they are recognised similarly by the conjugate anti-Fc FITC. It was argued that the enhanced fluorescence intensity might relate to enhancement binding capacity of srE2^{195}-Fc and not to srE2^{332}-Fc or possibly both. srE2^{195}-Fc was incubated first with the cells, and unbound proteins were removed by 2x proper washing. In addition, the native binding capacity of srE2^{195}-Fc alone (control) to 293T was poor with the cells. All this evidence suggests that measured enhanced binding capacity is related to srE2^{332}-Fc staining.

The further confirmatory experiment was conducted by labelling Fc domain fused with srE2^{332} peptide (not the srE2^{195} peptide) with a zenon-labelled Fab fragment. Unbound labelled fragments were removed by mixing reaction with non-specific IgG. The experiment was done again in the same order: treating the cells with srE2^{195}-Fc, 2x washing in PBS, the addition of 3 µg/ml srE2^{332}-Fc bound to Zenon conjugate, 2x rinsing in washing buffer and fixed with 0.5% PFA. The fortessa reading showed that Zenon Alexa Fluor 647 signal of 293T cell sample pre-incubated with 1µg/ml of srE2^{195}-Fc was sharply increased 3-fold over Zenon signal of srE2^{332}-Fc incubated with untreated 293T with srE2^{195}-Fc (**Fig. 4.6-1 B**). A further experiment was conducted using hepatoma

cell lines. Data demonstrated that pre-treatment of the cells with srE2^{195}-Fc was associated with increased Zenon Alexa Fluor 647 signal by approximately 3.7-fold (Huh7.0) and 2.8-fold (HepG2) compared with Zenon signal detected on untreated cells (**Fig. 4.6-1 B)**.

Overall, this indicates that enhanced binding capacity of fusion to the cell surface is specifically related to srE2^{332}-Fc interaction which is achieved due to pre-treatment of the cells with srE2^{195}-Fc. Our explanation for this event is that interaction of E2 containing an a.a. sequence between site E^{1} to T^{195} of the N-terminal domain (corresponding to E_{384} to T_{578} of the native HCV polypeptide sequence) to unknown factors on the cell membrane leads to exposure of possibly known HCV receptors (in particular CD81 or SR-B1) or unknown attachment factors which interact with E2 at region extensions downstream from site L^{196} to site K^{332} (corresponding to L_{579} to K_{715} of native HCV polypeptide sequence).

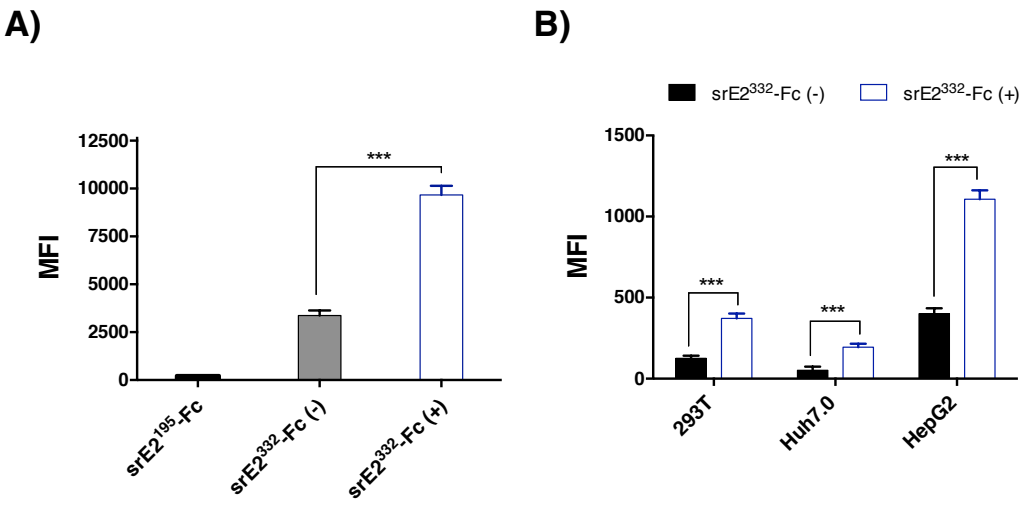

Figure 4.6-1 Improvement of srE2^{332}-Fc binding capacity to the pre-treated cells with srE2^{195}-Fc.

(A) srE2^{195}-Fc (30 µg/ml) was added to each sample containing 1x10^{6} the 293T cells in 1ml medium with 10% FBS and incubated for 60 minutes at RT. Unbound fusions were washed out twice and the cells pellet was resuspended in medium contained purified srE2^{332}-Fc (30 µg/ml) in 1ml DMEM medium with 10% FBS, and incubated for 60 minutes at RT. Cells were pelleted down and the cell pellet dissolved in fresh FBS-free DMEM and probed with FITC-conjugated goat anti-human Fc secondary (1:500). Unbound secondary antibodies were washed out twice and the cell pellet resuspended in 1ml of 0.5% PFA/PBS solution. A set of samples was treated only with srE2^{332}-Fc (no prior step of srE2^{195}-Fc addition) and used as a sample control. A set of samples was probed with tPA-Fc (negative control) and basal MFI from control was subtracted from each of the data point shown. (B) srE2^{195}-Fc (1 µg/ml) was added to each sample containing 1x10^{6} 293T cells in 1ml medium and incubated for 60 minutes at RT. Unbound fusions were washed out twice and pellet cells resuspended in medium containing 3 µg/ml purified srE2^{332}-Fc bound Zenon Alexa Fluor 647 and incubated for 60 minutes at RT. Cells were pelleted down and the cell pellet dissolved in 1ml of PBS (2x) and then were fixed with 0.5% PFA/PBS solution. FITC (panel A) and Zenon Alexa Fluor 647 (panel B) signals were measured using a fortessa machine. Methodology of labelling srE2^{332}-Fc fusion using: 5µl of the Zenon Alexa Fluor 647-labelled goat Fab fragments were added to 1µg srE2^{332}-Fc in 20 µl PBS (3:1 molar ratio of Fab to human Fc domain) and incubated for 5 minutes at RT. Then, 5µl of the Zenon blocking reagent (containing non-specific IgG) was added and incubated for 5 minutes at RT. The prepared complex was added to the cells within 30 minutes. Zenon human IgG labelling kit (cat. No. Z-25408) was supplied by Molecular Probes. Panel (A) represents binding capacity of fusion to 293T and panel (B) interaction of srE2^{332}-Fc-bound Zenon Alexa 647 Fab fragments to 293T, Huh7.0 and HepG2. Interaction of srE2^{332}-Fc to untreated cells with srE2^{195}-Fc is represented by (-) and to pre-treated the cells with srE2^{195}-Fc is represented by (+). Native binding of srE2^{195}-Fc to 293T cells is shown. Data values represent the mean of triplicate assays, error bars = SD. P-value was calculated between MFI of srE2^{332}-Fc interaction with control sample and with each individual pre-treated sample with srE2^{195}-Fc. T-test **: $p < 0.01$ and ***: $P < 0.001$.

4.6.2 Dose-dependent analysis of srE2^{332}-Fc binding to pre-incubated cells with srE2^{195}-Fc

As pre-incubation of cells with srE2^{195}-Fc promoted enhanced binding of srE2^{332}-Fc, we wanted to address whether this effect is receptor/attachment factor-dependent by examining the impact of a constant E2^{195}-Fc concentration on the dose-dependent binding capacity of srE2^{332}-Fc. Upon incubating cell lines (293T, Huh7.0, HepG2 and CD81-HepG2) pre-treated with srE2^{195}-Fc with increasing concentrations of E2^{332}-Fc, the cells exhibited a pronounced dose-dependent increase in E2^{332}-Fc-specific FITC fluorescence (**Fig. 4.6-2**). Importantly, this increase in fluorescence was considerably greater than that observed with cells that had not been pre-treated with srE2^{195}-Fc. This indicates that enhancement of fusion binding capacity in dose-dependent manner is specific to srE2^{332}-Fc fusion which is initiated by the interaction of srE2^{195}-Fc to the cells prior to exposing the target cells to srE2^{332}-Fc.

Importantly, we noticed that the HepG2 cells were most sensitive to the prior addition of srE2^{195}-Fc. The fluorescent signal of due to srE2^{332}-Fc binding (0.1µg/ml) to pre-treated HepG2 cells was improved 7,660-fold over native untreated HepG2. Pre-incubation of HepG2 with srE2^{195}-Fc resulted in enhanced interaction of 1.60µg/ml, 6.40µg/ml and 25.6µg/ml of srE2^{332}-Fc by 2,668.4, 51.64 and 10.22-fold respectively than native srE2^{332}-Fc interaction to HepG2 in the absence of srE2^{195}-Fc fusion. srE2^{195}-Fc preferentially enhances binding of low concentration of srE2^{332}-Fc. At high concentrations the cells are saturated with srE2^{332}-Fc and so the impact of srE2^{195}-Fc is less apparent. It may well have to do with the binding kinetics and affinity of the E2 with various receptors. Further work is required to determine the mechanism of enhanced binding in presence of srE2^{195}-Fc. Incubating pre-treated CD81-HepG2, 293T and Huh7.0 with 0.1µg/ml of srE2^{195}-Fc leads to improved binding of srE2^{332}-Fc by 12-fold, 3.8-fold and 4.5-fold respectively, and 25.6µg/ml of srE2^{332}-Fc results in approximately 2-fold enhanced interaction of srE2^{332}-Fc to the cell lines. Thus binding of srE2^{195}-Fc to a receptor that is distinct from CD81

results in enhanced binding of full-length srE2^{332}-Fc to cells; perhaps suggesting that pre-incubation with srE2^{195}-Fc results in exposure of new receptor binding sites and or improved expression of alternative receptors.

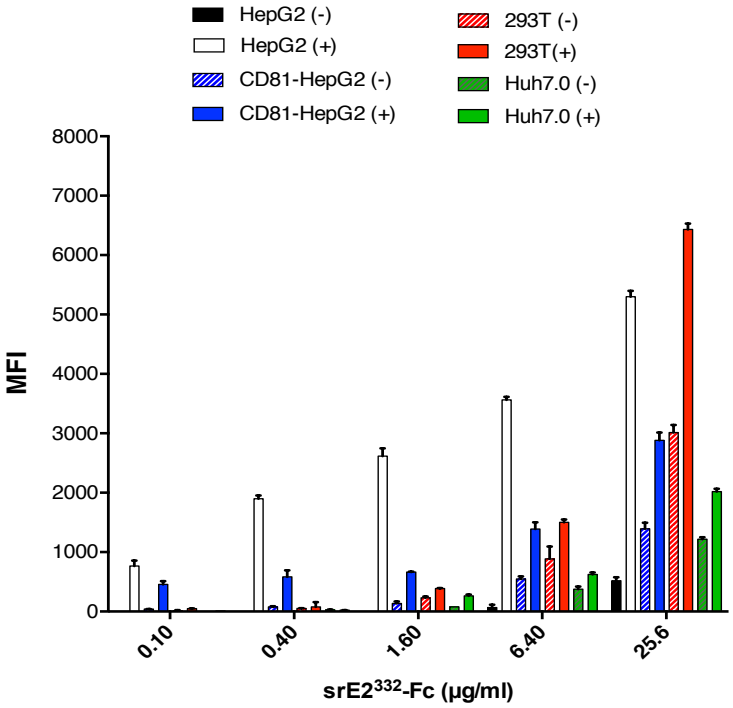

Figure 4.6-2 Interaction of srE2^{332}-Fc is markedly improved to HepG2 comparing with 293T, Huh7.0, and CD81-HepG2.

Order of reagent addition and FCM method were conducted exactly as done in the same section (legend 4.6-1 A) with the following modifications: addition of srE2^{195}-Fc (10 µg/ml) and a different concentration of srE2^{332}-Fc as shown (X axis). A set of samples was probed with tPA-Fc (negative control) and another set was probed with srE2^{195}-Fc. The basal MFI from tPA-Fc and from srE2^{195}-Fc readings were subtracted from each of the data points shown. The graph represents the binding capacity of srE2^{332}-Fc to 293T and hepatoma the cells in the following order: HepG2 (-), HepG2 (+), CD81-HepG2 (-), CD81-HepG2 (+), 293T (-), 293T (+), Huh7.0 (-) and Huh7.0 (+). Untreated the cells with srE2^{195}-Fc (control samples) were represented as (-) and pre-incubated the cells with srE2^{195}-Fc were represented as (+). Data values represent the mean of triplicate assays, error bars = SD.

4.6.3 Testing the effect of srE2^{195}-Fc presence on binding of srE2-Fc variants (295a.a, 278a.a and 265a.a)

We wanted to test if the interaction of srE2^{195}-Fc to 293T, Huh7.0, and HepG2 has an effect on the interaction of different srE2-Fc forms. An assay was conducted by treating the target cells with serial concentrations of srE2^{195}-Fc followed with washing to remove unbound protein. Then, the cells were incubated with srE2-Fc variants and probed with goat anti-human Fc FITC conjugate.

A fortessa reading showed that the FITC signal of srE2-Fc variants on the 293T cell sample incubated with 1.56 µg/ml of srE2^{195}-Fc was increased approximately 2-3-fold over the FITC signal of a srE2-Fc variant on untreated 293T with srE2^{195}-Fc (**Fig. 4.6-3 A, Table 4.6-1**). Interestingly, incubation of 293T with gradualy increasing concentrations of srE2^{195}-Fc up to 25 µg/ml showed further improvement of binding capacity of srE2-Fc variants by only 7-10% compared with enhanced interaction achieved with the addition of 1.56 µg/ml srE2^{195}-Fc. FITC signal of srE2-Fc variants on Huh7.0 cells treated with 1.56 µg/ml srE2^{195}-Fc was increased 2.5-3-fold over the FITC signal of a srE2-Fc variant on untreated 293T with srE2^{195}-Fc (**Fig. 4.6-3 B, Table 4.6-1**). Incubating the srE2-Fc form with Huh7.0 treated with 25 µg/ml of srE2^{195}-Fc in comparison with 1.56 µg/ml srE2^{195}-Fc leads to further enhancement of srE2^{332}-Fc, srE2^{295}-Fc, srE2^{278}-Fc and srE2^{265}-Fc interactions by 14%, 20.8%, 3.7% and 15%. The FITC signal of the srE2-Fc variants on HepG2 incubated with 1.56 µg/ml of srE2^{195}-Fc was improved approximately 2-3-fold over FITC signal of corresponding srE2-Fc variant on untreated HepG2 with srE2^{195}-Fc (**Fig. 4.6.3 C, Table 4.6-1**). Incubation of HepG2 with gradual increasing concentration of srE2^{195}-Fc up to 25 µg/ml showed further improvement of binding capacity of srE2^{332}-Fc, srE2^{295}-Fc, srE2^{278}-Fc and srE2^{265}-Fc by 39%, 7%, 13% and 2.6%. These variations in rate of enhancement among srE2-Fc variants have not yet been fully understood.

It is notable that all srE2-Fc forms showed improved binding capacity to 293T and hepatoma cells. In cells expressing CD81 (293T and Huh7.0), the order of

high binding capacity was achieved by srE2^{332}-Fc, then closely-related srE2^{295}-Fc and srE2^{278}-Fc, and finally with srE2^{265}-Fc. On CD81-deficient HepG2, the order was srE2^{332}-Fc, then srE2^{278} and finally with closely-related srE2^{295}-Fc and srE2^{265}-Fc. So, the full-length E2 was the best form in demonstrating interaction to treated the cells with srE2^{195}-Fc in particularly with HepG2 the cells.

Table 4.6-1 Percentage of enhancement in the binding of srE2-Fc forms when the cells pre-incubated with 1.56 µg/ml srE2^{195}-Fc.

Fusion	293T	Huh7.0	HepG2
srE2^{332}-Fc	65 %	59.31 %	68.55 %
srE2^{295}-Fc	50.81 %	59.64 %	64.72 %
srE2^{278}-Fc	50.26 %	61.42 %	50.13 %
srE2^{265}-Fc	64.81 %	65 %	61.42 %

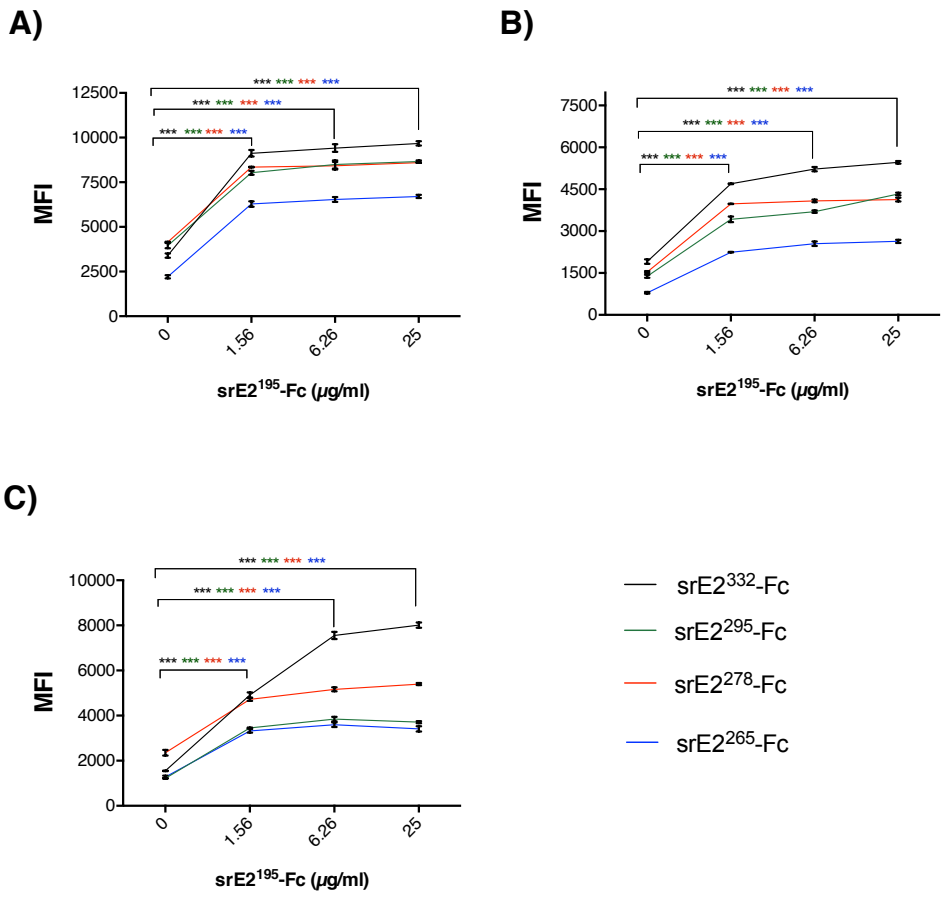

Figure 4.6-3 Binding of srE2-Fc variants are improved to pre-treated 293T and hepatoma the cells with srE2^{195}-Fc.

Order of reagent addition and FCM method were conducted exactly done in the same section (legend 4.6-1 A) with the following modifications: addition of srE2^{195}-Fc at different concentrations as indicated (x-axis), the addition of 30 µg/ml purified srE2-Fc variant to 293T and 25 µg/ml of the same fusions to Huh7.0 and HepG2. A set of samples was probed with tPA-Fc (negative control) and another set with srE2^{195}-Fc. The basal MFI from tPA-Fc and from srE2^{195}-Fc readings was subtracted from each of the data points shown. The graph represents binding of E2-Fc variants to 293T (panel A), Huh7.0 (panel B) and HepG2 (panel C). Zero point on the x-axis indicates natural binding of E2-Fc form to the cells without prior incubation of srE2^{195}-Fc with the cell (control sample). Data values represent the mean of triplicate assays, error bars = SD. P-value was calculated between MFI of srE2-Fc variant interaction with the control sample and with each individual pre-treated sample with srE2^{195}-Fc. T-test ***: P < 0.001.

4.7 The HepG2 cell bound to srE2^{195}-Fc becomes able to uptake srE^{332}-Fc

srE2^{332}-Fc was bound best the cells pre-treated with srE2^{195}-Fc in comparison of other srE2-Fc variants. Among the cell lines used, the HepG2 was highly sensitive in terms of enhancement of srE2^{332}-Fc binding capacity. So, we wanted to study if the same interaction could initiate uptake of srE2^{332}-Fc by HepG2. Two sets of live HepG2: one set was treated with srE2^{195}-Fc and another set not treated with srE2^{195}-Fc (control sample) and incubated in 5% CO_2 at 37°C for 60 minutes. Then, both sets of the cells were rinsed 2x in fresh MEM containing 10% FBS. srE2^{332}-Fc fusions bound to anti-Fc FITC conjugate was added to both sets of cells and incubated under the same conditions. Media were aspirated and the cells were fixed with PFA. Confocal imaging showed abundant cytoplasmic localisation of FITC staining and limited staining on the HepG2 cell membrane in cells pre-treated with srE2^{195}-Fc (**Fig. 4.7-1**). This indicates successful entry of srE2^{332}-Fc fusion in HepG2. However, the control the cells showed complete staining of the HepG2 cell membrane in the form of FITC discrete patches; no cytoplasmic staining was detected and the HepG2 cell still non-permissive for srE2^{332}-Fc as expected.

A further experiment was conducted applying exactly the same method of labelling srE2^{332}-Fc with a Zenon Alexa Fluor 647-labelled Fab fragment that targets the Fc domain fused with soluble envelope and including the addition of a blocking step in a solution containing non-specific IgG to remove unbound labelled fragments. Imaging analysis confirmed Alexa Fluor 647 signal detection in the cellular cytoplasm, which means that entry is specific to srE2^{332}-Fc and not srE2^{195}-Fc.

It was surprising how the susceptibility of CD81-deficient HepG2 cells to srE2^{332}-Fc entry is confered when the cells were pre-incubated with srE2^{195}-Fc. Our order of introducing the cells to srE2^{195} peptide possibly allowed optimum organisation of factors on HepG2. These factors might be present on the cell surface or intact at the inner side of the plasma membrane. The next step of

srE2^{332} peptide addition led to the interaction of high-affinity residues, located somewhere between sites 196 and 332, to HCV surface factors that might be already well exposed or involve binding with further factors and subsequently leads to efficient envelope entry. In contract, the initial introduction of the srE2^{332} peptide to HepG2 possibly does not permit such an order of events, high-affinity residue located after site 195 interact with the cell surface and may not allow the optimum interaction of certain residues located within the first 195 a.a. sequences. This probably results in condensation of E2 on the cell surface with no entry.

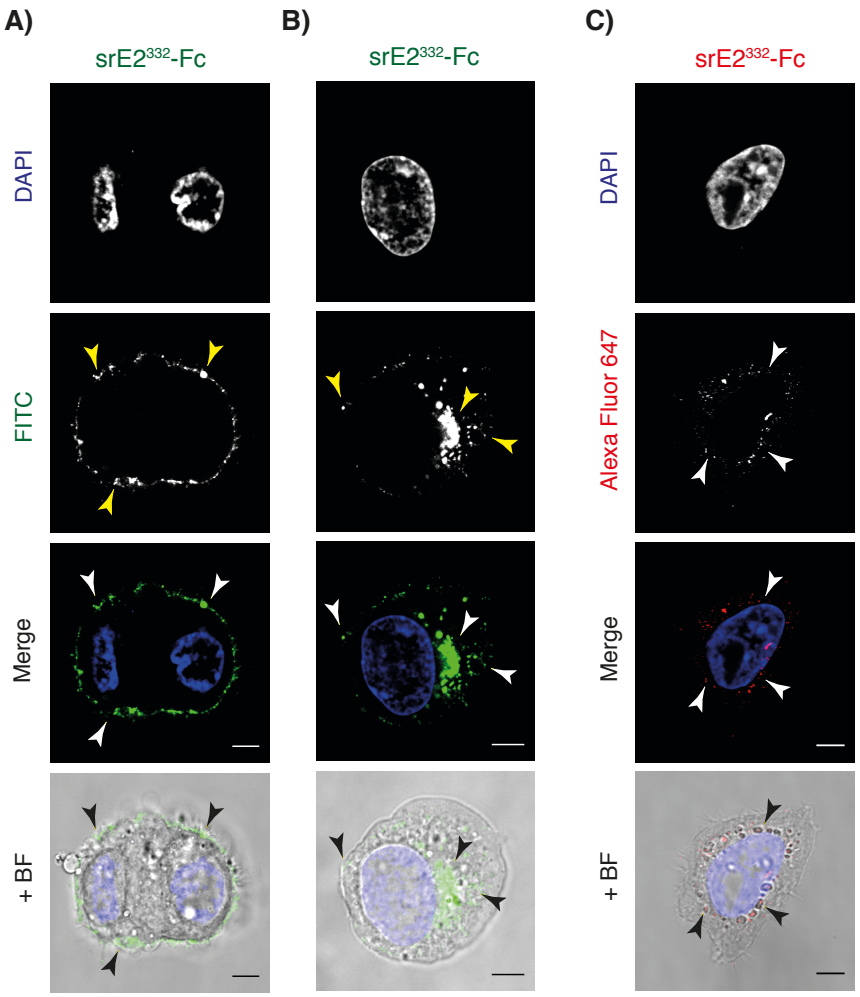

Figure 4.7-1 Treating the HepG2 with srE2^{195}-Fc leads to srE2^{332}-Fc entry.
Panel (A): live HepG2 (control sample) incubated with 25 µg/well srE2^{332}-Fc-bound anti-Fc FITC conjugate into 5% CO_2 incubator at 37°C for 60 minutes then the medium was aspirated. Panel (B): srE2^{195}-Fc (25 µg/well) was added to live HepG2 and incubated in 5% CO_2 at 37°C for 60 minutes. Unbound peptide fusion was removed, the cells were rinsed 2x in fresh medium and then incubated with 25 µg/well srE2^{332}-Fc-bound anti-Fc FITC conjugate in 5% CO_2 incubator at 37°C for 60 minutes. Panel (C): methodology was conducted as in panel (B) except srE2^{332}-Fc was labelled with Zenon Alexa Fluor 647-labelled Fab Fragment. For all panels, the cells were fixed with 4% PFA/PBS solution for 18 minutes at RT and followed with washing step 3x in PBS. Cells were counterstained with with DAPI, mounted and imaged by confocal micrscope. Merged nucleus (DAPI) and srE2^{332}-Fc (FITC or Zenon Alexa Fluor 647) +/- HepG2 the cell (BF) are presented. (Arrowheads indicate srE2^{332}-Fc staining located on the cell surface (panel A & B) or in the cytoplasm (panel B and C). Scale bar is 5 µM.

4.8 Discussion

4.8.1 Engagement of HCV receptors reveals alternative factor for srE2^{195}-Fc binding

Native purified srE2^{195}-Fc interaction with 293T and hepatoma cells is restricted to a limited binding site on the cell membrane. However treating HepG2 with srE2^{195}-Fc revealed higher binding capacity than compared to 293T and Huh7.0; it was still minimal binding when compared with other soluble E2-Fc fusions (332, 295, 278 and 265 a.a). In the insect cell expression system, srE2^{195}-Fc product is secreted into media as the correctly folded protein with the expected molecular size as evidenced by recognition of Fc domain by anti-Fc on WB membrane. Dense protein band stained with coomassie brilliant blue for srE2^{195}-Fc sample fraction collected by protein A column is achieved and indicates recognition of Fc domain that is fused with srE2^{195} domain. In addition, remarkable recognition of native or reduced denatured forms of srE2^{195}-Fc was achieved by hybridoma MAb (LBT 15B10) generated by immunizing mouse with srE2^{332} peptide. These findings support that hypothesis that poor interaction on the cell surface is not related to misfolding of srE2^{195}-Fc but reflects its natural recognition by factors on host cell surface. Incubating srE2^{195}-Fc with PFA fixed cells or live cells for up to 60 minutes revealed a prominent concentrated cap shaped binding site for the fusion peptide on the cell membrane. Extending incubation with HepG2 for 24 hours showed further binding sites in the form of spots located together and extended for short distance over cell membrane, which were smaller in size than the observed single concentrated structure. These spots were close to concentrated cap shaped interaction site for the srE2^{195}-Fc fusion on cell membrane. On HepG2 cells, we think that the presence of these spots (bound srE2^{195}-Fc) is related to an event occurred after binding of srE2^{195}-Fc fusion to the concentrate complex as treating cells for 60 minutes failed to show these small spots. So, we speculate that longer time of srE2^{195}-Fc incubation and

possibly binding to concentrate complex leads to slow spanning of presumably 'one or more' alternative binding domains for srE2^{195}-Fc.

We showed previously that anti-CD81 (5A6) Mab has the ability to block interaction of srE2^{332}-Fc, srE2^{295}-Fc, srE2^{278}-Fc and srE2^{265}-Fc to CD81 on 293T. Although srE2^{195}-Fc does not bind recombinant MBP-CD81 LEL, the binding capacity of srE2^{195}-Fc to 293T and Huh7.0 is promoted markedly when CD81 is recognised by 0.4µg/ml anti-CD81 after five minutes of incubation. Approximately 60 minutes of anti-CD81 incubation was required to show the beginning of an inhibitory effect on srE2^{332}-Fc interaction, while srE2^{195}-Fc achieved marked increase in interaction capacity to 293T surface. Imaging of live 293T and Huh7.0 pre-treated with anti-CD81 at different times in 5% CO_2 at 37°C followed by adding srE2^{195}-Fc after cell fixation demonstrates that the vast majority of enhanced binding of srE2^{195}-Fc fusions on cell surface sites are toward areas not occupied with CD81. Imaging analysis showed that instant stimulation of CD81 leads to robust dynamic spanning over the cell surface to form a capping structure at the side of target cells. This is consistent with published finding in which CD81 stimulation on Huh7 by anti-CD81 (JS-81) Mab, an antibody able to block entry of HCVcc and HCVpp in Huh7, for 60 minutes at 37°C result in CD81 relocalisation concentrated to areas of cell-cell contact (Brazzoli *et al.*, 2008).

Engagement of CD81 for a minimum of 20 minutes in 5% CO_2 at 37°C with Huh7.0 showed areas of plasma membrane comprising high incidence of different sizes of circular invaginations, decorated with CD81 and srE2^{195}-Fc. Extending the time of incubation showed that tubular invaginations occupied an area at the inner side of plasma membrane but were not budded in form of free vacuoles into cytoplasm. Treating live Huh7.0 with anti-CD81 in 5% CO_2 at 37°C for 30 minutes followed by addition of srE2^{195}-Fc before the fixation step showed of membranous invaginations decorated with both CD81 and srE2^{195}-Fc and obvious free localisation of srE2^{195}-Fc bound to alternative factors and CD81 in Huh7.0 cytoplasm with no overlap between both probes. These observations might indicate that live srE2^{195}-Fc/ alternative factor interaction in

presence of engaged CD81 is required to drive efficient post-binding entry in particular scission of vesicles that contain both srE2^{195}-Fc and CD81 from inner side of cell membrane to cytoplasm.

Harris *et al.*, (2008) demonstrated that treating Huh7.5 with anti-CD81 (M38) MAb, an antibody that has the ability to inhibit HCVcc and HCVpp infectivity in Huh7.5, for 60 minutes at 37°C increased the distance between tagged CD81/CD81 and had no effect on CD81/CLDN-1 which possibly means that engagement of CD81 has no effect on spanning of CLDN-1. CD81/anti-CD81 (5A6) interaction on Huh7.0 cell surface may have no effect on CD81/CLDN-1 interaction. In addition, enhanced srE2^{195}-Fc interaction on 293T cells which naturally express little CLDN-1 demonstrates that binding of srE2^{195}-Fc is unlikely with claudin-1. However observation of a few merged images between CD81 and srE2^{195}-Fc, flow cytometer data and most confocal imaging observations are in agreement, that srE2^{195}-Fc does not efficiently bind CD81. Missing critical residues involved in the interaction with the LEL of CD81 that locate at site Y^{230}, H^{234} and Y^{235} (Rothwang *et al.*, 2008) which are not included in srE2^{195} peptide are likely the reason behind residual binding to highly CD81 expressing 293T and null interaction with recombinant CD81 LEL.

Importantly, engaged very low CD81 with anti-CD81 (0.4µg/ml) on HepG2 was associated with remarkable improvement of srE2^{195}-Fc binding by approximately 335% compared with native binding. Moreover, the binding capacity on HepG2 was approximately 135% higher than that achieved on CD81 expressing Huh7.0. Imaging live HepG2 treated with anti-CD81 for 30 minutes in 5% CO_2 at 37°C followed with incubation with srE2^{195}-Fc demonstrated similar pattern to Huh7.0 in which srE2^{195}-Fc bound alternative factors present in the invaginations and underwent cytoplasmic localisation. It seems an undefined complicated process but it might be an indication that revealing, exposing or recruiting the alternative factor is not dependent on expression rate of the engaged receptor. It could be argued that anti-CD81 interactions with receptors might lead to optimum exposing of hidden epitopes on CD81 for better srE2^{195}-Fc interaction. Indeed, the rich binding of srE2^{195}-Fc

achieved on HepG2 cells, which naturally express little CD81, proves that srE2^{195}-Fc mainly deos not interact with CD81 even if anti-CD81 antibodies result in optimal epitope exposure of CD81 receptor.

Probing fixed HepG2 with antibodies targeting claudin-1 and srE2^{195}-Fc demonstrated no merged between abundantly distributed claudin-1 receptors and limited bound fusion peptide. This is in support of no immediate claudin-1/srE2^{195}-Fc interaction and in agreement with a report that no claudin-1/HCVpp interaction has been confirmed yet (Evans *et al.*, 2007). Similar results were achieved with live claudin-1 incubated with srE2^{195}-Fc before or after the PFA fixation step in terms of enhancement binding of fusion to claudin-1 free areas on surface and intracellular localisation of vacuoles decorated with claudin-1 and srE2^{195}-Fc. So this indicates that spanning and entry of alternative factors is by stimulation of claudin-1 and not due to binding of srE2^{195}-Fc.

Z-stack imaging of fixed HepG2 showed no overlay between abundant SR-B1 and srE2^{195}-Fc. After live SR-B1/anti-SRB1 interaction, obvious enhancement of srE2^{195}-Fc binding with HepG2 surface and some intracellular vacuoles decorated with srE2^{195}-Fc and SR-B1 were detected. Moreover, some srE2^{195}-Fc fusions are merged with engaged SR-B1 probably due to involving HVR1 (first N-terminal 1-27 a.a) which has previously been reported to include critical residues for SR-B1 binding at sites A^{14}, G^{15}, K^{25}, Q^{26} and N^{27} (Guan *et al.*, 2012). Scarselli *et al.*, (2002) reported that the interaction capacity of secreted deleted HVR1 $E2_{661}$ decreased only by approximately 30% compared to native $E2_{661,}$ which means existence of binding to surface factors other than SR-B1. Our data proved that the most increased srE2^{195}-Fc interaction on HepG2 cells are in areas free of SR-B1 with few merged sites detected which suggests at least some involvement of the remaining 168 residues located down-stream of HVR1 in binding to alternative factors other than SR-B1.

Among the identified 4 main receptors for HCV, srE2^{195}-Fc fusion concentrate merged with occludin on the surface of PFA fixed single HepG2 cells.

Incubating live HepG2 in 5% CO_2 at 37°C for 30 minutes followed with addition of srE2^{195}-Fc before or after PFA fixation resulted in spanning of OCLN over cell surface in association with srE2^{195}-Fc and led to formation of invaginations at inner side of plasma membrane and generated budding toward the cytoplasm of cells. In addition, the vast majority of srE2^{195}-Fc bind areas (small spots) on cell surface not occupied with occludin receptors (large spots) and are densely involved in decoration of detected invaginations. This is an indication that occludin has an impact on spanning of suggested alternative factors for srE2^{195}-Fc.

Brazzoli *et al.*, (2008) and Liu *et al.*, (2009) showed that treating Huh7.5 with JFH1 strain containing flag inserted at E2 HVR1, followed with pull down of flag-tagged proteins leads to E2-OCLN co-precipitation. The same report showed that E2-OCLN complex might be generated during the entry process or from cytosolic E2-OCLD complex and did not seem to indicate direct E2-OCLN interaction. A further report demonstrated an intracellular association between E2 (not core or NS3) and OCLN for virus replicon by immunofluorescence imaging and pull-down (Benedicto *et al.*, 2008). Despite different experimental methodology, our data showed absolute srE2^{195}-Fc/OCLN merge on plasma membranes which might indeed support a real E2-OCLN interaction. It is reported that OCLN is a post-binding late entry receptor which plays a part in the fusion process of HCV E1-E2. Knockdown of OCLN on Huh7 showed no difference in the expression rate and distribution of CD81, SR-B1 and CLDN-1 and clathrin mediated endocytosis of VSV (it caused reduction of HCVpp) compared with wild type Huh7 (Benedicto *et al.*, 2008; Benedicto *et al.*, 2009). This is an indication of no direct affect of OCLN on HCV main receptors and no effect on early stage of virion entry. Further reported data showed that recombinants GT1a $E2_{384\text{-}715}$ (which correspond to our E2^{332}) or $E1E2_{193\text{-}746}$ protein bind to Huh7 and complex with CD81 followed with lateral migration from apical surface to cell-cell contact region, which aggregate with CLDN-1, ZO-1 and OCLN. A remarkable decrease in co-localisation with TJs at head-head cell contact occurred when CD81 was

silenced (Brazzoli *et al.*, 2008). According to this order of events for HCV binding and entry, our data together demonstrate that the exposed binding site for srE2^{195}-Fc due to stimulation of OCLN probably is not CD81, SR-B1, CLDN-1. Occludin is part of TJs complexes which include CLDN-1 and ZO-1. So it might be logical to argue that engaged OCLN recruit ZO-1 which represents an alternative factor for srE2^{195}-Fc fusion. Current published data shows that silencing ZO-1 and JAMA on Huh7 had no inhibitory effect on HCVpp entry (Benedicto *et al.*, 2009), which implies no obvious involvement of ZO-1 in virus entry and provides no evidence for a srE2^{195}-Fc/ ZO-1 interaction.

Our data mainly achieved by the addition of specific antibodies which interfere with binding of HCV receptors, demonstrated a very complicated dynamic process and additionally suggested a novel unknown pathway. We explored the target epitope with antibodies and correlated it with available data related to function of targeted epitopes.

Anti-CLDN1 Mab (A-9) target epitopes located at the C-treminus of CLDN-1 between amino acids 168-207. The C-terminal domain of Claudin-1 has been reported to complex with other TJs proteins such as occludin, ZO-1 and JAM (Harris *et al.*, 2008; Heiskala *et al.*, 2001). So possibly binding of anti-CLDN1 to a target receptor may mediate disrupting/spanning of TJ protein complexes which have the capacity to bind srE2^{195}-Fc fusion and lead to clustering which can mediate entry of srE2^{195}-Fc via an alternative factor. Our Anti-OCLN (Y-12) targets OCLN of mouse origin, epitope mapped within an extracellular loop. Ploss *et al.*, (2009) reported that human OCLN shared 91% alignment identity with OCLN of mouse origin. In addition, the same author proved that expression of fused human or mouse OCLN ECL1 with human ECL2 (not mouse) on human 786-O cell has efficient infectivity for HCV. Extracellular loops of OCLN are reported to induce cell-cell interaction and ECL 2 has been reported to be responsible for aggregation with other TJs such as claudin-1 and JAM (Heiskala *et al.*, 2001; Nusrat *et al.*, 2005). Thus demonstrating extracellular loops of OCLN in particular ECL2 loop as critical for receptor

activity. Further data showed that the C-terminal domain is the most critical part of OCLN as introducing CLDN-1/OCLN partner fusion containing ECL1 and ECL2 of CLDN-1 linked with C- terminus of OCLN confered susceptibility for HCVpp infection into 293T. Substitution of CLDN-1 with both ECLs of OCLD and tail of CLDN-1 sustained 293T resistance for HCVpp infection (Liu *et al.*, 2009b). Combining these published data with our targeting of occludin, we might speculate that targeting ECLs of occludin with antibody results in signal transduction in the C-terminal domain and enhanced activation of other TJs components lead to recruitment of other related TJs or other domains with shared actions leading to offering of binding site for srE2^{195}-Fc. The target epitope of the monoclonal anti-CD81 (5A6) is not accurately known, but it was initially raised against human CD81 on B cell OCI-LY8 and has anti-proliferative effect on cells by an undefined mechanism (Oren *et al.*, 1990). Our previous data showed efficient recognition of rCD81 LEL that fused with MBP and an inhibitory effect on the interaction of srE2^{332}-Fc on 293T cells. This means that the anti-CD81 (5A6) targets LEL of CD81 and the exact specific epitope on LEL is not known yet. We might speculate that stimulated CD81 results in association with claudin-1 which in turn enhances binding/entry of srE2^{195}-Fc' alternative binding sites through association with TJ proteins. So, we think that the alternative receptor is probably of TJ origin, if not probably a factor affected by function of TJs complexes.

HSPG mediates indirect interaction of virion to cell surface through binding with ApoE and does not play a direct role in virus entry (Jiang *et al.*, 2012; Shi *et al.*, 2013). The pattern of srE2^{195}-Fc binding to fixed cells and internalisation of fusion peptide into Huh7.0 cells pre-treated with anti-CD81 or anti-CLDN-1 indicate that alternative factors are unlikely to be HSPG. Lupberger *et al.*, (2011) reported that EGFR is a post binding entry factor for HCV and works through promoting CD81/claudin-1 partnership. Diao *et al.*, (2012) showed that binding of HCVcc to CD81 on Huh7.5 (not CLDN-1) leads to EGFR activation before the clathrin mediate endocytosis step. The same author reported that adding Anti-CD81 (AP33 or JS-81), which blocks binding of E2 to CD81 on

cells, resulted in no activation of EGF. Treating Huh7.5 with TGF-alpha showed absolute co-localisation between EGF and CD81. All this indicates that our detected alternative factor is unlikely to be EGF. 293T cells are fibroblasts and not main sites for lipid interaction or uptake mechanism as hepatocytes. Thus, the enhancement of srE2^{195}-Fc binding to 293T cells might indicate that alternative factor is not lipid receptor.

We have shown increased srE2^{195}-Fc binding capacity, measured by flow cytometer, abundant imaged interaction to areas on cell surface of hepatocytes which did not merge with putative HCV receptors and cytoplasmic colocalisation of formed vacuoles decorated with srE2^{195}-Fc achieved by pre-targeting receptors with specific antibodies which suggest an unknown alternative factor recruited to the cell surface which possibly aids entry of virus. These data provide further insight to understand virus entry, encourage further investigation to identity this factor and to map the first N-terminus 195 residues of E2 sequence (corresponding to native peptide E2$_{384\text{-}578}$).

4.8.2 Enhancing binding capacity of srE2-Fc variants to cells already binding srE2^{195}-Fc

Although srE2^{332}-Fc efficiently interacts with 293T and hepatoma cells, our data demonstrate that pre-treatment of cells with srE2^{195}-Fc was associated with enhancment of srE2^{332}-Fc interaction by approximately 3 fold compared to that measured on cells which had not been treated with srE2^{195}-Fc. The result by detection of florescence intensity of anti-human FITC conjugate that binds Fc domain fused with srE2 forms is similar to the result measured by Zenon-labelled Fab fragment that bound only Fc tag fused with the srE2^{332} peptide. This indicates that the enhancement of binding capacity on cells is specifically for srE2^{332}-Fc and not for srE2^{195}-Fc. Assays revealed that adding 0.1 µg/ml of srE2^{332}-Fc to HepG2 pre-treated with srE2^{195}-Fc was improved 7660 fold compared to native binding to HepG2 in the absence of srE2^{195}-Fc addition. Overall higher binding capacity of srE2^{332}-Fc was measured on pre-treated HepG2 compared with 293T, Huh7.0 and CD81-HepG2. All experiments

demonstrated higher binding capacity of other forms (srE2^{295}-Fc, srE2^{278}-Fc and srE2^{265}-Fc) to cells bound srE2^{195}-Fc. On CD81 expressing cells (293T, Huh7.0 and CD81-HepG2), srE2^{332}-Fc was the best fusion product in gaining more binding capacity to pre-treated cells followed with closely related srE2^{295}-Fc and srE2^{278}-Fc and then srE2^{265}-Fc. On pre-treated HepG2, srE2^{332}-Fc fusion remained the best product in achieving increased binding capacity followed by srE2^{278}-Fc and then closely related srE2^{295}-Fc and srE2^{265}-Fc. Generally, this confirms that enhanced binding is related to residues located beyond residue L^{196} and fusion product with residues L^{196}-K^{332} seem to have the optimum folded structure to achieve such enhanced binding compared to other E2 variants. Interestingly, imaging analysis showed that HepG2 pre-treated with srE2^{195}-Fc followed by incubation with srE2^{332}-Fc bound to anti-Fc FITC or bound to Zenon Alexa Fluor 647 labelled Fab Fragment resulted in entry of srE2^{332}-Fc into the cytoplasmic compartment.

It is difficult to dissect the mechanism behind this promoted binding of srE2-Fc variants which strictly occurs when srE2^{195}-Fc interacts with the cell surface. The current literature is in agreement that cellular entry of HCV is receptor dependent (specifically CD81 and claudin-1) and requires clathrin mediated endocytosis. However, HepG2 cells express exceedingly low CD81 but our data showed non-efficient entry of srE2^{332}-Fc after an extensive period of incubation (at least 6 hours) and we have already shown that ectopic CD81 expression on HepG2 leads to srE2^{332}-Fc fusion uptaken within 30 minutes of incubation. Here, we demonstrate that restricted binding of srE2^{195}-Fc to HepG2 not only enhanced binding of srE2^{332}-Fc to the cell surface but also mediate its internalisation into cytoplasm of HepG2.

Matsuda *et al.*, (2014) reported that infectivity of trans-complemented HCV particles (HCVtcp), which were derived from HCV GT2a and mimic features of HCVcc, is markedly decreased in Huh7.0 and CD81-HepG2 harbouring silenced clathrin heavy chain or dynamine 2 and no inhibitory effect is detected in Huh7.5.1 and Hep3B/miR122 cell line. In both Huh7.0 and Huh7.5.1, knockdown of caveolin has no effect on HCVtcp infectivity indicating that

caveolin-mediate endocytosis is not an entry pathway for HCV. So the author believes that there is an alternative pH-dependent endocytosis pathway which is independent of clathrin or dynamin2. We previously showed that efficient entry of srE2^{332}-Fc into CD81-HepG2 is via clathrin-mediated endocytosis. In addition, we showed binding of srE2^{332}-Fc to HepG2 surface recruited clathrin with observed vesicle adherence to the inner side of the plasma membrane decorated with both clathrin and fusion protein. So, we think that the srE2^{332}-Fc fusion entry into pre-treated HepG2 with srE2^{195}-Fc are probably dependent on the presence of clathrin and further investigations are necessary to ensure if srE2^{195}-Fc bound HepG2 cells uptake srE2^{332}-Fc via clathrin-mediated endocytosis or not. It is difficult to understand the events associated with srE2^{332}-Fc after the interaction of srE2^{195}-Fc with the cell surface. Nevertheless, it seems that the order of events after initial binding of certain residues present in srE2^{195}-Fc to an unknown factor on HepG2 cell surface has a role in accelerating the rate of full length E2 interaction and entry which strictly relies on known HCV receptors and clathrin pathway.

In summary, our data provides clues for understanding novel aspects of the molecular mechanisms of HCV E2^{195} binding to unidentified cell surface receptors, binding to E2 domain from residues at L^{196} toward K^{332}. We believe this is the first data in E2 only with the absence of E1 or hybrids which identify possible alternative factors and activation mechanisms for viral binding and cell entry.

Chapter 5 Summary and future directions

5.1 Summary

Surface interaction and entry of virus into hepatocytes is the first step of the HCV life cycle and infection. Despite the published works which enlightened our understanding of virus attachment and entry leading us to believe it to be compulsorily dependent on presence of both viral E1 and E2 glycoproteins; our data show that srE2^{332}-Fc fusion is sufficient for binding and efficient entry into the cytoplasm of hepatoma cells via clathrin-mediated endocytosis with no need for E1 involvement in these process. Resonant with the unique internalisation tropism of HCV in cell cultures and E2-pseudotyped virus-like particles, target cells differ remarkably in their permissiveness for srE2^{332}-Fc entry. Huh7.0 cells support entry whereas HepG2 cells and 293T cells failed to inetranlise srE2^{332}-Fc fusion. The HCV-permissive Huh 7.0 cell line, which expresses copious amounts of CD81, CLDN-1 and OCLN, allows fast binding and rapid srE2^{332}-Fc entry into clathrin-enriched regions of the cytoplasm. By contrast, HepG2 cells support binding of srE2^{332}-Fc and express abundant CLDN-1, SR-B1 and OCLN, but express exceedingly few CD81 molecules. Distinctively, HepG2 cells do not have efficient susceptibility for srE2^{332}-Fc internalisation. Notably, the srE2^{332}-Fc internalisation phenotype can be markedly improved in HepG2 cells transfected with CD81; suggesting that while other cell surface markers are sufficient for E2 binding these markers are unable to support rapid E2 internalisation in the absence of CD81. Although 293T cells express abundant CD81 and are competent for srE2^{332}-Fc interaction; they do not permit efficient entry of E2 which might be as a result of low levels of the important factors essential for rapid E2 entry. Another important finding from our study is that E2^{332}-immunoadhesin to the 293T cell surface is associated with rapid coalescence into large CD81 and CLDN1-associated aggregates compared with longer time required for srE2^{265}-Fc (shortest form to interact with CD81) to form similar localisation and capping

formation over 293T cell surface. In comparison to the binding capacity of srE2^{295}-Fc, srE2^{278}-Fc and srE2^{265}-Fc, srE2^{332}-Fc is the ideal form to support higher affinity interaction to native CD81 and recombinant MBP-CD81 LEL. This stresses the importance of the presence of full N-terminal domains for highly efficient binding and localisation of virus on cell surface.

The novel finding of this project is the indication of the presence of an alternative factor which enhances binding of HCV when known HCV receptors (CD81, SR-B1, CLDN-1 and OCLN) were first blocked with antibodies prior to addition of E2 immunoadhesins. Comparison of native residual binding of srE2^{195}-Fc to 293T, Huh7.0 and HepG2 cell lines proved that the alternative factors target area of envelope E2 is within the first N-terminus 195 residues of E2 sequence (correspond to native peptide E2$_{384-578}$). Interestingly, native binding of E2^{195}-Fc boosted the binding of srE2^{332}-Fc and other variants to the cell surface. It is difficult to understand the exact mechanism behind this result from our experimental tools and further investigation is required. Nevertheless, our data added evidence in how E2^{195} binding site could be a critical factor to the molecular mechanism of HCV binding and entry.

5.2 Future directions

It is clear that our panel of E2^{332}-derived immunoadhesin and its variants provide a valuable set of tools to further dissect the HCV E2-dependent entry mechanism at molecular level and serve the concept of selecting envelope E2 as potential target for therapeutic strategies.

1- Besides the known HCV receptors, distinctive binding of srE2 variants (332a.a, 295a.a, 278a.a, 265a.a) to Huh7.0 and HepG2 cell lines indicate the presence of other host surface factors. The binding of srE2^{195} immunoadhesin to native hepatoma cell lines could be used with proteomic analysis of E2-associated complexes to identify the factors

which may play a role at any step: binding, localisation and entry of HCV.

2- Mapping epitopes of HCV E2 that are required for neutralizing binding and entry of virus.

3- Robust entry of srE2^{332}-Fc into hepatocyte might be used as carrier vehicles for hepatocyte targeted drug and gene therapy.

4- Pre-incubation of target hepatoma cells with srE2^{195}-Fc may be used to study the enhancement of peptides drugs interaction with cell surface or even improve their entry into cytoplasmic compartment of target cells.

LIST OF REFERENCES

Abban, C. Y., Bradbury, N. A. & Meneses, P. I. (2008). HPV16 and BPV1 infection can be blocked by the dynamin inhibitor dynasore. *American Journal of Therapeutics* **15**, 304-311.

Acton, S. L., Scherer, P. E., Lodish, H. F. & Krieger, M. (1994). Expression cloning of SR-BI, a CD36-related class B scavenger receptor. *Journal Biological Chemistry* **269**, 21003-21009.

Acton, S., Rigotti, A., Landschulz, K. T., Xu, S., Hobbs, H. H. & Krieger, M. (1996). Identification of scavenger receptor SR-BI as a high density lipoprotein receptor. *Science* **271**, 518-520.

Adamson, A. L., Chohan, K., Swenson, J. & LaJeunesse, D. (2011). A Drosophila model for genetic analysis of influenza viral/host interactions. *Genetics* **189**, 495-506.

Ahmed, A. & Felmlee, D. J. (2015). Mechanisms of Hepatitis C Viral Resistance to Direct Acting Antivirals. *Viruses-Basel* **7**, 6716-6729.

Akbar, S. M. F., Horiike, N., Onji, M. & Hino, O. (2001). Dendritic cells and chronic hepatitis virus carriers. *Intervirology* **44**, 199-208.

Allander, T., Forns, X., Emerson, S. U., Purcell, R. H. & Bukh, J. (2000). Hepatitis C virus envelope protein E2 binds to CD81 of tamarins. *Virology* **277**, 358-367.

Alter, H. J. & Seeff, L. B. (2000). Recovery, persistence, and sequelae in hepatitis C virus infection: A perspective on long-term outcome. *Seminars in Liver Disease* **20**, 17-35.

Alter, H. J., Holland, P. V. & Purcell, R. H. (1975). The emerging pattern of post-transfusion hepatitis. *Am J Med Sci* **270**, 329-334.

Alter, H. J., Purcell, R. H., Shih, J. W., Melpolder, J. C., Houghton, M., Choo, Q. L. & Kuo, G. (1989). Detection of antibody to hepatitis-c virus in

prospectively followed transfusion recipients with acute and chronic non-a-hepatitis, non-b-hepatitis. *New England Journal of Medicine* **321**, 1494-1500.

Alter, H. J., Sanchezpescador, R., Urdea, M. S., Wilber, J. C., Lagier, R. J., Dibisceglie, A. M., Shih, J. W. & Neuwald, P. D. (1995). Evaluation of branched dna signal amplification for the detection of hepatitis-c virus-RNA. *Journal of Viral Hepatitis* **2**, 121-132.

Alter, M. J. (2007). Epidemiology of hepatitis C virus infection. *World J Gastroenterol* **13**, 2436-2441.

Altmann, S. W., Davis, H. R., Zhu, L. J. & other authors (2004). Niemann-Pick C1 like 1 protein is critical for intestinal cholesterol absorption. *Science* **303**, 1201-1204.

Andre, P., Komurian-Pradel, F., Deforges, S. & other authors (2002). Characterization of low- and very-low-density hepatitis C virus RNA-containing particles. *Journal of Virology* **76**, 6919-6928.

Andre, P., Perlemuter, G., Budkowska, A., Brechot, C. & Lotteau, V. (2005). Hepatitis C virus particles and lipoprotein metabolism. *Seminars in Liver Disease* **25**, 93-104.

Angelichio, M. L., Beck, J. A., Johansen, H. & Iveyhoyle, M. (1991). Comparison of several promoters and polyadenylation signals for use in heterologous gene-expression in cultured drosophila cells. *Nucleic Acids Research* **19**, 5037-5043.

Banchereau, J., Briere, F., Caux, C., Davoust, J., Lebecque, S., Liu, Y. T., Pulendran, B. & Palucka, K. (2000). Immunobiology of dendritic cells. *Annual Review of Immunology* **18**, 767-+.

Bartenschlager, R. (2002). Hepatitis C virus replicons: potential role for drug development. *Nature Reviews Drug Discovery* **1**, 911-916.

Barth, H., Schafer, C., Adah, M. I. & other authors (2003). Cellular binding of hepatitis C virus envelope glycoprotein E2 requires cell surface heparan sulfate. *Journal of Biological Chemistry* **278**, 41003-41012.

Bartosch, B. & Cosset, F. L. (2006). Cell entry of hepatitis C virus. *Virology* **348**, 1-12.

Bartosch, B. & Cosset, F. L. (2009). Studying HCV cell entry with HCV pseudoparticles (HCVpp). *Methods in Molecular Biology* **510**, 279-293.

Bartosch, B., Bukh, J., Meunier, J. C., Granier, C., Engle, R. E., Blackwelder, W. C., Emerson, S. U., Cosset, F. L. & Purcell, R. H. (2003a). In vitro assay for neutralizing antibody to hepatitis C virus: Evidence for broadly conserved neutralization epitopes. *Proceedings of the National Academy of Sciences of the United States of America* **100**, 14199-14204.

Bartosch, B., Dubuisson, J. & Cosset, F. L. (2003b). Infectious hepatitis C virus pseudo-particles containing functional E1-E2 envelope protein complexes. *Journal of Experimental Medicine* **197**, 633-642.

Bartosch, B., Verney, G., Dreux, M., Donot, P., Morice, Y., Penin, F., Pawlotsky, J. M., Lavillette, D. & Cosset, F. L. (2005). An interplay between hypervariable region 1 of the Hepatitis C Virus E2 glycoprotein, the scavenger receptor BI, and high-density lipoprotein promotes both enhancement of infection and protection against neutralizing antibodies. *Journal of Virology* **79**, 8217-8229.

Baumert, T. F., Ito, S., Wong, D. T. & Liang, T. J. (1998). Hepatitis C virus structural proteins assemble into viruslike particles in insect cells. *Journal of Virology* **72**, 3827-3836.

Benedicto, I., Molina-Jimenez, F., Barreiro, O., Madonado-Rodriguez, A., Prieto, J., Moreno-Otero, R., Aldabe, R., Lopez-Cabrera, M. & Majano, P. L. (2008). Hepatitis C virus envelope components alter localization of hepatocyte tight junction-associated proteins and promote occludin retention in the endoplasmic reticulum. *Hepatology* **48**, 1044-1053.

Benedicto, I., Molina-Jimenez, F., Bartosch, B. & other authors (2009). The tight junction-associated protein occludin is required for a postbinding step in hepatitis C virus entry and infection. *Journal of Virology* **83**, 8012-8020.

Blanchard, E., Belouzard, S., Goueslain, L., Wakita, T., Dubuisson, J., Wychowski, C. & Rouille, Y. (2006). Hepatitis C virus entry depends on clathrin-mediated endocytosis. *Journal of Virology* **80**, 6964-6972.

Bornhorst, J. A. & Falke, J. J. (2000). Purification of proteins using polyhistidine affinity tags. *Applications of Chimeric Genes and Hybrid Proteins, Part A*. **326**, 245-254.

Bowen, D. G. & Walker, C. M. (2005). Adaptive immune responses in acute and chronic hepatitis C virus infection. *Nature* **436**, 946-952.

Bradley, D. W., Maynard, J. E., Popper, H., Cook, E. H., Ebert, J. W., McCaustland, K. A., Schable, C. A. & Fields, H. A. (1983). Posttransfusion non-A, non-B hepatitis: physicochemical properties of two distinct agents. *Journal of Infectious Diseases* **148**, 254-265.

Bradley, D. W., McCaustland, K. A., Cook, E. H., Schable, C. A., Ebert, J. W. & Maynard, J. E. (1985). Posttransfusion non-A, non-B hepatitis in chimpanzees - physicochemical evidence that the tubule-forming agent is a small, enveloped virus. *Gastroenterology* **88**, 773-779.

Brazzoli, M., Bianchi, A., Filippini, S., Weiner, A., Zhu, Q., Pizza, M. & Crotta, S. (2008). CD81 is a central regulator of cellular events required for hepatitis C virus infection of human hepatocytes. *Journal of Virology* **82**, 8316-8329.

Breiner, K. M., Schaller, H. & Knolle, P. A. (2001). Endothelial cell-mediated uptake of a hepatitis B virus: A new concept of liver targeting of hepatotropic microorganisms. *Hepatology* **34**, 803-808.

Brennan, T. & Shrank, W. (2014). New Expensive Treatments for Hepatitis C Infection. *Jama-Journal of the American Medical Association* **312**, 593-594.

Bressanelli, S., Stiasny, K., Allison, S. L., Stura, E. A., Duquerroy, S., Lescar, J., Heinz, F. X. & Rey, F. A. (2004). Structure of a flavivirus envelope glycoprotein in its low-pH-induced membrane fusion conformation. *Embo Journal* **23**, 728-738.

Brighty, D. W. & Rosenberg, M. (1994). A cis-acting repressive sequence that overlaps the Rev-responsive element of human immunodeficiency virus type 1 regulates nuclear retention of env mRNAs independently of known splice signals. *Proceedings of the National Academy of Sciences of the United States of America* **91**, 8314-8318.

Brighty, D. W., Rosenberg, M., Chen, I. S. & Ivey-Hoyle, M. (1991). Envelope proteins from clinical isolates of human immunodeficiency virus type 1 that are refractory to neutralization by soluble CD4 possess high affinity for the CD4 receptor. *Proceedings of the National Academy of Sciences of the United States of America* **88**, 7802-7805.

Brown, R. S. (2005). Hepatitis C and liver transplantation. *Nature* **436**, 973-978.

Bunch, T. A., Grinblat, Y. & Goldstein, L. S. B. (1988). Characterization and use of the drosophila metallothionein promoter in cultured *Drosophila-melanogaster* cells. *Nucleic Acids Research* **16**, 1043-1061.

Cai, Z. H., Zhang, C., Chang, K. S., Jiang, J. Y., Ahn, B. C., Wakita, T., Liang, T. J. & Luo, G. X. (2005). Robust production of infectious hepatitis C virus (HCV) from stably HCV cDNA-transfected human hepatoma cells. *Journal of Virology* **79**, 13963-13973.

Castelli, M., Clementi, N., Sautto, G. A. & other authors (2014). HCV E2 core structures and mAbs: something is still missing. *Drug Discovery Today* **19**, 1964-1970.

Catanese, M. T., Uryu, K., Kopp, M., Edwards, T. J., Andrus, L., Rice, W. J., Silvestry, M., Kuhn, R. J. & Rice, C. M. (2013). Ultrastructural analysis of hepatitis C virus particles. *Proceedings of the National Academy of Sciences of the United States of America* **110**, 9505-9510.

Centers for Disease Control and Prevention. (1998). Recommendations for prevention and control of hepatitis C virus (HCV) infection and HCV-related chronic disease. *MMWR Recommendations and Reports* **47**, 1-39.

Chandran, K., Sullivan, N. J., Felbor, U., Whelan, S. P. & Cunningham, J. M. (2005). Endosomal proteolysis of the Ebola virus glycoprotein is necessary for infection. *Science* **308**, 1643-1645.

Chang, K. S., Jiang, J. Y., Cai, Z. H. & Luo, G. X. (2007). Human apolipoprotein E is required for infectivity and production of hepatitis C virus in cell culture. *Journal of Virology* **81**, 13783-13793.

Charrin, S., Manie, S., Thiele, C., Billard, M., Gerlier, D., Boucheix, C. & Rubinstein, E. (2003). A physical and functional link between cholesterol and tetraspanins. *European Journal of Immunology* **33**, 2479-2489.

Chen, S. L. & Morgan, T. R. (2006). The natural history of hepatitis C virus (HCV) infection. *International Journal of Medical Sciences* **3**, 47-52.

Chevaliez, S. & Pawlotsky, L. M. (2007). Hepatitis C virus: Virology, diagnosis and management of antiviral therapy. *World Journal of Gastroenterology* **13**, 2461-2466.

Choo, Q. L., Kuo, G., Weiner, A. J., Overby, L. R., Bradley, D. W. & Houghton, M. (1989). Isolation of a cDNA clone derived from a blood-borne non-A, non-B viral hepatitis genome. *Science* **244**, 359-362.

Choo, Q. L., Richman, K. H., Han, J. H. & other authors (1991). Genetic organization and diversity of the hepatitis-c virus. *Proceedings of the National Academy of Sciences of the United States of America* **88**, 2451-2455.

Choukhi, A., Pillez, A., Drobecq, H., Sergheraert, C., Wychowski, C. & Dubuisson, J. (1999). Characterization of aggregates of hepatitis C virus glycoproteins. *Journal of General Virology* **80**, 3099-3107.

Choukhi, A., Ung, S., Wychowski, C. & Dubuisson, J. (1998). Involvement of endoplasmic reticulum chaperones in the folding of hepatitis C virus glycoproteins. *Journal of Virology* **72**, 3851-3858.

Chung, R. T. (2005). Acute hepatitis C virus infection. *Clinical Infectious Diseases* **41**, S14-S17.

Ciczora, Y., Callens, N., Penin, F., Pecheur, E. I. & Dubuisson, J. (2007). Transmembrane domains of hepatitis C virus envelope glycoproteins: Residues involved in E1E2 heterodimerization and involvement of these domains in virus entry. *Journal of Virology* **81**, 2372-2381.

Clarke, B. (1997). Molecular virology of hepatitis C virus. *Journal of General Virology* **78**, 2397-2410.

Cocquerel, L., Kuo, C. C., Dubuisson, J. & Levy, S. (2003). CD81-dependent binding of hepatitis C virus E1E2 heterodimers. *Journal of Virology* **77**, 10677-10683.

Cocquerel, L., Meunier, J. C., Pillez, A., Wychowski, C. & Dubuisson, J. (1998). A retention signal necessary and sufficient for endoplasmic reticulum localization maps to the transmembrane domain of hepatitis C virus glycoprotein E2. *Journal of Virology* **72**, 2183-2191.

Cocquerel, L., Voisset, C. & Dubuisson, J. (2006). Hepatitis C virus entry: potential receptors and their biological functions. *Journal of General Virology* **87**, 1075-1084.

Cocquerel, L., Wychowski, C., Minner, F., Penin, F. & Dubuisson, J. (2000). Charged residues in the transmembrane domains of hepatitis C virus glycoproteins play a major role in the processing, subcellular localization, and assembly of these envelope proteins. *Journal of Virology* **74**, 3623-3633.

Coller, K. E., Berger, K. L., Heaton, N. S., Cooper, J. D., Yoon, R. & Randall, G. (2009). RNA Interference and Single Particle Tracking Analysis of Hepatitis C Virus Endocytosis. *Plos Pathogens* **5**,e1000702

Cormier, E. G., Durso, R. J., Tsamis, F., Boussemart, L., Manix, C., Olson, W. C., Gardner, J. P. & Dragic, T. (2004a). L-SIGN (CD209L) and DC-SIGN (CD209) mediate transinfection of liver cells by hepatitis C virus. *Proceedings of the National Academy of Sciences of the United States of America* **101**, 14067-14072.

Cormier, E. G., Tsamis, F., Kajumo, F., Durso, R. J., Gardner, J. P. &

Dragic, T. (2004b). CD81 is an entry coreceptor for hepatitis C virus. *Proceedings of the National Academy of Sciences of the United States of America* **101**, 7270-7274.

Coyne, C. B. & Bergelson, J. M. (2006). Virus-induced Abl and Fyn kinase signals permit Coxsackievirus entry through epithelial tight junctions. *Cell* **124**, 119-131.

Coyne, C. B., Le, S., Turner, J. R. & Bergelson, J. M. (2007). Coxsackievirus entry across epithelial tight junctions requires occludin and the small GTPases Rab34 and Rab5. *Cell Host & Microbe* **2**, 181-192.

Cukierman, L., Meertens, L., Bertaux, C., Kajumo, F. & Dragic, T. (2009). Residues in a highly conserved claudin-1 motif are required for hepatitis C virus entry and mediate the formation of cell-cell contacts. *Journal of Virology* **83**, 5477-5484.

Cun, W., Jiang, J. Y. & Luo, G. X. (2010). The C-terminal alpha-helix domain of apolipoprotein E is required for interaction with nonstructural protein 5A and Assembly of hepatitis C virus. *Journal of Virology* **84**, 11532-11541.

Czajkowsky, D. M., Hu, J., Shao, Z. & Pleass, R. J. (2012). Fc-fusion proteins: new developments and future perspectives. *Embo Molecular Medicine* **4**, 1015-1028.

Da Costa, D., Turek, M., Felmlee, D. J., Girardi, E., Pfeffer, S., Long, G., Bartenschlager, R., Zeisel, M. B. & Baumert, T. F. (2012). Reconstitution of the Entire Hepatitis C Virus Life Cycle in Nonhepatic Cells. *Journal of Virology* **86**, 11919-11925.

Dammacco, F. & Sansonno, D. (1992). Antibodies to hepatitis-C virus in essential mixed cryoglobulinemia. *Clinical and Experimental Immunology* **87**, 352-356.

Dash, S., Halim, A. B., Tsuji, H., Hiramatsu, N. & Gerber, M. A. (1997). Transfection of HepG2 cells with infectious hepatitis C virus genome. *American Journal of Pathology* **151**, 363-373.

De Beeck, A. O., Voisset, C., Bartosch, B., Ciczora, Y., Cocquerel, L., Keck, Z., Foung, S., Cosset, F. L. & Dubuisson, J. (2004). Characterization of functional hepatitis C virus envelope glycoproteins. *Journal of Virology* **78**, 2994-3002.

Deleersnyder, V., Pillez, A., Wychowski, C., Blight, K., Xu, J., Hahn, Y. S., Rice, C. M. & Dubuisson, J. (1997). Formation of native hepatitis C virus glycoprotein complexes. *Journal of Virology* **71**, 697-704.

Delos, S. E., Gilbert, J. M. & White, J. M. (2000). The central proline of an internal viral fusion peptide serves two important roles. *Journal of Virology* **74**, 1686-1693.

Deng, L., Ma, L., Virata-Theimer, M. L. & other authors (2014). Discrete conformations of epitope II on the hepatitis C virus E2 protein for antibody-mediated neutralization and nonneutralization. *Proceedings of the National Academy of Sciences of the United States of America* **111**, 10690-10695.

Deol, H. K., Varghese, R., Wagner, G. F. & DiMattia, G. E. (2000). Dynamic regulation of mouse ovarian stanniocalcin expression during gestation and lactation. *Endocrinology* **141**, 3412-3421.

Diao, J. Y., Pantua, H., Ngu, H., Komuves, L., Diehl, L., Schaefer, G. & Kapadia, S. B. (2012). Hepatitis c virus induces epidermal growth factor receptor activation via CD81 binding for viral internalization and entry. *Journal of Virology* **86**, 10935-10949.

Ding, Q., von Schaewen, M. & Ploss, A. (2014). The Impact of Hepatitis C Virus Entry on Viral Tropism. *Cell Host & Microbe* **16**, 562-568.

Dixit, N. M., Layden-Almer, J. E., Layden, T. J. & Perelson, A. S. (2004). Modelling how ribavirin improves interferon response rates in hepatitis C virus infection. *Nature* **432**, 922-924.

Dreux, M., Pietschmann, T., Granier, C. & other authors (2006). High density lipoprotein inhibits hepatitis C virus-neutralizing antibodies by stimulating cell entry via activation of the scavenger receptor BI. *Journal of*

Biological Chemistry **281**, 18285-18295.

Drummer, H. E. & Poumbourios, P. (2004). Hepatitis C virus glycoprotein E2 contains a membrane-proximal heptad repeat sequence that is essential for E1E2 glycoprotein heterodimerization and viral entry. *Journal of Biological Chemistry* **279**, 30066-30072.

Drummer, H. E. & Poumbourios, P. (2004). Hepatitis C virus glycoprotein E2 contains a membrane-proximal heptad repeat sequence that is essential for E1E2 glycoprotein heterodimerization and viral entry. *Journal of Biological Chemistry* **279**, 30066-30072.

Drummer, H. E., Boo, I. & Poumbourios, P. (2007). Mutagenesis of a conserved fusion peptide-like motif and membrane-proximal heptad-repeat region of hepatitis C virus glycoprotein E1. *Journal of General Virology* **88**, 1144-1148.

Drummer, H. E., Boo, I., Maerz, A. L. & Poumbourios, P. (2006). A conserved Gly436-Trp-Leu-Ala-Gly-Leu-Phe-Tyr motif in hepatitis C virus glycoprotein E2 is a determinant of CD81 binding and viral entry. *J Virol* **80**, 7844-7853.

Drummer, H. E., Wilson, K. A. & Poumbourios, P. (2002). Identification of the hepatitis C virus E2 glycoprotein binding site on the large extracellular loop of CD81. *Journal of Virology* **76**, 11143-11147.

Dubuisson, J., Helle, F. & Cocquerel, L. (2008). Early steps of the hepatitis C virus life cycle. *Cellular Microbiology* **10**, 821-827.

Dubuisson, J., Hsu, H. H., Cheung, R. C., Greenberg, H. B., Russell, D. G. & Rice, C. M. (1994). Formation and intracellular-localization of hepatitis-c virus envelope glycoprotein complexes expressed by recombinant vaccinia and sindbis viruses. *Journal of Virology* **68**, 6147-6160.

Duvet, S., Cocquerel, L., Pillez, A., Cacan, R., Verbert, A., Moradpour, D., Wychowski, C. & Dubuisson, J. (1998). Hepatitis C virus glycoprotein complex localization in the endoplasmic reticulum involves a determinant for

retention and not retrieval. *Journal of Biological Chemistry* **273**, 32088-32095.

Duvet, S., Op De Beeck, A., Cocquerel, L., Wychowski, C., Cacan, R. & Dubuisson, J. (2002). Glycosylation of the hepatitis C virus envelope protein E1 occurs posttranslationally in a mannosylphosphoryldolichol-deficient CHO mutant cell line. *Glycobiology* **12**, 95-101.

Eksioglu, E. A., Bess, J. R., Zhu, H., Xu, Y., Dong, H. J., Elyar, J., Nelson, D. R. & Liu, C. (2010). Hepatitis C virus modulates human monocyte-derived dendritic cells. *Journal of Viral Hepatitis* **17**, 757-769.

Evans, M. J., von Hahn, T., Tscherne, D. M. & other authors (2007). Claudin-1 is a hepatitis C virus co-receptor required for a late step in entry. *Nature* **446**, 801-805.

Falkowska, E., Kajumo, F., Garcia, E., Reinus, J. & Dragic, T. (2007). Hepatitis C virus envelope glycoprotein E2 glycans modulate entry, CD81 binding, and neutralization. *Journal of Virology* **81**, 8072-8079.

Farci, P., Alter, H. J., Wong, D., Miller, R. H., Shih, J. W., Jett, B. & Purcell, R. H. (1991). A long-term study of hepatitis-c virus-replication in non-A, non-B hepatitis. *New England Journal of Medicine* **325**, 98-104.

Farquhar, M. J. & McKeating, J. A. (2008). Primary hepatocytes as targets for Hepatitis C virus replication. *Journal of Viral Hepatitis* **15**, 849-854.

Farquhar, M. J., Hu, K., Harris, H. J. & other authors (2012). Hepatitis C Virus Induces CD81 and Claudin-1 Endocytosis. *Journal of Virology* **86**, 4305-4316.

Fattovich, G., Stroffolini, T., Zagni, I. & Donato, F. (2004). Hepatocellular carcinoma in cirrhosis: Incidence and risk factors. *Gastroenterology* **127**, S35-S50.

Feinman, C. V., Berris, B., Sinclair, J. C. & Wrobel, D. (1980). Hepatitis non-A, non-B. *Can Med Assoc J* **123**, 181-184.

Feinstone, S. M., Kapikian, A. Z. & Purcell, R. H. (1973). Hepatitis-a -

detection by immune electron-microscopy of a viruslike antigen associated with acute illness. *Science* **182**, 1026-1028.

Feinstone, S. M., Kapikian, A. Z., Purcell, R. H., Alter, H. J. & Holland, P. V. (2001). Transfusion-associated hepatitis not due to viral hepatitis type A or B. 1975. *Reviews in Medical Virology* **11**, 3-8

Feinstone, S. M., Mihalik, K. B., Kamimura, T., Alter, H. J., London, W. T. & Purcell, R. H. (1983). Inactivation of hepatitis-b virus and non-A, non-B hepatitis by chloroform. *Infection and Immunity* **41**, 816-821.

Feld, J. J. & Hoofnagle, J. H. (2005). Mechanism of action of interferon and ribavirin in treatment of hepatitis C. *Nature* **436**, 967-972.

Feneant, L., Levy, S. & Cocquerel, L. (2014). CD81 and Hepatitis C Virus (HCV) Infection. *Viruses-Basel* **6**, 535-572.

Flajnik, M. (1994). Lines of defence. Review of: G. Beck, E. L. Cooper, G. S. Habicht, and J. J. Marchalonis (eds.) 1994. Primordial immunity: Foundations for the vertebrate immune system. Academy of *Science* **265**, 1254-1255.

Flint, M., Dubuisson, J., Maidens, C., Harrop, R., Guile, G. R., Borrow, P. & McKeating, J. A. (2000). Functional characterization of intracellular and secreted forms of a truncated hepatitis C virus E2 glycoprotein. *Journal of Virology* **74**, 702-709.

Flint, M., Maidens, C., Loomis-Price, L. D., Shotton, C., Dubuisson, J., Monk, P., Higginbottom, A., Levy, S. & McKeating, J. A. (1999a). Characterization of hepatitis C virus E2 glycoprotein interaction with a putative cellular receptor, CD81. *Journal of Virology* **73**, 6235-6244.

Flint, M., Thomas, J. M., Maidens, C. M., Shotton, C., Levy, S., Barclay, W. S. & McKeating, J. A. (1999b). Functional analysis of cell surface-expressed hepatitis C virus E2 glycoprotein. *Journal of Virology* **73**, 6782-6790.

Flint, M., von Hahn, T., Zhang, J., Farquhar, M., Jones, C. T., Balfe, P., Rice, C. M. & McKeating, J. A. (2006). Diverse CD81 proteins support hepatitis C virus infection. *Journal of Virology* **80**, 11331-11342.

Forns, X., Allander, T., Rohwer-Nutter, P. & Bukh, J. (2000a). Characterization of modified hepatitis C virus E2 proteins expressed on the cell surface. *Virology* **274**, 75-85.

Forns, X., Emerson, S. U., Tobin, G. J., Mushahwar, I. K., Purcell, R. H. & Bukh, J. (1999). DNA immunization of mice and macaques with plasmids encoding hepatitis C virus envelope E2 protein expressed intracellularly and on the cell surface. *Vaccine* **17**, 1992-2002.

Forns, X., Thimme, R., Govindarajan, S., Emerson, S. U., Purcell, R. H., Chisari, F. V. & Bukh, J. (2000b). Hepatitis C virus lacking the hypervariable region 1 of the second envelope protein is infectious and causes acute resolving or persistent infection in chimpanzees. *Proceedings of the National Academy of Sciences of the United States of America* **97**, 13318-13323.

Fournillier, A., Wychowski, C., Boucreux, D., Baumert, T. F., Meunier, J. C., Jacobs, D., Muguet, S., Depla, E. & Inchauspe, G. (2001). Induction of hepatitis C virus E1 envelope protein-specific immune response can be enhanced by mutation of N-glycosylation sites. *Journal of Virology* **75**, 12088-12097.

Foy, E., Li, K., Sumpter, R. & other authors (2005). Control of antiviral defenses through hepatitis C virus disruption of retinoic acid-inducible gene-I signaling. *Proceedings of the National Academy of Sciences of the United States of America* **102**, 2986-2991.

Foy, E., Li, K., Wang, C. F., Sumpter, R., Ikeda, M., Lemon, S. M. & Gale, M. (2003). Regulation of interferon regulatory factor-3 by the hepatitis C virus serine protease. *Science* **300**, 1145-1148.

Frank, C., Mohamed, M. K., Strickland, G. T. & other authors (2000). The role of parenteral antischistosomal therapy in the spread of hepatitis C virus in Egypt. *Lancet* **355**, 887-891.

Frick, D. N. (2006). HCV Helicase: Structure, Function, and Inhibition. In Hepatitis C Viruses: Genomes and Molecular Biology. Edited by S. L. Tan.

Norfolk (UK): *Horizon Bioscience*, 207-244

Furuse, M. & Tsukita, S. (2006). Claudins in occluding junctions of humans and flies. *Trends in Cell Biology* **16**, 181-188.

Furuse, M., Hata, M., Furuse, K., Yoshida, Y., Haratake, A., Sugitani, Y., Noda, T., Kubo, A. & Tsukita, S. (2002). Claudin-based tight junctions are crucial for the mammalian epidermal barrier: a lesson from claudin-1-deficient mice. *Journal of Cell Biology* **156**, 1099-1111.

Galbraith, R. M., Eddleston, A. L., Portmann, B., Williams, R. & Gower, P. E. (1975). Chronic liver disease developing after outbreak of HBsAG-negative hepatitis in haemodialysis unit. *Lancet* **2**, 886-890.

Gardner, J. P., Durso, R. J., Arrigale, R. R., Donovan, G. P., Maddon, P. J., Dragic, T. & Olson, W. C. (2003). L-SIGN (CD 209L) is a liver-specific capture receptor for hepatitis C virus. *Proceedings of the National Academy of Sciences of the United States of America* **100**, 4498-4503.

Garry, R. F. & Dash, S. (2003). Proteomics computational analyses suggest that hepatitis C virus E1 and pestivirus E2 envelope glycoproteins are truncated class II fusion proteins. *Virology* **307**, 255-265.

Gavel, Y. & Vonheijne, G. (1990). Sequence differences between glycosylated and nonglycosylated asn-x-thr ser acceptor sites-implications for protein engineering. *Protein Engineering* **3**, 433-442.

Geijtenbeek, T. B. H., Kwon, D. S., Torensma, R. & other authors (2000). DC-SIGN, a dendritic cell-specific HIV-1-binding protein that enhances trans-infection of T cells. *Cell* **100**, 587-597.

Gerlach, J. T., Diepolder, H. M., Zachoval, R. & other authors (2003). Acute hepatitis C: High rate of both spontaneous and treatment-induced viral clearance. *Gastroenterology* **125**, 80-88.

Ghany, M. G., Strader, D. B., Thomas, D. L. & Seeff, L. B. (2009). Diagnosis, Management, and Treatment of Hepatitis C: An Update. *Hepatology* **49**, 1335-1374.

Goffard, A., Callens, N., Bartosch, B., Wychowski, C., Cosset, F. L., Montpellier, C. & Dubuisson, J. (2005). Role of N-linked glycans in the functions of hepatitis C virus envelope glycoproteins. *Journal of Virology* **79**, 8400-8409.

Goossens, N. & Hoshida, Y. (2015). Hepatitis C virus-induced hepatocellular carcinoma. *Clinical Molecular Herpetology* **21**, 105-114.

Grove, J., Huby, T., Stamataki, Z. & other authors (2007). Scavenger receptor BI and BII expression levels modulate hepatitis C virus infectivity. *Journal of Virology* **81**, 3162-3169.

Gu, C., Yaddanapudi, S., Weins, A., Osborn, T., Reiser, J., Pollak, M., Hartwig, J. & Sever, S. (2010). Direct dynamin-actin interactions regulate the actin cytoskeleton. *Embo Journal* **29**, 3593-3606.

Guan, M., Wang, W. B., Liu, X. Q. & other authors (2012). Three Different Functional Microdomains in the Hepatitis C Virus Hypervariable Region 1 (HVR1) Mediate Entry and Immune Evasion. *Journal of Biological Chemistry* **287**, 35631-35645.

Guidotti, L. G., Rochford, R., Chung, J., Shapiro, M., Purcell, R. & Chisari, F. V. (1999). Viral clearance without destruction of infected cells during acute HBV infection. *Science* **284**, 825-829.

Gumbiner, B. M. (1993). Breaking through the tight junction barrier. *Journal of Cell Biology* **123**, 1631-1633.

Gupta, E., Bajpai, M. & Choudhary, A. (2014). Hepatitis C virus: Screening, diagnosis, and interpretation of laboratory assays. *Asian Journal of Transfusing Science* **8**, 19-25.

Hagan, H., Snyder, N., Hough, E., Yu, T. J., McKeirnan, S., Boase, J. & Duchin, J. (2002). Case-reporting of acute hepatitis B and C among injection drug users. *Journal of Urban Health-Bulletin of the New York Academy of Medicine* **79**, 579-585.

Halliday, J., Klenerman, P. & Barnes, E. (2011). Vaccination for hepatitis C

virus: closing in on an evasive target. *Expert Review of Vaccines* **10**, 659-672.

Hanafiah, K. M., Groeger, J., Flaxman, A. D. & Wiersma, S. T. (2013). Global epidemiology of hepatitis C virus infection: New estimates of age-specific antibody to HCV seroprevalence. *Hepatology* **57**, 1333-1342.

Harris, H. J., Farquhar, M. J., Mee, C. J. & other authors (2008). CD81 and claudin 1 coreceptor association: Role in hepatitis C virus entry. *Journal of Virology* **82**, 5007-5020.

Hart, P. D. & Young, M. R. (1991). Ammonium-chloride, an inhibitor of phagosome-lysosome fusion in macrophages, concurrently induces phagosome-endosome fusion, and opens a novel pathway - studies of a pathogenic mycobacterium and a nonpathogenic yeast. *Journal of Experimental Medicine* **174**, 881-889.

Hartsock, A. & Nelson, W. J. (2008). Adherens and tight junctions: Structure, function and connections to the actin cytoskeleton. *Biochimica Et Biophysica Acta-Biomembranes* **1778**, 660-669.

He, L. F., Alling, D., Popkin, T., Shapiro, M., Alter, H. J. & Purcell, R. H. (1987). Determining the size of non-A, non-B hepatitis virus by filtration. *Journal of Infectious Diseases* **156**, 636-640.

He, Y., Staschke, K. A. & Tan, S. L. (2006). HCV NS5A: a multifunctional regulator of cellular pathways and virus replication. In hepatitis C viruses: Genomes and molecular biology. Edited by S. L. Tan. Norfolk (UK): *Horizon Bioscience,* 267-292.

Hebert, D. N., Zhang, J. X., Chen, W., Foellmer, B. & Helenius, A. (1997). The number and location of glycans on influenza hemagglutinin determine folding and association with calnexin and calreticulin. *Journal of Cell Biology* **139**, 613-623.

Heinz, F. X., Stiasny, K. & Allison, S. L. (2004). The entry machinery of flaviviruses. *Archives of Virology* **18**,133-137.

Heiskala, M., Peterson, P. A. & Yang, Y. (2001). The roles of claudin

superfamily proteins in paracellular transport. *Traffic* **2**, 92-98.

Higginbottom, A., Quinn, E. R., Kuo, C. C. & other authors (2000). Identification of amino acid residues in CD81 critical for interaction with hepatitis C virus envelope glycoprotein E2. *Journal of Virology* **74**, 3642-3649.

Hijikata, M., Kato, N., Ootsuyama, Y., Nakagawa, M. & Shimotohno, K. (1991). Gene-mapping of the putative structural region of the hepatitis-c virus genome by invitro processing analysis. *Proceedings of the National Academy of Sciences of the United States of America* **88**, 5547-5551.

Hino, K., Fujii, K., Korenaga, M., Murakami, C., Okazaki, M., Okuda, M. & Okita, K. (1997). Correlation between relative number of circulating low-density hepatitis C virus particles and disease activity in patients with chronic hepatitis C. *Digestive Diseases and Sciences* **42**, 2476-2481.

Hinshaw, J. E. (2000). Dynamin and its role in membrane fission. *Annual Review of Cell and Developmental Biology* **16**, 483-519.

Hofmann, W. P., Sarrazin, C. & Zeuzem, S. (2012). Current Standards in the Treatment of Chronic Hepatitis C Reply. *Deutsches Arzteblatt International* **109**, 755-756.

Hollinger, F. B., Gitnick, G. L., Aach, R. D. & other authors (1978). Non-A, non-B hepatitis transmission in chimpanzees: a project of the transfusion-transmitted viruses study group. *Intervirology* **10**, 60-68.

Hoofnagle, J. H. (2002). Course and outcome of hepatitis C. *Hepatology* **36**, S21-S29.

Hoofnagle, J. H., Gerety, R. J., Tabor, E., Feinstone, S. M., Barker, L. F. & Purcell, R. H. (1977). Transmission of non-A, non-B hepatitis. *Annuals of Internal Medicine* **87**, 14-20.

Howell, C., Jeffers, L. & Hoofnagle, J. H. (2000). Hepatitis C in African Americans: Summary of a workshop. *Gastroenterology* **119**, 1385-1396.

Hsu, M., Zhang, J., Flint, M., Logvinoff, C., Cheng-Mayer, C., Rice, C. M. & McKeating, J. A. (2003). Hepatitis C virus glycoproteins mediate pH-dependent cell entry of pseudotyped retroviral particles. *Proceedings of the National Academy of Sciences of the United States of America* **100**, 7271-7276.

Hughes, T. T., Allen, A. L., Bardin, J. E., Christian, M. N., Daimon, K., Dozier, K. D., Hansen, C. L., Holcomb, L. M. & Ahlander, J. (2012). Drosophila as a genetic model for studying pathogenic human viruses. *Virology* **423**, 1-5.

Huijbers, M. M. E. & van Berkel, W. J. H. (2015). High yields of active Thermus thermophilus proline dehydrogenase are obtained using maltose-binding protein as a solubility tag. *Biotechnology Journal* **10**, 395-403.

Huss, M., Ingenhorst, G., Konig, S., Gassel, M., Drose, S., Zeeck, A., Altendorf, K. & Wieczorek, H. (2002). Concanamycin a, the specific inhibitor of V-ATPases, binds to the V-o subunit c. *Journal of Biological Chemistry* **277**, 40544-40548.

Ivey-Hoyle, M., Culp, J. S., Chaikin, M. A., Hellmig, B. D., Matthews, T. J., Sweet, R. W. & Rosenberg, M. (1991). Envelope glycoproteins from biologically diverse isolates of immunodeficiency viruses have widely different affinities for CD4. *Proceedings of the National Academy of Sciences of the United States of America* **88**, 512-516.

Jansson, B., Uhlen, M. & Nygren, P. A. (1998). All individual domains of staphylococcal protein A show Fab binding. *Fems Immunology and Medical Microbiology* **20**, 69-78.

Jarvis, D. L. & Summers, M. D. (1989). Glycosylation and secretion of human-tissue plasminogen-activator in recombinant baculovirus-infected insect cells. *Molecular and Cellular Biology* **9**, 214-223.

Jassal, S. R., Lairmore, M. D., Leigh-Brown, A. J. & Brighty, D. W. (2001). Soluble recombinant HTLV-1 surface glycoprotein competitively inhibits

syncytia formation and viral infection of cells. *Virus Research* **78**, 17-34.

Jayakumar, A., Huang, W. Y., Raetz, B., Chirala, S. S. & Wakil, S. J. (1996). Cloning and expression of the multifunctional human fatty acid synthase and its subdomains in Escherichia coli. *Proceedings of the National Academy of Sciences of the United States of America* **93**, 14509-14514.

Jiang, J. Y., Cun, W., Wu, X. F., Shi, Q., Tang, H. L. & Luo, G. X. (2012). Hepatitis C virus attachment mediated by apolipoprotein E binding to cell surface heparan sulfate. *Journal of Virology* **86**, 7256-7267.

Johannsdottir, H. K., Mancini, R., Kartenbeck, J., Amato, L. & Helenius, A. (2009). Host cell factors and functions involved in vesicular stomatitis virus entry. *Journal of Virology* **83**, 440-453.

Johnson, L. S., Dunn, K. W., Pytowski, B. & McGraw, T. E. (1993). Endosome acidification and receptor trafficking - bafilomycin A (1) slows receptor externalization by a mechanism involving the receptors internalization motif. *Molecular Biology of the Cell* **4**, 1251-1266.

Jorge, S. A. C., Santos, A. S., Spina, A. & Pereira, C. A. (2008). Expression of the hepatitis B virus surface antigen in drosophila S2 cells. *Cytotechnology* **57**, 51-59.

Kagi, J. H. & Kojima, Y. (1987). Chemistry and biochemistry of metallothionein. *Experientia Supplementum* **52**, 25-61.

Kamili, S., Drobeniuc, J., Araujo, A. C. & Hayden, T. M. (2012). Laboratory diagnostics for hepatitis C virus infection. *Clinical Infectious Diseases* **55**, S43-S48.

Kapust, R. B. & Waugh, D. S. (1999). Escherichia coli maltose-binding protein is uncommonly effective at promoting the solubility of polypeptides to which it is fused. *Protein Science* **8**, 1668-1674.

Kato, T., Furusaka, A., Miyamoto, M., Date, T., Yasui, K., Hiramoto, J., Nagayama, K., Tanaka, T. & Wakita, T. (2001). Sequence analysis of hepatitis

C virus isolated from a fulminant hepatitis patient. *Journal of Medical Virology* **64**, 334-339.

Keck, Z. Y., Sung, V. M. H., Perkins, S., Rowe, J., Paul, S., Liang, T. J., Lai, M. M. C. & Foung, S. K. H. (2004). Human monoclonal antibody to hepatitis C virus El glycoprotein that blocks virus attachment and viral infectivity. *Journal of Virology* **78**, 7257-7263.

Kenny-Walsh, E. & Irish Hepatol Res, G. (1999). Clinical outcomes after hepatitis C infection from contaminated anti-D immune globulin. *New England Journal of Medicine* **340**, 1228-1233.

Khan, A. G., Whidby, J., Miller, M. T. & other authors (2014). Structure of the core ectodomain of the hepatitis C virus envelope glycoprotein 2. *Nature* **509**, 381-384.

Kirkpatrick, R. B., Ganguly, S., Angelichio, M., Griego, S., Shatzman, A., Silverman, C. & Rosenberg, M. (1995). Heavy-chain dimers as well as complete antibodies are efficiently formed and secreted from drosophila via a bip-mediated pathway. *Journal of Biological Chemistry* **270**, 19800-19805.

Kong, L., Giang, E., Nieusma, T. & other authors (2013). Hepatitis C Virus E2 Envelope Glycoprotein Core Structure. *Science* **342**, 1090-1094.

Korenaga, M., Hino, K., Katoh, Y., Yamaguchi, Y., Okuda, M., Yoshioka, K. & Okita, K. (2001). A possible role of hypervariable region 1 quasispecies in escape of hepatitis C virus particles from neutralization. *Journal of Viral Hepatitis* **8**, 331-340.

Koutsoudakis, G., Kaul, A., Steinmann, E., Kallis, S., Lohmann, V., Pietschmann, T. & Bartenschlager, R. (2006). Characterization of the early steps of hepatitis C virus infection by using luciferase reporter viruses. *Journal of Virology* **80**, 5308-5320.

Krey, T., Thiel, H. J. & Rumenapf, T. (2005). Acid-resistant bovine pestivirus requires activation for pH-triggered fusion during entry. *Journal of Virology* **79**, 4191-4200.

Krieger, M. (2001). Scavenger receptor class B type I is a multiligand HDL receptor that influences diverse physiologic systems. *Journal of Clinical Investigation* **108**, 793-797.

Krieger, S. E., Zeisel, M. B., Davis, C. & other authors (2010). Inhibition of Hepatitis C Virus Infection by Anti-claudin-1 Antibodies is mediated by neutralization of E2-CD81-claudin-1 associations. *Hepatology* **51**, 1144-1157.

Landschulz, K. T., Pathak, R. K., Rigotti, A., Krieger, M. & Hobbs, H. H. (1996). Regulation of scavenger receptor, class B, type I, a high density lipoprotein receptor, in liver and steroidogenic tissues of the rat. *Journal of Clinical Investigation* **98**, 984-995.

Lauletta, G. (2013). HCV, Mixed Cryoglobulinemia and Malignant Lymphoproliferation. In Practical Management of Chronic Viral Hepatitis. Edited by In G. Serviddio. *InTech*, DOI: 10.5772/55474.

Lavallie, E. R., Diblasio, E. A., Kovacic, S., Grant, K. L., Schendel, P. F. & McCoy, J. M. (1993). A Thioredoxin gene fusion expression system that circumvents inclusion body formation in the *Escherichia-coli* cytoplasm. *Biotechnology* **11**, 187-193.

Lavanchy, D. (1999). Hepatitis C: public health strategies. *Journal of Hepatology* **31 Supplement 1**, 146-151.

Lavie, M., Goffard, A. & Dubuisson, J. (2007). Assembly of a functional HCV glycoprotein heterodimer. *Current Issues in Molecular Biology* **9**, 71-86.

Lavillette, D., Bartosch, B., Nourrisson, D., Verney, G., Cosset, F. L., Penin, F. & Pecheur, E. I. (2006). Hepatitis C virus glycoproteins mediate low pH-dependent membrane fusion with liposomes. *Journal of Biological Chemistry* **281**, 3909-3917.

Lavillette, D., Pecheur, E. I., Donot, P., Fresquet, J., Molle, J., Corbau, R., Dreux, M., Penin, F. & Cosset, F. L. (2007). Characterization of fusion determinants points to the involvement of three discrete regions of both E1 and E2 glycoproteins in the membrane fusion process of hepatitis C virus. *Journal*

of Virology **81**, 8752-8765.

Law, J. L. M., Chen, C., Wong, J. & other authors (2013). a hepatitis C virus (HCV) vaccine comprising envelope glycoproteins gpE1/gpE2 derived from a single isolate elicits broad cross-genotype neutralizing antibodies in humans. *Plos One* **8**, e59776

Lefevre, F., Remy, M. H. & Masson, J. M. (1997). Alanine-stretch scanning mutagenesis: a simple and efficient method to probe protein structure and function. *Nucleic Acids Research* **25**, 447-448.

Levy, S. (2014). Function of the tetraspanin molecule CD81 in B and T cells. *Immunologic Research* **58**, 179-185.

Levy, S., Todd, S. C. & Maecker, H. T. (1998). CD81 (TAPA-1): a molecule involved in signal transduction and cell adhesion in the immune system. *Annual Review of Immunology* **16**, 89-109.

Lin, C. (2006). HCV NS3-4A Serine Protease. In Hepatitis C Viruses: Genomes and Molecular Biology. Edited by S. L. Tan. Norfolk (UK): *Horizon Bioscience,* 163-206

Lin, X. H. (2004). Functions of heparan sulfate proteoglycans in cell signaling during development. *Development* **131**, 6009-6021.

Lindenbach, B. D. & Rice, C. M. (2001). Flaviviridae: The Viruses and Their Replication. In Fields Virology. Edited by D.M Knipe. D.M & P.M. Howley. Philadelphia (USA):*Lippincott Williams& Wilkins* **4**, 991-1042.

Lindenbach, B. D. & Rice, C. M. (2005). Unravelling hepatitis C virus replication from genome to function. *Nature* **436**, 933-938.

Lindenbach, B. D. & Rice, C. M. (2013). The ins and outs of hepatitis C virus entry and assembly. *Nature Reviews Microbiology* **11**, 688-700.

Liu, S. F., Yang, W., Shen, L., Turner, J. R., Coyne, C. B. & Wang, T. Y. (2009). Tight junction proteins claudin-1 and occludin control hepatitis C virus entry and are downregulated during infection to prevent superinfection. *Journal*

of Virology **83**, 2011-2014.

Lohmann, V. & Bartenschlager, R. (2014). On the history of hepatitis C virus cell culture systems. *Journal of Medicinal Chemistry* **57**, 1627-1642.

Lohmann, V., Korner, F., Koch, J. O., Herian, U., Theilmann, L. & Bartenschlager, R. (1999). Replication of subgenomic hepatitis C virus RNAs in a hepatoma cell line. *Science* **285**, 110-113.

Longman, R. S., Talal, A. H., Jacobson, I. M., Albert, M. L. & Rice, C. M. (2004). Presence of functional dendritic cells in patients chronically infected with hepatitis C virus. *Blood* **103**, 1026-1029.

Lozach, P. Y., Amara, A., Bartosch, B., Virelizier, J. L., Arenzana-Seisdedos, F., Cosset, F. L. & Altmeyer, R. (2004). C-type lectins L-SIGN and DC-SIGN capture and transmit infectious hepatitis C virus pseudotype particles. *Journal of Biological Chemistry* **279**, 32035-32045.

Lozach, P. Y., Lortat-Jacob, H., de Lacroix de Lavalette, A. & other authors (2003). DC-SIGN and L-SIGN are high affinity binding receptors for hepatitis C virus glycoprotein E2. *Journal of Biological Chemistry* **278**, 20358-20366.

Lucas, M., Tsitoura, E., Montoya, M. & other authors (2003). Characterization of secreted and intracellular forms of a truncated hepatitis C virus E2 protein expressed by a recombinant herpes simplex virus. *Journal of General Virology* **84**, 545-554.

Ludwig, I. S., Lekkerkerker, A. N., Depla, E., Bosman, F., Musters, R. J., Depraetere, S., van Kooyk, Y. & Geijtenbeek, T. B. (2004). Hepatitis C virus targets DC-SIGN and L-SIGN to escape lysosomal degradation. *J Virol* **78**, 8322-8332.

Lupberger, J., Zeisel, M. B., Xiao, F. & other authors (2011). EGFR and EphA2 are host factors for hepatitis C virus entry and possible targets for antiviral therapy. *Nature Medicine* **17**, 589-U109.

MacKenzie, J. M. & Westaway, E. G. (2001). Assembly and maturation of the

flavivirus Kunjin virus appear to occur in the rough endoplasmic reticulum and along the secretory pathway, respectively. *Journal of Virology* **75**, 10787-10799.

Magiorkinis, G., Magiorkinis, E., Paraskevis, D., Ho, S. Y. W., Shapiro, B., Pybus, O. G., Allain, J. P. & Hatzakis, A. (2009). The Global Spread of hepatitis C virus 1a and 1b: a phylodynamic and phylogeographic analysis. *Plos Medicine* **6**, e1000198

Maheshwari, A., Ray, S. & Thuluvath, P. J. (2008). Acute hepatitis C. *Lancet* **372**, 321-332.

Maina, C. V., Riggs, P. D., Grandea, A. G., Slatko, B. E., Moran, L. S., Tagliamonte, J. A., McReynolds, L. A. & Diguan, C. (1988). An *Escherichia.coli* vector to express and purify foreign proteins by fusion to and separation from maltose-binding protein. *Gene* **74**, 365-373.

Marshall, R. D. (1974). The nature and metabolism of the carbohydrate-peptide linkages of glycoproteins. *Biochemical Society Symposium* **40***,* 17-26.

Martin, D. N. & Uprichard, S. L. (2013). Identification of transferrin receptor 1 as a hepatitis C virus entry factor. *Proceedings of the National Academy of Sciences of the United States of America* **110**, 10777-10782.

Matsuda, M., Suzuki, R., Kataoka, C., Watashi, K., Aizaki, H., Kato, N., Matsuura, Y., Suzuki, T. & Wakita, T. (2014). Alternative endocytosis pathway for productive entry of hepatitis C virus. *Journal of General Virology* **95**, 2658-2667.

Meertens, L., Bertaux, C. & Dragic, T. (2006). Hepatitis C virus entry requires a critical postinternalization step and delivery to early endosomes via clathrin-coated vesicles. *Journal of Virology* **80**, 11571-11578.

Meola, A., Sbardellati, A., Bruni Ercole, B. & other authors (2000). Binding of hepatitis C virus E2 glycoprotein to CD81 does not correlate with species permissiveness to infection. *Journal of Virology* **74**, 5933-5938.

Messina, J. P., Humphreys, I., Flaxman, A., Brown, A., Cooke, G. S.,

Pybus, O. G. & Barnes, E. (2015). Global Distribution and Prevalence of Hepatitis C Virus Genotypes. *Hepatology* **61**, 77-87.

Mettlen, M., Pucadyil, T., Ramachandran, R. & Schmid, S. L. (2009). Dissecting dynamin's role in clathrin-mediated endocytosis. *Biochemical Society Transactions* **37**, 1022-1026.

Meunier, J. C., Fournillier, A., Choukhi, A., Cahour, A., Cocquerel, L., Dubuisson, J. & Wychowski, C. (1999). Analysis of the glycosylation sites of hepatitis C virus (HCV) glycoprotein E1 and the influence of E1 glycans on the formation of the HCV glycoprotein complex. *Journal of General Virology* **80**, 887-896.

Meunier, J. C., Russell, R. S., Goossens, V. & other authors (2008). Isolation and characterization of broadly neutralizing human monoclonal antibodies to the E1 glycoprotein of hepatitis C virus. *Journal of Virology* **82**, 966-973.

Michalak, J. P., Wychowski, C., Choukhi, A., Meunier, J. C., Ung, S., Rice, C. M. & Dubuisson, J. (1997). Characterization of truncated forms of hepatitis C virus glycoproteins. *Journal of General Virology* **78**, 2299-2306.

Milic, S., Mikolasevic, I., Orlic, L., Devcic, E., Starcevic-Cizmarevic, N., Stimac, D., Kapovic, M. & Ristic, S. (2016). The Role of Iron and Iron Overload in Chronic Liver Disease. *Medical Science Monitor* **22**, 2144-2151.

Miller, F. D. & Abu-Raddad, L. J. (2010). Evidence of intense ongoing endemic transmission of hepatitis C virus in Egypt. *Proceedings of the National Academy of Sciences of the United States of America* **107**, 14757-14762.

Miller, R. H. & Purcell, R. H. (1990). Hepatitis-c virus shares amino-acid-sequence similarity with pestiviruses and flaviviruses as well as members of 2 plant-virus supergroups. *Proceedings of the National Academy of Sciences of the United States of America* **87**, 2057-2061.

Molenkamp, R., Kooi, E. A., Lucassen, M. A., Greve, S., Thijssen, J. C. P., Spaan, W. J. M. & Bredenbeek, P. J. (2003). Yellow fever virus replicons as

an expression system for hepatitis C virus structural proteins. *Journal of Virology* **77**, 1644-1648.

Mondelli, M. U., Cerino, A., Segagni, L., Meola, A., Cividini, A., Silini, E. & Nicosia, A. (2001). Hypervariable region 1 of hepatitis C virus: immunological decoy or biologically relevant domain? *Antiviral Research* **52**, 153-159.

Moriya, K., Fujie, H., Shintani, Y. & other authors (1998). The core protein of hepatitis C virus induces hepatocellular carcinoma in transgenic mice. *Nature Medicine* **4**, 1065-1067.

Mosley, J. W., Redeker, A. G., Feinstone, S. M. & Purcell, R. H. (1977). Multiple hepatitis viruses in multiple attacks of acute viral-hepatitis. *New England Journal of Medicine* **296**, 75-78.

Mues, M. B., Cheshenko, N., Wilson, D. W., Gunther-Cummins, L. & Herold, B. C. (2015). Dynasore disrupts trafficking of herpes simplex virus proteins. *Journal of Virology* **89**, 6673-6684.

Narbus, C. M., Israelow, B., Sourisseau, M., Michta, M. L., Hopcraft, S. E., Zeiner, G. M. & Evans, M. J. (2011). HepG2 cells expressing microRNA miR-122 support the entire hepatitis C virus life cycle. *Journal of Virology* **85**, 12087-12092.

Negre, D., Duisit, G., Mangeot, P. E., Moullier, P., Darlix, J. L. & Cosset, F. L. (2002). Lentiviral vectors derived from simian immunodeficiency virus. *Lentiviral Vectors* **261**, 53-74.

Nguyen, T., Ghebrehiwet, B. & Peerschke, E. I. B. (2000). Staphylococcus aureus protein A recognizes platelet gC1qR/p33: a novel mechanism for staphylococcal interactions with platelets. *Infection and Immunity* **68**, 2061-2068.

Nielsen, S. U., Bassendine, M. F., Burt, A. D., Bevitt, D. J. & Toms, G. L. (2004). Characterization of the genome and structural proteins of hepatitis C virus resolved from infected human liver. *Journal of General Virology* **85**, 1497-1507.

Nielsen, S. U., Bassendine, M. F., Burt, A. D., Martin, C., Pumeechockchai, W. & Toms, G. L. (2006). Association between hepatitis C virus and very-low-density lipoprotein (VLDL)/LDL analyzed in iodixanol density gradients. *Journal of General Virology* **80**, 2418-2428.

Nielsen, S. U., Bassendine, M. F., Martin, C., Lowther, D., Purcell, P. J., King, B. J., Neely, D. & Toms, G. L. (2008). Characterization of hepatitis C RNA-containing particles from human liver by density and size. *Journal of General Virology* **89**, 2507-2517.

Nusrat, A., Brown, G. T., Tom, J., Drake, A., Bui, T. T. T., Quan, C. & Mrsny, R. J. (2005). Multiple protein interactions involving proposed extracellular loop domains of the tight junction protein occludin. *Molecular Biology of the Cell* **16**, 1725-1734.

Oren, R., Takahashi, S., Doss, C., Levy, R. & Levy, S. (1990). TAPA-1, the target of an antiproliferative antibody, defines a new family of transmembrane proteins. *Molecular and Cellular Biology* **10**, 4007-4015.

Orozco, I. J., Kim, S. J. & Martinson, H. G. (2002). The poly(A) signal, without the assistance of any downstream element, directs RNA polymerase II to pause in vivo and then to release stochastically from the template. *Journal of Biological Chemistry* **277**, 42899-42911.

Owsianka, A. M., Timms, J. M., Tarr, A. W. & other authors (2006). Identification of conserved residues in the E2 envelope glycoprotein of the hepatitis C virus that are critical for CD81 binding. *Journal of Virology* **80**, 8695-8704.

Paris, L., Tonutti, L., Vannini, C. & Bazzoni, G. (2008). Structural organization of the tight junctions. *Biochimica et Biophysica Acta* **1778**, 646-659.

Patel, J., Patel, A. H. & McLauchlan, J. (2001). Transmembrane domain of the hepatitis C virus E2 glycoprotein is required for correct folding of the E1 glycoprotein and native complex formation. *Virology* **279**, 58-68.

Pawlotsky, J. M., Germanidis, G., Frainais, P. O., Bouvier, M., Soulier, A., Pellerin, M. & Dhumeaux, D. (1999). Evolution of the hepatitis C virus second envelope protein hypervariable region in chronically infected patients receiving alpha interferon therapy. *Journal of Virology* **73**, 6490-6499.

Penin, F., Dubuisson, J., Rey, F. A., Moradpour, D. & Pawlotsky, J. M. (2004). Structural biology of hepatitis C virus. *Hepatology* **39**, 5-19.

Pereira, A. A. & Jacobson, I. M. (2009). New and experimental therapies for HCV. *Nature Reviews Gastroenterology & Hepatology* **6**, 403-411.

Petracca, R., Falugi, F., Galli, G. & other authors (2000). Structure-function analysis of hepatitis C virus envelope-CD81 binding. *Journal of Virology* **74**, 4824-4830.

Pileri, P., Uematsu, Y., Campagnoli, S. & other authors (1998). Binding of hepatitis C virus to CD81. *Science* **282**, 938-941.

Ploss, A., Evans, M. J., Gaysinskaya, V. A., Panis, M., You, H. N., de Jong, Y. P. & Rice, C. M. (2009). Human occludin is a hepatitis C virus entry factor required for infection of mouse cells. *Nature* **457**, 882-886.

Polyak, S. J., Klein, K. C., Shoji, I., Miyamura, T. & Lingappa, J. R. (2006). Assemble and Interact: Pleiotropic Functions of the HCV core Protein. In Hepatitis C Viruses: Genomes and Molecular Biology. Edited by S. L. Tan. Norfolk (UK): *Horizon Bioscience*, 89-119

Ponka, P. & Lok, C. N. (1999). The transferrin receptor: role in health and disease. *International Journal of Biochemistry & Cell Biology* **31**, 1111-1137.

Poynard, T., Bedossa, P. & Opolon, P. (1997). Natural history of liver fibrosis progression in patients with chronic hepatitis C. *Lancet* **349**, 825-832.

Prince, A. M., Grady, G. F., Hazzi, C., Brotman, B., Kuhns, W. J., Levine, R. W. & Millian, S. J. (1974). Long-incubation post-transfusion hepatitis without serological evidence of exposure to hepatitis-b virus. *Lancet* **2**, 241-246.

Prince, A. M., HuimaByron, T., Parker, T. S. & Levine, D. M. (1996).

Visualization of hepatitis C virions and putative defective interfering particles isolated from low-density lipoproteins. *Journal of Viral Hepatitis* **3**, 11-17.

Proudfoot, N. J. (1989). how RNA polymerase-II terminates transcription in higher eukaryotes. *Trends in Biochemical Sciences* **14**, 105-110.

Proudfoot, N. J., Furger, A. & Dye, M. J. (2002). Integrating mRNA processing with transcription. *Cell* **108**, 501-512.

Pryor, K. D. & Leiting, B. (1997). High-level expression of soluble protein in Escherichia coli using a His(6)-tag and maltose-binding-protein double-affinity fusion system. *Protein Expression and Purification* **10**, 309-319.

Puro, V., Petrosillo, N., Ippolito, G. & other authors (1995). Risk of hepatitis-c seroconversion after occupational exposures in health-care workers. *American Journal of Infection Control* **23**, 273-277.

Pybus, O. G., Barnes, E., Taggart, R. & other authors (2009). Genetic History of Hepatitis C Virus in East Asia. *Journal of Virology* **83**, 1071-1082.

Rahn, E., Petermann, P., Hsu, M.-J., Rixon, F. J. & Knebel-Morsdorf, D. (2011). Entry Pathways of Herpes Simplex Virus Type 1 into Human Keratinocytes Are Dynamin- and Cholesterol-Dependent. *Plos One* **6**, e25464

Ralston, R., Thudium, K., Berger, K. & other authors (1993). Characterization of hepatitis-c virus envelope glycoprotein complexes expressed by recombinant vaccinia viruses. *Journal of Virology* **67**, 6753-6761.

Ranjith-Kumar, C. T. & Kao, C. C. (2006). Biochemical Activities of the HCV NS5B RNA-Dependent RNA Polymerase. In Hepatitis C Viruses: Genomes and Molecular Biology. Edited by S. L. Tan. Norfolk (UK): *Horizon Bioscience*, 293-310 .

Rehermann, B. (2009). Hepatitis C virus versus innate and adaptive immune responses: a tale of coevolution and coexistence. *Journal of Clinical Investigation* **119**, 1745-1754.

Rhainds, D., Bourgeois, P., Bourret, G., Huard, K., Falstrault, L. & Brissette, L. (2004). Localization and regulation of SR-BI in membrane rafts of

HepG2 cells. *Journal of Cell Science* **117**, 3095-3105.

Rhainds, D., Falstrault, L., Tremblay, C. & Brissette, L. (1999). Uptake and fate of class B scavenger receptor ligands in HepG2 cells. *European Journal of Biochemistry* **261**, 227-235.

Rigotti, A., Acton, S. L. & Krieger, M. (1995). The class-B scavenger receptors SR-BI and CD36 are receptors for anionic phospholipids. *Journal of Biological Chemistry* **270**, 16221-16224.

Roberts, E. A. & Yeung, L. (2002). Maternal-infant transmission of hepatitis C virus infection. *Hepatology* **36**, S106-S113.

Roccasecca, R., Ansuini, H., Vitelli, A. & other authors (2003). Binding of the hepatitis C virus E2 glycoprotein to CD81 is strain specific and is modulated by a complex interplay between hypervariable regions 1 and 2. *Journal of Virology* **77**, 1856-1867.

Rothwang, K. B., Manicassamy, B., Uprichard, S. L. & Rong, L. (2008). Dissecting the role of putative CD81 binding regions of E2 in mediating HCV entry: Putative CD81 binding region 1 is not involved in CD81 binding. *Virology Journal* **5**-46

Sabahi, A. (2009). Hepatitis C Virus entry: the early steps in the viral replication cycle. *Virology Journal* **6**-117

Sainz, B., Barretto, N., Martin, D. N. & other authors (2012). Identification of the Niemann-Pick C1-like 1 cholesterol absorption receptor as a new hepatitis C virus entry factor. *Nature Medicine* **18**, 281-285.

Sainz, B., Jr., Barretto, N. & Uprichard, S. L. (2009). Hepatitis C Virus Infection in Phenotypically Distinct Huh7 Cell Lines. *Plos One* **4**, e6561

Sandrin, V., Boson, B., Salmon, P., Gay, W., Negre, D., Le Grand, R., Trono, D. & Cosset, F. L. (2002). Lentiviral vectors pseudotyped with a modified RD114 envelope glycoprotein show increased stability in sera and augmented transduction of primary lymphocytes and CD34+ cells derived from human and nonhuman primates. *Blood* **100**, 823-832.

Santos, M. G., Jorge, S. A. C., Brillet, K. & Pereira, C. A. (2007). Improving heterologous protein expression in transfected Drosophila S2 cells as assessed by EGFP expression. *Cytotechnology* **54**, 15-24.

Scarselli, E., Ansuini, H., Cerino, R. & other authors (2002). The human scavenger receptor class B type I is a novel candidate receptor for the hepatitis C virus. *Embo Journal* **21**, 5017-5025.

Schwarz, A. K., Grove, J., Hu, K., Mee, C. J., Balfe, P. & McKeating, J. A. (2009). Hepatoma cell density promotes claudin-1 and scavenger receptor BI expression and hepatitis C virus internalization. *Journal of Virology* **83**, 12407-12414.

Selby, M. J., Glazer, E., Masiarz, F. & Houghton, M. (1994). Complex processing and protein-protein interactions in the E2-NS2 region of HCV. *Virology* **204**, 114-122.

Sheares, B. T. (1988). Site-specific glycosylation in animal cells. Substitution of glutamine for asparagine 293 in chicken ovalbumin does not allow glycosylation of asparagine 312. *Journal of Biological Chemistry* **263**, 12778-12782.

Shi, Q., Jiang, J. Y. & Luo, G. X. (2013). Syndecan-1 Serves as the Major Receptor for Attachment of Hepatitis C Virus to the Surfaces of Hepatocytes. *Journal of Virology* **87**, 6866-6875.

Shin, H. S., Lim, H. J. & Cha, H. J. (2003). Quantitative monitoring for secreted production of human interleukin-2 in stable insect Drosophila S2 cells using a green fluorescent protein fusion partner. *Biotechnology Progress* **19**, 152-157.

Siller, R., Greenhough, S., Naumovska, E. & Sullivan, G. J. (2015). Small-molecule-driven hepatocyte differentiation of human pluripotent stem cells. *Stem cell reports* **4**, 939-952.

Simmonds, P., Alberti, A., Alter, H. J. & other authors (1994). A proposed system for the nomenclature of hepatitis C viral genotypes. *Hepatology* **19**, 1321-1324.

Skjeldal, F. M., Strunze, S., Bergeland, T., Walseng, E., Gregers, T. F. & Bakke, O. (2012). The fusion of early endosomes induces molecular-motor-driven tubule formation and fission. *Journal of Cell Science* **125**, 1910-1919.

Sklan, E. H. & Glenn, J. S. (2006). HCV NS4B: From Obscurity to Central Stage. In Hepatitis C Viruses: Genomes and Molecular Biology. Edited by S. L. Tan. Norfolk (UK): *Horizon Bioscience,* 245-266.

Smith, D. B., Bukh, J., Kuiken, C., Muerhoff, A. S., Rice, C. M., Stapleton, J. T. & Simmonds, P. (2014). Expanded classification of hepatitis C virus into 7 genotypes and 67 subtypes: updated criteria and genotype assignment web resource. *Hepatology* **59**, 318-327.

Smyth, D. R., Mrozkiewicz, M. K., McGrath, W. J., Listwan, P. & Kobe, B. (2003). Crystal structures of fusion proteins with large-affinity tags. *Protein Science* **12**, 1313-1322.

Stadler, K., Allison, S. L., Schalich, J. & Heinz, F. X. (1997). Proteolytic activation of tick-borne encephalitis virus by furin. *Journal of Virology* **71**, 8475-8481.

Stiasny, K. & Heinz, F. X. (2006). Flavivirus membrane fusion. *Journal of General Virology* **87**, 2755-2766.

Sun, X. J., Yau, V. K., Briggs, B. J. & Whittaker, G. R. (2005). Role of clathrin-mediated endocytosis during vesicular stomatitis virus entry into host cells. *Virology* **338**, 53-60.

Tabor, E., Drucker, J. A., Hoofnagle, J. H., April, M., Gerety, R. J., Seeff, L. B., Jackson, D. R., Barker, L. F. & Pinedatamondong, G. (1978). Transmission of non-A, non-B hepatitis from man to chimpanzee. *Lancet* **1**, 463-466.

Takada, A., Robison, C., Goto, H., Sanchez, A., Murti, K. G., Whitt, M. A. & Kawaoka, Y. (1997). A system for functional analysis of Ebola virus glycoprotein. *Proceedings of the National Academy of Sciences of the United States of America* **94**, 14764-14769.

Tan, S. L., Nakao, H., He, Y. P., Vijaysri, S., Neddermann, P., Jacobs, B. L., Mayer, B. J. & Katze, M. G. (1999). NS5A, a nonstructural protein of hepatitis C virus, binds growth factor receptor-bound protein 2 adaptor protein in a Src homology 3 domain/ligand-dependent manner and perturbs mitogenic signaling. *Proceedings of the National Academy of Sciences of the United States of America* **96**, 5533-5538.

Terrault, N. A. (2002). Sexual activity as a risk factor for hepatitis C. *Hepatology* **36**, S99-S105.

Thiel, HJ., Collett, MS., Gould, EA., Heinz, FX., Houghton, M., Meyers, G., Purcell, RH. & Rice, CM. (2005). Family Flaviviridae. In Viruses Taxonomy. Edited by CM. Fauquet, MA. Mayo, J. Maniloff, U. Desselberger & LA. Ball, LA. VIIIth Report of the International Committee on Taxonomy of Viruses. London (UK): *Elsevier/Academic Press*, 979–996

Thimme, R., Oldach, D., Chang, K. M., Steiger, C., Ray, S. C. & Chisari, F. V. (2001). Determinants of viral clearance and persistence during acute hepatitis C virus infection. *Journal of Experimental Medicine* **194**, 1395-1406.

Thomas, D. L., Astemborski, J., Rai, R. M. & other authors (2000). The natural history of hepatitis C virus infection-host, viral, and environmental factors. *Journal of the American Medical Association* **284**, 450-456.

Thomson, B. J. (2009). Hepatitis C virus: the growing challenge. *British Medical Bulletin* **89**, 153-167.

Timpe, J. M., Stamataki, Z., Jennings, A. & other authors (2008). Hepatitis C virus cell-cell transmission in hepatoma cells in the presence of neutralizing antibodies. *Hepatology* **47**, 17-24.

Tovey, M. G., Streuli, M., Gresser, I., Gugenheim, J., Blanchard, B., Guymarho, J., Vignaux, F. & Gigou, M. (1987). Interferon messenger-RNA is produced constitutively in the organs of normal individuals. *Proceedings of the National Academy of Sciences of the United States of America* **84**, 5038-5042.

Troesch, M., Meunier, I., Lapierre, P., Lapointe, N., Alvarez, F., Boucher, M.

& Soudeyns, H. (2006). Study of a novel hypervariable region in hepatitis C virus (HCV) E2 envelope glycoprotein. *Virology* **352**, 357-367.

Tscherne, D. M., Jones, C. T., Evans, M. J., Lindenbach, B. D., McKeating, J. A. & Rice, C. M. (2006). Time- and temperature-dependent activation of hepatitis C virus for low-pH-triggered entry. *Journal of Virology* **80**, 1734-1741.

Tsugawa, Y., Kato, H., Fujita, T., Shimotohno, K. & Hijikata, M. (2014). Critical role of interferon-alpha constitutively produced in human hepatocytes in response to RNA virus infection. *PLoS One* **9**, e89869.

Van Eck, M., Hoekstra, M., Out, R., Bos, I. S. T., Kruijt, J. K., Hildebrand, R. B. & Van Berkel, T. J. C. (2008). Scavenger receptor BI facilitates the metabolism of VLDL lipoproteins in vivo. *Journal of Lipid Research* **49**, 136-146.

van Kooyk, Y. & Geijtenbeek, T. B. H. (2003). DC-sign: escape mechanism for pathogens. *Nature Reviews Immunology* **3**, 697-709.

Vogt, M., Lang, T., Frosner, G. & other authors (1999). Prevalence and clinical outcome of hepatitis C infection in children who underwent cardiac surgery before the implementation of blood-donor screening. *New England Journal of Medicine* **341**, 866-870.

Voisset, C., Callens, N., Blanchard, E., Dubuisson, J. & Vu-Dac, N. (2005). High density lipoproteins facilitate hepatitis C virus entry through the scavenger receptor class B type I. *Journal of Biological Chemistry* **280**, 7793-7799.

Wakita, T., Pietschmann, T., Kato, T. & other authors (2005). Production of infectious hepatitis C virus in tissue culture from a cloned viral genome. *Nature Medicine* **11**, 905-905.

Wang, L. H., Rothberg, K. G. & Anderson, R. G. W. (1993). Mis-assembly of clathrin lattices on endosomes reveals a regulatory switch for coated pit formation. *Journal of Cell Biology* **123**, 1107-1117.

Wei, X. P., Decker, J. M., Wang, S. Y. & other authors (2003). Antibody neutralization and escape by HIV-1. *Nature* **422**, 307-312.

Welbourn, S. & Pause, A. (2006). HCV NS2/3 Protease. In Hepatitis C Viruses: Genomes and Molecular Biology. Edited by S. L. Tan. Norfolk (UK): *Horizon Bioscience,* 151-162

White, J. M., Delos, S. E., Brecher, M. & Schornberg, K. (2008). Structures and mechanisms of viral membrane fusion proteins: Multiple variations on a common theme. *Critical Reviews in Biochemistry and Molecular Biology* **43**, 189-219.

Wu, L. J., Gerard, N. P., Wyatt, R. & other authors (1996). CD4-induced interaction of primary HIV-1 gp120 glycoproteins with the chemokine receptor CCR-5. *Nature* **384**, 179-183.

Xu, Y., Martinez, P., Seron, K., Luo, G. X., Allain, F., Dubuisson, J. & Belouzard, S. (2015). Characterization of hepatitis C virus interaction with heparan sulfate proteoglycans. *Journal of Virology* **89**, 3846-3858.

Yagnik, A. T., Lahm, A., Meola, A., Roccasecca, R. M., Ercole, B. B., Nicosia, A. & Tramontano, A. (2000). A model for the hepatitis C virus envelope glycoprotein E2. *Proteins* **40**, 355-366.

Yamaguchi, A., Tazuma, S., Nishioka, T., Ohishi, W., Hyogo, H., Nomura, S. & Chayama, K. (2005). Hepatitis C virus core protein modulates fatty acid metabolism and thereby causes lipid accumulation in the liver. *Digestive Diseases and Sciences* **50**, 1361-1371.

Yang, W., Qiu, C., Biswas, N., Jin, J., Watkins, S. C., Montelaro, R. C., Coyne, C. B. & Wang, T. Y. (2008). Correlation of the tight junction-like distribution of Claudin-1 to the cellular tropism of hepatitis C virus. *Journal of Biological Chemistry* **283**, 8643-8653.

Yi, M., Villanueva, R. A., Thomas, D. L., Wakita, T. & Lemon, S. M. (2006). Production of infectious genotype 1a hepatitis C virus (Hutchinson strain) in cultured human hepatoma cells. *Proceedings of the National Academy of Sciences of the United States of America* **103**, 2310-2315.

Yokomizo, A. Y., Jorge, S. A. C., Astray, R. M., Fernandes, I., Ribeiro, O.

G., Horton, D. S. P. Q., Tonso, A., Tordo, N. & Pereira, C. A. (2007). Rabies virus glycoprotein expression in Drosophila S2 cells. I. Functional recombinant protein in stable co-transfected cell line. *Biotechnology Journal* **2**, 102-109.

Yoo, B. J., Selby, M. J., Choe, J. & other authors (1995). Transfection of a differentiated human hepatoma-cell line (Huh7) with in vitro-transcribed Hepatitis-C virus (HCV) RNA and establishment of a long-term culture persistently infected with HCV. *Journal of Virology* **69**, 32-38.

Yu, L. (2008). The structure and function of Niemann-Pick C1-like 1 protein. *Current Opinion in Lipidology* **19**, 440-440.

Zein, N. N. (2000). Clinical significance of hepatitis C virus genotypes. *Clinical Microbiology Reviews* **13**, 223-235.

Zeisel, M. B., Fofana, I., Fafi-Kremer, S. & Baumert, T. F. (2011). Hepatitis C virus entry into hepatocytes: molecular mechanisms and targets for antiviral therapies. *Journal of Hepatology* **54**, 566-576.

Zhang, J., Randall, G., Higginbottom, A., Monk, P., Rice, C. M. & McKeating, J. A. (2004a). CD81 is required for hepatitis C virus glycoprotein-mediated viral infection. *Journal of Virology* **78**, 1448-1455.

Zhang, M., Gaschen, B., Blay, W., Foley, B., Haigwood, N., Kuiken, C. & Korber, B. (2004b). Tracking global patterns of N-linked glycosylation site variation in highly variable viral glycoproteins: HIV, SIV, and HCV envelopes and influenza hemagglutinin. *Glycobiology* **14**, 1229-1246.

Zhao, L. J., Wang, L., Ren, H., Cao, J., Li, L., Ke, J. S. & Qi, Z. T. (2005). Hepatitis C virus E2 protein promotes human hepatoma cell proliferation through the MAPK/ERK signaling pathway via cellular receptors. *Experimental Cell Research* **305**, 23-32.

Zhong, J., Gastaminza, P., Cheng, G. F. & other authors (2005). Robust hepatitis C virus infection in vitro. *Proceedings of the National Academy of Sciences of the United States of America* **102**, 9294-9299.